Novel Applications of
Optical Coherence Tomography

for Diagnosis and Treatment Monitoring
of Patients with Macula-on Retinal Detachment
and Age-related Macular Degeneration

Jan Hendrik de Jong

ACKNOWLEDGEMENTS

Novel Applications of Optical Coherence Tomography
for Diagnosis and Treatment Monitoring
of Patients with Macula-on Retinal Detachment
and Age-related Macular Degeneration

Nieuwe toepassingen van optische coherentie tomografie
voor diagnose en monitoring van de behandeling
van patiënten met macula-aan netvliesloslatingen
en leeftijdsgebonden maculadegeneratie

Proefschrift

ter verkrijging van de graad van doctor aan de
Erasmus Universiteit Rotterdam
op gezag van de rector magnificus

Prof.dr. R.C.M.E. Engels

en volgens besluit van het College voor Promoties.

De openbare verdediging zal plaatsvinden op
woensdag 13 november 2019 om 9:30 uur

door
Jan Hendrik de Jong
geboren te Rotterdam

Erasmus University Rotterdam

Doctoral committee

Promotor: Prof.dr. J.C van Meurs

Other members: Prof.dr. J.R. Vingerling

Prof.dr. M. La Cour

Dr. E. Kilic

Copromotor: Dr.ir. K.A. Vermeer

'Een verstandig mens verwerft kennis, een wijze is gespitst op inzicht.'

Voor Christine, Eline en Naomi

Table of contents

Chapter

1

General introduction

The retina

The retina is the innermost, light-sensitive layer of the eye and is a crucial part of the visual system. The light that enters the eye is projected through the cornea, crystalline lens and vitreous body unto the retina and transformed into a two-dimensional image of the visual field. The rods and cones in the photoreceptor layer, which forms the outermost layer of the retina, convert the light into neural impulses. While the rods are responsible for detecting light and dark, the cones can process different light colors into electrical signals. These electrical signals travel via the retinal nerve fiber layer and optic nerve to the visual cortex in the occipital part of the brain. In the visual cortex, the information coming from the photoreceptor cells of both eyes is combined into a conscious perception of the visual fields.

The central part of the retina is called the macula and is approximately 5.5 mm in diameter. The concentration of photoreceptor cells is higher in the macula than in the peripheral retina, and therefore it is responsible for central vision.[1] In the fovea, the center of the macula with a diameter of approximately 1.5 mm, the photoreceptor layer consist of an even higher concentration of rods.[1,2] Therefore, the fovea is responsible for visual functions requiring detailed, sharp vision, like reading, face recognition and driving a car. The retinal pigment epithelium (RPE), Bruch's membrane and choroid are located under the retina (**Figure 1**). These structures support the function of the retina by providing nutrients and oxygen to the retina and by carrying off waste materials.
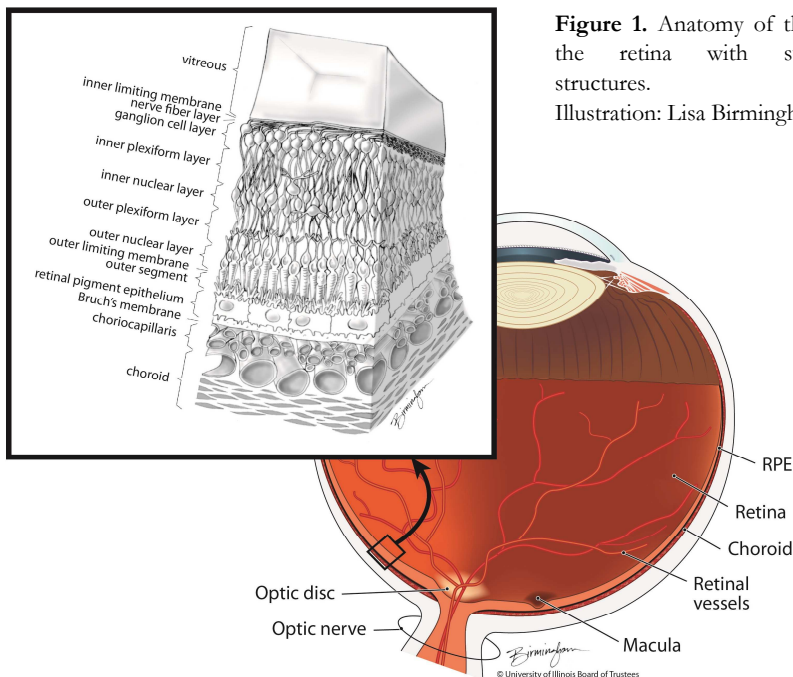
Figure 1. Anatomy of the eye and the retina with surrounding structures.
Illustration: Lisa Birmingham

© University of Illinois Board of Trustees

Retinal adhesion and detachment

A retinal detachment (RD) is a progressive, sight-threatening separation of the neurosensory retina from the RPE and has an incidence of 12-18 out of 10.000.[3,4] An RD occurs when the forces maintaining retinal adhesion are overwhelmed by forces of detachment.[5,6] Retinal adhesion is normally maintained by at least four mechanisms.[6] Firstly, fluid is driven passively from the vitreous to the choroid by both intraocular pressure and osmotic pressure of the extracellular fluid in the choroid. Since the retina and RPE provide substantial resistance to water movement, the outward movement of fluid acts to push the retina against the RPE.[7] Secondly, the RPE cells actively pump fluid from the (virtual) subretinal space to the choroid at a rate of 3.5 mL a day, which is more than half of the vitreous volume.[8] Thirdly, RPE microvilli wrap closely around the tips of the outer segments of the photoreceptors. Close ensheathment provides a frictional and possibly electrostatic resistance to withdrawal like a finger is hard to pull from a narrow tube.[6] Fourthly, the interphotoreceptor matrix between the retina and RPE contains proteins and proteoglycans which serve as a 'glue'.[9,10]

The pathology of the most common form of RD, rhegmatogenous RD, starts with liquefication and shrinking of the vitreous due to aging.[5,11,12] This allows head and eye movements to cause intraocular currents of vitreous gel and intravitreal fluid, which can lead to a complete or incomplete posterior vitreous detachment from the retina (**Figure 2**).[5,12,13] Dynamic traction exerted by the vitreous on the retina at places of vitreoretinal adhesion causes a retinal tear if the forces of retinal adhesion are overwhelmed.[5,6] Through the tear, the subretinal space may become accessible and intraocular currents allow intravitreal fluid to enter and accumulate in the subretinal space.
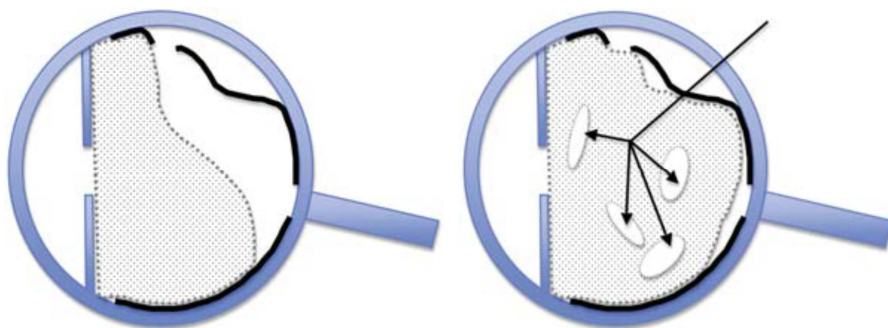
Figure 2. Schematic representation of two possible configurations of the vitreous in patients with a retinal detachment. (Left) a retinal detachment with partial posterior vitreous detachment and (right) an RD with the vitreous still attached to the detached part of the retina showing areas of liquefied vitreous (arrows). In both configurations, head and eye movements cause intraocular currents of subretinal fluid, intravitreal fluid and vitreous. As a result, dynamic traction on the retina and on the hinge of detachment results in the development and progression of RD. The lens and the macula are not shown for simplicity. Illustration from Kuhn et al.[5]

Because the oxygenation of the outer retina is dependent on the choroidal supply,[14] photoreceptors start to become apoptotic within 12 hours after retinal detachment.[15] Therefore, rapid surgical repair and prevention of macular involvement are critical in preserving central vision in patients with RD.[16-19]

Treatment of retinal detachment

Surgical repair of retinal detachments is performed by closing the retinal tear and relieving the vitreous traction on the retina, which can be accomplished by an internal or external approach. The internal approach uses pars plana vitrectomy to remove the vitreous as the source of retinal traction. After the vitrectomy, a temporary tamponade of gas or oil is left behind to close retinal tears and to approximate the retina to the RPE. The external approach uses a silicone explant which is sutured to the sclera at the location of the retinal tear. The explant causes an indentation, or 'buckles', the sclera, which relieves the vitreous traction on this part of the retina. The subretinal fluid is removed by external drainage and by spontaneous absorption by the RPE fluid pumps. After reattachment of the retina, it takes 6 weeks before the normal adhesion strength is reached.[20]

Patients with a macula-off retinal detachment are usually scheduled for surgery within a week, [21,22] although recent literature indicates that surgery within 3 days may result in a better outcome.[23] Patients with a macula-on retinal detachment are scheduled for early surgery to prevent macular detachment. As many clinics cannot provide same-day surgery for all patients and therefore, the majority of patients may have to wait for surgery for 1 or 2 days. However, the risk of RD progression toward macula-off is reported to be 0-3% in the 2-3 days before surgery.[24-27] Therefore, preoperative posturing consisting of bed rest and positioning is
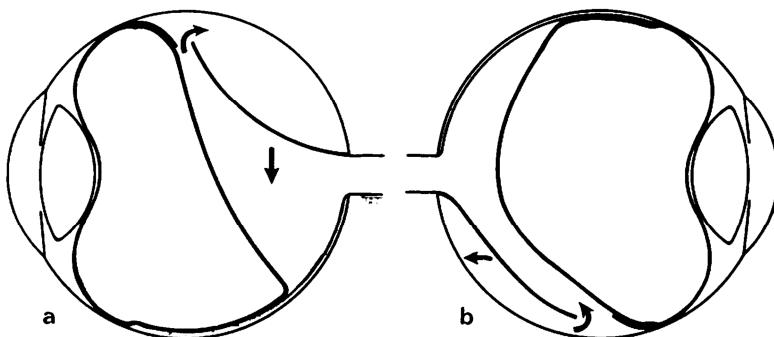
Figure 3. The effect of positioning in a patient with a superior retinal detachment (RD). (a) During the development of a bullous superior RD the retina may descend through the retrovitreal fluid. This fluid redistributes through the retinal tear from a preretinal to a postretinal position. (b) Positioning of the patient with the retinal hole dependent or on the side were the RD is mainly located allows reposition of the retina and transfer of fluid in the reverse direction. Illustration from Lean et al.[30]

traditionally prescribed to patients with macula-on RD to limit RD progression toward the fovea. Bed rest aims to restrict forces related to head and eye movement and the additional positioning of patients aims to address the potentially unfavorable effect of the force of gravity (**Figure 3**).[28-33] A supine position is advised for RD in the superior quadrants and a sitting position for RD in the inferior quadrants. It is not known whether this preoperative posturing advice is effective in limiting RD progression toward the fovea.

Exudative age-related macular degeneration
Age-related macular degeneration (AMD) is a progressive disease of the macula and the leading cause of irreversible legal blindness in elderly people in industrialized countries.[34,35] In AMD, a combined malfunctioning of retinal cells, RPE, Bruch's membrane and choroid leads to visual impairment. Two distinct variants can be differentiated. The first is dry, or atrophic, AMD, which is a slowly progressive subtype characterized by drusenoid deposits of waste material on the Bruchs' membrane and an atrophic and dysfunctional choriocapillaris, which leads to hypoxia of the adjacent RPE cells. The second is wet, or exudative, AMD, which is a more rapidly progressive subtype characterized by abnormal neovascularizations of the choroid or retinal vessels. These newly formed vessels cause fluid leakage and hemorrhages in the retina or in the subretinal space. Acute submacular hemorrhages cause immediate and irreversible damage to the retina and RPE and may severely compromise visual acuity without treatment.[36,37]

Exudative AMD can be classified further into three subtypes. In type 1, the neovascularizations are originating from the choroid and have penetrated the Bruch's membrane, but are restricted to the sub-RPE space. In type 2, the neovascularizations are from the choroidal origin as well and have grown through the RPE layer into the subretinal space. In type 3, the neovascularization is located intraretinally and may have an origin in the choroid, in the retinal vasculature, or both (**Figure 4**).[38] This subtype is traditionally called retinal angiomatous proliferation (RAP) and represents approximately 15-30% of newly diagnosed patients with exudative AMD.[39,40] The prognosis of RAP is poor with a typical rapid progression ending in a disciform scar and atrophy if not treated.[41]

Standard treatment for exudative AMD consists of intraocular anti-vascular endothelial growth factor injections (anti-VEGF), in selected cases combined with photodynamic laser therapy (PDT).[42] However, especially for the RAP subtype, there is no consensus on the optimal treatment strategy.
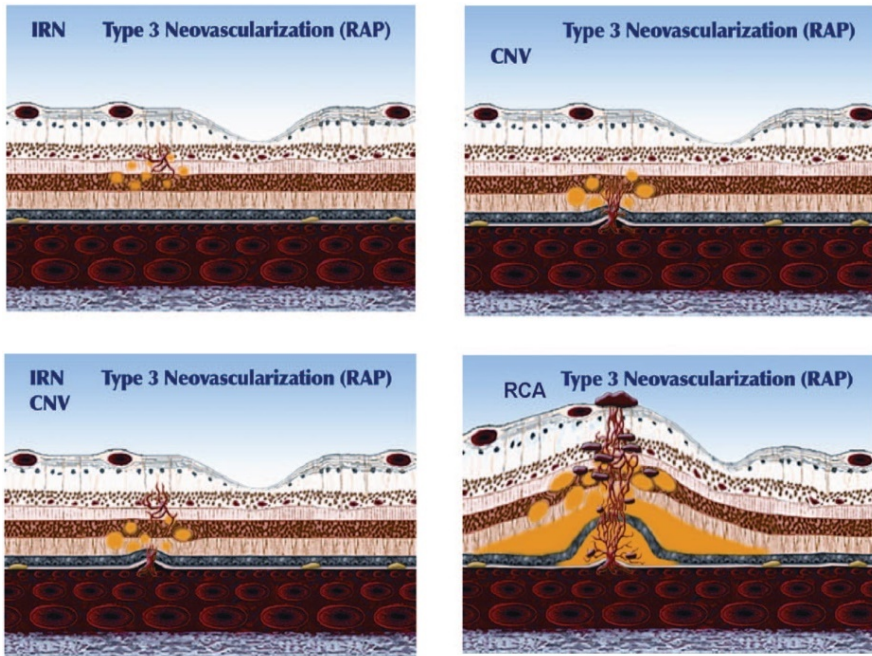
Figure 4. Schematic diagram of retinal angiomatous proliferation or type 3 neovascularization. Three variants of RAP are shown: an initial focal intraretinal neovascularization (IRN, top left), an initial choroidal neovascularization (CNV, top right) and a simultaneous retinal and choroidal proliferation (bottom left). These three variants may all rapidly progres into the mature stage of RAP including a retinal choroidal anastomosis (RCA), pigment epithelium detachment, subretinal fluid, and intraretinal hemorrhages (bottom right). Illustration from Yannuzzi et al.[38]

Monotherapy with anti-VEGF injections requires repeated administration and shows conflicting long-term results, while a combination treatment of anti-VEGF with PDT seems to lead to rapid resolution of the RAP lesion.[42] Surgical treatment by retinal rotation or RPE graft transplantation is optional in patients not responding to standard care or patients with severe complications like RPE-tears or submacular fibrosis.[43-45] In case of an acute submacular hemorrhage, surgical pneumatic displacement of the blood cloth can be considered. With this technique, recombinant tissue plasminogen activator (rtPA) is administrated to liquefy the blood cloth and an intravitreal gas tamponade is applied to displace the hemorrhage from the submacular region.[46,47] Two treatment modalities are currently practiced. The first is pars plana vitrectomy with subretinal administration of rtPA and intravitreal gas, the second is intravitreal administration of rtPA and gas. The efficacy of both treatment options seems to be similar based on the literature review. However, the intravitreal administration of rtPA technique might be less invasive.[47]

Imaging the posterior eye using optical coherence tomography

In the past two decades, optical coherence tomography (OCT) has revolutionized the imaging of the posterior eye and the understanding of retinal diseases.[48] OCT has evolved into a valuable tool in clinical ophthalmic practice and is used to diagnose and monitor a variety of retinal diseases affecting the vitreoretinal interface, the neurosensory retina, the RPE and choroid. OCT was revolutionary because it allows for a cross-section and *en face* representation of the posterior eye with a histology-like axial resolution up to 3 μm in a patient-friendly, noninvasive and non-contact manner. This in contrast to conventional imaging methods like fluorescence angiography which require intravenous injections of fluorescein dye to identify pathologic changes.

The central principle of OCT is low coherence interferometry, in which polarized light source back-scattered from the layers in the posterior eye is allowed to interfere with light that traveled a known distance. This is achieved by a Michelson interferometer, in which a beam splitter divides the emitted light from the laser source into a reference arm, which reflects on a mirror, and a sample arm, which reflects on the sample layers (**Figure 5A**). Within the coherence length of the light source, interference can be detected. The first implementation of OCT was time-domain OCT (TD-OCT), in which a movable mirror was used to vary the optical path length to detect interference fringes from different depths within the sample. Today, Fourier-domain OCT (FD-OCT) is mainly applied in commercial and experimental systems. FD-OCT can be implemented in two forms: spectral-domain OCT (SD-OCT) and swept source OCT (SS-OCT). SD-OCT uses a spectrometer to diffract the different wavelengths within the bandwidth of the laser source and detect them as multiple small wavelength bands on a charge-coupled device array (**Figure 5A**). SS-OCT, also known as optical frequency domain imaging (OFDI), uses a narrow band laser that rapidly sweeps in time over a broad spectral bandwidth. Subsequently, Fourier transformation is applied in both SD-OCT and SS-OCT systems to transform the composite spectral interference fringes into a reflectance pattern corresponding to the intensity of the reflected signal and its depth within the sample (**Figure 5B**). FD-OCT has a higher sensitivity and much greater acquisition speed than TD-OCT and therefore, yields an improved resolution with fewer artifacts due to sample movement.[49,50] SS-OCT is even less sensitive to fringe loss due to sample movement, gives lower signal decay in depth compared to SD-OCT and is currently used in most experimental systems.[51,52] In both systems, eye-tracking has been used to reduce artifacts and improve image quality.

A recent development of the standard OCT technique is OCT angiography, which is aimed at discriminating blood vessels from static tissue in a noninvasive and depth-resolved manner. Two approaches for OCT-A to visualize the retinal vasculature can be distinguished, which are combined in some commercially

available systems.[53] The first uses intensity changes between repeated OCT measurements to detect changes caused by moving light scattering particles. The second approach uses phase changes between successive OCT measurements caused by moving particles and is also referred to as Doppler OCT.[54-56] In contrast to intensity based OCT-A, phase-based OCT-A is also suited for measuring flow velocities and directions.

Figure 4. Spectral domain OCT. A) Schematic drawing of a spectral-domain OCT setup, which uses a spectrometer consisting of a diffraction grating, a lens and a CCD array. The spectrometer allows for detection of spectrally resolved interference signals along the full depth of an A-line using a single measurement. B) An example of a SD-OCT signal detection corresponding to a threefold partial reflector (top image). Fourier decomposition is used to transform the composite spectral fringes (middle image) to the depth in which the three peaks are observed at the locations of the three partial reflectors (bottom image).
Illustration adapted from Braaf B, The principles of Optical Coherence Tomography for posterior eye imaging; Academic thesis, 2015, Chapter 2, Figure 2.2 and 2.3, 13-34.

However, a few limitations of the current OCT-systems have to be considered. Firstly, OCT-imaging of the peripheral retina is challenging due to the small field of view of the OCT-systems. Wide-field systems have been developed which are able to visualize the retina up to the equator. However, a part of the retina remains 'invisible' for the current OCT systems, which is disadvantageous in studies on disease of the vitreous base. Secondly, the amount of data captured with a complete OCT volume scan is enormous and cannot be interpreted fully in a clinical setting. *En face* reconstructions of the retina at different depths have been developed to lower the time needed for interpretation, but layer segmentation algorithms are vulnerable to artifacts in case of severe distortions by retinal pathology.[57] Thirdly, morphological changes on OCT do not always correlate to leakage information on fluorescein angiography. The velocity of fluid leakage is too low for OCT-systems to detect, thereby withholding the clinical information on

the quality of visualized blood vessels. Fourthly, the quality of the OCT-signal is dependent on the clarity of the cornea, lens and vitreous, which can be hugely affected by various diseases, like corneal fibrosis, cataract, vitreous hemorrhages, and uveitis. Especially in elderly people, these factors limit the possibilities of the OCT system to visualize the pathology of the posterior eye.

Aims and outline of this thesis

The goals of this thesis were, making use of a novel application of OCT, to study: 1) if preoperative posturing of macula-on RD influences RD progression; 2) what risk factors for RD progression could be identified; 3) which role head orientation, movement and eye movement play in RD progression; 4) whether intravitreal or subretinal administration of rtPA better stimulates displacement of acute subretinal hemorrhages in AMD; 5) what advantage OCT-A has over conventional imaging in diagnosing and treatment monitoring of RAP.

In **chapter 2** the results of the first cohort of patients of a clinical trial studying the effect of preoperative posturing on RD progression are presented. RD progression was determined by measuring the RD–fovea distance with OCT before and after intervals of posturing and interruptions for meals and toilet visits. Additionally, risk factors for RD progression were studied within this first group of patients. In **chapter 3**, the effect of prolonging the duration of posturing interruptions by sitting upright is evaluated. Three cohorts of patients with macula-on RD were compared with an average interruption duration of 20, 40 and 60 minutes respectively. Besides re-evaluating the risk factors as studied in the first cohort, ultrasound imaging was used in cohort 3 to evaluate the amount of subretinal fluid at baseline as a risk factor for RD progression.

Chapter 4 focusses on the role of compliance to the preoperative posturing and head movement on RD progression. We used an inertial measurement unit (IMU) to measure head orientation and head movements and related the outcome of the IMU parameters to RD progression as measured with OCT. We evaluated whether compliance with the preoperative posturing advice or head motility plays a larger role in RD progression.

In **chapter 5**, numerical modeling is presented which was used to explore whether eye movement or head movement plays the largest role in RD progression. This was done because a clinical trial using RD progression OCT measurement and eye movement measurement would be invasive and therefore far more challenging to execute.

Chapter 6 discusses the results of a randomized clinical trial comparing the most effective and safe administration technique of rtPA and gas for the displacement of acute submacular hemorrhage in AMD. OCT was used to measure the amount of subretinal hemorrhage before and after surgical treatment.

In **chapter 7**, we demonstrate that OCT-A was able to image transretinal neovascularizations in patients with RAP. The features of RAP on OCT-A were described and compared to conventional imaging, including structural OCT, fluorescence angiography and indocyanine green angiography. **Chapter 8** evaluates the advantage of OCT-A in monitoring treatment effects in patients with RAP by comparing OCT-A features on follow-up measurements with structural OCT.

Finally, in **chapter 9,** the clinical implications of the studies as mentioned above are discussed and novel applications of OCT for future studies are proposed.

References

1. Purves D, Augustine GJ, Fitzpatrick D. Neuroscience, Fourth edition, chapter 11, figure 11.13. . 2008.

2. Polyak S. *The retina.* Chicago: University of Chicago Press; 1941.

3. Van de Put MA, Hooymans JM, Los LI, Dutch Rhegmatogenous Retinal Detachment Study Group. The incidence of rhegmatogenous retinal detachment in the netherlands. *Ophthalmology.* 2013;120(3):616-622.

4. Haimann MH, Burton TC, Brown CK. Epidemiology of retinal detachment. *Arch Ophthalmol.* 1982;100(2):289-292.

5. Kuhn F, Aylward B. Rhegmatogenous retinal detachment: A reappraisal of its pathophysiology and treatment. *Ophthalmic Res.* 2014;51(1):15-31.

6. Marmor M. Mechanisms of normal retinal adhesion. *In Retina Stephen J. Ryan, Chapter 19.* 2013;1:447-464.

7. Fatt I, Shantinath K. Flow conductivity of retina and its role in retinal adhesion. *Exp Eye Res.* 1971;12(2):218-226.

8. Chihara E, Nao-i N. Resorption of subretinal fluid by transepithelial flow of the retinal pigment epithelium. *Graefes Arch Clin Exp Ophthalmol.* 1985;223(4):202-204.

9. Hollyfield JG, Varner HH, Rayborn ME, Osterfeld AM. Retinal attachment to the pigment epithelium. linkage through an extracellular sheath surrounding cone photoreceptors. *Retina.* 1989;9(1):59-68.

10. Hageman GS, Marmor MF, Yao XY, Johnson LV. The interphotoreceptor matrix mediates primate retinal adhesion. *Arch Ophthalmol.* 1995;113(5):655-660.

11. Le Goff MM, Bishop PN. Adult vitreous structure and postnatal changes. *Eye (Lond).* 2008;22(10):1214-1222.

12. Kirchhof B, Oh KT, Hartnett ME. Pathogenetic mechanisms of retinal detachment. *RETINA, Ryan S.J., Fifth edition.* 2013:1616.

13. Machemer R. The importance of fluid absorption, traction, intraocular currents, and chorioretinal scars in the therapy of rhegmatogenous retinal detachments. XLI edward jackson memorial lecture. *Am J Ophthalmol.* 1984;98(6):681-693.

14. Wangsa-Wirawan ND, Linsenmeier RA. Retinal oxygen: Fundamental and clinical aspects. *Arch Ophthalmol.* 2003;121(4):547-557.

15. Hisatomi T, Sakamoto T, Goto Y, et al. Critical role of photoreceptor apoptosis in functional damage after retinal detachment. *Curr Eye Res.* 2002;24(3):161-172.

16. Salicone A, Smiddy WE, Venkatraman A, Feuer W. Visual recovery after scleral buckling procedure for retinal detachment. *Ophthalmology.* 2006;113(10):1734-1742.

17. Zhou C, Lin Q, Chen F. Prevalence and predictors of metamorphopsia after successful rhegmatogenous retinal detachment surgery: A cross-sectional, comparative study. *Br J Ophthalmol.* 2016.

18. Rezar S, Sacu S, Blum R, Eibenberger K, Schmidt-Erfurth U, Georgopoulos M. Macula-on versus macula-off pseudophakic rhegmatogenous retinal detachment following primary 23-gauge vitrectomy plus endotamponade. *Curr Eye Res.* 2016;41(4):543-550.

19. Kaufman PL. Prognosis of primary rhegmatogenous retinal detachments. 2. accounting for and predicting final visual acuity in surgically reattached cases. *Acta Ophthalmol (Copenh).* 1976;54(1):61-74.

20. Yoon YH, Marmor MF. Rapid enhancement of retinal adhesion by laser photocoagulation. *Ophthalmology.* 1988;95(10):1385-1388.

21. Hassan TS, Sarrafizadeh R, Ruby AJ, Garretson BR, Kuczynski B, Williams GA. The effect of duration of macular detachment on results after the scleral buckle repair of primary, macula-off retinal detachments. *Ophthalmology.* 2002;109(1):146-152.

22. Diederen RM, La Heij EC, Kessels AG, Goezinne F, Liem AT, Hendrikse F. Scleral buckling surgery after macula-off retinal detachment: Worse visual outcome after more than 6 days. *Ophthalmology.* 2007;114(4):705-709.

23. van Bussel EM, van der Valk R, Bijlsma WR, La Heij EC. Impact of duration of macula-off retinal detachment on visual outcome: A systematic review and meta-analysis of literature. *Retina.* 2014;34(10):1917-1925.

24. Hajari JN, Kyhnel A, Bech-Azeddine J, la Cour M, Kiilgaard JF. Progression of foveola-on rhegmatogenous retinal detachment. *Br J Ophthalmol.* 2014;98(11):1534-1538.

25. Ho SF, Fitt A, Frimpong-Ansah K, Benson MT. The management of primary rhegmatogenous retinal detachment not involving the fovea. *Eye (Lond).* 2006;20(9):1049-1053.

26. Wykoff CC, Smiddy WE, Mathen T, Schwartz SG, Flynn HW,Jr, Shi W. Fovea-sparing retinal detachments: Time to surgery and visual outcomes. *Am J Ophthalmol.* 2010;150(2):205-210.e2.

27. Ehrlich R, Niederer RL, Ahmad N, Polkinghorne P. Timing of acute macula-on rhegmatogenous retinal detachment repair. *Retina.* 2013;33(1):105-110.

28. Algvere P, Rosengren B. Immobilization of the eye. evaluation of a new method in retinal detachment surgery. *Acta Ophthalmol (Copenh).* 1977;55(2):303-316.

29. Algvere P, Rosengren B. Active immobilization of the eye in the treatment of retinal detachment. *Mod Probl Ophthalmol.* 1977;18:286-291.

30. Lean JS, Mahmood M, Manna R, Chignell AH. Effect of preoperative posture and binocular occlusion on retinal detachment. *Br J Ophthalmol.* 1980;64(2):94-97.

31. Lincoff H, Stopa M, Kreissig I. Ambulatory binocular occlusion. *Retina.* 2004;24(2):246-253.

32. Lincoff H, Kreissig I, Uram D. Minor surgery for the repair of retinal detachment emanating from retinoschisis. *Acta Ophthalmol.* 2009;87(3):281-284.

33. Chen CY, Chen SN, Lin SM, Ho CL. Reduction of subretinal fluid after preoperative immobilization of the eyes with rhegmatogenous retinal detachment. *Chang Gung Med J.* 2001;24(12):799-804.

34. Gunnlaugsdottir E, Arnarsson A, Jonasson F. Prevalence and causes of visual impairment and blindness in icelanders aged 50 years and older: The reykjavik eye study. *Acta Ophthalmol.* 2008;86(7):778-785.

35. Congdon N, O'Colmain B, Klaver CC, et al. Causes and prevalence of visual impairment among adults in the united states. *Arch Ophthalmol.* 2004;122(4):477-485.

36. Scupola A, Coscas G, Soubrane G, Balestrazzi E. Natural history of macular subretinal hemorrhage in age-related macular degeneration. *Ophthalmologica.* 1999;213(2):97-102.

37. Hochman MA, Seery CM, Zarbin MA. Pathophysiology and management of subretinal hemorrhage. *Surv Ophthalmol.* 1997;42(3):195-213.

38. Yannuzzi LA, Freund KB, Takahashi BS. Review of retinal angiomatous proliferation or type 3 neovascularization. *Retina.* 2008;28(3):375-384.

39. Massacesi AL, Sacchi L, Bergamini F, Bottoni F. The prevalence of retinal angiomatous proliferation in age-related macular degeneration with occult choroidal neovascularization. *Graefes Arch Clin Exp Ophthalmol.* 2008;246(1):89-92.

40. Slakter JS, Yannuzzi LA, Schneider U, et al. Retinal choroidal anastomoses and occult choroidal neovascularization in age-related macular degeneration. *Ophthalmology.* 2000;107(4):742-53; discussion 753-4.

41. Viola F, Massacesi A, Orzalesi N, Ratiglia R, Staurenghi G. Retinal angiomatous proliferation: Natural history and progression of visual loss. *Retina.* 2009;29(6):732-739.

42. Tsai ASH, Cheung N, Gan ATL, et al. Retinal angiomatous proliferation. *Surv Ophthalmol.* 2017;62(4):462-492.

43. Machemer R, Steinhorst UH. Retinal separation, retinotomy, and macular relocation: II. A surgical approach for age-

related macular degeneration? *Graefes Arch Clin Exp Ophthalmol*. 1993;231(11):635-641.

44. van Meurs JC, Van Den Biesen PR. Autologous retinal pigment epithelium and choroid translocation in patients with exudative age-related macular degeneration: Short-term follow-up. *Am J Ophthalmol*. 2003;136(4):688-695.

45. van Zeeburg EJ, Maaijwee KJ, Missotten TO, Heimann H, van Meurs JC. A free retinal pigment epithelium-choroid graft in patients with exudative age-related macular degeneration: Results up to 7 years. *Am J Ophthalmol*. 2012;153(1):120-7.e2.

46. Heriot WJ. Intravitreal gas and tPA: An outpatient procedure for subretinal haemorrhage. proceedings of vail vitrectomy meeting. *Vail: American Society of Retina Specialists*. 1996.

47. van Zeeburg EJ, van Meurs JC. Literature review of recombinant tissue plasminogen activator used for recent-onset submacular hemorrhage displacement in age-related macular degeneration. *Ophthalmologica*. 2013;229(1):1-14.

48. Huang D, Swanson EA, Lin CP, et al. Optical coherence tomography. *Science*. 1991;254(5035):1178-1181.

49. de Boer JF, Cense B, Park BH, Pierce MC, Tearney GJ, Bouma BE. Improved signal-to-noise ratio in spectral-domain compared with time-domain optical coherence tomography. *Opt Lett*. 2003;28(21):2067-2069.

50. Leitgeb R, Hitzenberger C, Fercher A. Performance of fourier domain vs. time domain optical coherence tomography. *Opt Express*. 2003;11(8):889-894.

51. Yun SH, Tearney G, de Boer J, Bouma B. Pulsed-source and swept-source spectral-domain optical coherence tomography with reduced motion artifacts. *Opt Express*. 2004;12(23):5614-5624.

52. Potsaid B, Baumann B, Huang D, et al. Ultrahigh speed 1050nm swept source/fourier domain OCT retinal and anterior segment imaging at 100,000 to 400,000 axial scans per second. *Opt Express*. 2010;18(19):20029-20048.

53. Hagag AM, Gao SS, Jia Y, Huang D. Optical coherence tomography angiography: Technical principles and clinical applications in ophthalmology. *Taiwan J Ophthalmol*. 2017;7(3):115-129.

54. Leitgeb RA, Werkmeister RM, Blatter C, Schmetterer L. Doppler optical coherence tomography. *Prog Retin Eye Res*. 2014;41:26-43.

55. Braaf B, Vermeer KA, Sicam VA, van Zeeburg E, van Meurs JC, de Boer JF. Phase-stabilized optical frequency domain imaging at 1-micron for the measurement of blood flow in the human choroid. *Opt Express*. 2011;19(21):20886-20903.

56. Braaf B, Vermeer KA, Vienola KV, de Boer JF. Angiography of the retina and the choroid with phase-resolved OCT using interval-optimized backstitched B-scans. *Opt Express*. 2012;20(18):20516-20534.

57. Novosel J, Vermeer KA, de Jong JH, Ziyuan W, van Vliet LJ. Joint segmentation of retinal layers and focal lesions in 3-D OCT data of topologically disrupted retinas. *IEEE Trans Med Imaging*. 2017;36(6):1276-1286.

Part I

Macula-on retinal detachment

Chapter

2

Preoperative posturing of patients with macula-on retinal detachment reduces progression toward the fovea

Jan Hendrik de Jong
Juan Pedro Vigueras-Guillén
Tiarah C. Simon
Reinier Timman
Tunde Peto
Koenraad A. Vermeer
Jan C. van Meurs

ABSTRACT

Purpose: Traditionally, preoperative posturing consisting of bed rest and positioning is prescribed to patients with macula-on retinal detachment (RD) to prevent RD progression and detachment of the fovea. Execution of such advice can be cumbersome and expensive. This study aims to investigate if preoperative posturing affects the progression of RD.

Design: Prospective cohort study

Participants: Ninety-eight patients with macula-on RD were included. Inclusion criteria were: volume optical coherence tomography (OCT) scans could be obtained with sufficient quality, and the smallest distance from the fovea to the detachment border was 1.25 mm or more.

Methods: Patients were admitted to the ward for bed rest in anticipation of their surgery and were positioned on the side where the RD was mainly located. At baseline and before and after each interruption for meals or toilet visits, a 37°x45° OCT volume scan was performed using a wide angle Spectralis OCT (Heidelberg Engineering, Germany). The distance between the nearest point of the RD border and fovea was measured using a custom-built measuring tool.

Outcome measures: The RD border displacement and the average RD border displacement velocity moving toward (negative) or away (positive) from the fovea were determined for intervals of posturing and interruptions.

Results: The median duration of intervals of posturing was 3.0 hours (interquartile range (IQR): 1.8 – 14.0 hours; N=202) and of interruptions 0.37 hours (IQR: 0.26 – 0.50; N=197). The median RD border displacement was 2 μm (IQR: -65 to +251 μm) during posturing and -61 μm (IQR: -140 to 0 μm) during interruptions, which was statistically significantly different (Mann Whitney U-test, p<0.001). The median RD border displacement velocity was +1 μm/hour (IQR: -21 to +49) during posturing and -149 μm/hour (IQR: -406 to +1) during interruptions, a statistically significant difference (p<0.001).

Conclusions: By making use of usual interruptions of preoperative posturing we were able to show, in a prospective and ethically acceptable manner, that RD stabilizes during posturing and progresses during interruptions in patients with macula-on RD. Preoperative posturing is effective in reducing progression of RD.

INTRODUCTION

Retinal detachment (RD) is a progressive and, if left untreated, blinding disease. The annual incidence of primary rhegmatogenous RD was reported to be 18 per 100.000 people in The Netherlands[1] and 12 per 100.000 people in the United States.[2] Surgery is successful in reattaching the retina in more than 95% of patients.[3,4] The visual prognosis after successful RD surgery is determined primarily by the extent of the RD. When the macula is not yet involved, the visual outcome is significantly better.[5-8] Therefore, between diagnosis and surgical treatment, all efforts are aimed at keeping the macula attached.

Traditionally, preoperative posturing consisting of bed rest and positioning is prescribed to patients with macula-on RD. Bed rest aims to restrict forces related to head and eye movement that are believed to reduce the height and extent of RD.[9-15] Bed rest also allows positioning of patients to address the potentially unfavorable effect of the force of gravity. A supine position is advised for RD in the superior quadrants and a sitting position for RD in the inferior quadrants.[16-18]

Despite the major burden of posturing for patients and, when combined with hospital admission, on nursing staff, ward facilities and public health costs, little prospectively collected evidence for preoperative posturing has been presented as yet. We believe that the want of a sufficiently accurate measuring method for progression of RD toward the fovea is the reason for this lack of evidence. With optical coherence tomography (OCT), such a measuring tool has become available that allows accurate and precise measurements of changes in the distance between the edge of the RD and the fovea.[18]

Because it is generally accepted that RD patients interrupt their bed rest regimen for meals and other short breaks,[18] such intervals offer an excellent opportunity to acquire prospective and comparative data. The aim of this study was to investigate in an ethically acceptable manner whether preoperative posturing affects the progression of macula-on RD. Secondary objectives were to identify risk factors for progressive RD and to determine the reproducibility of the OCT measurements.

PATIENTS & METHODS

Study design

This study was designed as a prospective cohort study with OCT recordings of the distance between the RD and fovea during preoperative posturing and interruptions of posturing. The study was approved by the local internal review board of the Rotterdam Eye Hospital and the medical ethical committee of the Erasmus Medical Center, Rotterdam, The Netherlands (identifier, 2014-502; www.trialregister.nl identifier, NTR4884). This report concerns the outcome of the first of 3 planned cohorts of a larger prospective trial and includes patients with detachments observed up to 48 hours. The first cohort is the baseline cohort. The interruption intervals will be prolonged in the second and third cohort compared with the baseline interval, and we plan to include 50 patients. During the inclusion period of the 50 patients in the baseline cohort, we additionally included 48 patients with RD in the other retinal quadrants following the same eligibility criteria to explore the differences between RD locations and posturing advices. All patients were hospitalized and examined in the Rotterdam Eye Hospital, The Netherlands. The study was conducted in accordance with the tenets of the Declaration of Helsinki.

Inclusion and exclusion criteria

Inclusion criteria were: age 18 years or older, written informed consent, nearest point of the RD border at 1250 μm or more from the foveola (safety measure) and within the range of the OCT system, sufficiently clear media to obtain an OCT scan, sufficiently accurate OCT scan, and ability to perform OCT within 1 hour after admission of the patient to the ward. No exclusion criteria were specified. The safety border of 1250 mm from the foveola was defined by the traditional size of the fovea centralis (with a radius of approximately 750 mm) and parafovea (ring of 500 mm around the fovea) combined.[19]

Surgery planning and posturing advice

Patients diagnosed with macula-on RD were admitted to the ward for posturing while they were waiting for surgery the same day, the next day or occasionally the day after. Surgery was planned as soon as possible, but no later than 48 hours from the start of hospitalization. Patients were admitted to the ward and planned for surgery independently from study eligibility. If patients were included in the study and progressed more than 250 μm, the OCT measurements continued, but surgery was rescheduled to an earlier time point if possible. We hypothesized that the risk of foveal involvement does not increase substantially with RD progression of less than 250 μm Posturing consisted of 2 parts: bed rest and positioning. All patients were prescribed bed rest. Patients with RD mainly located in the superior quadrant

were positioned supine, patients with RD in the temporal quadrant were positioned on the temporal side of the affected eye, patients with RD in the nasal quadrant were positioned on the nasal side and patients with RD in the inferior quadrant were instructed to sit upright. Patients were allowed to interrupt their posturing for meals, toilet visits, refreshment in the morning and surgeon's examinations. Patients advised to sit upright interrupted their posturing by lying flat on the back for 20 minutes.

OCT progression measurements

Within 1 hour after arrival on the ward a baseline volume OCT scan was performed and eligibility was determined. The volume scan was obtained with a Heidelberg Spectralis OCT system (Heidelberg Engineering, Heidelberg, Germany) using a wide field lens (50°). The field of view of the volume scan was 37°x45°, the transverse resolution was 21 μm/pixel, 16 B-scans were averaged per retinal location and the spacing of B-scans was 125 μm. If the scanning time was estimated to exceed 1 minute (because of unstable fixation or peripheral RD location), the number of B-scans per volume scan was decreased, but resolution and spacing were kept the same. OCT measurements were performed at the beginning and the end of each interruption as often as logistically possible. Patients were transported from their bed to the OCT using a wheelchair (10 to 50 m distance). If fewer than 3 OCT measurements could be obtained, the patient was withdrawn from the study and the data were excluded from the analysis.

The initial distance measurements between fovea and the RD border were performed with the Heidelberg Spectralis OCT built-in measurement tool. After all OCT scans were obtained, a selection of 21 B-scans was made around the location of the estimated nearest point of the RD for a more accurate and reproducible distance measurement. The order of the scans was randomized per patient to blind the primary grader (J.H.d.J.) during the interpretation of the OCT scans. The location of the border of subretinal fluid was annotated in all B-scans using the annotation program ITK-SNAP (available at www.itksnap.org) (**Figure 1**).[19] The location of the fovea was identified in a separate volume scan with a transverse resolution of 21 μm/pixel and a 32 μm spacing of B-scans.

To calculate the shortest distance between fovea and RD border, the scanning laser ophthalmoscopy (SLO)-images corresponding to the OCT volume scans were registered using a custom built registration tool. To align the SLO-images, the primary grader annotated several points in each SLO image corresponding to common vessel crossings (**Figure 1**). Affine geometric transformation was applied involving translation, rotation, scale, and shear of the image to project all the annotations onto a single SLO-image. Finally, by using simple geometric calculations, the shortest distances could be computed.

The distance measurements then were used to calculate the change in distance and the average RD border displacement velocity (change in distance per hour) during posturing and interruption intervals. The change in distance and average progression velocity from baseline at each time point was determined as well.
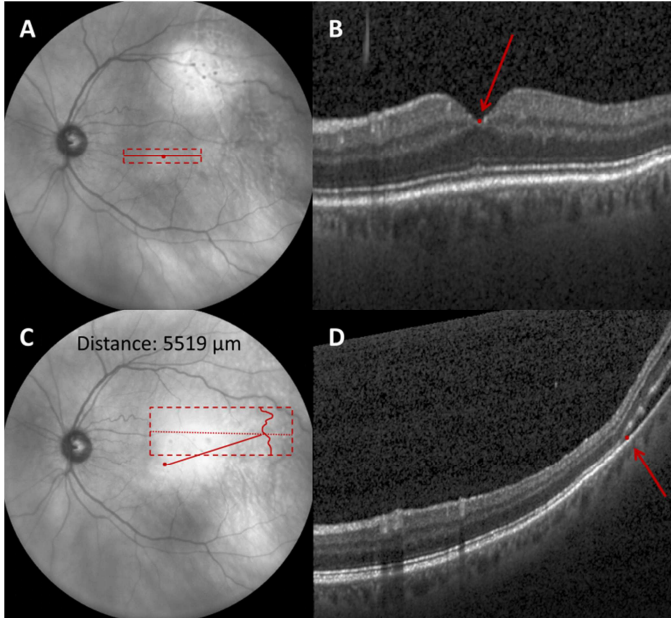
Figure 1. Measurement of the change in distance between fovea (**A, B**) and retinal detachment (RD) border (**C, D**). A small volume scan was performed to image the fovea (red dashed rectangle in panel **A**) and the central point of the fovea was identified (red dot, panel **B**). A second volume scan was aimed at the RD border around the estimated nearest point to the fovea (red dashed rectangle in panel **C**). The point of subretinal fluid closest to the attached part of the retina was annotated in all B-scans (see panel **D**). A custom-built software tool was used to merge the scanning laser ophthalmoscopy images of (**A**) the foveal volume scan and (C) the RD volume scan. The shortest distance between RD-border and fovea was then calculated to be 5519 μm.

The worst change from baseline was defined as the shortest distance measured in any of the OCT scans during follow-up. We calculated the average RD border displacement velocity to correct for the differences in interval duration and to enable a more valid comparison between posturing and interruptions.

Progression during interruptions was subdivided into progression of newly detached retina and previously detached retina (i.e. after reattachment). If the progression was partially of previously detached retina and partially of newly detached retina, the interval was assigned to the predominant type.

To compare for difference between RD locations, we divided the patients into a superior RD group with supine positioning, a temporal RD group with temporal

side positioning, a nasal RD group with nasal side positioning, and an inferior RD group with sitting upright positioning.

Secondary outcome measures
The following secondary outcome measures were recorded: age, gender, duration of visual field loss (days), duration of follow-up (hours), spherical equivalent refraction (diopters), baseline distance between RD border and fovea (micrometers), size of retinal breaks (clock hours), RD location (deviation from superior of the nearest point on the RD border at baseline, in degrees), extent of RD (degrees), angle between retina and retinal pigment epithelium (RPE) at the RD edge (degrees). Patients were interviewed to determine the existence and duration of visual field loss using identical questions for all patients. If patients did not report visual field loss, they were excluded from the analysis. The duration of follow-up was calculated between admission and the time point of the worst change from baseline and the last OCT. The size of retinal breaks was estimated by the operating surgeon. The baseline OCT and SLO were used to determine the extent of RD and the angle of the actual direction of the closest point on the RD border as well as the change of this direction over time. The angle between the retina and RPE was measured with ImageJ software (https:// imagej.nih.gov/ij/).

Reproducibility analysis
To evaluate the intrarater variability of the RD–fovea distance measurements, 25 patients were selected randomly from the total of 98 patients. A total of 125 volume scans belonging to these 25 patients were annotated 3 times by the primary grader (J.H.d.J.). The order of scans was rerandomized among the 3 datasets to make them unidentifiable and the annotation was repeated at a different time point. This was performed to estimate the intrarater variability caused by the interpretation of the primary grader. Additionally, the baseline volume OCT scan of 6 patients judged to be representative of the entire population were repeated 4 times. This was carried out within the shortest possible timeframe and the distance between fovea and RD border was measured. In between the repeated measurements the patient removed his head from the chinrest to include the variation caused by the repeated acquisition of an OCT scan in our estimate of the intrarater variability.

   To evaluate the interrater variability of the distance measurements, the same dataset used to evaluate the intrarater variability with a total of 125 volume scans was annotated by 5 graders of the Moorfields Reading Centre, London, United Kingdom. All graders were instructed to annotate the point of subretinal fluid closest to the attached part of the retina in all B-scans using ITK-SNAP[20] and were trained with 3 example volume scans before they started with the dataset of 125 volume scans. The order of the scans was randomized per patient to blind the

graders during interpretation of the OCT scans. The interrater variability of the change in distance of 100 intervals then was evaluated.

Statistical analysis

Linear mixed modeling was used to describe the intra- and interrater variability. The patient, image and grader effects were included as random effects. An univariate F-test and a pairwise comparison with Bonferroni correction were performed to test for differences between the graders. The intraclass correlation coefficient (ICC), and the 95% limits of agreement were determined as well (±1.96 * standard deviation, SD).

Because of the apparent skewed distribution of RD–fovea distance and velocity measurements, nonparametric testing (Mann–Whitney U test) was used to compare between posturing and interruptions intervals. Mann–Whitney U test was also performed to compare between progression of newly detached retina and previously detached retina, posturing at night and posturing during the day and between patients with a follow-up duration of 16 hours or less and more than 16 hours to relate our study outcome to the findings of Hajari *et al*.[18] The Kruskall–Wallis test and pairwise comparison of the Mann–Whitney U test with Bonferroni correction were used to test for differences between the RD location groups (superior, temporal, nasal and inferior RD).

Spearman's rho was used to test for correlations between the worst progression from baseline and the following supposed risk factors: duration of visual field loss, duration of follow-up, spherical equivalent refraction, baseline distance between RD border and fovea, size of retinal breaks, RD location, extent of RD, angle between retina and RPE. Statistical analyses were performed with SPSS version 21 (IBM Corporation, Armonk, NY).. Two-sided p-values below 0.05 were considered significant.

RESULTS

Patients

Between February 24, 2015 and January 26, 2016 391 macula-on RD patients were hospitalized before surgery in the Rotterdam Eye Hospital, 181 of whom were screened for eligibility. Of this screening pool, 71 patients were not eligible for this study. In 36, the distance between the fovea and RD was smaller than 1250 μm; in 16 patients, the border of the RD could not be determined because of a peripheral RD location beyond the limits of the OCT system, a bullous RD overhanging the RD border, or poor OCT quality; in 7 patients, even a narrowed volume scan protocol took more than 2 minutes because of poor fixation of the patient or a peripheral RD location; 11 patients declined to participate; 1 patient was demonstrated suspected methicillin-resistant *Staphylococcus aureus* and remained in a quarantine room. Of 110 included patients, 12 patients were sent to the operation room before 3 OCT measurements could be conducted and were withdrawn from this study and further analysis. In the remaining 98 included patients a total of 497 OCT scans were obtained (range 3-13 OCT scans per patient), and these are presented in this report. All patients with 2 or more OCT scans provided written informed consent.

Patient characteristics are summarized in **Table 1**. Of 98 patients, 24 were instructed to lie supine, 42 were instructed to lie on the temporal side, 22 were instructed to lie on the nasal side and 10 were instructed to sit upright. With the 497 OCT scans, 399 intervals were recorded comprising 202 posturing intervals and 197 interruptions. A description of the duration of hospitalization and measured intervals is given in **Table 2**. The course of RD progression differed extensively between patients as presented in **Figure 2**. The median change in direction from the fovea to the nearest point of the RD border was 4 degrees (interquartile range: 2–7; range 0–69) during follow-up.

Reproducibility

The intrarater variability (caused by the interpretation of the primary grader) was 23 μm (standard deviation (SD)) and the 95% limits of agreement of the intrarater variability were ±45 μm. The intrarater variability caused by both the interpretation of the primary grader and the OCT acquisition was 29 μm (SD), and the 95% limits of agreement of the intrarater variability were 58 μm. The ICC for repeated measurements was 0.999 (ICC type 3,1; 95% confidence interval (CI): 0.998 – 1.000).

Table 1. Patient characteristics

Characteristic	Data
No. of patients included the study	98
Age (years)	
Mean±SD	59±8
Gender (male:female; no.)	66:32
Phakic:pseudophakic (no.)	65:33
Snellen visual acuity	
Mean	20/25
Range	20/400 – 20/17
Refraction spherical equivalent (diopters)*	
Median (IQR)	-3.00 (-4.50 to 0.00)
Range	-10.00 to +5.75
Mean ± SD	-3.20±3.78
Moderate myopia (<6.0 and ≥3.0) (no.)	28
High myopia (≥6.0D) (no.)	23
Duration of visual field loss (days)	
Median (IQR)	4 (2-8)
Range	0.5 – 120
Mean ± SD	8±16
No complaints of visual field loss (no.)	24
Primary/recurrent RD (no.)	92/6
History of vitrectomy (no.)	3
History of scleral buckling (no.)	3
Posterior vitreous detachment (yes/no)	98/0
Extent of RD (°)	
Median (IQR)	105 (90 – 135)
Range	45 – 300
Mean ± SD	114±45
Size of retinal tear (no.)	
Single small (≤0.50 clock hours)	27
Multiple/large (>0.50 clock hours)	63
No breaks found	8
Angle between retina and RPE (°)	
Median (IQR)	8 (4 – 13)
Range	1 – 40
Mean ± SD	10±8
Posturing advice (N)	
Supine	24
Temporal side	42
Nasal side	22
Sitting upright	10

IQR = interquartile range, SD = standard deviation, RD = retinal detachment, RPE= retinal pigment epithelium
* In patients with pseudophakic lens status, the spherical equivalent refraction before cataract surgery was used.

Table 2. Hospitalization and timing of OCT's

Characteristic	Data
Time between baseline OCT and surgery (hours)	
Median (IQR)	21.5 (18.5–23.8)
Range	1.2–48.0
Mean±SD	20.9±10.0
Time between baseline OCT and last OCT (hours)	
Median (IQR)	16.5 (3.9–20.2)
Range	0.8–39.9
Mean±SD	14.8±9.5
Number of posturing intervals	202
Duration of posturing intervals (hours)	
Median (IQR)	3.0 (1.8–14.0)
Range	0.3–23.1
Mean±SD	6.8±6.1
Number of interruptions	197
Duration of interruptions (hours)	
Median (IQR)	0.37 (0.26–0.50)
Range	0.15–1.91
Mean±SD	0.42±0.24

IQR = inter quartile range; SD = standard deviation

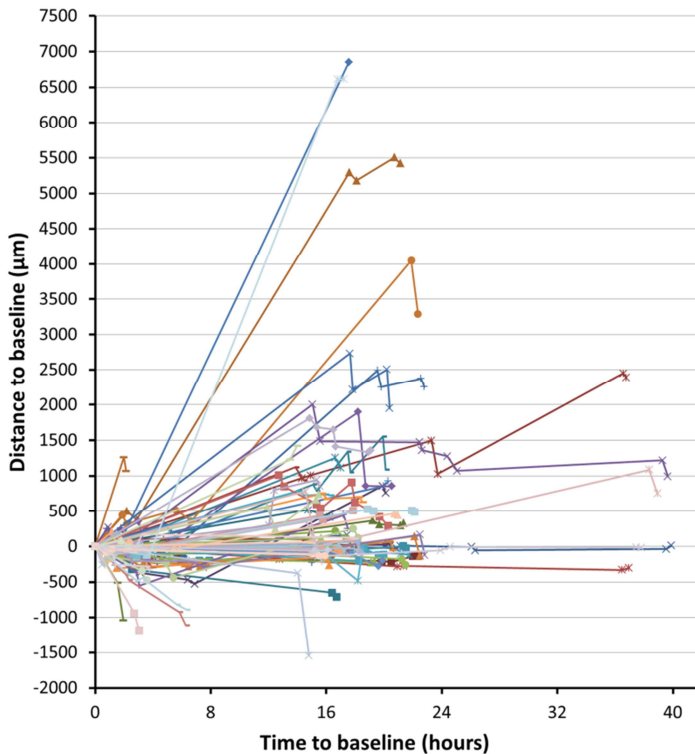**Figure 2**.
Graph showing the course of the change in distance between the retinal detachment border and fovea compared with baseline during the study follow-up period. Individual patients are represented by different colors. The markers on the lines represent the time points on which the OCT measurements were performed. The change in distance from baseline differed extensively between patients.

The interrater variability of distances was 47 µm (SD) and the residual variation in the model was 80 µm (SD). The 95% limits of agreement of the combined grader and residual effects were ±182 µm. The interrater ICC for distances was 1.000 (ICC type 3,k; CI: 1.000–1.000). The mean ± SD difference per grader with the mean of the 6 grader measurements was -25±69 µm for grader 1; -9±49 µm for grader 2; +97±115 µm for grader 3; -23±80 µm for grader 4; -22±47 µm for grader 5 and -17±53 µm for grader 6 (a positive difference indicates a systematically larger distance to the fovea). A univariate F-test showed a significant difference among the graders (P<0.001). Pairwise comparison showed that the annotations of grader 3 were statistically significantly different from those of the other graders (P<0.001).

Figure 3 shows 3 examples are shown of the three patients with the poorest agreement between grader 3 and the other graders. The presence of a low-reflective photoreceptor outer segment layer hanging under the detached and highly reflective ellipsoid zone seems to be the reason for the different interpretation of grader 3 (**Figure 3 A–C**). The arbitrary discrimination between photoreceptor outer segments and subretinal fluid is also demonstrated by the different interpretation of grader 1 in **Figure 3 B**.
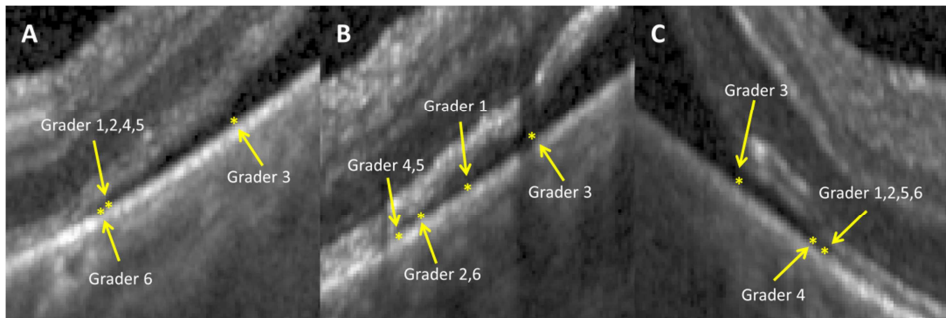
Figure 3. Examples of OCT images for which poor agreement on the border of subretinal fluid was found between grader 3 and the other graders. The annotation of the different graders is indicated with yellow asterisks. The graders were instructed to annotate the point of subretinal fluid closest to the attached part of the retina. The presence of a low-reflective photoreceptor outer segment layer hanging under the detached and highly reflective ellipsoid zone seems to be the reason for the different interpretation of grader 3 (**A, B, C**), but also for the different interpretation of grader 1 in (**B**).

The interrater variability of change in distance per interval was redundant and set to 0 by the model, but the residual variability was of 89 μm (SD) and the 95% limits of agreement of the interrater variability were ±175 μm. The interrater ICC for change per interval was 0.996 (ICC type 3,k; CI: 0.995-0.997). The mean ± SD difference per grader with the mean of the 6 grader measurements was 5±79 μm for grader 1, -5±64 μm for grader 2, 4±130 μm for grader 3, 4±74 μm for grader 4, -1±69 μm for grader 5, and -6±52 μm for grader 6. Although the mean differences between the graders were much smaller for change for intervals than for distances, the SDs are in the same order of magnitude.

Given the small mean difference of -6 μm and smallest standard deviation of 52 μm, the interpretation of the primary grader (J.H.d.J., grader 6) provided accurate and precise results for the change per interval. The 95% limits of agreement between the measurements of grader 6 and the average of all graders were ±102 μm. The interpretation of the primary grader was also used for the other 73 patients presented in this study, of which the order of scans per patient was randomized as well.

Example patient
An example of the change in distance between RD border and fovea of a patient with a superior temporal RD is shown in **Figure 4**. This patient regressed during nighttime posturing and progressed during interruptions. The last OCT 39.6 hours from admission revealed regression of 992 μm from baseline (see the first and the last measurement point in **Figure 4**). On the right, 3 example OCT scans are displayed, indicated by the red 1, 2 and 3 in the graph. During the posturing interval between OCT 1 and 2, 2085 μm of regression was found, and during the interruption between OCT 2 and 3, 519 μm of progression was found.

Comparison of posturing and interruptions
To elucidate whether preoperative posturing influences RD progression we compared displacement of the RD border during posturing intervals and interruptions. The median RD border displacement during posturing was 2 μm (interquartile range (IQR), -65 to +251 μm; n = 202) and the mean ± SD displacement was +265±919 μm. The median RD border displacement during interruptions was -61 μm (IQR, -140 to 0 μm; n = 197) and the mean ± SD displacement was -94±193 μm. The difference between posturing and interruptions was statistically significant (P<0.001; **Figure 5**). As reported in **Table 2**, the interval during interruptions was much shorter than during posturing intervals. The median interval during posturing was 3.0 hours (IQR, 1.8–14.0 hours) and that during interruptions was 22 (IQR, 15–30) minutes.
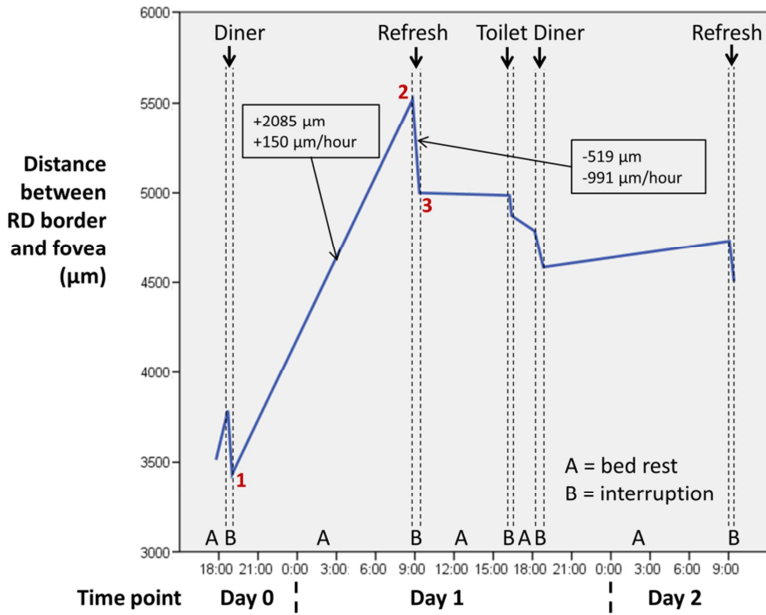
Figure 4. Example of the change in distance between retinal detachment (RD) border and fovea during the hospitalization of a patient with superior temporal RD in the left eye. On the graph on the top, the full course of hospitalization is shown and the reason for interrupting posturing is indicated. On the right, 3 example OCT scans are displayed, indicated by red numerals 1, 2 and 3 in the graph. The red dashed rectangle indicates the location and size of the volume scan, and the red line indicates the location of the B-scan. The fovea is indicated with a red dot, the RD border is indicated with a blue line, and the blue dashed line indicates the shortest distance to the fovea. The baseline OCT measurement provided a distance of 3434 µm (see OCT 1). During the posturing intervals in the night, the RD regressed (see OCT 2), and during interruptions, the RD progressed (see OCT 3). Between OCT 1 and 2, a regression of 2085 µm was found (+150 µm/hour) and between OCT 2 and 3, a progression of 519 µm was found (-991 µm/hour).
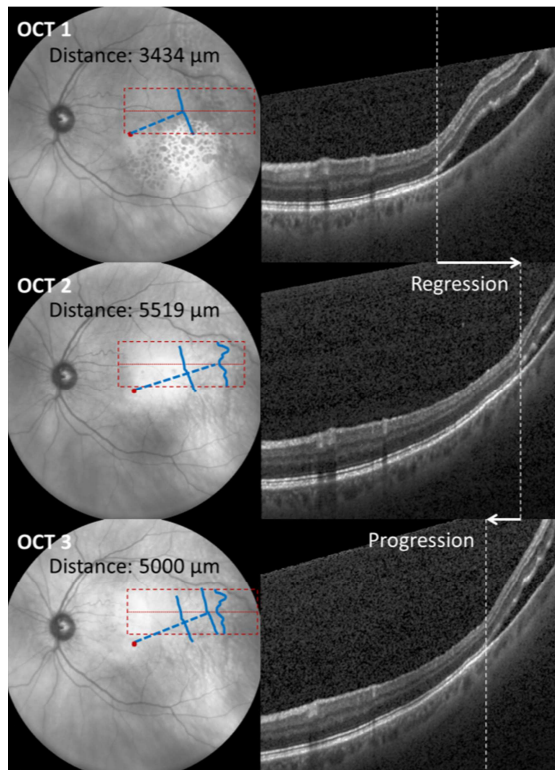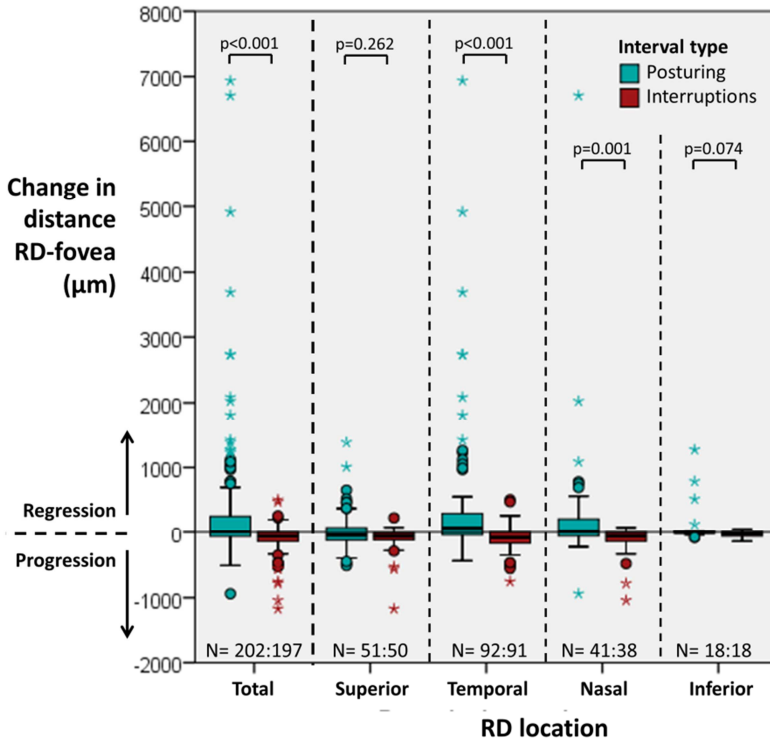
Figure 5. Retinal detachment (RD) border displacement (in μm) showing progression (negative change) or regression (positive change). The change during posturing and interruptions is shown for all patients (total) and is subdivided according to RD location and positioning advice. The difference between posturing and interruptions were statistically significantly different for the temporal and nasal RD group, but not for the superior or inferior RD group (see P-values in figure, Mann–Whitney U test). N = a:b indicates the number of intervals of posturing (a) and interruptions (b).

The median RD border displacement velocity during posturing was +1 (IQR, -21 to +49) μm/hour and the mean +19±122 μm/hour. The median RD border displacement velocity during interruptions was -149 (IQR, -406 to +1) μm/hour and the mean ± SD velocity was -259±535 μm/hour. The difference between posturing and interruptions was statistically significant (P<0.001; **Figure 6**).

We further compared posturing intervals during the day and during the night. The median RD border displacement velocity during daytime posturing intervals was -4 μm/hour (IQR, -51 to +47 μm/hour; N=128) and at night was +13 μm/hour (IQR, -1 to +59 μm/hour; N=74) and these differed statistically significantly from each other (P<0.001). The median duration of posturing intervals during the day was 2.1 hours and during the night was 14.5 hours.

We also compared progression during interruptions in previously detached retina (i.e. after reattachment) and in newly detached retina. The median progression velocity during interruptions in an area of previously detached retina was -312 μm/hour (IQR, -633 to -162 μm/hour; n = 86) and in an area of newly detached retina was -160 μm/hour (IQR, -358 to -78 μm/hour; n = 62). The RD progression during interruptions in previously detached retina was significantly faster (P<0.001) than RD progression of newly detached retina.

We further analyzed the effect of posturing on RD progression in different groups of patients based on the RD location and positioning advice. We found statistically significant differences for the change in distance toward the fovea between posturing and interruptions for the temporal and nasal RD group (P<0.001; **Figure 5**), but not for the superior and inferior RD group. The difference in RD border displacement velocity between posturing and interruptions was significantly different for all RD location groups (**Figure 6**).
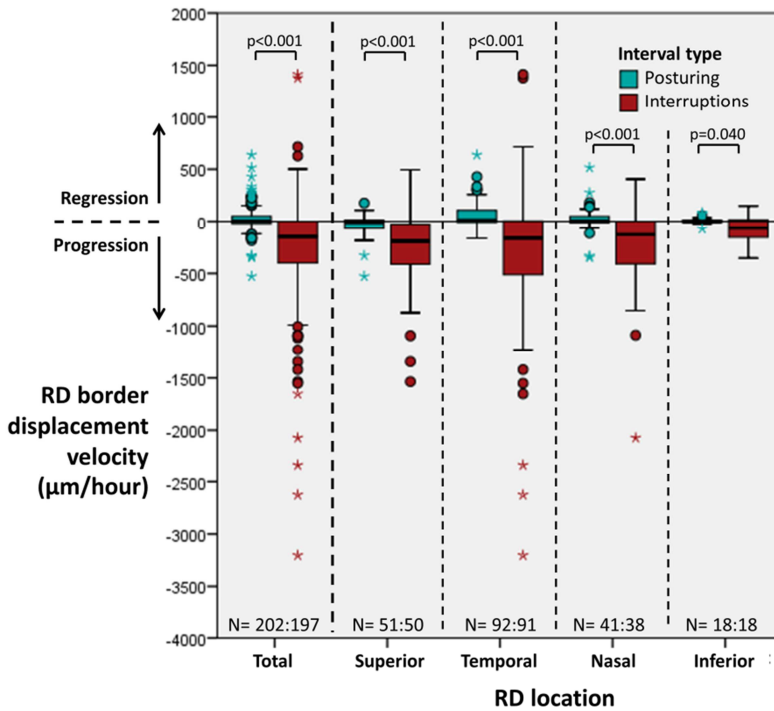
Figure 6. Retinal detachment (RD) border displacement velocity (in μm/hour) showing progression (negative velocity) or regression (positive velocity). The average velocity during posturing and interruptions is shown for all patients (total) and subdivided according to RD location. The difference between posturing and interruptions was statistically significantly different for all groups (see P-values in figure, Mann–Whitney *U* test). N = a:b indicates the number of intervals of posturing (a) and interruptions (b).

Change from baseline

Although posturing reduces progression compared with interruptions, some patients do progress from baseline. **Table 3** shows 3 time points: baseline OCT, worst change from baseline (smallest distance during follow-up) and the last OCT. At the worst change from baseline, a median change of -84 μm (IQR: -221 to -25; range -1544 to +1948 μm) was found, 21 of 98 patients showed more than 250 μm progression, 4 of 98 showed more than 1000 μm progression. The median duration from baseline to the point of worst change from baseline for the 21 patients with more than 250 mm of progression was 6.3 hours (IQR, 3.3e15.7 hours; range, 1.5e36.5 hours), and the average velocity was 87 mm/hour (IQR, 179 to 41 mm/hour; range, 535 to 9 mm/hour). The 4 patients with more than 1000 μm of progression from baseline all had primary, superior RD with multiple or large retinal tears and were phakic. Three of these 4 patients maintained supine positioning, and 1 of 4 patients was instructed to lie on the nasal side. One of 4 patients had myopia of more than 6.0 diopters. The extent of RD varied between 90º and 110º.

Table 3. Distance and change in distance between the retinal detachment border and the fovea

	RD–fovea distance at baseline (μm)	Change from baseline		
		Distance (μm)	Time (hour)	Average velocity (μm/hour)
Baseline OCT				
Median (95% CI)	4050 (3740 to 4837)	NA	NA	NA
Interquartile range	2741 to 6132			
Range	1256 to 14122			
Mean±SD	4982±2872			
Smallest distance during follow-up				
Median (95% CI)	4294 (3765 to 5090)	-84 (-122 to -58)	5.9 (3.6 to 12.5)	-11 (-21 to 6)
Interquartile range	2782 to 5854	-221 to 25	2.4 to 16.0	-48 to 3
Range	707 to 13819	-1544 to 1948	0.5 to 36.5	-535 to 499
Mean±SD	4926±2803	-54±472	9.2±7.7	-25±105
Last OCT				
Median (95% CI)	4674 (4017 to 5374)	-3 (-53 to 49)	16.5 (15.5 to 17.6)	0 (-4 to 6)
Interquartile range	3077 to 6284	-127 to 457		-11 to +27
Range	1358 to 13857	-1544 to 6850	3.9 to 20.2	-535 to 637
Mean±SD	5336±3019	356±1272	0.8 to 39.9 14.8±9.5	7±116

RD = retinal detachment, CI = confidence interval, SD = standard deviation

In 14 of 21 patients with more than 250 μm of progression, surgery was already planned for the first available time on the operation room program. In 6 of 21 patients, we were able to reschedule the patients a few hours earlier. In 1 of 21 patients, the patient underwent surgery after normal working hours and surgery was not postponed to the next day owing to the apparent progressive nature of the RD. After the worst change from baseline some patients showed regression, especially during the night, and the median change from baseline to the last OCT was -3 (IQR: -127 to +457) μm. The maximum progression from baseline was 1544 μm and the maximum regression from baseline was 6850 μm.

None of our patients progressed to macula-off RD during our follow-up. Only 1 patient progressed within 1000 μm of the fovea. This patient showed a baseline distance between the RD border and fovea of 1256 μm and progressed to 707 μm in 3 hours. The next morning, after 14 hours of posturing, the patient had regressed to an RD–fovea distance of 1698 μm. The patient with the maximum regression of 6850 μm regressed so extensively that at the last OCT before surgery, only a small amount of subretinal fluid was seen around the retinal hole at 12.4 mm from the fovea after regressing in 18 hours from a baseline distance of 5.5 mm.

Figure 7 displays progression from baseline for at worst change from baseline for all patients (total) and subdivided by RD location. The Kruskall-Wallis test resulted in a significant difference among the RD location groups (P = 0.026). There seemed to be more progression from baseline in the superior RD group, but pairwise comparison did not result in significant differences between the groups.
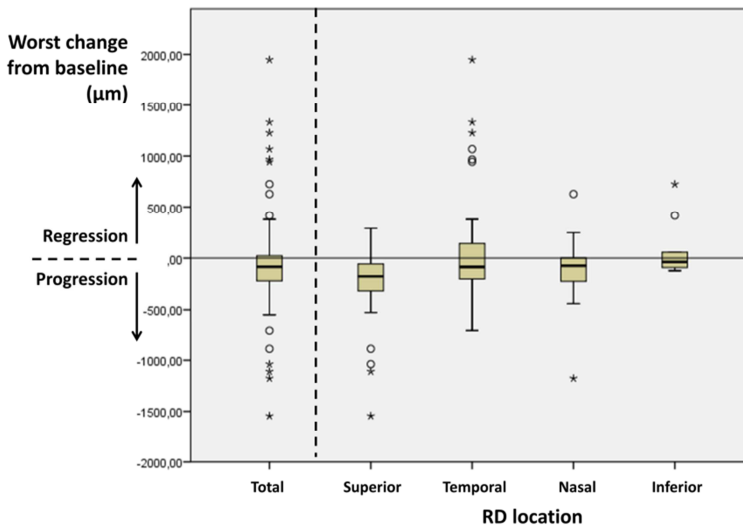
Figure 7. Graph showing the worst change from baseline in μm for the total of patients and a stratification according to retinal detachment (RD) location. The progression from baseline seemed to be larger in the superior RD group, although pairwise comparison did not reveal significant differences between the RD groups.

Risk factors for progression

Statistically significant correlations were found between the worst progression from baseline and a larger baseline distance between RD border and fovea, a shorter duration of visual field loss, an RD location with a smaller deviation from superior and a smaller extent of RD (**Table 4**). No significant correlation found between progression and the duration of follow-up, spherical equivalent refraction, the angle between retina and RPE and the size of retinal breaks.

Patients with a duration of follow-up 16 hours or fewer showed a median change from baseline to the last OCT of -26 µm (IQR, -211 to 53 µm; n = 44) and patients with more than 16 hours of follow-up showed a median change from baseline to the last OCT of 79 µm (IQR, -79 to 792 µm; n = 54), which was statistically significant different (P = 0.005). After exclusion of the 7 patients who were rescheduled to an earlier surgery time because of more than 250 µm of progression, the difference was still statistically significant (P = 0.008) with a median change from baseline in the group with a follow-up time of 16 hours or fewer of -18 µm (IQR, -142 to 56 µm; n = 41) and a median change from baseline in the group with a follow-up time of more than 16 hours of 114 µm (IQR, -69 to 873 µm; n = 50).

Table 4. Risk factors for progression from baseline

	Spearman's correlation coefficient with worst progression from baseline*	
	Rho (95% CI)	**P Value**
Baseline RD – fovea distance (mm)	-0.321 (-0.114 to -0.499)	0.001
Extent of RD (clock hours)	+0.262 (+0.068 to 0.438)	0.009
Duration of visual field loss (days)	+0.240 (+0.009 to +0.485)	0.039
Deviation from superior (degrees)	+0.229 (+0.031 to +0.400)	0.023
Duration of follow-up (hours)	-0.036 (-0.230 to 0.161)	0.725
Spherical equivalent refraction (diopters)	-0.144 (-0.344 to 0.065)	0.158
Angle between retina and RPE ( )	-0.156 (-0.341 to 0.032)	0.125
Size of retinal breaks (clock hours)	0.065 (-0.115 to 0.242)	0.523

CI = confidence interval, RD = retinal detachment
* A negative correlation means that a larger value for the risk factor results in more progression. A positive correlation means that a smaller value for the risk factor results in more progression.

DISCUSSION

Preoperative posturing advice has been given to patients with macula-on RD for decades all around the world, in some countries combined with hospital admission.[9-18,21] The first study performed using OCT to elucidate the progression rate of RD showed that delay of surgery beyond 16 hours was associated with a greater risk of progression.[18] Moreover and most importantly, this study highlighted the use of OCT as a precise research tool and allowed us to study the relationship between posturing and RD progression in an ethical manner. We could record progression safely with an OCT device located on the ward by using the accepted reasons for interrupting posturing, like toilet visits and meals. We were able to demonstrate that the median RD border displacement velocity during posturing was +1 (IQR, -21 to +49) μm/hour and -149 (IQR, -406 to +1) μm/hour during interruptions that was statistically significantly different (P<0.001). Therefore, we conclude that preoperative posturing significantly reduces progression of RD.

Retinal detachment progression is likely to be affected by several forces of different importance. Gravity is involved in specific positioning, with the detached retina in the lowermost position. However, it is considered unlikely that gravity will much affect intraocular fluid dynamics because the density differences between retina and vitreous are rather small.[22] Shear forces on the retina by eye and head movements are expected to affect RD progression as well.[23,24] Bed rest not only allows for specific positioning but also helps to reduce eye and head movements. Although there is no evidence available, posturing at home may increase the risk of RD progression because of the traveling time, the lack of nurse surveillance and the need to perform domestic duties. Therefore, while patients are awaiting surgery, in some European hospitals patients are admitted to the hospital instead of being sent home to improve their compliance with the posturing regimen.

In this study, superior and inferior RD patients seem to be less affected by the posturing advice than the temporal or nasal RD groups (**Figure 5**). Although the comparison of RD displacement velocity during posturing and interruptions showed that superior RD patients also benefitted from posturing (**Figure 6**), the progression from baseline seemed to be larger in these patients (**Figure 7**). A supine posturing advice may be suboptimal for superior RD, because the force of gravity is not directed from the fovea to the RD area and the tear.[24] Trendelenburg positioning would achieve that better, but is highly inconvenient to patients and impractical without hospital admission. Patients with inferior RD and sitting in an upright position interrupted their posturing by lying supine while maintaining bed rest, instead of interrupting bed rest, as did patients with RD in the superior quadrants. The smaller effect of posturing and the smaller progression rate from

baseline in these patients may point out that head and eye movement-related forces are responsible for the development of RD more than gravity alone.[24,25]

The progression velocity seemed to be twice as fast in previously detached areas of the retina compared with newly detached retina. This is in accordance with the retinal adhesion experiments of Yoon and Marmor,[26] who showed that the retinal adhesion strength gradually increases after spontaneous reattachment, but is still only 75% of the normal adhesion strength after 4 weeks. The median progression velocity in newly detached retina of 160 µm/hour during interruptions is clinically meaningful. If patients would not follow a posturing advice and their activity level is comparable with the light daily activities during bed rest interruptions of the patients in this study, then they are estimated to have on average 2.6 mm of progression on a 16-hour period. This extrapolation suggests that patients who the clinician believes may not comply with preoperative posturing may benefit from earlier surgical intervention. The higher regression rate during nighttime posturing compared with daytime posturing may be explained by better compliance with the posturing advice or fewer eye movements during the night.

Despite preoperative posturing, 21 of 98 patients progressed by more than 250 µm from baseline and 4 of 98 patients progressed more than 1000 µm from baseline. The median worst change from baseline was -84 (IQR: -221 to 25) µm, whereas the median change from baseline to the last OCT was +3 (IQR: -127 to 457) µm. This demonstrates that regression may follow earlier progression during the first days of posturing. Only one of the patients progressed within 1000 µm from the fovea during follow-up. This seems to indicate that the current policy of preoperative posturing and surgery within 48 hours is sufficient to prevent macula-off RD. It is also in accordance with the low rate of progression to macula-off status of patients awaiting surgery as reported by Ho *et al* (3%)[16], Ehrlich *et al* (2%)[17], Wykoff *et al* (0.5%)[27] and Hajari *et al* (1%)[18].

Patients with a superior RD location are slightly more at risk for progression than when the other quadrants are affected (**Table 4; Figure 7**).[28] We also found a slightly increased risk of progression from baseline of patients with a short duration of visual field loss, a larger baseline RD–fovea distance and a smaller extent of RD. The relationship between duration of visual field loss and progression may be explained by symptomatic patients who may be more inclined to seek medical attention than patients whose detachments are progressing slowly, resulting in minimal or no symptoms.[29] The increased risk of progression in case of a larger baseline RD–fovea distance and smaller extent of RD both may be explained by a weaker retinal adhesion in the periphery, allowing faster progression. When creating an RD for macular rotation or RPE-graft it is a common observation among surgeons that the peripheral retina detaches much more easily than the posterior retina, suggesting a difference in adhesion. This

phenomenon may be related to the greater photoreceptor density in the posterior pole.[30]

We did not find an increased risk for progression if surgery was postponed beyond 16 hours from admission, like Hajari *et al*.[18] On the contrary, a longer admission time significantly facilitated regression (P < 0.001) during the short follow-up of this study. In 1 patient, the RD almost completely disappeared after only 18 hours of posturing, which shows that in rare cases surgery may no longer be required after preoperative posturing. Even if we excluded the 7 patients who were rescheduled to an earlier surgery spot because of more than 250 μm progression, we found a significant difference between short (≤16 hours) and long (>16 hours) admission time. The reason for this different outcome might be that we followed the patients also during the first hours of admission, while Hajari *et al* only repeated the OCT every morning. When performing OCT scans in the morning, the progression during the previous day is likely concealed by reattachment during the night. However, the follow-up time of our study was limited with a median of 16.5 hours (IQR, 3.9–20.2). A surgery delay beyond the follow-up duration of our study might still result in more progression because of potentially poorer compliance to the posturing advice.

The 95% limits of agreement of the intrarater variability of the OCT distance measurements were ±58 μm, which was comparable with the 84 μm precision of the OCT measurements of Hajari *et al*.[18] The 95% limits of agreement of the combined intrarater and interrater variability of the change in distance were ±175 μm, which describes the maximum variability of our scan protocol if multiple graders are used to interpret the OCT measurements. The accuracy of the primary grader in determining the change in distance was -6 μm and the 95% limits of agreement were ±102 μm. To obtain this precision, an elaborate training of graders is necessary. If measurements of the RD–fovea distance change with a precision of more than ±102 μm are required, applying a higher scan resolution or larger number repeated B-scans per retinal location should be considered to improve the contrast between the photoreceptor outer segment layer and subretinal fluid.

The strengths of this study are the number of patients, the prospective nature of this study, the use of OCT on the ward allowing a safe and detailed analysis of the course of progression and the reproducibility analysis. Limitations of this study are the logistic constraints (no measurements were performed at night, surgery ended the follow-up period) and the shorter hospitalizations of patients who showed progression. One patient with a giant retinal tear was given a higher priority in operation time planning and had to be withdrawn from the study, which might have introduced a small selection bias and might have affected the rate of progression from baseline we found. Nevertheless, we could not find a relationship between the size of the retinal tear and progression from baseline in the 98 included patients (**Table 4**).

In conclusion, we showed that preoperative posturing reduces the progression of macula-on RD. Despite posturing, 21 of 98 patients progressed by more than 250 μm from baseline. For future studies, prolongation of interruptions may reveal whether traveling home increases patient risk of progression. Monitoring compliance with the posturing advice using positioning sensors may illuminate whether a restriction of head movements rather than gravity is related to RD progression. Further analysis of putative risk factors is required to be able to design a model that can predict progression of macula-on RD.

Acknowledgments

REFERENCES

1. Van de Put MA, Hooymans JM, Los LI, Dutch Rhegmatogenous Retinal Detachment Study Group. The incidence of rhegmatogenous retinal detachment in the netherlands. *Ophthalmology*. 2013;120(3):616-622.

2. Haimann MH, Burton TC, Brown CK. Epidemiology of retinal detachment. *Arch Ophthalmol*. 1982;100(2):289-292.

3. Thompson JA, Snead MP, Billington BM, Barrie T, Thompson JR, Sparrow JM. National audit of the outcome of primary surgery for rhegmatogenous retinal detachment. II. clinical outcomes. *Eye (Lond)*. 2002;16(6):771-777.

4. Johnson Z, Ramsay A, Cottrell D, Mitchell K, Stannard K. Triple cycle audit of primary retinal detachment surgery. *Eye (Lond)*. 2002;16(5):513-518.

5. Salicone A, Smiddy WE, Venkatraman A, Feuer W. Visual recovery after scleral buckling procedure for retinal detachment. *Ophthalmology*. 2006;113(10):1734-1742.

6. Zhou C, Lin Q, Chen F. Prevalence and predictors of metamorphopsia after successful rhegmatogenous retinal detachment surgery: A cross-sectional, comparative study. *Br J Ophthalmol*. 2016.

7. Rezar S, Sacu S, Blum R, Eibenberger K, Schmidt-Erfurth U, Georgopoulos M. Macula-on versus macula-off pseudophakic rhegmatogenous retinal detachment following primary 23-gauge vitrectomy plus endotamponade. *Curr Eye Res*. 2016;41(4):543-550.

8. Kaufman PL. Prognosis of primary rhegmatogenous retinal detachments. 2. accounting for and predicting final visual acuity in surgically reattached cases. *Acta Ophthalmol (Copenh)*. 1976;54(1):61-74.

9. Algvere P, Rosengren B. Immobilization of the eye. evaluation of a new method in retinal detachment surgery. *Acta Ophthalmol (Copenh)*. 1977;55(2):303-316.

10. Algvere P, Rosengren B. Active immobilization of the eye in the treatment of retinal detachment. *Mod Probl Ophthalmol*. 1977;18:286-291.

11. Lean JS, Mahmood M, Manna R, Chignell AH. Effect of preoperative posture and binocular occlusion on retinal detachment. *Br J Ophthalmol*. 1980;64(2):94-97.

12. Lincoff H, Stopa M, Kreissig I. Ambulatory binocular occlusion. *Retina.* 2004;24(2):246-253.

13. Lincoff H, Kreissig I, Uram D. Minor surgery for the repair of retinal detachment emanating from retinoschisis. *Acta Ophthalmol.* 2009;87(3):281-284.

14. Chen CY, Chen SN, Lin SM, Ho CL. Reduction of subretinal fluid after preoperative immobilization of the eyes with rhegmatogenous retinal detachment. *Chang Gung Med J.* 2001;24(12):799-804.

15. Adams GL, Yee RD, Hahn PM, Pearlman JT. Effect of binocular and monocular patching on eye movements. *Arch Ophthalmol.* 1973;90(2):117-120.

16. Ho SF, Fitt A, Frimpong-Ansah K, Benson MT. The management of primary rhegmatogenous retinal detachment not involving the fovea. *Eye (Lond).* 2006;20(9):1049-1053.

17. Ehrlich R, Niederer RL, Ahmad N, Polkinghorne P. Timing of acute macula-on rhegmatogenous retinal detachment repair. *Retina.* 2013;33(1):105-110.

18. Hajari JN, Kyhnel A, Bech-Azeddine J, la Cour M, Kiilgaard JF. Progression of foveola-on rhegmatogenous retinal detachment. *Br J Ophthalmol.* 2014;98(11):1534-1538.

19. Polyak S. The retina. Chicago: University of Chicago Press; 1941.

20. Yushkevich PA, Piven J, Hazlett HC, et al. User-guided 3D active contour segmentation of anatomical structures: Significantly improved efficiency and reliability. Neuroimage. 2006;31(3):1116-1128.

21. Mahmoudi S, Almony A. Macula-sparing rhegmatogenous retinal detachment: Is emergent surgery necessary? J Ophthalmic Vis Res. 2016;11(1):100-107.

22. Su X, Vesco C, Fleming J, Choh V. Density of ocular components of the bovine eye. Optom Vis Sci. 2009;86(10):1187-1195.

23. Repetto R, Tatone A, Testa A, Colangeli E. Traction on the retina induced by saccadic eye movements in the presence of posterior vitreous detachment. Biomech Model Mechanobiol. 2011;10(2):191-202.

24. Kuhn F, Aylward B. Rhegmatogenous retinal detachment: A reappraisal of its pathophysiology and treatment. Ophthalmic Res. 2014;51(1):15-31.

25. Machemer R. The importance of fluid absorption, traction, intraocular currents, and chorioretinal scars in the therapy of rhegmatogenous retinal detachments. XLI edward jackson memorial lecture. Am J Ophthalmol. 1984;98(6):681-693.

26. Yoon YH, Marmor MF. Rapid enhancement of retinal adhesion by laser photocoagulation. Ophthalmology. 1988;95(10):1385-1388.

27. Wykoff CC, Smiddy WE, Mathen T, Schwartz SG, Flynn HW,Jr, Shi W. Fovea-sparing retinal detachments: Time to surgery and visual outcomes. Am J Ophthalmol. 2010;150(2):205-210.e2.

28. Kontos A, Williamson TH. Rate and risk factors for the conversion of fovea-on to fovea-off rhegmatogenous retinal detachment while awaiting surgery. Br J Ophthalmol. 2016.

29. Goezinne F, La Heij EC, Berendschot TT, et al. Patient ignorance is the main reason for treatment delay in primary rhegmatogenous retinal detachment in the netherlands. Eye (Lond). 2009;23(6):1393-1399.

30. Jonas JB, Schneider U, Naumann GO. Count and density of human retinal photoreceptors. Graefes Arch Clin Exp Ophthalmol. 1992;230(6):505-510.

Chapter

3

The influence of prolongation of interruptions of preoperative posturing and other clinical factors on the progress of macula-on retinal detachment

Jan Hendrik de Jong
Juan Pedro Vigueras-Guillén
René J. Wubbels
Reinier Timman
Koenraad A. Vermeer
Jan C. van Meurs

ABSTRACT

Purpose: The primary aim of the current study was to evaluate whether prolongation of interruptions of preoperative posturing by sitting upright influences retinal detachment (RD) progression. The secondary objective was to find clinical factors to identify patients with a high risk for RD progression.

Design: Prospective cohort study.

Subjects: 198 patients divided over three cohorts of patients with macula-on RD were included. Inclusion criteria were: volume OCT scans of sufficient quality; smallest distance from the fovea to the detachment border at least 1.25 mm. In the second and third cohort, 50 patients with only superior temporal RD were included.

Methods: Patients were admitted to the ward in anticipation of their surgery. Preoperative bed rest and positioning were prescribed. The position of the RD border was determined based on OCT imaging performed at baseline, before and after the usual interruptions for meals or toilet visits. The duration of interruptions was prolonged with sitting upright for 20 minutes in cohort 2 and 40 minutes in cohort 3. Various secondary outcome measures were defined, such as the baseline area of subretinal fluid (SRF) as measured on ultrasound images in the third cohort.

Main outcome measures: The RD border displacement was determined. The worst RD progression from baseline was given by the shortest distance to the fovea in any of the OCT scans during follow-up. The worst relative RD progression from baseline was defined as the worst RD progression from baseline as a percentage of the baseline distance between RD border and fovea.

Results: The median duration of interruptions was 22, 41, and 58 minutes in the three cohorts respectively. The median RD border displacement during interruptions in patients with superior temporal RD was not significantly different between the cohorts (P = 0.28). The correlation coefficient between the SRF area at baseline and worst relative RD progression from baseline was 0.37 (95%CI: 0.04 to 0.66, P = 0.009).

Conclusions: We did not find a significant increase in RD progression after prolongation of interruptions by sitting upright. Patients with a larger area of SRF on ultrasound showed more RD progression from baseline.

INTRODUCTION

Macula-on retinal detachment (RD) is a progressive, sight-threatening disease affecting 12–18 out of 10,000 people per year.[1,2] The risk of clinically significant progress toward the fovea is reported to be 15–21% in the 2–3 days before surgery[3-5] and the risk of progression to macula-off is 0–3% .[3-7] If the macula is still attached, visual outcome is best and patients are scheduled for early surgery. However, same day surgery is challenging to accommodate because of an already full surgical schedule, the availability of a surgeon, anesthetist, nurses, or similar constraints. Therefore, many clinics do not provide same-day surgical treatment for all patients with macula-on RD. There is no consensus on the optimal preoperative policy for patients with one or two days surgery delay and the approach varies between inpatient or outpatient care with or without preoperative posturing.[3,4,6-13] Therefore, the safety of preoperative care and the risk factors for RD progression warrant further study.

Previously we have demonstrated that bed rest with positioning is effective in limiting the progression of macula-on RD in hospitalized patients waiting for surgery.[4] Optical coherence tomography (OCT) appeared to be highly suitable to study RD progression with an intra-rater variability of ±58μm. One of the main differences between inpatient and outpatient preoperative posturing is that patients would have to travel home in a car or taxi and sit upright during travel. Prolonging the duration of interruptions of posturing in hospitalized patients by sitting upright and monitoring the effect on RD progression by OCT might reveal whether cautiously traveling home with preoperative posturing at home can be considered as an alternative policy to inpatient care.

The evidence in the literature on putative risk factors for RD progression is limited. We previously found that a shorter duration of visual field defects and a superior RD location are weak risk factors for progression.[4] A bullous configuration has also been suggested as a risk factor for progression.[7,14] However, the only other prospective study using OCT to monitor RD progression by Hajari et al. could not find a relationship between bullous shape and RD progression.[3] A possible explanation might be that defining an RD as bullous based on funduscopic examination is rather subjective. Measuring the amount of subretinal fluid (SRF) by ultrasound might show whether such a relationship with RD progression exists.

The primary aim of this study was to evaluate whether prolongation of interruptions of preoperative posturing by sitting upright influences RD progression. The secondary objective was to find clinical factors to identify patients with a high risk for RD progression.

PATIENTS & METHODS

Study design

This study was designed as a prospective cohort study with OCT recordings of the distance between RD and fovea during preoperative posturing and interruptions of posturing. The study was approved by the Medical Ethical Committee of the Erasmus Medical Center, Rotterdam, the Netherlands, and registered at www.trialregister.nl (Trial number NTR4884). The study consisted of three cohorts of 50 patients and included patients with superior temporal RD. The first cohort was the baseline cohort in which we allowed the normal duration of posturing interruptions. In the second and third cohort, the interruption intervals were prolonged. During the inclusion period of the 50 patients in the baseline cohort, we additionally included 48 patients with RD in the other retinal quadrants following the same eligibility criteria to explore the differences between RD locations and posturing advices. The results of these 98 patients in the first cohort were reported previously.[4] All patients were hospitalized and examined in the Rotterdam Eye Hospital, The Netherlands. The study was conducted in accordance with the tenets of the Declaration of Helsinki.

Study procedures

The study procedures were described previously in more detail.[4] In brief, patients diagnosed with macula-on RD were admitted to the ward for posturing while they were waiting for surgery the same day, the next day or occasionally the day after. Surgery was planned as soon as possible, but no later than 48 hours from the start of hospitalization. Patients were admitted to the ward and scheduled for surgery independently of study eligibility.

Posturing consisted of two parts: bed rest and positioning. Patients with RD mainly located in the superior quadrant were positioned supine, patients with RD in the temporal quadrant on the temporal side of the affected eye, patients with RD in the nasal quadrant on the nasal side and patients with RD in the inferior quadrant were instructed to sit upright. Nurses regularly entered the wardrooms to check whether patients were adhering to the positioning advice, which was the standard clinical practice. Patients were allowed to interrupt their posturing for meals, toilet visits, short refreshment using a washcloth in the morning and surgeon's examinations. Such intervals offer an excellent opportunity to acquire prospective and comparative data in an ethically acceptable and safe manner.[4]

In the first cohort, the normal duration of interruptions was measured, which appeared to be 22 minutes on average.[4] In the second and third cohort, the duration of interruptions was prolonged by 20 and 40 minutes respectively. Toilet visits and other short breaks were prolonged from an average of 10 minutes in cohort 1 to 30 minutes in cohort 2 and 50 minutes in cohort 3. Dinner breaks and

other long breaks were prolonged from an average of 30 minutes in cohort 1 to 50 minutes in cohort 2 and 70 minutes in cohort 3.

During these prolongations, the patients were instructed to sit upright in their bed. The rationale behind this instruction was that sitting upright while traveling home was expected to be one of the main differences between the preoperative posturing advice in an outpatient or inpatient policy.

If included patients progressed more than 250 μm, surgery was rescheduled to an earlier time point if possible. We hypothesized that the risk of foveal involvement does not substantially increase with RD progression below 250 μm. In cohort 1, which was an observational cohort without intervention, OCT measurements continued if more than 250 μm progression was recorded. In cohort 2 and 3, OCT measurements were stopped to prevent further progression induced by prolonged interruptions. Measurements with progression exceeding 250 μm (cohort 1) were excluded for the comparison between the cohorts to enable a valid comparison. If the proportion of patients with RD progression of more than 250 μm from baseline would increase from cohort 1 to cohort 2 more than 10% (i.e., an increase of more than five patients), the study would be terminated.

Inclusion and exclusion criteria

Inclusion criteria were: age of 18 years or older, written informed consent, nearest point of the RD border more than 1250 μm away from the foveola (safety measure) and within the range of the OCT system, sufficiently clear media to obtain an OCT scan, sufficient quality of the OCT scan, and OCT performed within an hour after admission of the patient to the ward. In cohort 2 and 3: involvement of superior temporal retinal quadrant. No exclusion criteria were specified. The safety border of 1250 μm from the foveola was based on the traditional size of the fovea centralis (with a radius of 750 μm) and parafovea (ring of 500 μm around the fovea) combined.[15]

Retinal detachment progression measurements

Within one hour after arrival on the ward a baseline volume OCT scan was performed (Spectralis OCT, Heidelberg Engineering, Germany) and eligibility was determined. The smallest distance between RD border and fovea was measured according to our previously described method, with a 95% limit of agreement of the intra-rater variability of ±58 μm.[4] The measured distance on subsequent OCT scans were then used to calculate the RD border displacement and the average RD border displacement velocity (change in distance per hour) during posturing and interruption intervals. The latter measure adjusts for differences in interval duration and thereby enables a more consistent comparison between posturing intervals and interruptions. The worst RD progression from baseline was defined as change from baseline recorded at the time point when the shortest distance to

the fovea was measured in any of the OCT scans during follow-up. In patients who show RD progression from baseline, the threat of foveal detachment is larger if the baseline distance between the RD border and the fovea is smaller. Therefore, we calculated the worst relative RD progression from baseline, which was defined as the worst RD progression from baseline as a percentage of the baseline distance between the RD border and fovea.

Secondary outcome measures
The following secondary outcome measures were recorded: age, gender, reported duration of visual field loss (days), duration of follow-up (hours), spherical equivalent refraction (diopter), previous vitrectomy, previous scleral buckle, previous laser treatment for retinal breaks, lens status, baseline distance between RD border and fovea (μm), size of retinal breaks (clock hours), RD location (deviation from superior of the nearest point on the RD border at baseline in degrees, where superior is a 0 degrees deviation and inferior 180 degrees), extent of RD (clock hours relative to the fovea), angle between retina and retinal pigment epithelium (RPE) on OCT B-scan at the RD edge (degrees). Patients were interviewed to determine the existence and duration of visual field loss. If patients did not report visual field loss, they were excluded from the analysis. The duration of follow-up was defined as the time between admission and the last OCT scan. The size of retinal breaks was estimated by the operating surgeon. The baseline OCT was used to determine the extent of RD and the deviation from superior of the nearest point on the RD border. The angle between the retina and RPE was measured with ImageJ.

In cohort 3, ultrasound images (B-scan Plus, Accutome Inc, Malvern, USA) of the RD were acquired at baseline. During acquisition, patients were sitting upright and looking straight ahead or in the direction of the RD location (for example, superior gaze for superior detachments, temporal gaze for temporal detachments) to improve the visualization of the RD. A horizontal and vertical recording of the RD was performed, consisting of a series of B-scans of 14 seconds. To find the maximum area, height, and angle, the B-scan representing the estimated largest area, height or angle of the SRF pocket was selected from the B-scan series. The following features of the SRF pocket were measured: the area of SRF (mm²), the height of SRF (mm), the angle between the retina and RPE (degrees), convex shape (Yes/No) (**Figure 1)**. From the horizontal and vertical measurement, the maximum value was selected for further analysis. Intra-rater and inter-rater reproducibility of the SRF measurements on ultrasound were analyzed using different graders as described in **Supplemental material 3.1**.

We determined to smallest RD-fovea distance during follow-up to correlate this distance with the baseline RD-fovea distance, to find out whether the baseline RD-fovea distance has predictive value as was reported before by Ho et al.[5]
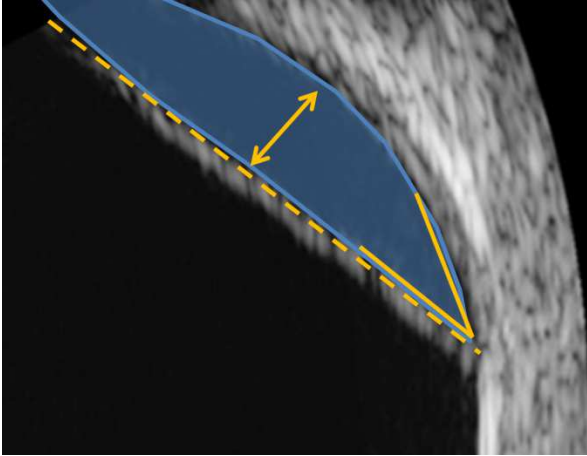
Figure 1.
Ultrasound measurements of the subretinal fluid (SRF) pocket features. The blue area represents the area of SRF, the yellow arrow the maximum height of the SRF, the yellow corner the angle between retina and RPE, and the dashed line represents a line connecting the (estimated) starting points of the SRF pocket revealing whether the RD had a convex shape.

Statistical analysis

Because of the non-Gaussian distribution of the worst RD progression from baseline and the progression during interruptions as well as the RD-fovea distance and velocity measurements (Shapiro-Wilk test of normality, $p<0.001$), non-parametric testing was performed. The Mann Whitney U test was used to compare the RD displacement between posturing and interruption intervals.

The Kruskal-Wallis test was performed to test for differences between the patient characteristics of the three cohorts with superior temporal RD. The Jonckheere trend test was used to test for a trend between the three cohorts concerning the RD border displacement during interruptions of posturing and concerning the worst RD progression from baseline. The chi-squared test was used for differences between the proportions per cohort of patients with more than 250 μm progression from baseline.

Spearman's rho was used to quantify correlations between the worst relative RD progression from baseline and the following risk factor candidates: area of SRF, height of SRF, angle between retina and RPE on ultrasound, convexity of SRF pocket, RD border displacement velocity during first bed rest interval, extent of RD, duration of visual field loss, duration of follow-up, baseline distance between RD border and fovea, size of retinal breaks, RD location, angle between retina and RPE. Because of the explorative purpose of these tests, we did not correct for multiple testing and considered p-values below 0.05 significant. Receiver operating characteristic (ROC) curves were produced to determine the optimal cut-off values and to calculate the diagnostic odds ratio (DOR). The optimal cut-off value was defined as the point on the ROC curve where Youden's index (sensitivity + specificity - 1) was maximized. The optimal cut-off values of the ultrasound features were corrected for the inter-rater reproducibility (**Supplemental material 3.1**) by subtracting the one-sided 95% limit of agreement value. Afterward, the DOR was recalculated.

Spearman's rho was used to test for a correlation between the baseline RD-fovea distance and the smallest RD-fovea distance during follow-up. Statistical analyses were performed with SPSS version 23.

RESULTS

Patients

Between February 24, 2015, and October 4, 2017, 1102 macula-on RD patients were hospitalized preoperatively in the Rotterdam Eye Hospital, 392 of whom were screened for eligibility. Out of this screening pool, 172 patients were not eligible for this study: in 73 of them the distance between fovea and RD was smaller than 1250 μm; in 54 patients the border of the RD could not be visualized with sufficient quality due to a peripheral RD location beyond the limits of the OCT system, a bullous RD overhanging the RD border, a vitreous hemorrhage, a giant retinal tear, or poor fixation of the patient; 23 patients had an RD which, based on OCT, was not superior temporally located and were excluded from cohort 2 or 3; 21 patients were unwilling to participate; 1 patient was methicillin resistant staphylococcus aureus-suspect and was kept in a quarantine room. Out of 220 eligible patients, 22 patients were sent to the operation room before 3 OCT measurements could be conducted and were withdrawn from this study and further analysis. In the remaining 198 included patients, a total of 1039 OCT scans were made (median 5, range 3–13 OCT scans per patient), the results of which are presented in this report. All included patients provided a written informed consent.

The course of progression from baseline

Patient characteristics are summarized in **Table 1**. With the 1039 OCT scans, 841 intervals were recorded, of which 434 posturing intervals and 407 interruptions. The median time between baseline OCT and last OCT was 16.6 hours (range: 0.8 to 57.1 hours). At the worst RD progression during follow-up, 35 out 198 patients (17.7%) showed more than 250 μm progression from baseline, and 8 out of 198 patients (4.0%) showed more than 1000 μm progression from baseline. Relative to baseline, 27 patients (13.6%) had more than 10% progression, and 12 patients (6.1%) showed more than 20% progression. The maximum worst RD progression from baseline was -3132 μm in a patient with a baseline distance of 8723 μm, which progressed to 5591 μm. The maximum worst relative RD progression from baseline was -59% in a patient with a baseline distance of 1918 μm, which progressed to 786 μm.

The correlation between baseline RD-fovea distance and smallest RD-fovea distance during follow-up had a coefficient of 0.98 (95%CI: 0.96 to 1.00, p<0.001, see also **Figure 2**), which is similar to the findings of Ho et al.[5]

Table 1. Patient characteristics

Characteristic	Data
Patients included the study (no.)	198
Age (years)	
Median (range)	61 (26 to 86)
Male : Female (no.)	128 : 70
Phakic : Pseudophakic (no.)	123 : 75
Snellen visual acuity at presentation	
Median (range)	20/27 (20/17 to 20/400)
Refraction spherical equivalent* (Diopter)	
Median (IQR)	-2.1 (-5.1 to 0.0)
Range	-18.5 to 5.75
Moderate myopia (≤6.0D and ≥3.0D) (no.)	42
High myopia (≥6.0D) (no.)	52
Duration of visual field loss (days)	
Median (IQR)	4.0 (2.0 to 8.5)
Range	0.5 to 120
No complaints of visual field loss (no.)	37
Primary / recurrent RD	184 / 14
History of vitrectomy (no.)	6
History of scleral buckling (no.)	8
History of argon laser (no.)	16
Extent of RD (clock hours)	
Median (IQR)	3.3 (2.7 to 4.3)
Range	1 to 10
Size of retinal tear (no.)	
Single small (≤0.50 clock hr.)	39
Multiple/large (>0.50 clock hr.)	142
No breaks found	17
Angle (degrees) between retina and RPE	
Median (IQR)	8.5 (4.8 to 13.3)
Range	1.3 to 40.2
Posturing advice (no.)	
Supine	50
Temporal side	93
Nasal side	45
Sitting upright	10

IQR = inter quartile range, SD = standard deviation, RD = retinal detachment, RPE= retinal pigment epithelium

* In patients with pseudophakic lens status, the spherical equivalent refraction before cataract surgery was used.
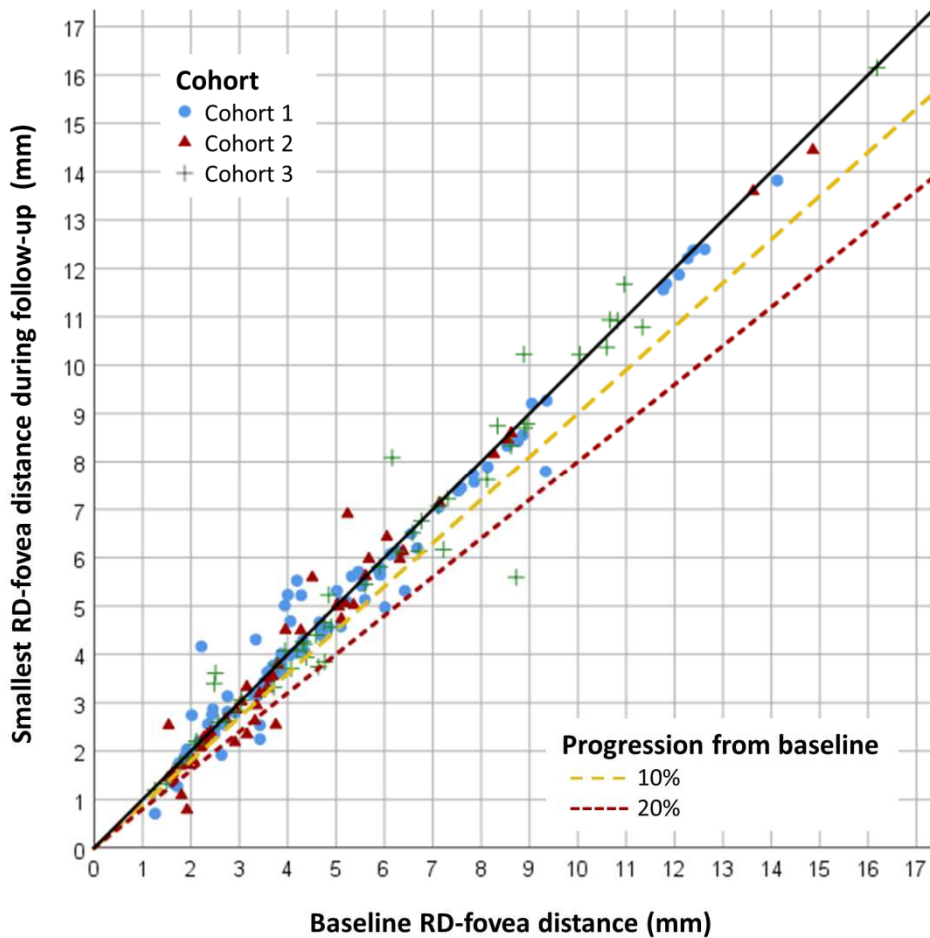
Figure 2. Scatter plot between the baseline RD-fovea distance and the smallest RD-fovea distance during follow-up. Each marker represents one patient and the corresponding cohort is indicated by the shape and color of the marker. Patients shown under the diagonal (black line) have progressed, patients above the diagonal have only regressed during the study period. Patients shown under the yellow dashed line progressed more than 10% from baseline, patients shown under the red dotted line progressed more than 20% from baseline. Most patients were stable or regressed from baseline, while 27 out of 198 patients (13.6%) revealed more than 10%

Comparison of progression in the three cohorts

For the comparison with the 50 superior temporal patients each in cohort 2 and 3, we selected the 50 superior temporal patients from cohort 1. The patient characteristics as reported in **Table 1** were only statistically significantly different among the three cohorts for the extent of RD (P = 0.02) and the duration of visual field defects (P = 0.014), which were both higher in cohort 2 compared to the other two cohorts. The duration of interruptions, the RD border displacement during these interruptions and the worst progression from baseline are presented in **Table 2**.

The difference between RD border displacement during interruptions was not significantly different between the three cohorts (P = 0.28, see also **Table 2**). In our previous study, we have shown a statistically and clinically significant difference between the displacement of the RD border during posturing intervals and interruptions in the patients from the first cohort of this study.[4] The difference between RD border displacement and RD border displacement velocity between posturing and interruptions was statistically significant for cohort 2 and 3 as well (P<0.001; **Table 2**).

The average RD border displacement velocity during day time posturing was -3 μm/hour (IQR, -37 to 40 μm/hour; n = 254) and during night time posturing 12 μm/hour (IQR, -2 to 73 μm/hour; n = 180), which differed statistically significantly (P < 0.001, difference of the medians 15 μm/hour).

Table 2. Progression in the three cohorts

	Cohort 1	Cohort 2	Cohort 3	
	Median [IQR]; N	*Median* [IQR]; N	*Median* [IQR]; N	p-value
Interruption duration (min.)	*22* [13, 30]; 99	*41* [33, 47]; 99	*58* [52, 66]; 105	<0.001
RD border displacement during interruptions (μm)	*-76* [-178, -7); 99	*-38* [-239, 10]; 99	*-85* [-211, -17]; 105	0.28
Worst RD progression from baseline (μm)	*-91* [-220, 210]; 50	*-89* [-245, -5]; 50	*-87* [-243, 52]; 50	0.94
RD border velocity during posturing (μm/h)	*1* [-21, 49]; 202	*6* [-12, 80]; 115	*-3* [-10, 40]; 117	<0.001*
RD border velocity during interruptions (μm/h)	*-149* [-406, 1]; 197	*-54* [-399, 17];103	*-81* [-194, -16]; 107	
	n/N, %	n/N, %	n/N, %	
>250 μm progression (n, %)	11/50, 22%	12/50, 24%	12/50, 24%	0.96

difference posturing-interruptions

Putative risk factors for RD progression

To determine which ultrasound SRF feature was the best predictor of progression of more than 10% from baseline, the following was analyzed: the area of SRF, the height of SRF, the angle between retina and RPE and convexity of the SRF pocket (see **Figure 1**). The Spearman correlation coefficient and area under the curve with optimal cut-off values are presented in **Table 3**. Based on the area under the ROC curves of more than 0.9, the area of SRF, the height of SRF and the angle between retina and RPE appeared to be strong tests to differentiate between high and low-risk patients. The convexity of the SRF pocket can be seen as a fair test with an area under the ROC curve of 0.77.

After correcting the optimal cut-off value as reported in **Table 3** for inter-rater variability, the DOR was 37 for the area of SRF (see also **Figure 3**), 26 for the height of SRF and 24 for the angle between retina and RPE. The area of SRF on ultrasound appeared to be the best candidate to select patients with a high risk for progression.

We performed the Spearman correlation test also for other putative risk factors with the worst relative RD progression from baseline. Three risk factors were significantly correlated with RD progression: the average RD border velocity during the first posturing interval, RD location as a deviation of the nearest point on the RD border from superior and the reported duration of visual field defects (see **Table 3**). RD displacement velocity in the first posturing interval was a good test with a diagnostic odds ratio of 8.8. The deviation from superior and the duration of visual field defects seem to be poor tests, although the diagnostic odds ratios were reasonable (5.5 and 6.2).

History of vitrectomy, scleral buckle or laser treatment

The median worst progression from baseline was -183 μm (IQR, -296 to -88 μm; n = 6) in vitrectomized patients and was -83 μm (IQR, -227 to 14 μm; n = 192) in non-vitrectomized patients, which was not significantly different (P = 0.14). The median worst progression from baseline was -86 μm (IQR, -271 to 4 μm; n=8) in patients with previous buckle surgery and was -85 μm (IQR, -230 to 10 μm; n = 190) in non-scleral buckle patients, which was not significantly different (P = 0.92). The median worst progression from baseline was -24 μm (IQR, -189 to 236 μm; n = 16) in patients with previous laser treatment for retinal defects alone (no vitrectomy or scleral buckle) and was -87 μm (IQR, -236 to 9 μm; n = 168) in patients without a history of argon laser, vitrectomy or scleral buckle, which was not significantly different (P = 0.18).

Table 3. Putative risk factors for RD progression

Putative risk factor	N	Spearman's Rho (95% CI)	P-value	Area under the ROC curve (95%CI)*	Optimal cut-off value**	Diagnostic odds ratio (95%CI)***
Area of SRF (mm²)	49	-0.37 (-0.66 to -0.04)	0.009	0.97 (0.93-1.00)	45 mm² (>)	150 (7-3200)
Height of SRF (mm)	49	-0.29 (-0.55 to 0.01)	0.045	0.91 (0.80-1.00)	5.7 mm (>)	61 (7-555)
Angle between retina and RPE on ultrasound (degrees)	49	-0.31 (-0.56 to -0.03)	0.030	0.92 (0.81-1.00)	71 degrees (>)	61 (7-555)
Convexity (Y/N)	49	-0.19 (-0.44 to 0.08)	0.203	0.77 (0.62-0.91)	Not applicable ****	15 (0.8-281)
RD displacement velocity in the first posturing interval (μm/hour)	198	0.65 (0.53 to 0.73)	<0.001	0.81 (0.71-0.92)	-76 μm/hour (<)	8.8 (3.3-23.6)
Deviation from superior (degrees)	198	0.21 (0.06 to 0.34)	0.004	0.70 (0.59-0.80)	44 degrees (<)	2.5 (1.9-16.0)
Duration of visual field loss (days)	161	0.24 (0.10 to 0.36)	0.002	0.66 (0.56-0.76)	7.5 days (<)	6.2 (1.1-33.5)
Extent of RD (clock hours)	198	-0.09 (-0.23 to 0.05)	0.194	0.66 (0.55-0.76)	3.6 hours (>)	5.5 (0.5-154.7)
Duration of follow-up (hours)	198	0.02 (-0.12 to 0.16)	0.804	0.53 (0.41-0.64)	17 hours (>)	1.4 (0.6-3.1)
Angle between retina and RPE on OCT (degrees)	198	-0.10 (-0.25 to 0.05)	0.174	0.53 (0.41-0.66)	13 degrees (>)	1.9 (0.8-4.5)
Size of retinal breaks (clock hours)	198	0.01 (-0.11 to 0.14)	0.861	0.52 (0.41-0.63)	0.4 hours (>)	2.7 (0.7-10.6)

*The predicted condition was worst RD progression from baseline of more than 10% from the baseline RD-fovea distance

** The optimal cut-off value was defined as the point of the ROC curve where the Youden's index was maximal (sensitivity + specificity -1). The sign behind the cut-off value indicates whether a higher (>) or lower (<) value is regarded as a positive test result.

*** Since the diagnostic odds ratio is undefined when the number of false negatives or false positives is zero, 0.5 was added to all cells of the contingency table to calculate the diagnostic odds ratios for all putative risk factors
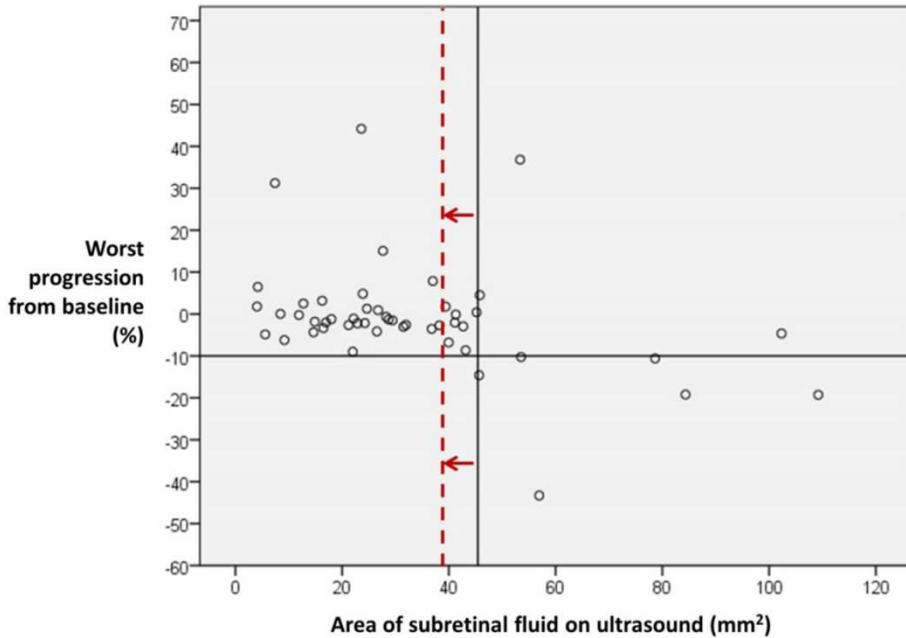
Figure 3. Scatter plot of the relationship between the area of subretinal fluid (SRF) as measured on ultrasound images and the worst relative RD progression from baseline. The cut-off point found using the Youden's index was 45 mm² (black vertical line). The 95% limits of agreement of the inter-rater variability of the area of SRF was ±7.3 mm². Lowering the cut-off point for the inter-rater variability results in a corrected cut-off point of 38 mm² (red dashed line) and a diagnostic odds ratio of 37.

DISCUSSION

Preoperative posturing is effective in reducing progression toward the fovea as we have shown in this and the previous study[4] and should be an important ingredient of the preoperative policy of macula-on RD patients with delayed surgery.[3,4] Since 12 out 198 patients (6.1%) progressed more than 20% of their baseline RD-fovea distance, offering same day surgery as much as possible is priority number one. However, when delayed surgery is inevitable due to limited resources, the strong correlation of 0.98 between baseline RD-fovea distance and the smallest RD-fovea distance during follow-up shows that patients with a small baseline RD-fovea distance may preferably be selected for urgent surgery. The area of SRF on ultrasound appeared to have an odds ratio of 37 (after correction for

reproducibility) in predicting more than 10% progression toward the fovea. Therefore, patients with a large area of SRF on ultrasound may also be given priority for urgent surgery and inpatient preoperative posturing if a ward is available.

Outpatient care may require patients to travel more extensively between their home and the clinic. During traveling by car or taxi, patients would have to sit upright for a prolonged time compared to inpatient posturing. We did not find a statistically significant difference between the three cohorts concerning RD progression from baseline or the progression during interruptions. The most plausible explanation for this is that movements of the head and eyes are likely to be the driving forces behind RD progression,[16-20] while patients were mostly sitting upright quietly during the prolongation of interruptions. Head and eye movements cause intraocular fluid currents, which exert a detachment force on the retina.[21] Since the density difference between the retina and vitreous fluid is rather small,[22] the force of gravity alone is not enough to detach the retina when a patient is quietly sitting upright. Indeed, in an explorative trial using a positioning device to monitor compliance to the preoperative posturing advice, we have shown that head motility affects RD progression more than head orientation.[23] Therefore, traveling up to 60 minutes, which was the average duration of interruptions in cohort 3, is expected to be safe. For the situation in the Netherlands, 60 minutes is a reasonable travel distance, which would see the majority of treated patients home. We realize that that does not apply to countries with more impressive travel distances. Future studies should increase the travel time to multiple hours to evaluate the safety of longer travel distances.

We have also shown that significantly more regression is achieved during night time posturing intervals than during day time posturing intervals. An advantage of outpatient care may be that patients can sleep in their own bed, which probably increases the duration of nighttime sleep compared to a noisy ward room and thereby facilitate RD regression.

Traveling home includes more than prolonged sitting upright alone, like walking to the car, getting in and out of the car, climbing the stairs in an apartment building, and domestic duties. However, the number of domestic activities should be minimized for the 1 or 2 days of surgery delay, or room or home mates may take over some of them. The referring ophthalmologist could play a key role in preventing unnecessary traveling by sending in patients to the tertiary clinic only on the day that there is operation time available. OCT and ultrasound measurements will be convenient in the communication between secondary and tertiary clinics. A large comparative non-inferiority trial would be required to more definitely study the safety of outpatient care by sending patients home and evaluate RD progression at their return.

As Ho *et al.* already demonstrated the strong correlation between RD-fovea distance at baseline and at operation using fundus drawings,[12] we now can confirm this strong relationship by more precise OCT measurements. A correlation of 0.98 between baseline RD-fovea distance and distance at the worst progression from baseline shows that a safety margin around the fovea would be able to differentiate between patients with an *a priori* low or high risk of macula-off status at the day of surgery. However, the overall risk of progression toward macula-off is only 0–3%[3-7], and the very strong correlation coefficient still fails to identify the small number of exceptions for which the preoperative emergency policy has been designed in the first place. To prevent all RD progression to macula-off status, a safety margin around the fovea alone is probably not enough.

We have studied various putative risk factors for progression from baseline, of which the area of SRF on ultrasound appeared to be the best predictor. Although the strength of the correlation coefficient was moderate ($r=0.37$), the ROC curve with progression of >10% showed an area under the curve of 0.97. The difference in test outcome is probably caused by a large number of stable patients showing a minimum amount of regression or progression (**Figure 3**), which affects the correlation coefficient, but not the ROC area under the curve. Based on the ROC analysis, ultrasound appears to be an excellent tool to select patients with a high risk for RD progression. This is in accordance with the theory that the inertia of subretinal fluid during head and eye movements exerts a detaching force on the retina.[3,19,21] The more fluid accumulates under the retina, the more likely the RD will further progress.

Although ultrasound as a single test seems to be sufficient to predict RD progression, the number of patients was limited to 49. Therefore, when considering to use ultrasound to select patients for urgent surgery, we would like to suggest also to apply a safety margin of 4 mm using the baseline distance as measured with OCT. Thereby, the maximum RD progression of 3132 μm or the maximum relative RD progression of 59% as found in this study will not cause progression into the 750 μm circle around the fovea representing the fovea centralis.

Three other risk factors were significantly correlated to RD progression from baseline: the progression during the first posturing interval, the RD location defined as a deviation from superior, and the duration of visual field loss at the time of diagnosis. Although the progression measured during the first posturing interval is not independent of the RD progression from baseline, the strong correlation of 0.7 shows the potential of a testing period of preoperative posturing to select progressive patients, although a measure hard to implement in practice. As shown before,[4] a superior RD location is more likely to progress towards the fovea. Supine posturing may be suboptimal for superior RD because the force of gravity is not directed from the fovea to the RD area and tear.[4,19] The few

vitrectomized patients showed a tendency towards more RD progression compared to non-vitrectomized patients. This might be explained by the role of the vitreous in damping fluid compartment currents.[21] Interestingly, lens status did not make any difference in RD progression, while it is a known risk factor for the occurrence of RD.

The strengths of this study are the number of patients, the prospective nature of this study, the use of OCT on the ward allowing a safe and detailed analysis of the course of progression and the reproducibility analysis. Limitations of this study are the logistic constraints (no measurements were performed at night, surgery ended the follow-up period), the shorter hospitalization of progressive patients and the uncertainty on the compliance of patients with the posturing advice since nurses regularly checked the compliance of patients, but patients were not surveilled continuously.

In conclusion, the baseline distance between RD and fovea on OCT and the area of SRF on ultrasound are essential measures to single out patients with a high risk for RD progression toward macula-off. Patients with a small baseline distance between RD and fovea (<4 mm), large area of SRF (>38mm^2) and a long traveling distance (>1 hour) from the clinic, should be selected for urgent surgery and inpatient preoperative posturing.

Acknowledgments

REFERENCES

1. Van de Put MA, Hooymans JM, Los LI, Dutch Rhegmatogenous Retinal Detachment Study Group. The incidence of rhegmatogenous retinal detachment in the netherlands. *Ophthalmology*. 2013;120(3):616-622.

2. Haimann MH, Burton TC, Brown CK. Epidemiology of retinal detachment. *Arch Ophthalmol*. 1982;100(2):289-292.

3. Hajari JN, Kyhnel A, Bech-Azeddine J, la Cour M, Kiilgaard JF. Progression of foveola-on rhegmatogenous retinal detachment. *Br J Ophthalmol*. 2014;98(11):1534-1538.

4. de Jong JH, Vigueras-Guillén JP, Simon TC, et al. Preoperative posturing of patients with macula-on retinal detachment reduces progression toward the fovea. *Ophthalmology*. 2017.

5. Ho SF, Fitt A, Frimpong-Ansah K, Benson MT. The management of primary rhegmatogenous retinal detachment not involving the fovea. *Eye (Lond)*. 2006;20(9):1049-1053.

6. Wykoff CC, Smiddy WE, Mathen T, Schwartz SG, Flynn HW,Jr, Shi W. Fovea-sparing retinal detachments: Time to surgery and visual outcomes. *Am J Ophthalmol*. 2010;150(2):205-210.e2.

7. Ehrlich R, Niederer RL, Ahmad N, Polkinghorne P. Timing of acute macula-on rhegmatogenous retinal detachment repair. *Retina.* 2013;33(1):105-110.

8. Algvere P, Rosengren B. Immobilization of the eye. evaluation of a new method in retinal detachment surgery. *Acta Ophthalmol (Copenh).* 1977;55(2):303-316.

9. Lean JS, Mahmood M, Manna R, Chignell AH. Effect of preoperative posture and binocular occlusion on retinal detachment. *Br J Ophthalmol.* 1980;64(2):94-97.

10. Lincoff H, Stopa M, Kreissig I. Ambulatory binocular occlusion. *Retina.* 2004;24(2):246-253.

11. Chen K, Weiland JD. Anisotropic and inhomogeneous mechanical characteristics of the retina. *J Biomech.* 2010;43(7):1417-1421.

12. Ho SF, Fitt A, Frimpong-Ansah K, Benson MT. The management of primary rhegmatogenous retinal detachment not involving the fovea. *Eye (Lond).* 2006;20(9):1049-1053.

13. Mahmoudi S, Almony A. Macula-sparing rhegmatogenous retinal detachment: Is emergent surgery necessary? *J Ophthalmic Vis Res.* 2016;11(1):100-107.

14. The repair of rhegmatogenous retinal detachments. american academy of ophthalmology. *Ophthalmology.* 1996;103(8):1313-1324.

15. Polyak S. *The retina.* Chicago: University of Chicago Press; 1941.

16. Machemer R. The importance of fluid absorption, traction, intraocular currents, and chorioretinal scars in the therapy of rhegmatogenous retinal detachments. XLI edward jackson memorial lecture. *Am J Ophthalmol.* 1984;98(6):681-693.

17. Foster WJ. Bilateral patching in retinal detachment: Fluid mechanics and retinal "settling". *Invest Ophthalmol Vis Sci.* 2011;52(8):5437-5440.

18. Repetto R, Tatone A, Testa A, Colangeli E. Traction on the retina induced by saccadic eye movements in the presence of posterior vitreous detachment. *Biomech Model Mechanobiol.* 2011;10(2):191-202.

19. Kuhn F, Aylward B. Rhegmatogenous retinal detachment: A reappraisal of its pathophysiology and treatment. *Ophthalmic Res.* 2014;51(1):15-31.

20. Vroon J, de Jong JH, Aboulatta A, et al. Numerical study of the effect of head and eye movement on progression of retinal detachment. *Biomech Model Mechanobiol.* 2018.

21. Marmor M. Mechanisms of normal retinal adhesion. *In Retina Stephen J. Ryan, Chapter 19.* 2013;1:447-464.

22. Su X, Vesco C, Fleming J, Choh V. Density of ocular components of the bovine eye. *Optom Vis Sci.* 2009;86(10):1187-1195.

23. de Jong JH, de Koning K, den Ouden T, van Meurs JC, Vermeer KA. The effect of compliance with preoperative posturing advice and head movements on the progression of macula-on retinal detachment. Translational vision science & technology. *Transl Vis Sci Technol.* 2019;8(2):4.

SUPPLEMENTAL MATERIAL 3.1

Reproducibility analysis of subretinal fluid measurements

Methods
To evaluate the intra-rater variability of the measurements of the subretinal fluid (SRF) pocket, 15 patients were randomly selected from all patients of cohort 3. The ultrasound device captured a series of B-scans during 14 seconds of acquisition. To find the maximum area, height, and angle, the B-scan representing the estimated largest area, height or angle of the SRF pocket was selected four times from the B-scan series with at least one day in between the selections. This was done to include both the grader interpretation and a part of the acquisition of B-scans in the reproducibility analysis. Both the horizontal and vertical cross-section of these 15 patients (30 cross-sections per repetition) were annotated by the primary grader (JHdJ).

To evaluate the inter-rater variability of the measurements of SRF pocket, the same dataset with a total of 30 B-scan series was used by 3 research physicians of the Rotterdam Ophthalmic Institute (H.N., T.K., and Y.C.) to select and annotate the SRF features on both the horizontal and vertical cross-sections.

A univariate Kruskal-Wallis test was done to test for differences between the graders of the ultrasound SRF features. The intraclass correlation coefficient (ICC), and the 95% limits of agreement were determined as well ($\pm 1.96 *$ standard deviation, SD).

Results
The 95% limits of agreement of the intra-rater variability of the ultrasound measurements were 3.6 mm² for the area of SRF, 0.45 mm for the height of SR, 8.2 degrees for the angle between retina and RPE.

The intraclass correlation coefficient (2.1, absolute agreement) of the inter-rater variability was 0.95 (95%CI: 0.89 to 0.98) for area of SRF, 0.97 (95%CI: 0.93 to 0.99) for height of SRF, 0.88 (95%CI: 0.67 to 0.96) for angle between retina and RPE. The 95% limits of agreement of the inter-rater variability of these measures were 7.3 mm² for the area of SRF, 0.67 mm for the height of SRF, 15.3 degrees for the angle between retina and RPE. The Kruskal-Wallis test did not reveal statically significant differences between the graders for any of the ultrasound features.

Chapter

4

The effect of compliance with preoperative posturing advice and head movements on the progression of macula-on retinal detachment

Jan Hendrik de Jong
Koen de Koning
Tom den Ouden
Johan Casper van Meurs
Koenraad Arndt Vermeer

ABSTRACT

Purpose
The aim of this study was to explore the relationship between compliance with preoperative posturing advice and progression of macula-on retinal detachment (RD) and to evaluate whether head positioning or head motility contributes most to RD progression.

Methods
Sixteen patients with macula-on RD were enrolled and admitted to the ward and instructed to posture preoperatively. The primary outcome parameter was compliance, which was defined as the average head orientation deviation from advised positioning. Secondary outcome parameters included the average rotational and linear head acceleration. The head orientation and acceleration were measured with a head-mounted inertial measurement unit (IMU, Shimmer 3, Shimmer Sensing, Ireland). OCT imaging was performed at baseline and during natural interruptions of posturing for meals and toilet visits to measure RD progression toward the fovea.

Results
The Spearman correlation coefficient with RD progression was 0.37 ($P = 0.001$, $r_s^2=0.13$) for compliance, 0.52 ($p<0.001$, $r_s^2=0.27$) for rotational acceleration, and 0.49 ($p<0.001$, $r_s^2=0.24$) for linear acceleration. The correlation coefficient between RD progression and rotational acceleration was statistically significantly higher than the correlation coefficient between RD progression and compliance ($P = 0.034$).

Conclusion
The strength of the correlation between RD progression and compliance was moderate. However, the correlation between RD progression and rotational and linear acceleration was much stronger. Preoperative posturing is effective by reducing head movements rather than enforcing head positioning.

Translational relevance
Monitoring the efficacy of preoperative posturing in macula-on RD using OCT and IMU measurements shows that a new and combined application of these technologies leads to clinically relevant insights.

INTRODUCTION

Retinal detachment (RD) is a progressive separation of the retina from the underlying retinal pigment epithelium that occurs in 12-18 per 100.000 people per year.[1, 2] Visual acuity may be severely affected if the RD extends to the macula.[3-5] To prevent macular involvement, preoperative posturing is prescribed while patients are waiting for surgery. Patients with macula-on RD are prescribed bed rest to reduce head and eye movements and related fluid currents.[6-13] Additionally, patients are positioned supine when RD is located in the superior quadrants of the retina and upright for RD in the inferior quadrants to address the effect of gravity. To improve the compliance with this posturing advice, in some clinics patients are hospitalized during the preoperative period. An alternative approach is to provide surgery on a 24-hour, 7-days-per-week basis. As both approaches are expensive policies, the understanding of the effectiveness of preoperative posturing warrants further study. Recently, we used optical coherence tomography (OCT) to demonstrate that preoperative posturing reduces the progression of macula-on RD by comparing posturing with interruptions for meals and other short breaks.[14] However, the strength of the relationship between compliance to preoperative posturing and RD progression is yet unknown.

Compliance with positioning advice has been quantified previously using gravity- and tilt-compensated sensors after macular hole surgery.[15-17] In this study, we used such sensors to measure the head orientation as well as the head's rotational and linear motility in patients with macula-on RD. Because the density differences between the retina and subretinal fluid are rather small, we would expect gravity to play a limited role in the progress of RD.[18] Therefore, we hypothesize that head movements and eye movements contribute more to progression of RD than does head positioning.

The primary aim of this study was to explore the relationship between compliance with the preoperative posturing advice and the progression of macula-on RD. The secondary objective was to evaluate whether head positioning or head motility contributes most to the progression of RD.

PATIENTS & METHODS

Study design
This study was designed as an explorative cohort study with recordings of head orientation, head motility, and the distance between the RD border and fovea during preoperative posturing of patients with macula on RD. The study was approved by the local internal review board of the Rotterdam Eye Hospital and the medical ethical committee of the Erasmus Medical Center, Rotterdam, The Netherlands (identifier, 2014-502; www.trialregister.nl identifier, NTR4884). The study evaluated a small cohort which was enrolled in addition to a larger prospective trial evaluating preoperative posturing.[14] The recordings of head orientation and head motility were performed only in the patients enrolled in the small additional cohort, which is presented in this report. All patients were hospitalized and examined in the Rotterdam Eye Hospital, Rotterdam, The Netherlands and all provided a written informed consent. The study was conducted in accordance with the tenets of the Declaration of Helsinki.

Study procedures
The study procedures were described previously in more detail.[14] In brief, patients diagnosed with macula-on RD were admitted to the ward for posturing while they were waiting for surgery the same day, the next day or occasionally the day after. Posturing consisted of two parts: bed rest and positioning. Patients with RD located mainly in the superior quadrant were positioned supine, patients with RD in the temporal quadrant on the temporal side of the affected eye, patients with RD in the nasal quadrant on the nasal side and patients with RD in the inferior quadrant were instructed to sit upright. Patients were allowed to interrupt their posturing for meals, toilet visits, refreshment in the morning and surgeon's examinations. Such intervals offer an excellent opportunity to acquire prospective and comparative data in an ethically acceptable manner.

Inclusion and exclusion criteria
Inclusion criteria were: age ≥ 18 years, written informed consent, nearest point of the RD border more than 1250 μm away from the foveola (safety measure) and within the range of the OCT system (estimated range was up to 10-12 mm from the fovea), sufficiently clear media to obtain an OCT scan, sufficient quality of the OCT scan, and OCT performed within an hour after admission of the patient to the ward. No exclusion criteria were specified. The safety border of 1250 μm from the foveola was defined by the traditional size of the fovea centralis (with a radius of approximately 750 μm) and parafovea (ring of 500 μm around the fovea) combined.[19]

Retinal detachment progression measurements

Within one hour after arrival on the ward a baseline volume OCT scan (Wide field Spectralis OCT, Heidelberg Engineering, Heidelberg, Germany) was performed and eligibility was determined. The distance between RD border and fovea was measured according to our previously described method.[14] The 95% limits of agreement of the intra-rater variability of these distance measurements was ±58 μm.[14] The distance measurements on subsequent OCT scans were then used to calculate the RD border displacement and the average RD border displacement velocity (change in distance per hour) during posturing and interruption intervals. The latter measure adjusts for differences in interval duration and thereby enables a more consistent comparison between OCT measurements and average head orientation and head movements per measured interval. The average progression velocity from baseline was determined at each time point as well.

Head-mounted inertial measurement unit

Measuring eye saccades over longer periods of time is not possible without invasive measures. However, measuring head orientation and motion is possible in a noninvasive manner by using a head-mounted electronic sensor, the Shimmer3 inertial measurement unit (IMU) (Shimmer Sensing, Glasnevin, Ireland). This IMU is small, lightweight, commercially available and CE-marked, which indicates conformity with several health and safety regulations within the European Economic Area. After eligibility of a patient was determined, the IMU was fixed on the forehead of the patient with hypoallergenic, waterproof and strongly adhesive plasters.

We configured the IMU to use three individual sensors: a low-noise accelerometer, a gyroscope and a magnetometer at a 512Hz sampling rate. The IMU was calibrated according to the north-west-up coordination system, which means that the X-axis points toward the north, the Y-axis toward the west and the Z-axis up, perpendicular to the earth's surface. To prevent gimbal lock, quaternions were used instead of Euler angels to describe the three-dimensional rotations. The quaternions were calculated using the Shimmer Matlab Instrument Driver software which estimates orientation data using magnetic angular rate and gravity (MARG) filtering. MARG filtering is reported to achieve orientation accuracy levels with less than 0.8° static error and less than 1.7° dynamic error.[19]

Outcome parameters

The primary outcome parameter of the IMU was defined as the orientation deviation from the advised positioning. We considered three secondary outcome parameters: the orientation deviation from the (presumed) optimal positioning, the rotational acceleration, and the linear acceleration.

Orientation deviation from advised positioning

To obtain the deviation from the advised positioning, we used the relative (inverse) direction of gravity measured by the IMU at each time point. At the beginning of the first posturing interval, when the patient was positioned according to the advice, we determined the reference orientation of gravity (**Figure 1A**). Subsequently, we used standard vector calculation to determine the smallest angle between the actual, measured gravity vector (**Figure 1B**) and the reference gravity vector. Note that rotations around the gravity axis are not relevant and are ignored in this analysis. This transformed the orientation deviation, which could vary between 0 and 180 degrees, into a compliance factor between 0 and 1, where 0 means perfect compliance and 1 means poor compliance.
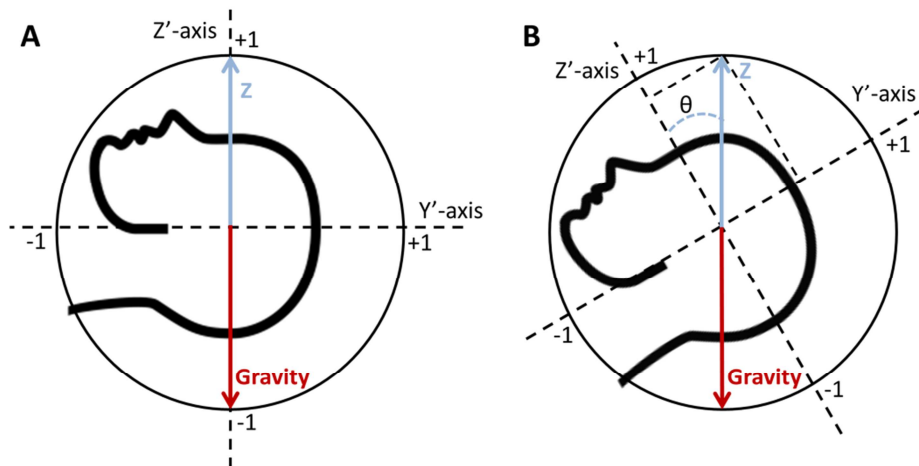
Figure 1. Schematic drawing of the position of the unit Z-vector(blue arrow) and gravity vector (red arrow) within the inertial measurement unit (IMU) coordinate system. When the patient is positioned supine with the IMU fixated on the forehead, the world Z-axis is aligned with the IMU Z'-axis (situation A). The coordinates of the unit Z-vector (blue arrow) on the IMU X'-, Y'- and Z'-axis will be 0, 0 and 1 respectively in situation A. In situation B, a 30° rotation (θ) around the world X-axis has resulted in a 30° tilt of the IMU Y'- and Z'-axis and in a change of the coordinates of the unit Z-vector on the Y'-axis (this will be sin(θ)) and Z'-axis (cos (θ)) . Rotation around the world Z-axis in either situation A or B will not change the coordinates of the unit Z-vector. progression and 12 out of 198 patients (6.1%) showed more than 20% progression from baseline.

Orientation deviation from a presumed optimal positioning

Positioning is mostly prescribed in four categories: supine, temporal side, nasal side and upright. This advice does not account for the distance between the fovea and the RD border or the precise location of the closest point on the RD border. For instance, positioning on the temporal side might be optimal for peripheral temporal RD, but a temporal RD that already has progressed close to the fovea

might be better positioned supine to support reattachment of the retina closest to the fovea. Patients with inferior temporal RD might be better positioned with half-upright on the temporal side instead of a choice between temporal side or upright. We hypothesize that in optimal positioning the gravitation forces are directed perpendicular to the detached retina that is closest to the fovea to facilitate reattachment of this part of the retina (**Figure 2**). Determining the presumed optimal position and using it as the reference position instead of the advised position might reveal whether patients would benefit from the optimization of the posturing advice. A more detailed description of how this parameter was calculated can be found in **Supplemental material 4.1**.
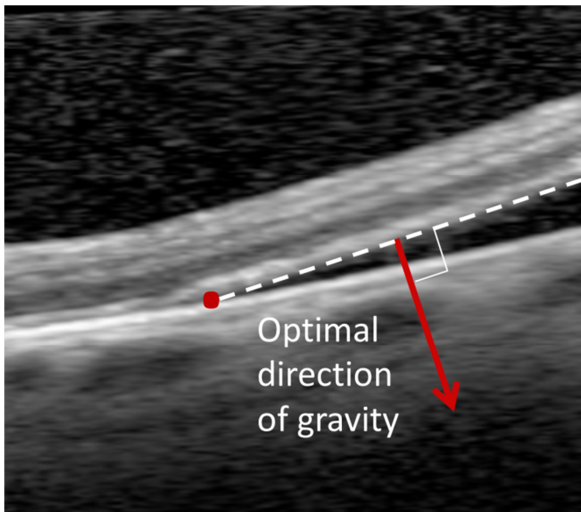
Figure 2. The optimal direction of gravity was defined as perpendicular to the detached retina closest to the fovea (red arrow).

<u>*Rotational and linear acceleration*</u>

Accelerations around the X, Y and Z axes, both clockwise and counterclockwise, were all assumed to be equally relevant and included in the analysis. To obtain the rotational acceleration, the rotational velocity of two consecutive time points were subtracted from each other and divided by the time difference for all gyroscope axes separately. The total rotational acceleration was then defined by the root mean square of the rotational acceleration of the three axes.

To obtain the residual linear acceleration, we first corrected the measured linear acceleration for gravity. The total linear acceleration was then estimated by the root mean square of the residual linear accelerations obtained with the three accelerometer axes.

IMU parameter outcome per interval

Because of the various durations of posturing and interruption intervals, the average of IMU parameter per interval was expected to provide the most consistent comparison to the average RD progression velocity per interval. The measured signal was corrected for the noise floor levels as seen during static test measurements and during the posturing intervals of the patient measurements.

We additionally wanted to determine whether head movements, in general, should be avoided by patients or whether sudden head movements with fast accelerations, in particular, should be avoided to prevent RD progression. Therefore, we determined the number of rotational and linear accelerations per interval per hour above a specific threshold and calculated the correlation with RD progression. We varied the threshold levels to evaluate whether higher thresholds would result in stronger correlation coefficients than the correlation coefficients between RD progression and the noise corrected averages of IMU parameters. We varied the rotational acceleration thresholds between 250 and 10.000 °/s² at increments of 250 °/s² and the linear acceleration thresholds between 0.25 and 10 m/s² at increments of 0.25 m/s².

Statistical analysis

Due to the exploratory nature of this study, 16 patients with continuous measurements between admission to the ward and surgery were assumed to be sufficient to show general trends. We did not assume normally distributed data and therefore, nonparametric testing (Mann Whitney U-test) was used to compare RD progression and IMU parameters between posturing and interruptions intervals. We expected a monotonic but possibly non-linear relationship between RD progression and the IMU parameters. Therefore, Spearman's correlation coefficient was calculated to describe the relationship between RD progression and average IMU parameters. The correlation analysis was performed for all measured intervals as well as for the progression from baseline. For all IMU parameters, a positive correlation demonstrates an association with RD regression and a negative correlation an association with RD progression. Statistical significant differences between correlation coefficients were tested according to the methods of Meng et al.[20] To determine whether the duration of follow-up (defined as the time between baseline OCT and last OCT measurement) influences the rate of RD progression from baseline, we also used the Spearman's correlation coefficient to describe the relationship.

RESULTS

Patient measurements and example patient

Sixteen consecutive patients were enrolled between the 7th of December, 2016 and the 13th of June, 2017. All patients were prescribed bed rest; 3 patients were positioned supine, 7 on the nasal side, 2 on the temporal side and 4 with sitting upright. A total of 94 OCT scans was performed to record the RD displacement toward the fovea during 41 posturing intervals and 37 interruptions. The median duration of follow-up with OCT and the IMU was 18.1 hours (range 2.1 to 35.7 hours). All patients provided a written informed consent. Patients' characteristics are summarized in **Table 1**.

Figure 3 gives an example of the RD progression and head orientation deviation from the advised positioning of a patient with a superior temporal RD. This figure demonstrates that a larger orientation deviation results in more RD progression in this patient. During the day there was moderate progression in both posturing intervals and fast progression during the interruptions. However, 2591 μm regression was seen during the posturing interval that included the night rest and the lowest average IMU parameters were found during this interval as well, which demonstrates the efficacy of immobilization.

RD progression and IMU parameters

A summary of the RD progression measurements is provided in **Table 2**. The median RD border displacement during posturing intervals was 10 μm (interquartile range (IQR), -84 to 177 μm) and during interruptions -52 μm (IQR, -220 to 1 μm), which was statistically significantly different (P = 0.003). The median RD border displacement velocity during posturing intervals was -1 μm/hour (IQR: -9 to 34 μm/hour) and during interruptions -202 μm/hour (IQR, -491 to 0 μm/hour), which was statistically significantly different as well (P<0.001).

The average IMU parameters for all posturing and interruption intervals, as well as the intervals from baseline are described in **Table 3**. The applied noise thresholds were 1.8° for orientation deviation, $200°/s^2$ for rotational acceleration, and $0.8 m/s^2$ for linear acceleration. The difference between posturing intervals and interruptions was statistically significant for all four IMU parameters (P<0.001).

Correlation analysis

The correlations of RD border displacement velocity and the IMU parameters are provided in **Table 3** as well. **Figure 4** shows the scatter plots of RD progression and IMU parameters. The strongest Spearman's rho correlation coefficients (r_s) between RD progression and the IMU parameters were found for rotational acceleration ($r_s = 0.52$) and linear acceleration ($r_s = 0.49$). The r_s^2 can be interpreted

as a proportion of explained variance if the IMU parameters and the RD progression are presented as ranked variables. The higher this proportion, the more variance is explained by a specific variable. The r_s^2 was 0.13 for orientation deviation from the advised positioning, 0.13 for the orientation deviation from optimal positioning, 0.27 for the rotational acceleration and 0.24 for the linear acceleration. This means that rotational acceleration, as well as linear acceleration, seems to explain twice as much of the variance of RD progression than orientation deviation from advised or optimal positioning. The correlation coefficient between RD progression and rotational acceleration was statistically significantly higher than the correlation coefficient between RD progression and compliance ($P = 0.034$, see also **Table 3**).
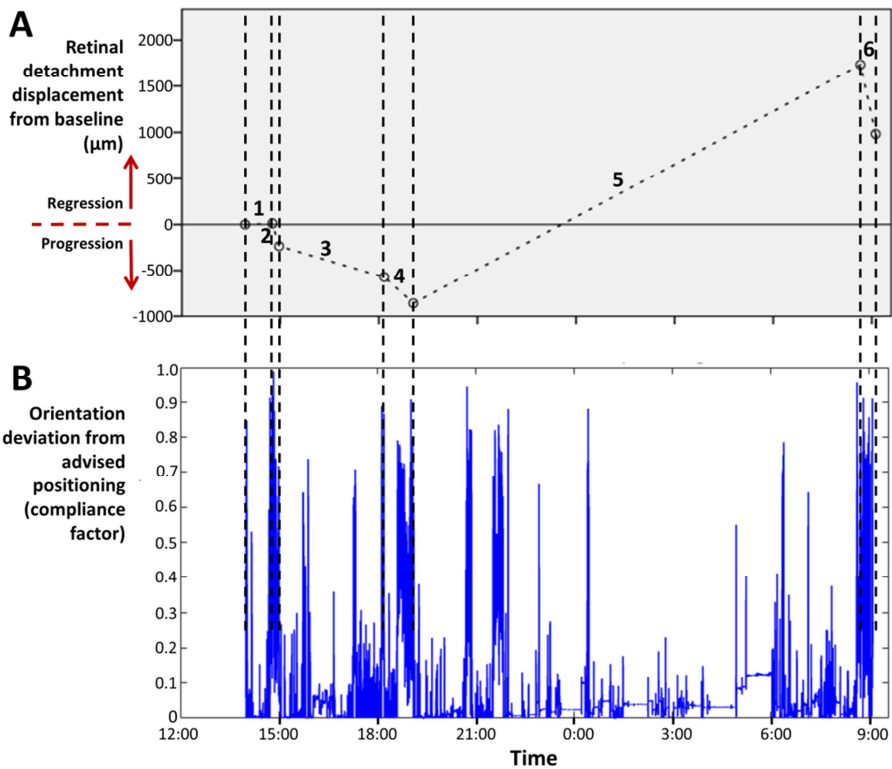
Figure 3. Example of the course of progression and the inertial measurement unit (IMU) parameters of a 56 years old patient. The patient had a retinal detachment in the superior temporal quadrant of the right eye and supine posturing. During the day most intervals showed progression, while during the night regression of 2591 μm was seen (**A**). The orientation deviation was lower during posturing intervals than during interruptions, especially during the night (**B**, interval 5).

Table 1. Patient and retinal detachment characteristics

Characteristic	Data
Patients included the study (no.)	16
Age (years)	
Median (range)	56 (18-73)
Male : Female (no.)	12 : 4
Phakic : Pseudophakic (no.)	9 : 7
Snellen visual acuity	
Median (range)	20/25 (20/33 – 20/17)
Moderate myopia (≤6.0D and ≥3.0D) (no.)	3
High myopia (≥6.0D) (no.)	5
Duration of visual field loss (days)	
Median (range)	5 (0.25 – 40)
No complaints of visual field loss (no.)	1
Primary : recurrent RD (no.)	14 : 2
History of vitrectomy (no.)	1
History of scleral buckling (no.)	1
Posterior vitreous detachment (yes/no)	16
Extent of RD (degree)	
Median (IQR)	62 (57 – 121)
Range	47 – 151
Size of retinal tear (no.)	
Single small (≤0.50 clock hr.)	2
Multiple/large (>0.50 clock hr.)	12
No breaks found	2
Posturing advice (no.)	
Supine	2
Temporal side	3
Nasal side	7
Sitting upright	4
Baseline RD-fovea distance on OCT (μm)	
Median (IQR)	6535 (3304 to 8306)
Range	1813 to 12190
Time between baseline OCT and surgery (hours)	
Median (IQR)	21.3 (18.4 to 23.0)
Range	4.6 to 36.6
Time between baseline OCT and last OCT (hours)	
Median (IQR)	18.1 (13.3 to 19.4)
Range	2.1 to 35.7
Change of RD-fovea distance from baseline to the last OCT (μm)	
Median (IQR)	-19 (-56 to 562)
Range	-847 to 1934

IQR = interquartile range, RD = retinal detachment
* In patients with pseudophakic lens status, the spherical equivalent refraction before cataract surgery was used.

Table 2. Comparison of RD progression and IMU outcome parameters
between posturing intervals and interruptions

	RD border displacement (µm)	Duration (hour)	RD border displacement velocity (µm/hour)
Posturing intervals (N=41)			
Median (IQR)	10 (-84 to 177)	3.5 (1.8 to 11.4)	1 (-24 to 64)
Range	-538 to 2590	0.7 to 15.1	-147 to 871
Interruptions (N=37)			
Median (IQR)	-52 (-220 to 1)	0.4 (0.2 to 0.5)	-202 (-491 to 0)
Range	-749 to 96	0.1 to 1.0	-1625 to 227
Difference between posturing intervals and interruptions			
P-value	0.002	<0.001	<0.001

Table 2. Extended

	Average orientation deviation from advised positioning (compliance factor)	Average orientation deviation from optimal positioning (optimal compliance factor)	Average rotational acceleration (°/s²)	Average linear acceleration (m/s²)
Posturing intervals (N=41)				
Median (IQR)	0.04 (0.02 to 0.05)	0.20 (0.10 to 0.37)	66 (56 to 97)	0.06 (0.04 to 0.10)
Range	0.01 to 0.20	0.04 to 0.56	43 to 193	0.01 to 0.33
Interruptions (N=37)				
Median (IQR)	0.30 (0.10 to 0.38)	0.46 (0.31 to 0.65)	181 (145 to 213)	0.26 (0.17 to 0.42)
Range	0.01 to 0.52	0.09 to 0.84	79 to 427	0.05 to 0.73
Difference between posturing intervals and interruptions				
P-value	<0.001	<0.001	<0.001	<0.001

Table 3. Correlation analysis of four IMU outcome parameters
against RD border displacement velocity

	Average orientation deviation from advised positioning (compliance factor)	Average orientation deviation from optimal positioning (optimal compliance factor)
Posturing intervals and interruptions (N=78)		
Correlation with RD border displacement velocity		
Spearmans rho (95% CI)	-0.37* (-0.56 to -0.13)	-0.36* (-0.53 to -0.14)
P-value†	0.001	0.001
Difference between correlation coefficients (column 1 against 2, 3 and 4)		
Spearmans rho difference (95% CI)	NA	-0.01 (-0.24 to 0.22)
P-value (single-sided)†		0.465
Change from baseline (N=78)		
Correlation with RD border displacement velocity		
Spearmans rho (95% CI)	-0.06 (-0.30 to 0.19)	0.11 (-0.13 to 0.34)
P-value†	0.58	0.35
Difference between correlation coefficients (column 1 against 2, 3 and 4)		
Spearmans rho difference (95% CI)	NA	-0.17 (-0.45 to 0.14)
P-value (single-sided)†		0.143

Table 3. Extended

	Average rotational acceleration ($°/s^2$)	Average linear acceleration (m/s^2)
Posturing intervals and interruptions (N=78)		
Correlation with RD border displacement velocity		
Spearmans rho (95% CI)	-0.52* (-0.68 to -0.30)	-0.49* (-0.69 to -0.25)
P-value†	<0.001	<0.001
Difference between correlation coefficients (column 1 against 2, 3 and 4)		
Spearmans rho difference (95% CI)	0.15 (-0.01 to 0.37)	0.12 (-0.03 to 0.32)
P-value (single-sided)†	0.034	0.054
Change from baseline (N=78)		
Correlation with RD border displacement velocity		
Spearmans rho (95% CI)	-0.36* (-0.15 to -0.53)	-0.30 (-0.50 to -0.11)
P-value†	0.001	0.007
Difference between correlation coefficients (column 1 against 2, 3 and 4)		
Spearmans rho difference (95% CI)	0.29 (0.04 to 0.52)	0.24 (0.05 to 0.42)
P-value (single-sided)†	0.012	0.008

* this correlation is still statistically significant after Bonferroni correction for the 14 correlation analyses (P-level 0.05/14 = 0.004)

† P-value without Bonferroni correction
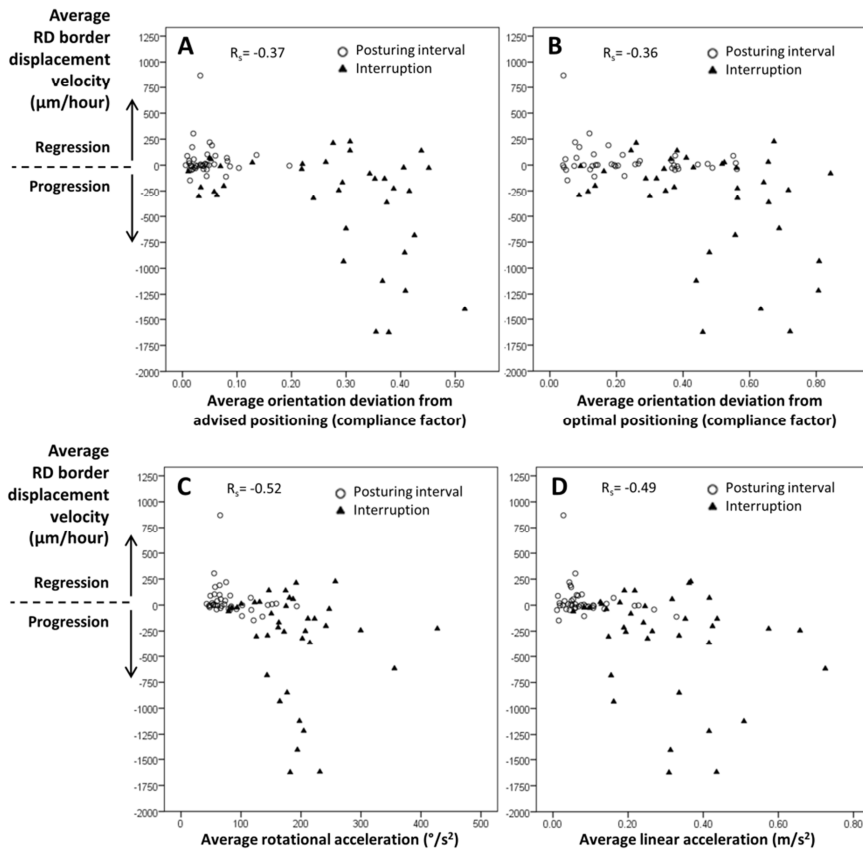
Figure 3. Example of the course of progression and the inertial measurement unit (IMU) parameters of a 56 years old patient. The patient had a retinal detachment in the superior temporal quadrant of the right eye and supine posturing. During the day most intervals showed progression, while during the night regression of 2591 μm was seen (**A**). The orientation deviation was lower during posturing intervals than during interruptions, especially during the night (**B**, interval 5).

The Spearman's correlation coefficient between orientation deviation from advised positioning with the other three IMU parameters was 0.52 (r_s^2=0.27) for orientation deviation from optimal positioning, 0.68 (r_s^2=0.46) for rotational acceleration and 0.72 (r_s^2=0.49) for linear acceleration. This means that the secondary IMU parameters are codependent with the primary IMU parameter (orientation deviation from advised positioning), but they are not the same.

The average head orientation deviation was not significantly correlated with RD progression from baseline (**Table 3**, row 2). However, RD progression from

baseline was statistically significantly correlated with the average rotational acceleration (r_s = -0.36; P = 0.001).

The correlation between the duration of follow-up and the change of RD-fovea distance from baseline to the last OCT measurement was 0.08 (95% confidence interval (CI) -0.42 to 0.58; P = 0.76).

Correlation with the number of accelerations per interval
We studied the correlation between RD progression and the average number of accelerations above various thresholds per posturing and interruption interval. The strongest Spearman's correlation coefficient was 0.51 at a threshold level of 2000 °/s^2 for rotational acceleration and 0.51 at a threshold level of 1.25 m/s^2 for linear acceleration (see for full analysis **Supplemental material 4.2**). The increase of threshold levels did not result in substantially higher correlation coefficients than the correlation between RD progression and average IMU parameters per interval as presented in **Table 3**.

DISCUSSION

To our knowledge, the compliance with preoperative posturing advice in patients with macula-on RD and the correlation with RD progression has not been studied previously. We showed that the strength of the correlation between RD progression and head orientation deviation from advised and optimal positioning was moderate. However, the correlation of RD progression with rotational and linear acceleration was much stronger, both for the progression during posturing and interruption intervals and the progression from baseline. Therefore, we conclude that preoperative posturing is effective by reducing head movements rather than enforcing head positioning.

The clinical significance of the strong correlation between RD progression and head motility is that patients will benefit from moving their head as little as possible during the preoperative period. This can be accomplished by bed rest and by avoiding unnecessary activities involving head motion. Any required transportation may be done by bed or wheelchair (preferably with suspension) to minimize the amount of head and eye movements. Previous research showed that a reduction of eye movements (saccades) by double patching the eyes or suturing the eye muscles to the bulbus resulted in a reduction of subretinal fluid.[6-11] Apparently, a reduction of head movements is also beneficial to prevent RD progression.

Several other factors may affect RD progression. Most importantly, we measured head movements, whereas saccades are traditionally expected to be able to overcome the forces of retinal adhesion.[21, 22] The rotational velocity and

acceleration of saccades are typically faster than those of active head rotations.[23-27] However, the radius of the head is greater than the radius of the eye, whereas the magnitude of saccades is smaller than that of head movements.[28] Therefore, the tangential linear acceleration of the components of RD may be in the same range. During a head rotation, the movement of the eye approximates a translational movement. The direction of acceleration and deceleration forces of the fluids at opposite sides of the eye will be almost parallel during rotational head movements and precisely parallel during linear head movements. As a result, the effect on fluid currents within the eye may be limited. During a saccadic eye rotation, however, the direction of acceleration and deceleration forces will be opposite on the opposite sides of the eye, which is likely to create strong fluid currents of both liquefied vitreous and subretinal fluid. Nevertheless, the number and strength of saccades can partly be predicted by the number and strength of head movements as measured in the current study.[29, 30] Therefore, if saccades would be measured independently from head movements, we expect that only a small additional part of the variance of RD progression could be explained.

There are at least four other factors that may play a role in RD progression. Firstly, the retinal adhesion strength differs between retinal locations and is especially higher at the macula. It is a common observation among surgeons that the peripheral retina detaches much more easily than does the posterior retina when creating an RD for macular rotaton or retinal pigment epithelium-choroid-graft, suggesting a difference in adhesion.[31] We previously demonstrated that a small RD in the periphery has a higher progression risk, suggesting a difference in retinal adhesion as well.[14] Secondly, the amount of subretinal fluid and the shape of the detachment differs between RDs. It is expected that the retina reattaches faster in a flat RD than in a bullous RD with the same area of detachment, because the subretinal fluid volume is smaller and will be reabsorbed earlier.[12, 33-36] Thirdly, the size, number, and type of retinal breaks differ between RD patients, where a large horseshoe shaped retinal tear is more likely to facilitate inflow of liquefied vitreous into the subretinal space than do small round holes.[12, 13, 37] Finally, the contractile properties of the detached, incompletely detached or not detached vitreous differs among patients, mostly due to the effects of aging of the vitreous.[38, 39] Progressive traction of contractile vitreous may detach the retina surrounding the retinal break, allowing more liquefied vitreous to enter the subretinal space.[12, 13] Because of all these factors, head and eye movements can only be partly accountable for the variance in RD progression.

Evaluation of the orientation deviation from optimal positioning did not reveal a stronger correlation with RD progression than did the orientation deviation from advised positioning. This suggests that the optimization of positioning would not significantly reduce RD progression. It also suggests that the role of gravity is

limited, which is expected because the density difference between the retina and subretinal fluid is small.[18]

Evaluation of the number of accelerations per interval above various thresholds did not reveal a substantially higher correlation with RD progression than did the average of IMU parameters per interval. This might indicate that relatively slow head accelerations are also able to induce RD progression, or it might be that patients did not frequently perform sudden head movements during their hospitalization and the number of fast head accelerations was too low to reveal a stronger relationship. We cannot conclude that only strong or sudden head movements should be avoided. Evaluation of the relationship between the duration of follow-up and the change of RD-fovea distance from baseline did not reveal a statistically significant relationship. As pointed out above, RD progression can be explained by factors other than the duration of follow-up.

Our method by which we measured head orientation might be used, in combination with OCT distance measurements, to evaluate the effect of delayed surgery for 1 day with preoperative posturing at home. This alternative policy might be cost-saving for both clinics that aim to provide 7 days per week surgery service and clinics that hospitalize patients preoperatively. However, such a study should take into account the expected differences in characteristics and behavior between hospitalized patients and patients who are asked to stay quiet at home. IMU devices might also be used for other areas of ophthalmology where the effect of posturing regimes warrants validation, such as postoperative positioning after macular hole surgery,[15-17] after RD surgery when intraocular gas is used, after pneumatic displacement of submacular hemorrhages, and after corneal transplantation when air bubbles are used to facilitate attachment of the graft.

Strengths of this study include the objective measurements of head orientation, head movements, and RD progression and the reasonable amount of 78 monitored intervals. Limitations include the small number of patients, the variation in RD localization and subsequent positioning advice, and the differences in follow-up duration. In addition, the patient might have touched the device causing false rotational and linear accelerations. Since this would result only in short acceleration peaks, we think that the influence on the averages and number of accelerations per interval is small.

In conclusion, preoperative posturing advice should emphasize a reduction of head movements, although positioning might be beneficial to prevent RD progression as well. This study may be an important step toward an evidence-based policy for optimal preoperative posturing in patients with macula-on RD.

REFERENCES

1. Van de Put MA, Hooymans JM, Los LI, Dutch Rhegmatogenous Retinal Detachment Study Group. The incidence of rhegmatogenous retinal detachment in The Netherlands. Ophthalmology. 2013;120:616-622.

2. Haimann MH, Burton TC, Brown CK. Epidemiology of retinal detachment. Arch Ophthalmol. 1982;100:289-292.

3. Salicone A, Smiddy WE, Venkatraman A, Feuer W. Visual recovery after scleral buckling procedure for retinal detachment. Ophthalmology. 2006;113:1734-1742.

4. Zhou C, Lin Q, Chen F. Prevalence and predictors of metamorphopsia after successful rhegmatogenous retinal detachment surgery: a cross-sectional, comparative study. Br J Ophthalmol. 2016.

5. Rezar S, Sacu S, Blum R, Eibenberger K, Schmidt-Erfurth U, Georgopoulos M. Macula-On Versus Macula-Off Pseudophakic Rhegmatogenous Retinal Detachment Following Primary 23-Gauge Vitrectomy Plus Endotamponade. Curr Eye Res. 2016;41:543-550.

6. Adams GL, Yee RD, Hahn PM, Pearlman JT. Effect of binocular and monocular patching on eye movements. Arch Ophthalmol. 1973;90:117-120.

7. Algvere P, Rosengren B. Active immobilization of the eye in the treatment of retinal detachment. Mod Probl Ophthalmol. 1977;18:286-291.

8. Algvere P, Rosengren B. Immobilization of the eye. Evaluation of a new method in retinal detachment surgery. Acta Ophthalmol (Copenh). 1977;55:303-316.

9. Lean JS, Mahmood M, Manna R, Chignell AH. Effect of preoperative posture and binocular occlusion on retinal detachment. Br J Ophthalmol. 1980;64:94-97.

10. Chen CY, Chen SN, Lin SM, Ho CL. Reduction of subretinal fluid after preoperative immobilization of the eyes with rhegmatogenous retinal detachment. Chang Gung Med J. 2001;24:799-804.

11. Lincoff H, Stopa M, Kreissig I. Ambulatory binocular occlusion. Retina. 2004;24:246-253.

12. Machemer R. The importance of fluid absorption, traction, intraocular currents, and chorioretinal scars in the therapy of rhegmatogenous retinal detachments. XLI Edward Jackson memorial lecture. Am J Ophthalmol. 1984;98:681-693.

13. Kuhn F, Aylward B. Rhegmatogenous retinal detachment: a reappraisal of its pathophysiology and treatment. Ophthalmic Res. 2014;51:15-31.

14. de Jong JH, Vigueras-Guillén JP, Simon TC, et al. Preoperative Posturing of Patients with Macula-On Retinal Detachment Reduces Progression Toward the Fovea. Ophthalmology. 2017.

15. Leitritz MA, Ziemssen F, Voykov B, Bartz-Schmidt KU. Usability of a gravity- and tilt-compensated sensor with data logging function to measure posturing compliance in patients after macular hole surgery: a pilot study. Graefes Arch Clin Exp Ophthalmol. 2014;252:739-744.

16. Forsaa VA, Krohn J. POSTOPERATIVE POSITIONING IN MACULAR HOLE SURGERY: An Objective Evaluation of Nonsupine Positioning and the Effect of the "Tennis Ball Technique". Retina. 2016;36:1081-1086.

17. Alberti M, la Cour M. GAS-FOVEAL CONTACT: A New Approach to Evaluating Positioning Regimens in Macular Hole Surgery. Retina. 2017.

18. Su X, Vesco C, Fleming J, Choh V. Density of ocular components of the bovine eye. Optom Vis Sci. 2009;86:1187-1195.

19. Madgwick SO, Harrison AJ, Vaidyanathan A. Estimation of IMU and MARG

orientation using a gradient descent algorithm. IEEE Int Conf Rehabil Robot. 2011;2011:5975346.

20. Meng XL, Rosenthal R, Rubin DB. Comparing correlated correlation coefficients. Psychological Bulletin. 1992;111(1):172-175.

21. Machemer R. The importance of fluid absorption, traction, intraocular currents, and chorioretinal scars in the therapy of rhegmatogenous retinal detachments. XLI Edward Jackson memorial lecture. Am J Ophthalmol. 1984;98:681-693.

22. Repetto R, Tatone A, Testa A, Colangeli E. Traction on the retina induced by saccadic eye movements in the presence of posterior vitreous detachment. Biomech Model Mechanobiol. 2011;10:191-202.

23. Demer JL, Viirre ES. Visual-vestibular interaction during standing, walking, and running. J Vestib Res. 1996;6:295-313.

24. Wilson SJ, Glue P, Ball D, Nutt DJ. Saccadic eye movement parameters in normal subjects. Electroencephalogr Clin Neurophysiol. 1993;86:69-74.

25. Abrams RA, Meyer DE, Kornblum S. Speed and accuracy of saccadic eye movements: characteristics of impulse variability in the oculomotor system. J Exp Psychol Hum Percept Perform. 1989;15:529-543.

26. Bussone W. Linear and Angular Head Accelerations in Daily Life. Master of Science Thesis, Faculty of Mechanical Engineering of the Virginia Polytechnic Institute and State University. 2005.

27. Arndt S, Cargill R, Selim Hammoud P. Head Accelerations Experienced during Everyday Activities and While Riding Roller Coaster. Proceedings of the Human Factors and Ergonomics Society Annual Meeting. 2004;48:1973-1977.

28. Bahill AT, Adler D, Stark L. Most naturally occurring human saccades have magnitudes of 15 degrees or less. Invest Ophthalmol. 1975;14:468-469.

29. Freedman EG, Sparks DL. Coordination of the eyes and head: movement kinematics. Exp Brain Res. 2000;131:22-32.

30. Pelz J, Hayhoe M, Loeber R. The coordination of eye, head, and hand movements in a natural task. Exp Brain Res. 2001;139:266-277.

31. Ryan SJ. RETINA. 5th ed. Los Angeles, CA, USA: ELSEVIER Saunders; 2013:2010-2018.

32. Yoon YH, Marmor MF. Rapid enhancement of retinal adhesion by laser photocoagulation. Ophthalmology. 1988;95:1385-1388.

33. Quintyn JC, Brasseur G. Subretinal fluid in primary rhegmatogenous retinal detachment: physiopathology and composition. Surv Ophthalmol. 2004;49:96-108.

34. Ehrlich R, Niederer RL, Ahmad N, Polkinghorne P. Timing of acute macula-on rhegmatogenous retinal detachment repair. Retina. 2013;33:105-110.

35. The repair of rhegmatogenous retinal detachments. American Academy of Ophthalmology. Ophthalmology. 1996;103:1313-1324.

36. Marmor M. Mechanisms of normal retinal adhesion. 2001:pp 1849–1869.

37. Foster WJ. Bilateral patching in retinal detachment: fluid mechanics and retinal "settling". Invest Ophthalmol Vis Sci. 2011;52:5437-5440.

38. Pokki J, Ergeneman O, Sevim S, Enzmann V, Torun H, Nelson BJ. Measuring localized viscoelasticity of the vitreous body using intraocular microprobes. Biomed Microdevices. 2015;17:85-015-9988-z.

39. Sebag J. Age-related changes in human vitreous structure. Graefes Arch Clin Exp Ophthalmol. 1987;225:89-93

SUPPLEMENTAL MATERIAL 4.1

Description of the calculation of orientation deviation from optimal positioning

To determine the optimal unit Z-vector we used the OCT scan to measure the angle between the RPE and retina in the part of the detachment closest to the fovea (**Supplemental figure 4.1A**). We assumed that according to the standard orientation of the IMU on the forehead of the patient, the IMU Z' axis would be aligned with the anterior-posterior axis of the eye. We also assumed that the average eye gaze direction was straight ahead during any position of the head. We calculated the angle between the presumed optimal vector and the Z'-axis using formula (1), see also **Supplemental figure 4.1**.

$$\beta = 2 \cdot \arcsin\left(\frac{0,5 \cdot L}{R}\right) + \alpha \tag{1}$$

Where β is the angle between the optimal vector and the Z'-axis in degree, L is the shortest distance between the fovea and the RD border in mm, R is the radius of the eye, which was set to 12 mm for all patients and α is the angle between the retinal pigment epithelium and the retina in degree (**Supplemental figure 4.1A**).

The coordinates of the unit Z-vector were then calculated for the situation that the patient would be positioned with the unit Z-vector pointing in the opposite direction of the direction of gravity using formula (2), see also **Supplemental figure 4.1**.

$$\begin{bmatrix} Z_{X'} \\ Z_{Y'} \\ Z_{Z'} \end{bmatrix} = \begin{matrix} -\sin(\beta) \cdot \sin(\gamma) \\ -\sin(\beta) \cdot \cos(\gamma) \\ \cos(\beta) \end{matrix} \tag{2}$$

Where $Z_{X'}$, $Z_{Y'}$, $Z_{Z'}$ are the X', Y' and Z'-coordinates of the unit Z-vector during a presumed optimal positioning (for an explanation of the unit Z-vector and IMU axis X', Y' and Z', see also Figure 1 in the manuscript), β the angle between the optimal vector and the Z'-axis in degree (derived from formula 1), γ the clockwise angle between 12 o-clock and the line between fovea and the closest point to the fovea on the RD border (in degree, see **Supplemental figure 4.1B**).

The deviation from the presumed optimal positioning was then calculated for all time points in degrees and a cosine transformation (compliance factor = 0.5 - cos(angle)/2) was performed as well which resulted in a compliance factor between 0 and 1 (where 0 means perfect compliance and 1 means poor compliance).
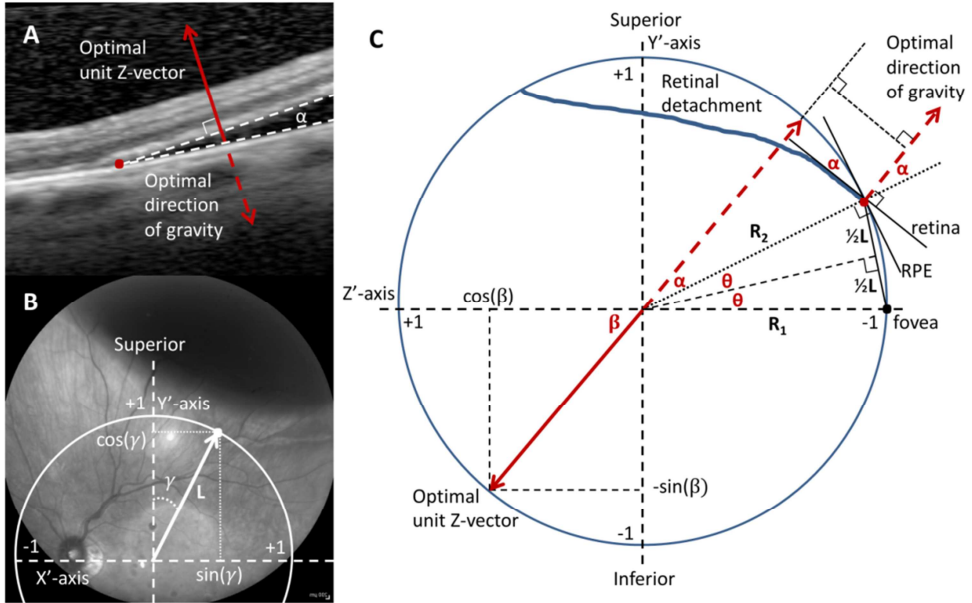
Supplemental figure 4.1. Definition of the coordinates of the presumed optimal unit Z-vector on the IMU X', Y' and Z'-axis. The optimal direction of gravity was defined as perpendicular to the first part of the detached retina in the direction of the retinal pigment epithelium (**A**, dashed red arrow) and the optimal unit Z-vector as the inverse vector (**A**, red arrow).

To determine the coordinates of the presumed optimal unit Z-vector, we first defined the angle between the Z'-axis and the normal (**C**, R_2) of the closest point to the fovea on the RD border (**C**, red dot). The distance between the fovea (**C**, black dot) and the closest point to the fovea on the RD border (C, red dot) was measured with OCT and is called L (see **B** and **C**). This line L forms a isosceles triangle with the Z' axis (**C**, R_1) and the black dotted normal-line (C, R_2). If we bisect this triangle, we can calculate θ by the following formula: $\theta = \sin^{-1} (0.5 \times L / R)$, where R is the radius of the eye, which was defined as 12 mm for all patients.

Next step was to rotate the normal further towards the direction of gravity by angle α. We assumed that the tangents of the closest point on the RD border (**C**, red dot) closely resembles the curvature of the retinal pigment epithelium (RPE) in the first part of the detachment (**A**, lower dashed line and C, RPE-line). Since the RPE-line has an angle of 90 degrees with the normal (**C**, RPE-line and R_2), the normal has to rotate with angle α to find the presumed optimal direction of gravity. The angle β between the Z'-axis and the unit Z-vector was then calculated with the following formula: $\beta = 2 \times \theta + \alpha = 2 \times \sin^{-1} (0.5 \times L / R) + \alpha$. The Z' coordinate of the unit Z-vector was then defined as $Z_{Z'} = \cos(\beta)$. To find the X' and Y' coordinates, we measured the deviation γ of L from the superior or 12 o-clock line (see γ and L in B). Then the X' coordinate of the unit Z-vector could be defined as $Z_{X'} = -\sin(\beta) \times \sin(\gamma)$ and the Y' coordinate as $Z_{Y'} = -\sin(\beta) \times \cos(\gamma)$.

SUPPLEMENTAL MATERIAL 4.2
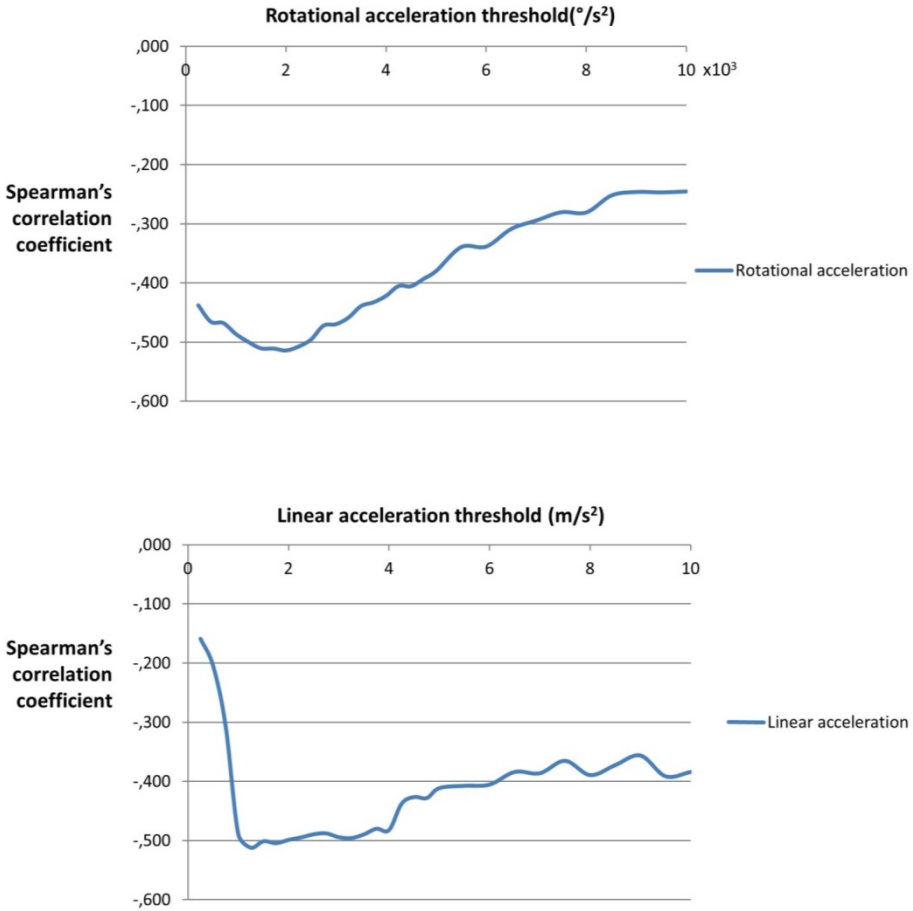
Supplemental figure 4.2. The correlation between RD progression and the average number of accelerations above various thresholds. The strongest Spearman's correlation coefficient found was -0.51 at a threshold level of 2000 °/s² for rotational acceleration (top figure) and -0.51 at a threshold level of 1.25 m/s² for linear acceleration (lower figure)

.

Chapter

5

Numerical study of the effect of head and eye movement on progression of retinal detachment

J. Vroon*
J. H. de Jong*
A. Aboulatta
A. Eliasy
F. C. T. van der Helm
J. C. van Meurs
D. Wong
A. Elsheikh

*Joint principal authorship

ABSTRACT

Rhegmatogenous retinal detachment (RD) is a sight-threatening condition. In this type of RD a break in the retina allows retrohyaloid fluid to enter the subretinal space. The prognosis concerning the patients' visual acuity is better if the RD has not progressed to the macula. The patient is given a posturing advice of bed rest and semi-supine positioning (with the RD as low as possible) to allow the utilization of gravity and immobilization in preventing progression of the RD. It is, however, unknown what external loads on the eye contribute the most to the progression of an RD. The goal of this exploratory study is to elucidate the role of eye movements caused by head movements and saccades on the progression of an RD. A finite element model is produced and evaluated in this study. The model is based on geometric and material properties reported in the literature. The model shows that a mild head movement and a severe eye movement produce similar traction loads on the retina. This implies that head movements—and not eye movements—are able to cause loads that can trigger and progress an RD. These preliminary results suggest that head movements have a larger effect on the progression of an RD than saccadic eye movements. This study is the first to use numerical analysis to investigate the development and progression of RD and shows promise for future work.

INTRODUCTION

Retinal detachment (RD) is a serious condition that can lead to blindness, in the affected eye, if left untreated. The most common type of retinal detachment is rhegmatogenous.[1] Approximately 12–18 in 100,000 people per year are diagnosed with a primary rhegmatogenous RD.[2,3] In this type of RD the interaction between the vitreous and the retina creates a break in the retina, allowing retrohyaloid fluid to enter the subretinal space.

The prognosis concerning the patients' visual ability is better if RD has not progressed to the macula.[4] Therefore, common management methods aim to keep the macula attached by slowing or halting the progression of the RD. Patients with an RD with an attached macula are scheduled for surgery as soon as possible. While waiting for surgery, these patients are advised to follow a posturing advice of bed rest and positioning on the side where the RD is mainly located. This posturing advice is often inconvenient and uncomfortable for the patient, and costly if combined with hospital admission.

Traction of the vitreous is likely to prevent reattachment of the retina. The properties of the vitreous might allow settling of the retina driven by gravity. As the retina is slightly denser than the surrounding liquefied vitreous and subretinal fluid, positioning and bed rest are prescribed to utilize the force of gravity. It is considered unlikely, however, that gravity will much affect intraocular fluid dynamics because the density difference between retina and vitreous is small.[5] It has long been theorized that bed rest reduces the loads on the retina caused by eye movements caused by head movements and saccades, therefore, halting progression and even causing regression of an RD.[6,7] Recently, it was shown that bed rest and positioning will reduce the progression of RD. De Jong and associates[8] also showed that during periods of interruption of bed rest the RD progresses. The progression of RD during these interruptions was caused by every day activities, like toilet visits and meal consumption. Therefore, we hypothesize that every day head movements, rather than saccadic eye movements, are a significant factor in the progression of an RD.

Performing clinical studies to investigate this hypothesis is likely to impose unacceptable risks to the patient: risking blindness by intentionally causing progression of a patients RD would be unethical, and therefore, a modeling study is indicated.

In the past, finite element models have been used to investigate impact damage in human eyes.[9-13] These models have also proven useful when investigating RD due to impact.[14,15] Finite element modeling provides a tool to investigate the human eye without ethical constraints. These previous studies investigated loads due to trauma, but the effect of every day eye and head movements on the progression of an existing RD has not yet been studied using finite element

modeling. Numerical simulation will help to identify what conditions specifically promote extension of retinal detachment in patients where the most critical part of the retina, namely the macula, is still attached. The aim of this study is to produce a finite element model that accurately represents the human eye with an RD and elucidate the role of head and saccadic eye movements in the development and progression of an RD.

MATERIAL AND METHODS

In this study we built finite element models of the eye and defined its geometry, the material properties, and two load cases, representing a saccadic eye movement and a head movement. Finally, we performed a parameter sensitivity analysis. The traction load on the retina generated by the two load cases was compared to each other. The general kinematics of the models were compared to ultrasound images obtained in vivo for human eyes (Accutome B-scan Plus, Malvern, USA, and Quantel Medical cinescan B-scan, Cournon d'Auvergne, France).

All models were run with a commercial finite elements software (ABAQUS Release 6.14-2, Dassault Systemes, Johnston, Rhode Island, USA). All models' geometry were generated with a custom made code run by a commercial programming software package (MATLAB Release 2015b, The MathWorks, Inc., Natick, Massachusetts, USA).

Geometry
First, we created a model involving the cornea, limbus, sclera, retina and vitreous with the dimensions shown in **Figure 1a**. The 3D model is axisymmetric around the anterior–posterior axis (**Figure 1a**). For the purpose of simplicity, the increased thickness around the optic nerve head has not been modeled. The thickness of the retina is indicated in **Figure 1c**, based on Chen et al.[16,17], Liu et al.[18] and Grover et al. [19]. The impact of tissues in the orbit surrounding the eye was assumed to be minimal during everyday head and eye movements. Therefore, these structures were not implemented in the model.

The mesh was based on the configuration of diamatic domes as described by Nooshin and Tomatsuri[20] and used previously by Elsheikh and Wang[21]. The cornea consisted of eleven rings of elements, the limbus consists of two rings and the sclera consists of 19 rings (**Figure 2**). The cornea, limbus, sclera, and retina are represented by elements organized in one layer. All elements had a triangular prismatic shape (type C3D6). The vitreous filled the entire inner volume of the model and was made up of ten layers of elements. The three outermost element layers consist of 32 rings of elements (similar to cornea, limbus, and sclera).
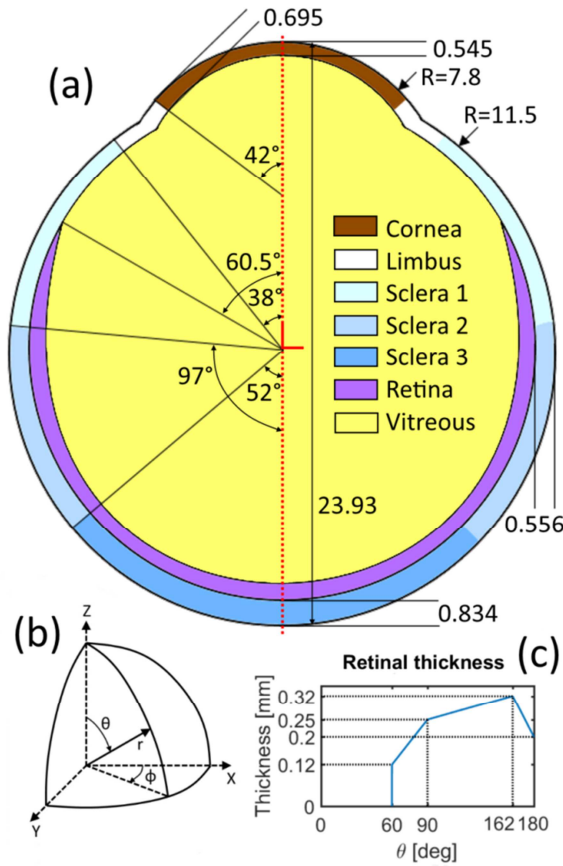
Figure 1. (a) Schematic image (not to scale) of a cross section of the model through the xz-plane. All measurements are in millimetres and all angles in degrees. The colours indicate different sections of the model with different material properties (see **Table 1**). The red lines indicate the location of the origin of the coordinate system. The model is axisym-metric around the z-axis (red dotted line). (**b**) Direction and orientation of the Cartesian and polar coordinates used in the model. The z-axis runs anterior–posteriorly. **c** Graph of the thickness of the retina, as a function of θ (**b**). The graph starts at 60° because at lower θ angles the retina is not present.

Figure 2. A 3D rendering of the model showing the mesh layout. The mesh was based on the design for a diamatic dome as described by Nooshin and Tomatsuri.[20] The cornea (brown) plus one ring of the limbus count twelve rings of elements. The sclera (various shades of blue) plus one ring of the limbus count 20 rings, making for a total of 32 rings of elements. All elements have a triangular prism shape.
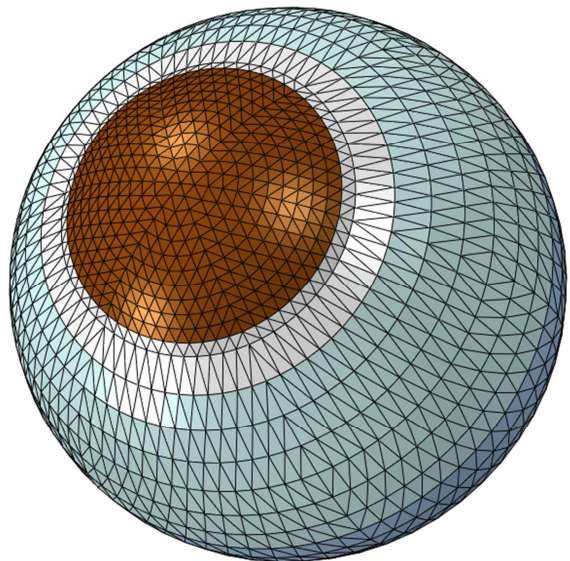
The next set of three layers, towards the center, consist of 16 rings of elements and the three innermost layers consisted of eight rings of elements. The center was filled with 192 tetrahedral elements to fill the remaining space. The elements were attached to the adjacent elements using a tie constraint. See **Table 1** for an overview of all elements in the model.

We now have the model as shown in **Figure 3a**. Next, the vitreous was shrunk posteriorly to create a posterior vitreous detachment. This was accomplished by transposing nodes of the vitreous inward. The amount is described with the following equations:

Table 1. Regions of the model with element types, number of elements and material properties

Region	# of elements	Density (kg/m³)	Stiffness
Cornea	726	1061	Ogden: $n = 1$ $\mu = 54100$ Pa $a = 110.4$
Limbus	288	1076	Ogden: $n = 1$ $\mu = 270910.5$ Pa $a = 150$
Sclera1	1044	1076	Ogden: $n = 1$ $\mu = 270910.5$ Pa $a = 150$
Sclera2	720	1076	Ogden: $n = 1$ $\mu = 133, 279$ Pa $a = 150$
Sclera3	294	1076	Ogden: $n = 1$ $\mu = 133, 279$ Pa $a = 150$
Vitreous	12,288	1005	Young's: $E = 15$ Pa $v = 0.495$
Retina	1536	1033	Ogden: $n = 1$ $\mu = 12021$ Pa $a = 145$

$$r_{new} = r * f_{shrink}(\theta) \qquad (1)$$

where r is the r-coordinate of the node as described by the spherical coordinate system shown in **Figure 1b**. The term $f_{shrink}(\theta)$ is described as:

$$f_{shrink}(\theta) = \begin{cases} 1 & for & 0 \leq \theta \leq 86° \\ -\frac{8}{3}\theta & for & 86° < \theta \leq 144° \\ \frac{1}{2\cos\pi-\theta} & for & 144° < \theta \leq 180° \end{cases} \qquad (2)$$

where θ is the θ-coordinate as described by the polar coordinate system shown in **Figure 1b**. Thus, Equation (1) defines a new r-coordinate for all nodes of the vitreous dependent on the θ-coordinate. See **Figure 3b**.

Finally, an RD was created by transposing the nodes of the retina and the nodes of the vitreous towards the center. The transposing was done in a similar way as before (see Equation 1) but now with an extra factor dependent on φ (see **Figure 1b**).

$$r_{new} = r * \left(1 - 0.06 * f_{rd}(\theta) * f_{rd}(\phi)\right) \tag{3}$$

where $f_{rd}(\theta)$ is defined in Equation (4) and $f_{rd}(\phi)$ is defined in Equation (5).

$$f_{rd}(\theta) = \begin{cases} -10\left(\theta - \frac{29}{50}\pi\right)^2 + 4 & for \quad 66° \leq \theta \leq 144° \\ 0 & for \quad all\ other\ \theta \end{cases} \tag{4}$$

$$f_{rd}(\theta) = \begin{cases} -5\phi^2 + 1 & for \quad -26° \leq \phi \leq 26° \\ 0 & for \quad all\ other\ \phi \end{cases} \tag{5}$$

Thus, Equation (3) gives a definition for the new r-coordinate of all nodes of the vitreous and the retina dependent on the θ-coordinate and the φ-coordinate. The transposing of the nodes finalizes the model geometry (**Figure 3c**).

The previous equations, defining the vitreous detachment and the RD, have been defined in consultation with a veteran vitreoretinal surgeon (J.C.v.M) to create a realistic pathological case.
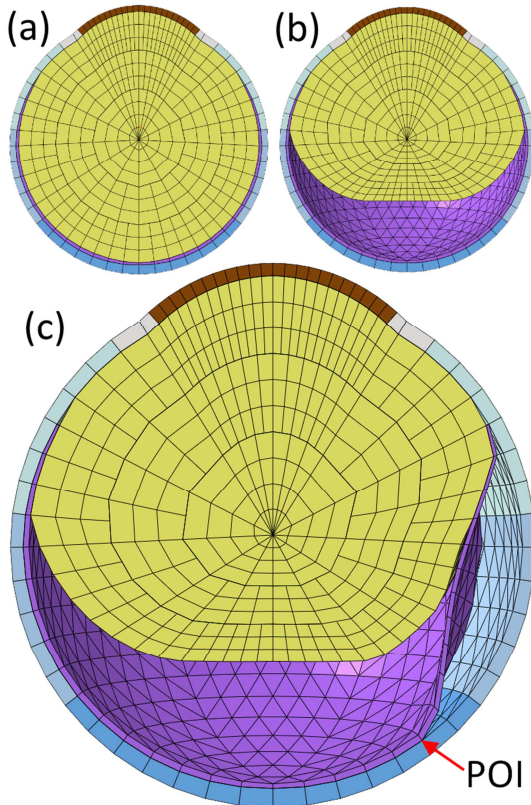
Figure 3. The steps in building the geometry of the model. Shown is a cross section through the xz-plane (Figure 1b). The colours correspond to the materials as seen in Figure 1a. **(a)** First step in building the model, exactly like Figure 1a. **(b)** Second step, the model with a detached vitreous (see Equation 3). **(c)** Final step, the model with a detached vitreous and an RD. The red arrow indicates the location of the point of interest (POI) where the results are measured.

Materials

The material properties used in the model are shown in **Table 1**. Material properties of the cornea, limbus, and sclera were based on in house measurements performed by the University of Liverpool (most recent publication by Whitford et al.[22]). The properties of the vitreous were based on the average of four publications.[23-26] The properties of the retina were based on data provided and published by Chen et al.[17] Due to the lack of more accurate measurements, the vitreous was modeled as a solid using a Young's modulus combined with a Poisson ratio. All other material stiffnesses were approximated with hyperelastic Ogden material constitutive models.[27] More accurate material models are known for the cornea, sclera, and limbus that may also incorporate microstructures. These properties were not found necessary to be used in this study. These components are much stiffer than the vitreous and retina and therefore acting as a rigid body during everyday head and eye movements. Authors believe that other components of the eye including lens, iris and optic nerve head will not play a significant role for the purpose of this study, and since the material characteristics of these components are not accurately known, these implementation could result in a less reliable numerical models and increases uncertainties.

The free liquefied vitreous between vitreous and retina, and in the subretinal space between retina and sclera, was modeled using the FLUID CAVITY option available in ABAQUS. The fluid cavity was characterized by an enclosing surface and a bulk modulus that describes the compressibility. The bulk modulus was set at 1 kPa to simulate (near) incompressible behavior. This adds a constraint to the enclosed volume of the fluid cavity of compressibility in compliance with the defined bulk modulus. The cavity will therefore act as one big element that can deform at will but must keep its volume constant.

The mass of the free fluid was added evenly to the elements surrounding a cavity using the NON STRUCTURAL MASS option. The cavities (one above and one underneath the retina) can exchange fluid with each other through a retinal break based on pressure difference, viscosity, flow area and flow coefficient. Liquefied vitreous is very similar to water in physical and mechanical properties;[28] therefore, the viscosity was set to that of water (0.001 Pa s). The flow area was set to 1 mm^2 which is a typical size for a retinal break.[29,30] The flow constant was set to 0.65; this is comparable to flow through a hole in a thin plate.

All models were solved using the explicit solver in ABAQUS. No convergence issues were observed and the average run time of the models was about two hours (Intel i7, 2.50 GHz, 16 GB RAM). A mesh study was performed to arrive at an optimum mesh density that provided stable behavior predictions with the smallest number of elements. (see **Supplemental material 5.1**)

Load cases

Two load cases were defined to investigate the differences between head and saccadic eye movements. These load cases were selected to be representative for an everyday head and eye movement. Saccadic eye movements are involuntary, and all saccades are similar, even between subjects. The load case used to represent eye movement was a saccadic eye movement of 10°. This is a large and fast saccade, larger than 95% of all saccades.[31] Saccades can be expressed with the following equation:

$$\alpha(t) = \frac{\alpha_0}{2}\left(1 - \cos\frac{\pi}{T}t\right) \tag{6}$$

where α is the rotation angle over time, t, in degrees, α_0 is the saccade angle in degrees, T is the duration of the saccade in seconds, and t is the time in seconds.[32] The duration of a saccade is related to the saccade angle with the empirical equation:

$$T = 0.021\alpha_0^{2/5} \tag{7}$$

Equations 6 and 7 were used to define a rotation over time that is imported into ABAQUS.

The head movement was defined as a translations with a size of 2 mm and a time span similar to that of the saccadic eye movement (0.1 s). The accelerations caused by this movement are comparable to a cough motion or sitting down on a chair.[33] The accelerations are larger than those created by walking but smaller than those created by jogging.[34] The head movement was defined using an equation similar to Equation 6 for the progress over time:

$$s(t) = \frac{80}{2}\left(1 - \cos\frac{\pi}{T}t\right) \tag{8}$$

where s is the translation over time, s_0 is the size of the translation in millimeters, T is the duration of the movement in seconds, and t is the time in seconds.

Both these load cases consisted of the defined movements plus a second of stationary simulation. The movements were implemented at the outside nodes of the model (cornea, limbus and sclera). The saccadic eye rotation was defined as a counterclockwise rotation around the y-axis, and the head movements were defined as a translation in the negative x-direction (**Figure 1b**).

Parametric study

To investigate the dependency of the model on certain parameters and to investigate to what accuracy these parameters must be known, a parametric study was conducted with varying parameters related to the material properties as depicted in **Table 2**. One parameter has been changed at a time to investigate the effect on the models' results.

We determined the traction load on the point of interest (POI) of the retina (see **Figure 3c**) perpendicular to the sclera where traction pulling the retina and sclera apart is defined as positive. First, the results of the control set of parameters were determined. The control set of parameters represent the most recent and reliable value found in the literature (**Table 2**). The size of the variation is roughly based on the amount of variation seen in the literature. The vitreous density is based on Su et al.[5], the vitreous stiffness is based on Pokki et al.[23], Swindle et al.[24], Bettelheim and Wang[25] and Zimmerman[26], the retinal density is based on Su et al.[5], the retinal stiffness is based on Chen et al.[17], the fluid viscosity is based on Godtfredsen,[28] the fluid density is based on Quintyn and Brasseur,[35] and the retinal break area is based on Miura and Ideta[29] and Neumann and Hyams.[30]

Next, the effect of all parameter variations was determined and normalized to the loads produced by the control set of parameters. Finally, the ratio of the loads that result from the two load cases is compared for all parameter variations.

Table 2. The parameters of the model that are varied to investigate dependency and needed accuracy.

	Control	Variations (%)			
Vitreous density	1005 kg/m^3	90	95	105	110
Vitreous Young's	15 Pa	25	50	200	400
Retina density	1033 kg/m^3	90	95	105	110
Retina ogden (μ)	12021 Pa	25	50	200	400
Fluid viscosity	0.001 Pa $*$ s	60	80	120	140
Fluid density	1000 kg/m^3	60	80	120	140
Retinal break	10^{-6} m^2	25	50	200	400

RESULTS

Figure 4 shows the traction on the POI of the model with the control set of parameters for both load cases. For both load cases, the peaks in traction load are between 30 and 35 Pa. It can be seen that in both cases oscillation of the vitreous cause traction loads on the POI long after the eye has stopped moving or rotating (**Figure 5**).

The results of the parametric study are shown in **Figure 6**. The models result is most dependent on changes of the vitreal and retinal material properties, and also on fluid density. Note that the normalized traction load never exceeds a factor of two.

The results of the comparison between the head and saccadic eye movements are shown in **Figure 7**. It shows that the ratio of the load caused by saccadic eye movements divided by the load caused by head movements is around one for most variations. Thus, head movements result in similar loads on the retina compared to saccadic eye movement.
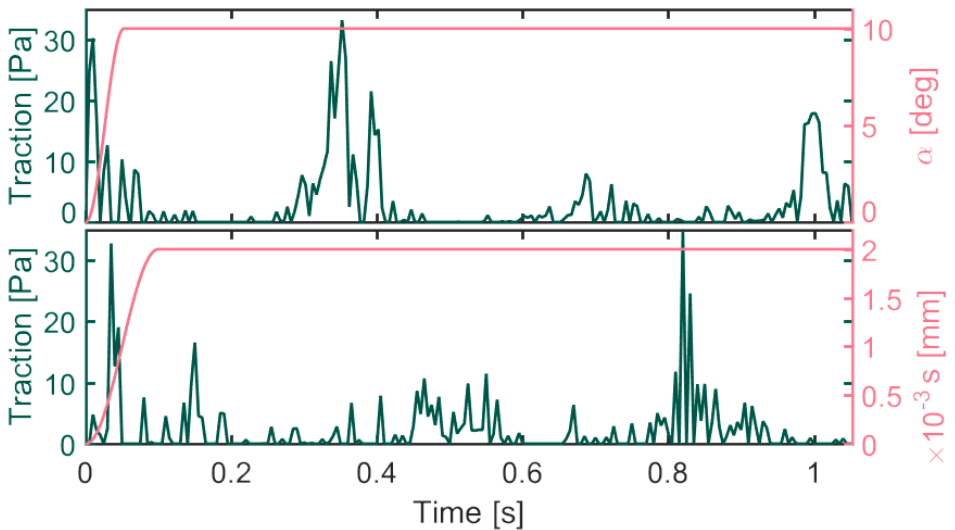
Figure 4. Traction on the POI (see Fig. 3c) over time, for both load cases. The top graph shows the results for the eye movement (blue) and the rotation (pink) over time. The bottom graph shows the results for the head movement (blue) and the translation (pink) over time. It can be seen that in both cases oscillation of the vitreous cause traction loads on the POI long after the eye has stopped moving or rotating.
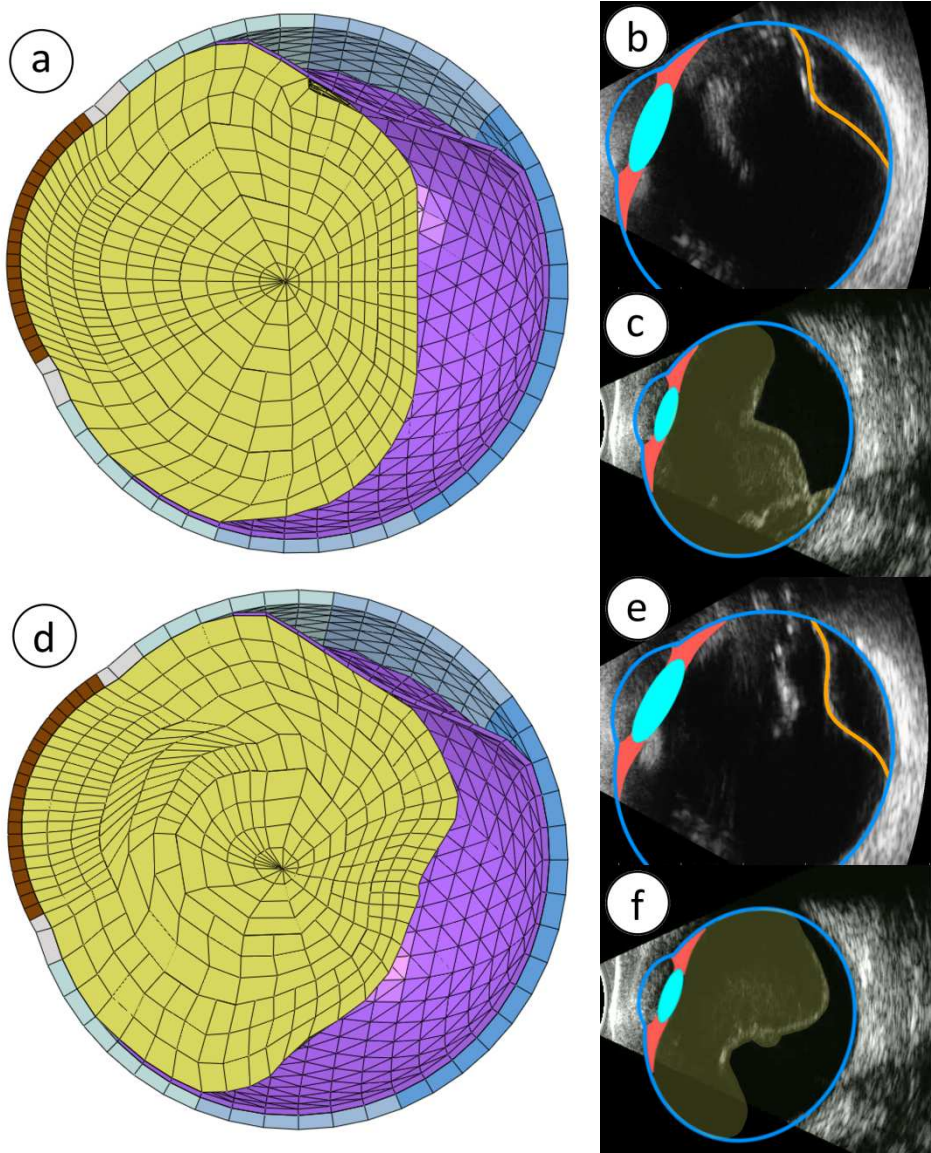
Figure 5. Stills of the supplementary video file (**Supplemental video 5.1**). The figure shows ultrasound imaging of two different patients: one with a retinal detachment (**b, e**) and one with only a vitreous detachment (**c, f**). Also shown is the model in similar states as the ultrasound images (**a, d**). The top three images **a–c** show the onset of eye rotation; the bottom three images **d–f** show the situation after rotation. The movements of the vitreous and the deformation of the retina in the ultrasound images are larger and more dampened than the movements seen in the model.

The model has been visually compared to ultrasound images of human eyes (see **Supplemental video 5.1**, or **Figure 5**). There were clearly some differences in the shape of the vitreous bodies and the retinal detachment. Therefore, only general differences between the ultrasound recordings and the model could be observed. Two differences can be observed when comparing the model to the images. First, the vitreous in the model oscillates for a long time (also seen in **Figure 4**). The ultrasound images show a single dampened movement of the vitreous. Secondly, the ultrasound images show a more mobile retina compared to the model.
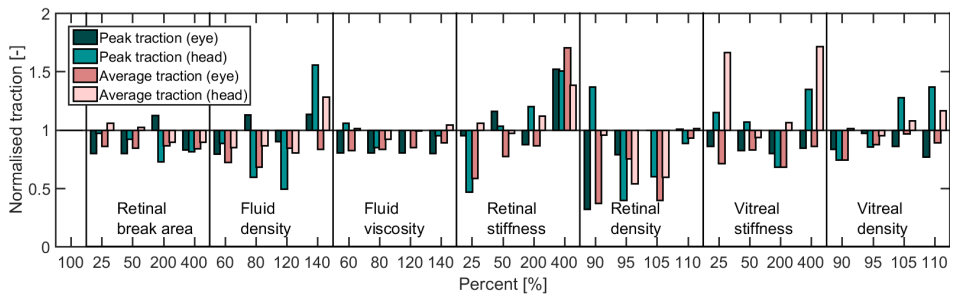
Figure 6. Peak and average traction loads on the point of interest (nor-malised to the load present in the simulation with the control set of parameters) are shown on the y-axis. All variations of parameters are shown in the x-axis. The model is most sensitive for changes of the vitreal and retinal material properties.
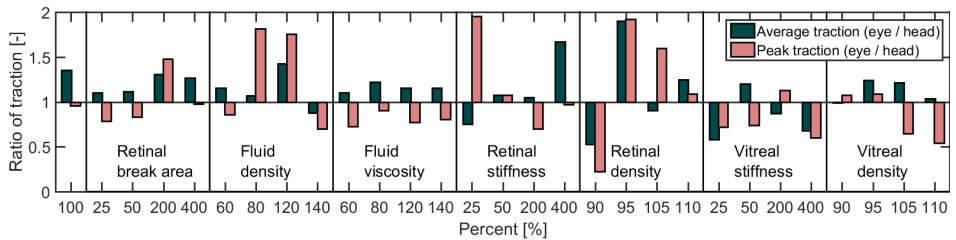
Figure 7. The load of the rotation (eye movement) divided by the load of the translation (head movement) for all parameter variations. The ratio is shown in the y-axis, and the variations are shown in the x-axis. It can be seen that the ratio is around one for most variations. This shows that the translation (head movement) results in similar loads on the retina compared to the rotation (eye movement).

CONCLUSION AND DISCUSSION

The peak of the traction loads on the retina caused by eye movements caused by head movements and saccades (**Figure 4**) is within the range 30–35 Pa. **Figure 6** shows that, for both load cases and all parameter variations, the traction will never change by a factor of more than two outside this 30–35 Pa range. This is a factor of ten lower than what is measured to be the adhesion force of the retina by Liu et al.[15] which was 340 Pa. Since the defined saccadic eye movement was larger than 95% of all saccadic eye movements,[31] it is unlikely that traction caused by most saccadic eye movement will be large enough to overcome the retinal adhesion. However, the defined head movement was small compared to those created by other everyday activities. Therefore, it is likely that only head movements are able to create traction loads in the same order of magnitude as the retinal adhesion. These preliminary results suggest that head movements are the major factor in the progression of an RD.

Although the ultrasound images display a simplified 2d representation of the retinal detachment, they enabled a rough comparison with the numerical model. Two observations were made when comparing the model to the ultrasound images. First, the vitreous in the model oscillates for a long period, while the real vitreous does not. This lack of damping is most likely caused by the simplifications adopted in the material properties of the vitreous and the fluid-structure interaction between vitreous and liquefied vitreous. Second, the ultrasound images show a more mobile retina compared to the model. The stiffness properties used for the retina are based on the best measurements from the literature.[17] It is clear that these material properties have not been measured in a way that is physiologically representative. Only the linear material properties of the vitreous were implemented in the model, due to a lack of proper characterization of the nonlinear and viscoelastic material properties of the vitreous in the literature. Future work is therefore needed to measure the properties of the vitreous and retina more accurately. A better comparison to ultrasound images should also be made since there is (although small) a difference in the size of the detachment between the used ultrasound images and the model.

The results of the parametric study (**Figure 6**) show that the models result is most sensitive to changes in the properties of the vitreous and retina. This adds to the claim that these properties should be measured more accurately to improve the model. It should also be noted that the stiffness properties of the retina and the vitreous are known to be anisotropic and inhomogeneous.[16,36,37] The model is less sensitive to changes in the other tissue properties. The model also shows a dependency on the densities of the liquefied vitreous, the retina and the vitreous. However, density measurements are comparatively easy and accurate. The densities

are known to a greater accuracy than the stiffness;[5] therefore, the focus should be on measuring the stiffnesses.

This study has focused on the load produced by eye movements caused by head movements and saccades. Therefore, gravity has been taken out of the analysis. This allowed us to purely consider the stresses produced by eye movements. Future work should aim to include gravity forces to improve the simulation. Although a realistic case was chosen in this study, it would be interesting to investigate the different presentations of the vitreous and retinal detachments and their influence on RD progression.

This study has been exploratory in nature to investigate internal eye dynamics, and it yields useful results on elucidating the role of head and saccadic eye movements in the development and progression of RD. It is the first time a finite element model has been used to investigate the pathology of an RD. The most accurate and most recent material data have been used in this model. Its preliminary results indicate that head movements are the major factor in the progression of an RD. This result could explain the results of an earlier study on the effectiveness of the posturing advice.[8] This suggests to the authors of the present paper that this modeling technique is useful in understanding the progression of RD. The fact that a relatively simple model like this produces worthwhile results shows the authors that continuation of this research will lead to a better understanding of RD and could improve its treatment to minimize the risk of blindness for patients.

REFERENCES

1. Johnston PB (1991) Traumatic retinal detachment. Br J Opthalmol 75:18–21

2. Van De Put MAJ, Hooymans JMM, Los LI (2013) The incidence of rhegmatogenous retinal detachment in the Netherlands. Ophthal-mology 120(3):616–622.

3. Haimann MH, Burton TC, Brown CK (1982) Epidemiology of retinal detachment. Arch Ophthalmol 100(2):289–292.

4. Salicone A, Smiddy WE, Venkatraman A, Feuer W (2006) Visual recovery after scleral buckling procedure for retinal detachment. Oph-thalmology 113(10):1734–1742.

5. Su X, Vesco C, Fleming J, Choh V (2009) Density of ocular components of the bovine eye. Optom Vis Sci 86(10):1187–95.

6. Algvere P, Rosengren B (1977) Immobilization of the eye. Evaluation of a new method in retinal detachment surgery. Acta Ophthalmol 55(2):303–16

7. Lean JS, Mahmood M, Manna R, Chignell AH (1980) Effect of preoperative posture and binocular occlusion on retinal detachment. Br J Ophthalmol 64(2):94–97

8. De Jong JH, Vigueras-Guillén JP, Simon TC, Timman R, Peto T, Vermeer KA, van Meurs JC (2017) Preoperative posturing of patients with macula-on retinal detachment reduces progression toward the fovea. Ophthalmology 124:1–13.

9. Uchio E, Ohno S, Kudoh J, Aoki K, Kisielewicz LT (1999) Simulation model of an eyeball based on finite element analysis on a super-computer. J Opthalmol 83:1106–1111

10. Stitzel JD, Duma SM, Cormier JM, Herring IP (2002) A nonlinear finite element model of the eye with experimental validation for the prediction of globe rupture. Stapp Car Crash J 46:81–102

11. Rossi T, Boccassini B, Esposito L, Iossa M, Ruggiero A, Tamburrelli C, Bonora N (2011) The pathogenesis of retinal damage in blunt eye trauma: finite element modeling. Invest Ophthalmol Vis Sci 52(7):3994–4002.

12. Karimi A, Razaghi R, Navidbakhsh M, Sera T, Kudo S (2016a) Computing the stresses and deformations of the human eye components due to a high explosive detonation using fluid-structure interaction model. Injury 47(5):1–9.

13. Karimi A, Razaghi R, Navidbakhsh M, Sera T, Kudo S (2016b) Quantifying the injury of the human eye components due to tennis ball impact using a computational fluid-structure interaction model. Injury 19(2):1–9.

14. Hans SA, Bawab SY, Woodhouse ML (2009) A finite element infant eye model to investigate retinal forces in shaken baby syndrome. Graefe's Archive Clin Exp Ophthalmol 247(4):561–571.

15. Liu X, Wang L, Wang C, Sun G, Liu S, Fan Y (2013) Mechanism of traumatic retinal detachment in blunt impact: a finite element study. J Biomech 46(7):1321–1327.

16. Chen K, Rowley AP, Weiland JD (2010) Elastic properties of porcine ocular posterior soft tissues. J Biomed Mater Res Part A 93(2):635–645.

17. Chen K, Rowley AP, Weiland JD, Humayun MS (2014) Elastic properties of human posterior eye. J Biomed Mater Res Part A 102(6):2001–2007.

18. Liu T, Hu AY, Kaines A, Yu F, Schwartz SD, Hubschman JP (2011) A pilot study of normative data for macular thickness and volume measurements using cirrus high-definition optical coherence tomography. Retina 31(9):1944–1950.

19. Grover S, Murthy RK, Brar VS, Chalam KV (2010) Normative data for macular thickness by high-definition spectral-domain optical coherence tomography (spectralis). Invest Ophthalmol Vis Sci 148(2):2644–2647.

20. Nooshin H, Tomatsuri H (1995) Diamatic transformations. In: Giuliani C (ed) Proceedings of the symposium on spatial structures: heritage, present and future, Milan, pp 71–82

21. Elsheikh A, Wang D (2007) Numerical modelling of corneal biomechanical behaviour. Comput Methods Biomech Biomed Eng 10(2):85–95.

22. Whitford C, Studer H, Boote C, Meek KM, Elsheikh A (2015) Biomechanical model of the human cornea: considering shear stiffness and regional variation of collagen anisotropy and density. J Mech Behav Biomed Mater 42:76–87.

23. Pokki J, Ergeneman O, Sevim S, Enzmann V, Torun H, Nelson BJ (2015) Measuring localized viscoelasticity of the vitreous body using intraocular microprobes. Biomed Microdevices 17(5):85.

24. Swindle KE, Hamilton PD, Ravi N (2008) In situ formation of hydrogels as vitreous substitutes: viscoelastic comparison to porcine vitreous. J Biomed Mater Res Part A 87(3):656–665.

25. Bettelheim FA, Wang TJY (1976) Dynamic viscoelastic properties of bovine vitreous. Exp Eye Res 23(4):435–441.

26. Zimmerman RL (1980) In vivo measurements of the viscoelasticity of the human vitreous humor. Biophys J 29(3):539–44.

27. Ogden RW (1972) Large deformation isotropic elasticity–on the cor-relation of theory and experiment for incompressible rubberlike solids. Proc R Soc A Math Phys Eng Sci 326(1567):565–584.

28. Godtfredsen E (1949) Investigations into hyaluronic acid and hyaluronidase in the subretinal fluid in retinal detachment, partially due to ruptures and partly

secondary to malignant choroidal melanoma. Br J Ophthalmol 33(12):721–732.

29. Miura M, Ideta H (2000) Factors related to subretinal proliferation in patients with primary rhegmatogenous retinal detachment. J Retin Vitreous Dis 20(5):465–468

30. Neumann E, Hyams S (1972) Conservative management of retinal breaks. A follow-up study of subsequent retinal detachment. Br J Ophthalmol 56(6):482–6.

31. Bahill AT, Adler D, Stark L (1975) Most naturally occurring human saccades have magnitudes of 15 degrees or less. Investig Ophthalmol 14(June):468–469

32. Yarbus AL (1967) Eye movements and vision. In: Haigh B, Riggs LA, Ballou LH (eds) Eye movements and vision. Plenum Press, New York, pp 129–146 (Chap IV Saccadi)

33. Arndt SR, Cargill II RS, Hammoud S (2004) Head acceleration experienced during everyday activities and while riding roller coasters. In: Human factors, pp 1973–1977

34. Kavanagh JJ, Barrett RS, Morrison S (2004) Upper body accelerations during walking in healthy young and elderly men. Gait Posture 20(3):291–298.

35. Quintyn JC, Brasseur G (2004) Subretinal fluid in primary rhegmatogenous retinal detachment: physiopathology and composition. Surv Ophthalmol 49(1):96–108.

36. Chen K, Weiland JD (2010) Anisotropic and inhomogeneous mechanical characteristics of the retina. J Biomech 43(7):1417–1421.

37. Colter J, Williams A, Moran P, Coats B (2015) Age-related changes in dynamic moduli of ovine vitreous. J Mech Behav Biomed Mater 41:315–324.

SUPPLEMENTAL MATERIAL 5.1

Mesh convergence study

A mesh convergence study has been performed to arrive at the best mesh. The best mesh would be fine enough to not influence the result but not too fine, to keep computation times low. This has been achieved by defining different meshes with an increasing amount of elements (see **Supplemental figure 5.2**).

The displacement of six different points of the vitreous is investigated for all different meshes. The load case is the same for all models. The six nodes that are investigated and their results are shown in **Supplemental figure 5.1**. It can be seen that to the right of the dotted line the result of all six nodes have converged. Therefore the chosen mesh is that of the dotted line which is 12288 elements in the vitreous.
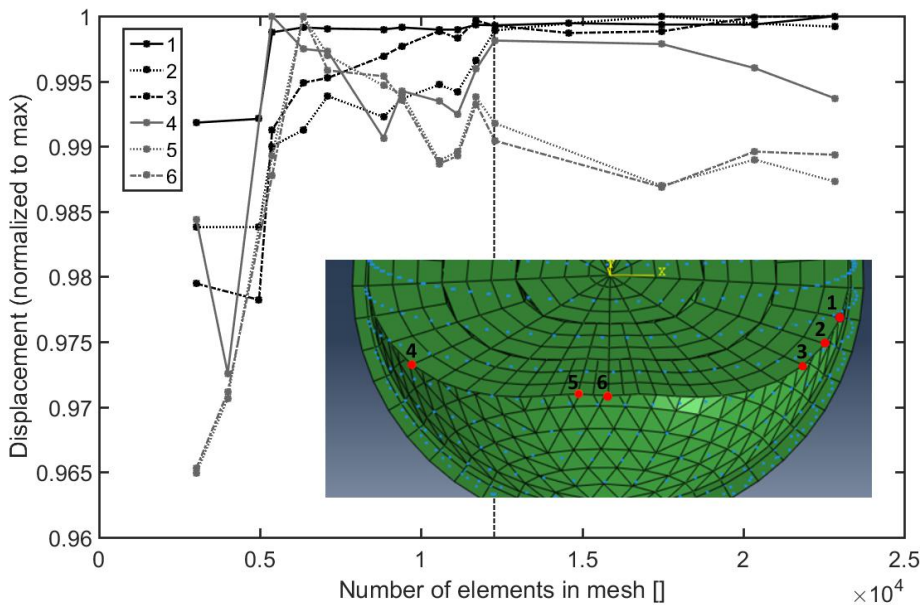
Supplemental figure 5.1: Results of the mesh convergence study. The absolute maximum displacement of the node, normalised to the maximum between meshes, is shown on the y-axis. The number of elements is shown on the x-axis. The colours correspond to the different nodes. The chosen mesh has 12288 elements in the vitreous (see dotted line).
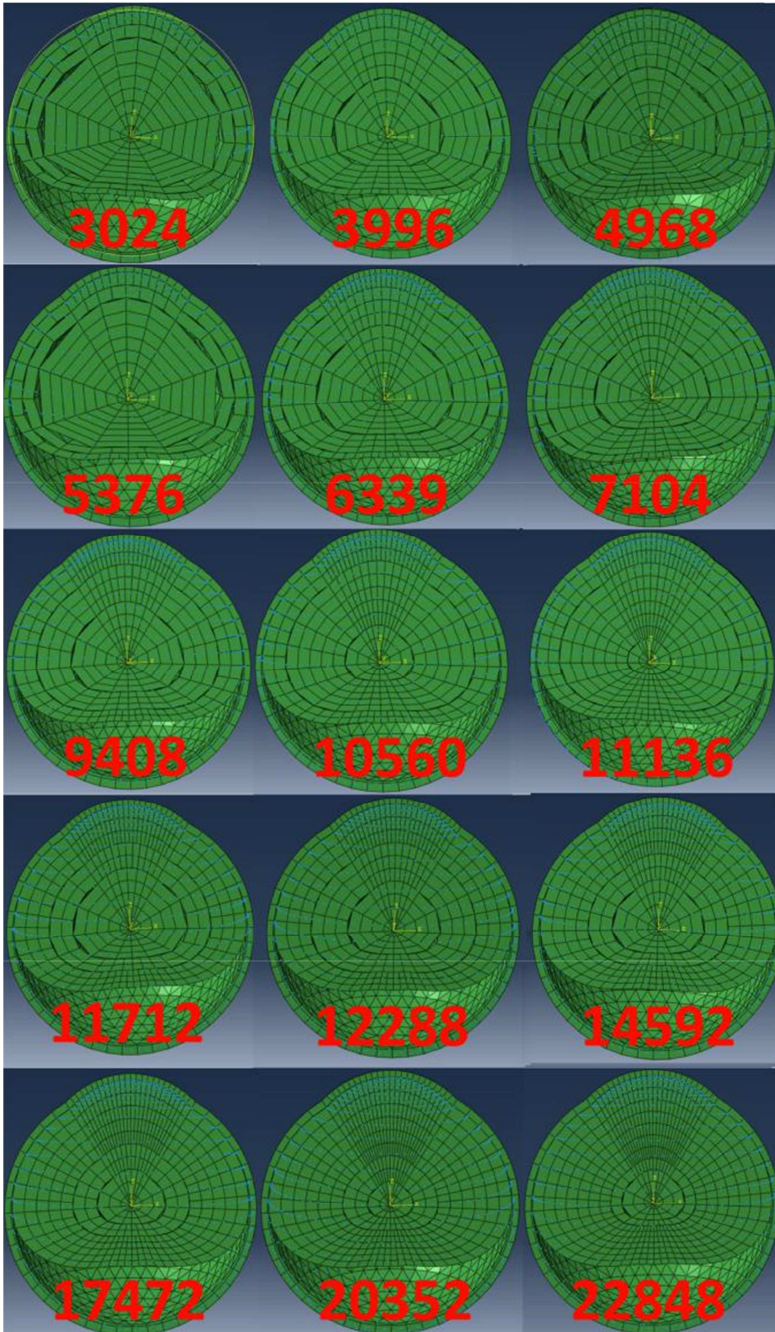
Supplemental figure 5.2: All iterations of the mesh convergence study. Shown in red are the number of elements of the vitreous. The "gaps" between some of the elements are an artefact and are not present in the nal calculation of these models.

Part II

Age-related macular degeneration

Chapter

6

Intravitreal versus subretinal administration of recombinant tissue plasminogen activator combined with gas for acute submacular hemorrhages due to age-related macular degeneration: an exploratory prospective study

Jan Hendrik de Jong*
Elsbeth J. T. van Zeeburg*
Matteo G. Cereda
Mirjam E.J. van Velthoven
K. Faridpooya
Koenraad A. Vermeer
Jan C. van Meurs

*Joint principal authorship

ABSTRACT

Purpose
Current management of submacular hemorrhage (SMH) favors vitrectomy and gas with subretinal administration of recombinant tissue plasminogen activator (rtPA) over mere intravitreal rtPA injections and gas. In this study, we aimed to compare the effectiveness of both treatment modalities to displace submacular blood.

Methods
Twenty-four patients with SMH secondary to age-related macular degeneration were included. The SMH had to exist ≤14 days at time of surgery and SMH thickness had to be between 250 μm and 1,250 μm. Patients were randomized to either intravitreal injections of rtPA, perfluoropropane (C_3F_8) gas and bevacizumab (n = 12) or vitrectomy with subretinal rtPA administration, intravitreal C_3F_8 gas and bevacizumab (n = 12). The SMH volume change was measured on SD-OCT postoperatively within a 2.5-mm cylinder centered at the fovea.

Results
Median relative volume reduction of subretinal blood at 6 weeks postoperatively was 97% (95% confidence interval: 91 – 99%) in the intravitreal rtPA group and 100% (95 – 100%) in the subretinal rtPA group and did not differ significantly between groups (P = 0.56).

Conclusion
Both treatment modalities effectively displaced SMH in this exploratory clinical trial. To more definitely study the noninferiority of intravitreal rtPA with gas to subretinal rtPA, vitrectomy with gas, a larger clinical trial would be necessary.

INTRODUCTION

Submacular hemorrhage (SMH) is a severe complication of exudative age-related macular degeneration (AMD) causing immediate and extensive loss of visual acuity and irreversible damage to the retina and retinal pigment epithelial (RPE) cells.[1,2] SMH can be aggravated in AMD patients taking anticoagulant medications,[3,4] and without treatment, the visual outcome is poor.[5] Damage to the sensory retinal tissue is due to a limited passage of nutrients to the retina, shrinkage of the outer retinal layers by clot formation with fibrin contraction[2,6] and toxicity of iron and hemosiderin.[7-9] Toxic effects of the SMH can occur already within 24 hours,[6] and resolution of the hemorrhage is associated with formation of a macular scar by fibrous tissue proliferation.[10]

Retrospective case studies have shown that recombinant tissue plasminogen activator (rtPA), injected either subretinally or intravitreally in combination with expansible gas or a gas/air tamponade, can displace the hemorrhage from the macula, resulting in improved visual acuity.[11-18] rtPA is supposed to liquefy the fresh hemorrhage,[19] whereas gas helps to displace the SMH,[20] either by a steam roller action or by gravity,[21] to a location where the hemorrhage can be resorbed over time causing less functional damage. In patients with exudative AMD, a major step forward was combining blood displacement with anti-vascular endothelial growth factor (anti-VEGF) injections, to treat and prevent progression of the underlying choroidal neovascularization (CNV).[22-28]

To the best of our knowledge, no randomized controlled trial has been performed to compare subretinal with intravitreal administration of rtPA. According to the published data, the current management trend is toward subretinal administration of rtPA combined with vitrectomy and gas tamponade,[11] possibly because the concentration of rtPA in the subretinal blood clot is assumed to be larger when rtPA is administrated subretinally. However, Kamei et al[29] demonstrated that rtPA can diffuse through microscopic retinal tears after intravitreal administration in rabbit eyes. These microscopic tears might be present secondary to a subretinal hemorrhage in AMD. Moreover, intravitreal rtPA administration combined with intravitreal gas is a procedure that can be performed in the office instead of an operation room and potentially at a shorter notice. Intravitreal rtPA is also a less invasive procedure than subretinal rtPA and might therefore cause fewer complications, although this is not clearly stated in the literature.[11]

Displacement of the blood clot is an important predictive factor for visual outcome after SMH treatment.[30] In most studies, fundus examination is used to define displacement based on the extent of hemorrhage with rather arbitrary and subjective categories like total, partial or no displacement. No attention is paid to the thickness of the hemorrhage under the fovea, even though this is likely to be

the most important factor in the functional impairment of the overlying retina.[6] Spectral domain optical coherence tomography (SD-OCT) provides three-dimensional high-quality images of the involved macular area, which enables measurements of the volume and thickness of the hemorrhage and other structural changes. In this study, we used such SD-OCT volume scans as a measure of hemorrhage displacement. Because subretinal blood is likely to cause most direct damage to the photoreceptors,[2,6] subretinal blood, subretinal fluid (SRF) and sub-RPE blood were delineated separately. The aim of this exploratory randomized controlled trial is to compare the effectiveness in terms of hemorrhage displacement of intravitreal versus subretinal administration of rtPA using quantitative volumetric SD-OCT analysis of SMH.

METHODS

Study objectives
The primary study objective of this exploratory study was to examine whether intravitreal administration of rtPA is as effective as subretinal administration of rtPA with respect to displacement and volume reduction of SMH at 4, 6, and 12 weeks follow-up. Secondary study objectives were to compare visual acuity and safety between both groups at 12 weeks follow-up.

Study design
This study was designed as a prospective, randomized, exploratory intervention study with hemorrhage displacement as primary endpoint as preparation for a larger clinical trial with visual acuity as primary endpoint. The study was approved by the local internal review board of the Rotterdam Eye Hospital and the Medical Ethical Committee of the Erasmus Medical Center (Rotterdam, the Netherlands). The study was registered at www.trialregister.nl as "Intravitreal versus submacular injection of rtPA for acute submacular hemorrhages." (Trial number NTR3359). All surgical procedures and examinations were performed at the Rotterdam Eye Hospital, The Netherlands. A data safety monitoring board was established and authorized to suspend or terminate recruitment if a significant safety problem would arise. The study was conducted in accordance with the tenets of the Declaration of Helsinki.

Inclusion and exclusion criteria
Inclusion criteria were: SMH existing no longer than 14 days at time of surgery (as determined by patient's history); SMH thicker than 250 μm under the fovea, but thinner than 1250 μm (limited by the SD-OCT system to fit a total retinal thickness up to 1,500 μm); age 45 years or older. Exclusion criteria were: Known

etiology of SMH other than exudative AMD; use of anticoagulants: International normalized ratio (INR) >2 or when the treating cardiologist did not allow an INR <2.

After determination of eligibility of consecutive cases from the clinic population, and directly after written consent was received, all patients were randomized into two treatment groups. Although this was an exploratory study, 24 assignment envelopes were prepared (12x intravitreal rtPA group and 12x subretinal rtPA group), of which one was randomly drawn after inclusion of a patient (only the affected eye was included). After treatment allocation, surgery was planned as soon as possible, but no later than 14 days after the onset of the hemorrhage.

Treatment

Patients in Group 1 were treated with intravitreal rtPA, perfluoropropane (C_3F_8) gas and bevacizumab. Patients in Group 2 were treated with pars plana vitrectomy, subretinal rtPA, a 10 % C_3F_8 gas/air tamponade and bevacizumab. For each patient, a vial with 2 mg rtPA powder (alteplase, Actilyse Cathflo, Boehringer Ingelheim BV) was reconstituted to a concentration of 1 mg/mL rtPA with the supplied solvent. The reconstituted solution was diluted further with sterile sodium chloride 9 mg/mL (0.9 %) solution to a final concentration of 0.25 mg/mL rtPA. This procedure was performed under aseptic conditions within an hour before injection, according to good manufacturing practice (GMP) guidelines. Alteplase is not labeled for the use under discussion.

Procedure intravitreal rtPA group: rtPA (25 µg in 0.1 mL) and bevacizumab (1.25 mg in 0.05 mL) were injected in the vitreous, followed by injection of 0.4 mL pure C_3F_8 gas as a tamponade, using 30 gauge needles. During the procedure, a paracentesis was performed to minimize the risk of intraocular hypertonia. If the complete volume of 0.4 mL C_3F_8 gas could not be administered during the first procedure (after manual assessment of highly increased intraocular pressure (IOP)), an additional injection of C_3F_8 gas was given the next day to complement a total of 0.4 mL of C_3F_8 gas and to achieve a tamponade size of >50% of the vitreous cavity.

Procedure subretinal rtPA group: after induction of a posterior vitreous detachment (if needed), a complete vitrectomy was performed. A 41 gauge cannula was used to inject 0.1 mL rtPA solution (25 µg rtPA) into the SMH, creating a local retinal detachment encompassing (part of) the blood clot.[18] The inner limiting membrane (ILM) was peeled at the macula (encompassing fovea and injection site) assisted by the surgical adjunct Membrane Blue (DORC, Zuidland, the Netherlands), to decrease the risk of a secondary macular hole or pucker. Although macular holes seem to be a rare complication after subretinal administration of rtPA, several cases have been reported in the literature.[11,27,31] As the senior author

(J.C.v.M.) has repeatedly observed that during the injection of subretinal volume and the subsequent ballooning of the macula, blood escapes through the fovea, ILM peel might prevent postoperative macular hole formation. However, this personal impression does not represent evidence that ILM removal reduces the incidence of macular hole and we realize that ILM peel may cause microscotomas.[32] A fluid-air exchange was performed and a nonexpansible mixture of C_3F_8 (10%) and air was left as a tamponade. At the end of surgery bevacizumab (1.25 mg) was injected with a 30 gauge needle through the pars plana into the vitreous cavity. In phakic patients with significant cataract, the treatment was combined with cataract surgery. In case of cataract development during the course of the study, cataract surgery was allowed during follow-up.

To prevent or treat a rise in IOP, apraclonidine (1%), was applied in all patients and acetazolamide (250 mg) tablets, timolol (0.5%) and dorzalazomide (20 mg/ml) eye drops were administered as often as necessary. Surgery in this study was performed by two experienced surgeons, J.C.v.M. and K.F.. Immediately after the operation patients were instructed to position their face in a 45° forward or laterally tilted position 6 hours per day for 4 weeks and at night sleeping on the side were most blood is located, left or right from the fovea. Postoperatively all patients were treated with bevacizumab at Week 5 and 10, and subsequently when there was persistence of neovascular activity defined as blood seen with ophthalmoscopy or intraretinal or subretinal fluid on OCT.

Examinations and outcome measures

The visual acuity was measured in logMAR (logarithm of the minimal angle of resolution) with Early Treatment Diabetic Retinopathy Study (ETDRS) charts according to a standard operation procedure (SOP) and converted to Snellen notation for publication. Imaging was performed with SD-OCT (Spectralis HRA; Heidelberg Engineering, Heidelberg, Germany), fundus photography (TRC 50 DX, Type 1A, TOPCON, Tokyo, Japan) and autofluorescence imaging (TRC 50 DX, Type 1A or Spectralis HRA).

Preoperative and postoperative examinations included SD-OCT, ETDRS visual acuity, fundus photography, fundus autofluorescence, dilated funduscopy, and IOP measurement. The extent of hemorrhage was measured preoperatively on fundus photography using the Topcon IMAGEnet area measurement tool. Duration of vision loss of the study eye, the number of anti-VEGF injections and other treatment modalities given before inclusion and the use of anticoagulants were recorded. Postoperative examinations were performed for subjects of both arms at day 1 and at 1, 2, 4, 6, and 12 weeks. At each visit, adverse events were recorded. The size of the gas bubble was estimated during funduscopy and the compliance to posturing was estimated by patient interview and recorded every visit.

The SD-OCT volume scans consisted of at least 25 B-scans centered at the fovea with a lateral resolution of 12 µm and axial resolution of 4 µm. The distance between B-scans was 120 µm and the number of averages was set to 51 per B-scan. Hemorrhage volume size was measured with SD-OCT by two masked retina specialists (M.E.J.v.V. and M.G.C.). After delineating the hemorrhage in every other frame of the volumetric OCT scan using the segmentation tool ITK-SNAP[33] (**Figure 1**), a conversion to volume was performed. With each pixel representing a known physical space, the volume of the hemorrhage was calculated from the number of pixels inside the delineated volume in a 2.5 mm cylinder around the foveal center, which corresponds to the traditional definition of the size of the fovea (1.5 mm) and parafovea (ring of 0.5 mm around the fovea) combined.
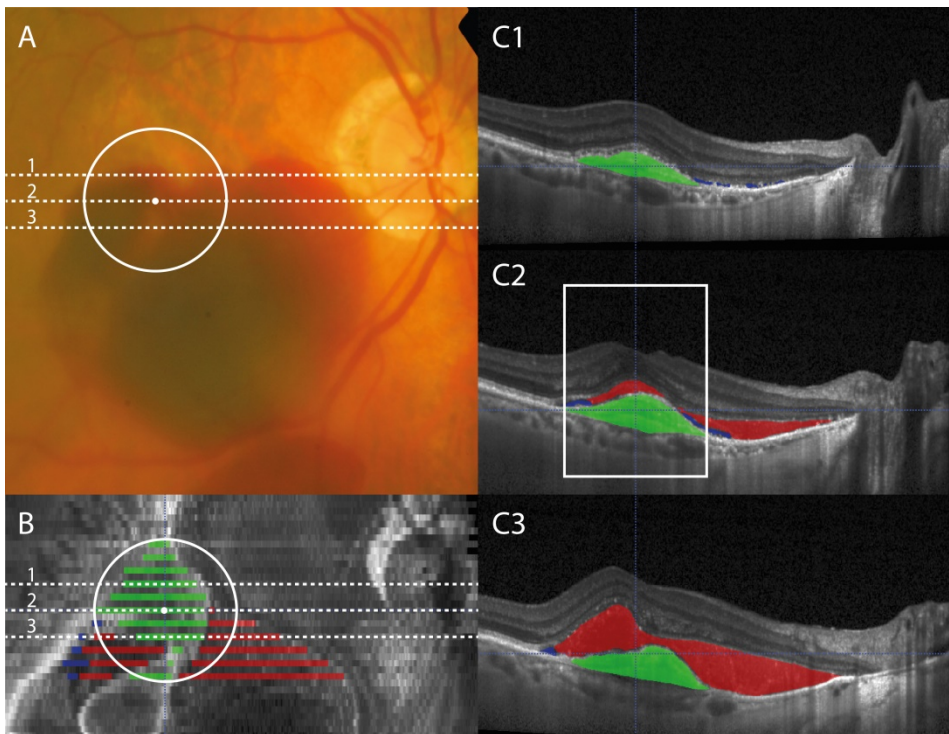
Figure 1. Example of the delineation of SMH parts on SD-OCT. On the fundus examination (**A**) a hemorrhage partly covers the 2.5 mm cylinder around the fovea (white dot). A confocal reconstruction (**B**) is shown of the complete OCT volume scan. Three horizontal B-scans (**C1-3**) demonstrate the differences between three parts of the hemorrhage. The location of the B-scans is annotated with white dashed lines on the fundus examination and OCT *en face* images (**A** and **B**, lines 1, 2 and 3). Segmentation colors: red= subretinal blood; blue= subretinal fluid; green= sub-RPE volume. The white circles and rectangle represent the 2.5 mm cylinder around the foveal center.

Statistical analysis

Because this study was exploratory, we assumed that 24 patients was an acceptable sample size. It was also taken into consideration that it was likely that this number of patients could be recruited within an acceptable period of time. We determined the intraclass correlation coefficients (ICC) to compare the OCT volume measurements of the two graders. We used the nonparametric Wilcoxon signed rank test to test for treatment effects and the Mann–Whitney U test to test for differences between treatment groups, because the data were not normally distributed. Baseline characteristics and visual acuity of both groups were also compared using the Mann–Whitney U test.

Table 1: Patient characteristics

Characteristic	Intravitreal rtPA, gas and bevacizumab (n=12)	Subretinal rtPA, vitrectomy, gas and bevacizumab (n=12)	P-value
Age (yrs)			
Median (range)	81.5 (76-93)	78.5 (68-94)	0.38
Male:Female (%)	4:8 (33:67%)	5:7 (42:58%)	0.76
Days of vision loss before surgery			
Median (range)	5 (1-11)	6 (1-14)	0.84
Ophthalmic history study eye			
Number of anti-VEGF injections			
Median (range)	0 (0-7)	4.5 (0-19)	0.012
Duration of exudative AMD			
Median	7 days	21.5 months	0.05
Range	(4 days – 9 months)	1 day - 59 months	
Number of patients taking anti-coagulant medication (%)	7 (58%)	4 (33%)	0.32
Phakic:Pseudophakic lens (%)	4:8 (33:67%)	5:7 (42:58%)	0.76
Extent of hemorrhage			
Disc areas			
Median (range)	11.1 (0.5-31.0)	9.7 (2.9-20.2)	0.89
Absolute area (mm^3)			
Median (range)	30.2 (1.6-94.1)	28.8 (7.3-50.8)	1.00

rtPA= recombinant tissue plasminogen activator; anti-VEGF= anti-vascular endothelial growth factor; AMD = age related macular degeneration

RESULTS

Patients

Twenty-five consecutive patients with a SMH were included in this prospective randomized trial between June 13, 2012 and the December 23, 2013. All patients provided a written informed consent for the surgical procedure and the preoperative and postoperative examinations. In one patient, the underlying condition causing the SMH turned out to be a retinal macroaneurysm. The randomization assignment envelop was replaced in the randomization pool to be able to complete the inclusion of 12 patients in both arms. Twelve patients were treated with intravitreal rtPA, C_3F_8 gas and bevacizumab and 12 were treated with subretinal rtPA, vitrectomy, C_3F_8 gas and bevacizumab. Patient characteristics of both groups are summarized in **Table 1**. Both groups were comparable regarding age, sex, time of vision loss before surgery and lens status. In the intravitreal group the extent of hemorrhage was slightly larger, but not statistically significant (P = 0.89). The number of prior anti-VEGF injections was statistically significant larger (P = 0.012) and duration of exudative AMD before surgery was longer in the subretinal rtPA group (P = 0.05).

Reliability of OCT measurements

One patient in each group was excluded from OCT analysis owing to a retinal detachment before Week 4. Two more measurements were excluded at Week 4, one in Group 1 because of cataract formation (which was operated in Week 5) and one in Group 2 because of vitreous opacities. One measurement was excluded at Week 12 in group 1 due to recurrent SMH and autologous RPE-choroid graft surgery at Week 7.

With an ICC of 0.98 (95% Confidence Interval (CI): 0.96–0.99) both graders excellently agreed on the pre-operative subretinal blood measurements. Post-operatively the ICC of the subretinal blood volume was lower but acceptable with 0.73 (0.55–0.84). The ICC for sub-RPE volume was 0.99 (0.98–0.99) and was consistent pre- and postoperatively. The ICC for SRF was overall 0.17 (-0.18–0.42) and did not differ significantly from 0, which means that both graders mostly disagreed on the amount of SRF in the OCT volume scans.

Effect of treatment on hemorrhage volume reduction

The measured volumes of subretinal blood, SRF and sub-RPE volume in a 2.5 mm cylinder around the foveal center are displayed in **Figure 2**. Absolute volume reduction in both groups is shown in a **Supplemental table 6.1**. Because of the small absolute changes of sub-RPE blood and subretinal fluid, only the relative subretinal blood volume reduction was displayed in **Table 2**.
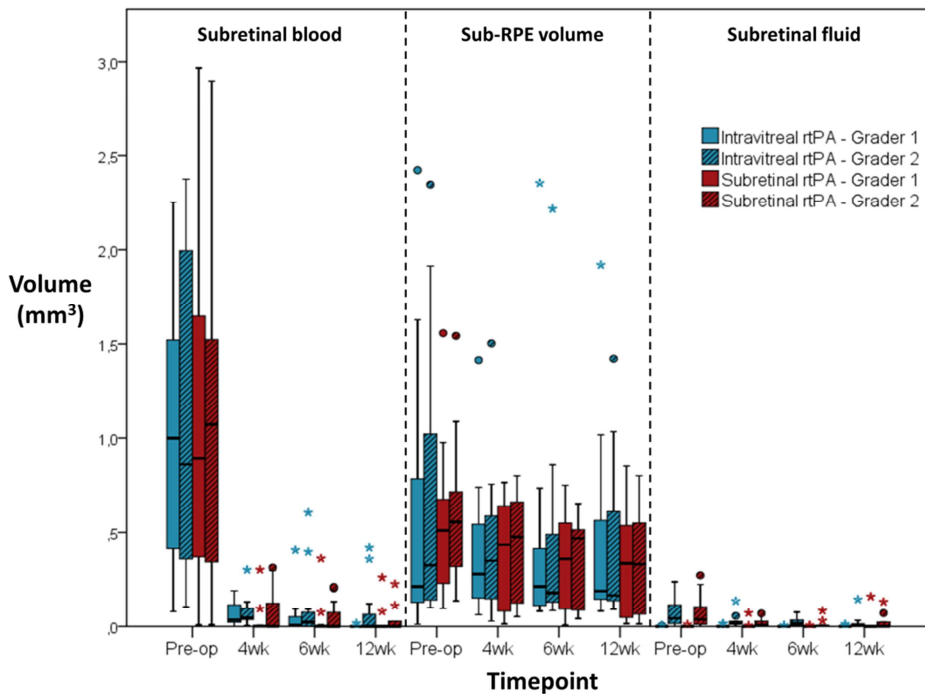
Figure 2. Volumetric measurements of SMH and subretinal fluid (SRF) volume pre-operatively and at 4, 6 and 12 weeks after surgery. Volumes were measured by two graders in a 2.5mm cylinder around the fovea. The SMH was subdivided in subretinal blood and sub-RPE volume. Explanation of the box-plots: horizontal lines = median; boxes = middle 50% of measurements; whiskers = data points up till 1.5 x box length; circles = mild outliers; asterisks = extreme outliers. Median subretinal blood volume was reduced from approximately 0.95 mm3 pre-operatively to less than 0.05 mm3 at 4, 6 and 12 weeks in both groups. Median sub-RPE volume and SRF volume slightly reduced in both groups postoperatively.

The median subretinal blood volume was reduced significantly from 0.93 mm³ (0.40–1.66) (average between graders, median ± 95%CI) pre-operatively to 0.02 mm³ (0.00–0.14) at 6 weeks (P = 0.003) in the intravitreal rtPA group and from 0.98 mm³ (0.39–1.39) pre-operatively to 0.00 mm³ (0.00–0.10) (P = 0.003) in the subretinal rtPA group. The median subretinal blood volume reduction from baseline to 6 weeks was 0.62 mm³ (-0.36–1.64) in the intravitreal rtPA group and 0.70 mm³ (-0.39–1.39) in the subretinal rtPA group. The median relative volume reduction of subretinal blood in the intravitreal rtPA group was 97% (91–99%) at 6 weeks after surgery and 100% (95–100%) in the subretinal rtPA group. Examples of OCT, autofluorescence and fundus examinations to demonstrate hemorrhage displacement for both treatment strategies are shown in **Figure 3** and **Figure 4**.

The median sub-RPE volume reduced from 0.27 mm³ (0.11–0.91) (average between graders, median ± 95%CI) pre-operatively to 0.20 mm³ (0.11-0.55) at 6 weeks after surgery (P = 0.21) in the intravitreal rtPA group and from 0.50 mm³

(0.31–0.66) pre-operatively to 0.41 mm³ (0.11–0.52) (P = 0.25) in the subretinal rtPA group. The median sub-RPE volume reduction from baseline to 6 weeks was 0.02 mm³ (-0.04–0.12) in the intravitreal rtPA group and 0.03 mm³ (0.00–0.08) in the subretinal rtPA group.

The median volume of SRF decreased during follow-up from 0.04 mm³ (95%CI: 0.01–0.11) at baseline to 0.02 mm³ (0.00–0.04) at 6 weeks in the intravitreal group and from 0.04 mm³ (0.01–0.09) to 0.00 mm³ (0.00–0.01) mm³ in the subretinal rtPA group, based on the measurements of Grader 2. Median SRF volumes of Grader 1 were smaller than 0.001 mm³ at baseline and at six weeks in both groups.

Comparison between treatment groups

No significant differences between both treatment groups were found pre-operatively and at 4, 6 and 12 weeks after surgery regarding absolute and relative volume change of subretinal blood, SRF and sub-RPE volume. These findings were consistent for both graders. The comparison of relative volume reduction of subretinal blood is shown in **Table 2**. The largest mean difference between groups regarding relative volume reduction of subretinal blood was found at 4 weeks with a 6% larger volume reduction in the subretinal rtPA group. However, this difference was also not significant (P = 0.08).

Table 2: Relative volume reduction of subretinal blood (in %); average of two graders

	Week 4	Week 6	Week 12
			11
Intravitreal rtPA, gas and bevacizumab		11	81 – 100 %
Number	10	55 – 100 %	100 (99– 100)
Range	68 – 100 %	97 (91 – 99) %	%
Median (95%CI)	91 (78 – 96) %	91 (82 – 100)	97 (93 – 101)
Mean (95%CI)	88 (80 – 95) %	%	%
Subretinal rtPA, vitrectomy, gas and	10	11	10
bevacizumab	69 – 100 %	68 – 100 %	75 – 100 %
Number	100 (92 – 100)	100 (95 – 100)	100 (99 – 100)
Range	%	%	%
Median (95%CI)	93 (86 – 101)	92 (83 – 100)	96 (89 – 102)
Mean (95%CI)	%	%	%
Comparison of treatment groups			
P-value	0.07	0.55	0.72
Median difference* (95%CI)	-5 (-14 – 1) %	-3 (-9 – 5) %	0 (-1 – 0) %
Mean difference* (95%CI)	-6 (-16 – 4) %	-1 (-12 – 11) %	1 (-6 – 8) %

rtPA = recombinant tissue plasminogen activator; CI = confidence interval.
*A positive difference means that the volume reduction in the intravitreal rtPA group was larger than in the subretinal rtPA group, a negative difference means the opposite
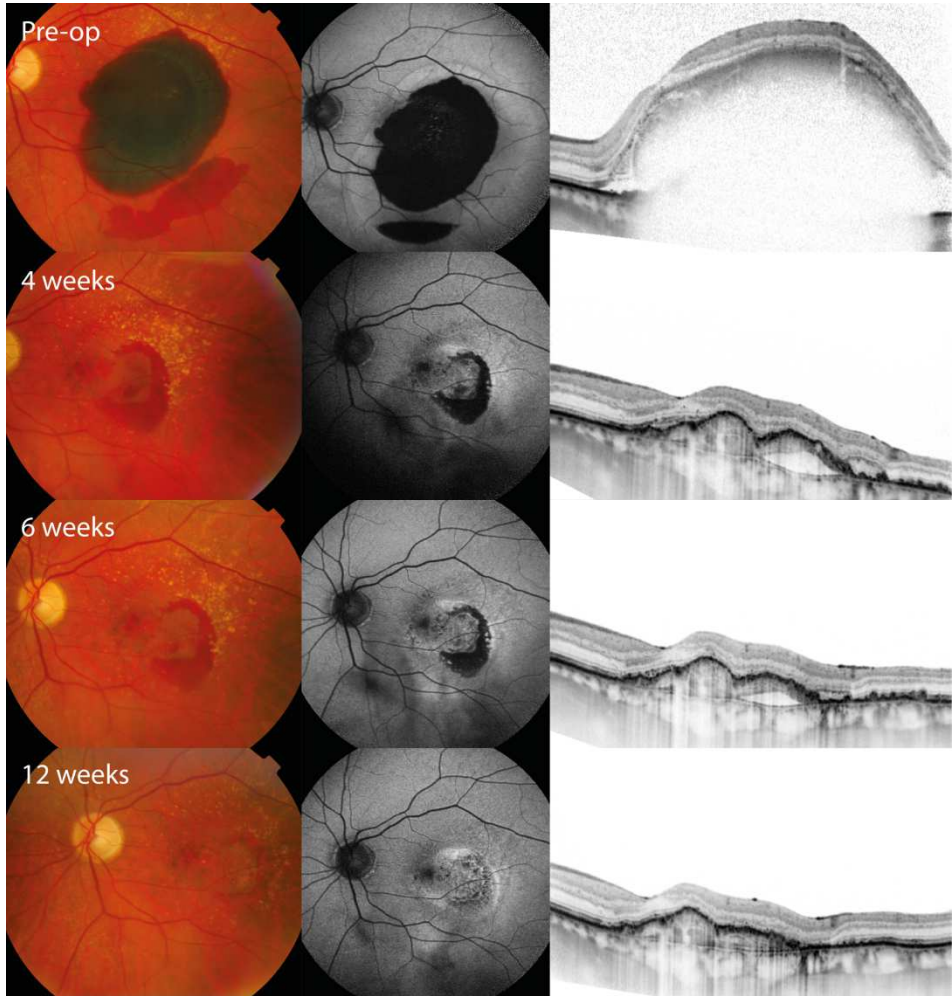
Figure 3. Displacement of submacular hemorrhage secondary to AMD in patient 19 treated with intravitreal rtPA, gas, and bevacizumab at baseline and at 5 and 10 weeks after the initial procedure. Shown are the fundus examination (left), autofluorescence (middle) and horizontal SD-OCT (right) pre-operatively and at 4, 6, and 12 weeks. Visual acuity improved from 20/209 Snellen pre-operatively to 20/26, 20/25, and 20/28 Snellen at 4, 6, and 12 weeks respectively.
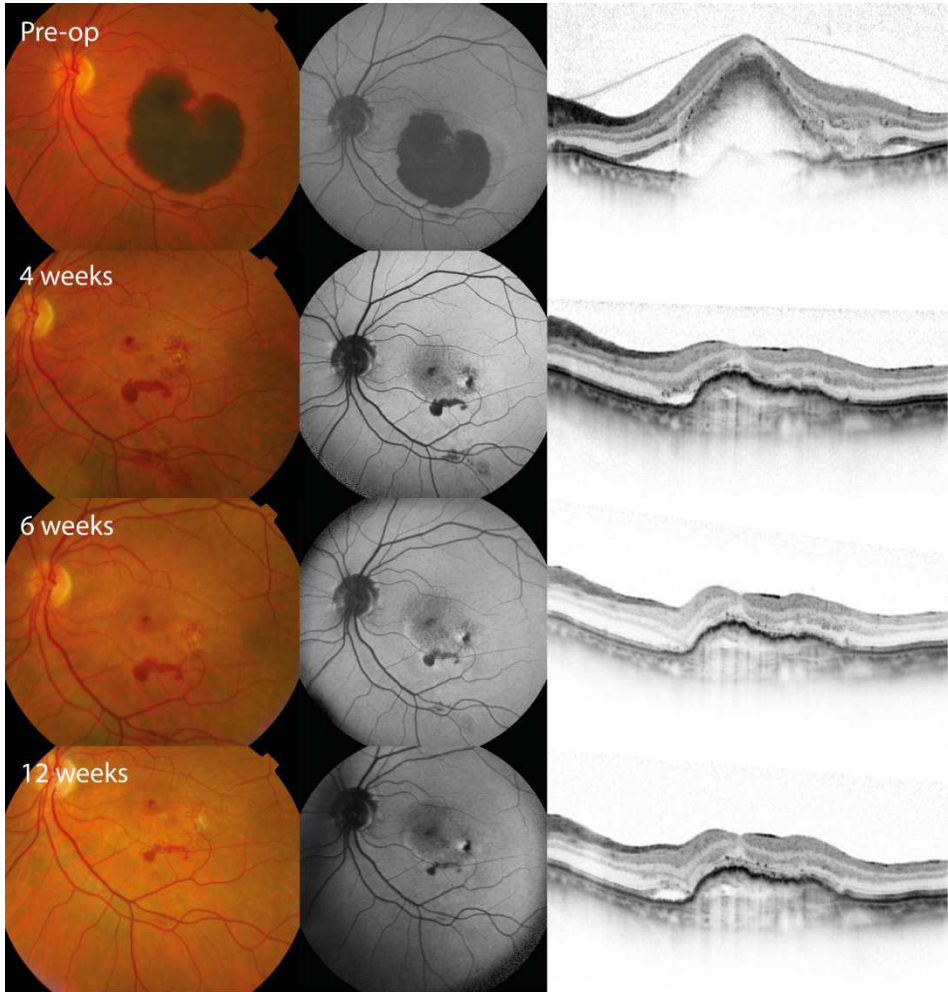
Figure 4. Displacement of submacular hemorrhage secondary to AMD in patient 9 treated with pars plana vitrectomy, subretinal rtPA, intraocular gas, and bevacizumab at baseline and at 5 and 10 weeks postoperatively. Shown are the fundus examination (left), autofluorescence (middle) and horizontal SD-OCT (right) pre-operatively and at 4, 6, and 12 weeks. Visual acuity changed from 20/66 Snellen pre-operatively to 20/126, 20/42, and 20/69 Snellen at 4, 6, and 12 weeks respectively.

Visual acuity

Two measurements at Week 4 were excluded from visual acuity analysis: one in Group 1 due to a temporary gas cataract and one in Group 2 due to vitreous opacities. Two measurements were excluded at Week 6, one in each group due to retinal detachment surgery at Week 4. One measurement was excluded at Week 12 in group 1 due to recurrent SMH at week 7. This patient was submitted to autologous RPE-choroid graft transplantation.

Visual acuity at baseline and at 4, 6 and 12 weeks postoperative are displayed in **Table 3**, in absolute values and as a percentage of patients who gained, lost or had stable visual acuity at each time point compared to preoperative assessment. Median visual acuity improvement in ETDRS lines at week 4 was +2.0 lines (95%CI +0.8 – +3.2; range -7.8 – +9.0; N=11) in the intravitreal rtPA group and +0.6 lines (CI -2.4 – +2.6; range -3.8 – +3.8; N=11) in the subretinal rtPA group (no significant differences between groups, P = 0.65). Median visual acuity improved from baseline to Week 6 with +1.4 lines (CI -1.0 - +5.0; range -4.8 – +9.2; N=11) in the intravitreal rtPA group and +2.9 lines (CI +0.9 – +3.2; range -3.6 – +3.6; N=11) from baseline to Week 6 in the subretinal rtPA group (P = 0.70). Median visual acuity improvement from baseline to Week 12 was +1.8 lines (CI: 0.0 – +6.3; range -4.8 – +8.8; N=12) in the intravitreal rtPA group and +1.4 lines (CI -0.8 – +2.4; range -5.0 – +4.2; N=11) in the subretinal rtPA group (P = 0.24). The proportion of patients with an ETDRS visual acuity of >20/200 increased from 58% (7/12) preoperatively to 92% (11/12) at 12 weeks in the intravitreal group and was stabile in the subretinal rtPA group, from 83% (10/12) preoperatively to 82% (9/11).

Postoperative course

Complications in the intravitreal rtPA group were: 3 increased IOP > 50 mmHg, 2 vitreous hemorrhages, 1 retinal detachment and 1 recurrent SMH. In the 3 patients with increased IOP, a second paracentesis was performed after applanation tonometry outcome of > 50mmHg within 4 hours after injection. Despite a third paracentesis with subsequent pulsatile retinal arteries, one patient was considered to have ischemic disk damage due to a prolonged high intraocular pressure. Both patients with vitreous hemorrhage were taking anticoagulant medication and 1 out of 3 patients with recurrent SMH was taking anticoagulants. Complications in the subretinal rtPA group were: 2 retinal detachments and 2 recurrent SMHs. Cataract surgery was performed in 4 out of 5 phakic patients in the subretinal rtPA group, in 3 during the study procedure and for one at Week 5 (visualization of the fundus impossible due to cataract formation after first surgery).

Table 3: Best corrected visual acuity preoperatively, and at week 4, 6, and 12 (in Snellen*)

	Intravitreal rtPA, gas, and bevacizumab	Subretinal rtPA, vitrectomy, gas, and bevacizumab
Preoperative		
Number	12	12
Median (range)	20/115 (20/834-20/53)	20/112 (20/551-20/23)
Mean (95%CI)	20/163 (20/289-20/98)	20/115 (20/195-20/71)
Week 4		
Number	11	11
Median (range)	20/91 (20/726-20/26)	20/126 (20/480-20/48)
Mean (95%CI)	20/103 (20/178-20/62)	20/123 (20/187-20/80)
Week 6		
Number	11	11
Median (range)	20/87 (20/364-20/25)	20/60 (20/276-20/42)
Mean (95%CI)	20/100 (20/159-20/63)	20/89 (20/132-20/60)
Week 12		
Number	12	11
Median (range)	20/85 (20/364-20/24)	20/91 (20/317-20/60)
Mean (95%CI)	20/87 (20/135-20/56)	20/107 (20/152-20/80)
Line difference Week 4		
Gain ≥2 lines	7/11 (63.6%)	5/11 (45.5%)
Stable	2/11 (18.2%)	2/11 (18.2%)
Loss ≥2 lines	2/11 (18.2%)	4/11 (36.4%)
Line difference Week 6		
Gain ≥2 lines	5/11 (45.5%)	7/11 (63.6%)
Stable	5/11 (45.5%)	2/11 (18.2%)
Loss ≥2 lines	1/11 (9.1%)	2/11 (18.2%)
Line difference Week 12		
Gain ≥2 lines	6/12 (50%)	4/11 (36.4%)
Stable	5/12 (41.7%)	5/11 (45.5%)
Loss ≥2 lines	1/12 (8.3%)	2/11 (18.2%)

rtPA = recombinant tissue plasminogen activator; CI=95% confidence interval
*The visual acuity was measured in logMAR (logarithm of the minimal angle of resolution) with Early Treatment Diabetic Retinopathy Study (ETDRS) charts and converted to Snellen notation.

In the intravitreal rtPA group 6 patients were reinjected with C_3F_8 gas at day one after the initial procedure to complement a total injection of 0.4 cc C_3F_8 (and achieve an acceptable tamponade of > 50 %). One patient was reinjected 2 weeks after surgery, because at the follow-up examination the gas bubble was considered to be too small to be still effective. In the subretinal rtPA group one patient was reinjected at Day 1 because the tamponade size was less than 50%, probably due to a leak at the sclerotomy sites. The gas bubble size was (1 week / 2 weeks postoperatively; mean ± 95%CI) 52 ± 8% / 44 ± 7% in the intravitreal rtPA group and 61 ± 5% / 48 ± 4% in the subretinal rtPA group. **Figure 5** shows the gas bubble sizes in both groups at the postoperative visits up till 6 weeks .

In both treatment groups 7 out of 12 patients followed the postoperative posturing advice more than 5 hours per day and 5 out of 12 followed it less than 5 hours of the advised 6 hours per day.
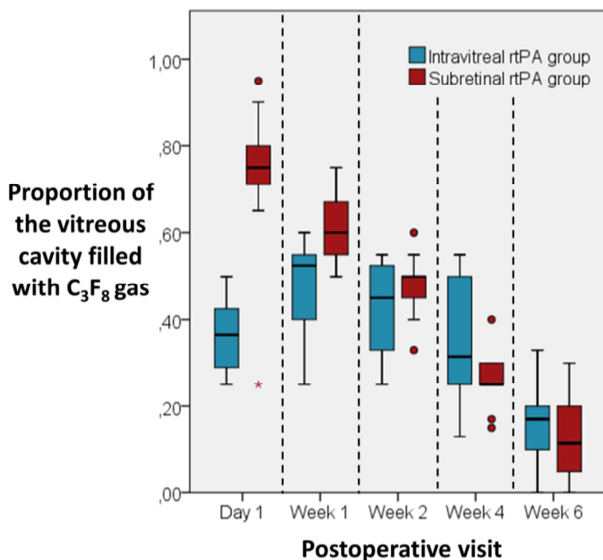
Figure 5. Size of the perfluoropropane (C_3F_8) gas bubble. The size of the gas bubble is shown as a proportion of the vitreous cavity as estimated during funduscopy at Day 1 and at Week 1, 2 , 4, and 6 postoperatively. Patients in the intravitreal rtPA group received a tamponade through intravitreal injection of 0.4 ml C_3F_8 gas at Day 0. Six of twelve patient were reinjected with intravitreal C_3F_8 at Day 1. In patients in the subretinal rtPA group a tamponade of 10% C3F8 gas and air was left after vitrectomy.

DISCUSSION

This study is, to our knowledge, the first randomized controlled trial to compare intravitreal versus subretinal administration of rtPA as tools for the pneumatic displacement of acute SMH in AMD patients. Despite a lack of evidence when reviewing the available data in 2013,[11] in the 10 most recent publications on the use of rtPA for SMH secondary to AMD rtPA was administered subretinally in 291 eyes (six publications)[28, 34-38] and intravitreally in only 48 eyes (four publications)[30, 39-41] (search performed in March 2015 on PubMed using keywords 'recombinant tissue plasminogen activator' AND 'submacular hemorrhage'). Although the application of intravitreal rtPA and gas might be underreported, there seems to be a preference for the subretinal application of rtPA and vitrectomy. This preference is possibly related to the assumed larger concentration of rtPA in the subretinal blood clot compared to intravitreal administration[29] and the introduction of smaller gauge vitrectomy equipment.

In this study, we did not find any significant differences between the volume reductions of subretinal blood, sub-RPE blood, and SRF in both groups at any time point. The large decrease in subretinal blood volume demonstrates the effectivity of both strategies. However, this outcome clarifies neither the exact role and penetration of rtPA nor the mechanism of gas displacement. Penetration of intravitreally injected tPA to the subretinal space was demonstrated in rabbit models by Tal K et al. (Penetration of Intravitreal Injected Tissue Plasminogen Activator to the Retina - Rats Model Study; ARVO Annual Meeting, May 03, 2015). It should be further investigated whether the subretinal concentrations of rtPA after intravitreal injection are sufficient to liquefy the blood clot, or whether the tamponade is more essential for displacement than is generally assumed.

The effect on sub-RPE hemorrhage was much less pronounced. The decrease in sub-RPE volume might be underestimated because, in the presence of large pre-operative subretinal hemorrhage, the sub-RPE component is not fully visible on OCT. Besides, sub-RPE volume partially consists of neovascular and old fibrous tissue, which is not expected to be affected significantly by pneumatic displacement treatment. Subretinal fluid disappeared in most patients after treatment, but persisted in some patients, owing to the ongoing activity of the underlying choroidal neovascularization.

The advantage of OCT measurements over standard fundus examinations is that it enables differentiation between subretinal blood and sub-RPE blood or -volume. Subretinal volume reduction of a hemorrhage is more likely to correlate with survival of the overlying retina than the extent of the area of hemorrhage, because important subretinal hemorrhage thickness changes are not masked by a thin remaining subretinal or sub-RPE hemorrhage residue. Therefore, we hypothesize that volume measurements are a clinically more meaningful and

sensitive tool than fundus examinations. Finally, because most hemorrhages display a heterogeneous distribution of blood in the cylinder of 2.5 mm (see the example in **Figure 1**), volume measurements are also expected to yield a more accurate hemorrhage quantification than macular thickness measurements using individual B-scans.

Six out of 12 patients gained more than 2 ETDRS visual acuity lines between baseline and 12 weeks in the intravitreal rtPA group and 4 out of 11 patients in the subretinal rtPA group. The visual acuity improvement in this study was much lower than reported in most retrospective studies.[11, 22-28, 30, 34-41] An explanation could be that preoperative visual acuity measurements are often underestimated on the accident and emergency departments owing to lack of time, no need for an accurate visual acuity measurement strategy and low contrast optotypes. In comparison, our preoperative visual acuity measurements were performed with high contrast ETDRS chart optotypes under trial standard operation procedure conditions, which most likely reveals a much better initial visual acuity. Nevertheless, the final visual acuity at 12 weeks was >20/200 in 92% in the intravitreal rtPA group and 82% in the subretinal rtPA group, which was a higher percentage than most retrospective studies have reported after treatment of SMH secondary to AMD.

Favorable anatomical and functional outcomes in both groups were obtained despite the occurrence of serious complications in both groups: retinal detachments and recurrent hemorrhages, as well as an elevated IOP after intravitreal rtPA and gas injection causing ischemic disk damage in one patient. To avoid undue pressure peaks after intravitreal gas injection, we suggest dividing the amount of injected gas over 2 days.

The strengths of this study are the prospective design, the randomization of the patients, the masked observers for volume measurements, balanced baseline characteristics and the use of rtPA prepared according to good manufacturing practice. In most published series the rtPA/tPA used has been prepared and stored in different ways with potentially uncertain or invalidated biological activity. In this study, for each patient we prepared rtPA within an hour before administration. Having biologically active tPA may be more important when applying it intravitreally than subretinally, because some dilution of the clot may be induced by the subretinal injection of fluid. Thus, in our study, both arms were tested on their true potential.

Limitations of this study are the small number of patients in each group. Randomization in a small study, like this one, may result in uneven distribution of variables, like the duration of AMD and the number of intraocular injections before the intervention. The longer duration of AMD, as well as the number of preoperative injections, could have caused more fibrosis in the subretinal rtPA group. However, this would not affect our primary outcome measure blood

displacement as blood and fibrosis can be distinguished from each other on OCT cross-sections (fibrosis being more hyperreflective than subretinal blood). If function recovery would have been the main endpoint, these variables would be more likely to result in a poorer functional outcome.

In conclusion, both the combination treatment of intravitreal rtPA with gas and subretinal rtPA, vitrectomy and gas were able to displace, on average, more than 90% of the subretinal blood volume between baseline and 4, 6 and 12 weeks postoperatively of acute SMH due to AMD with a hemorrhage size thinner than 1,250 µm. No significant differences in hemorrhage volume reduction were found between the two treatment modalities in this exploratory randomized controlled trial. To more definitely study the noninferiority of intravitreal rtPA with gas to subretinal rtPA, vitrectomy with gas concerning efficacy, safety, and function, a larger clinical trial would be necessary.

REFERENCES

1. Benner JD, Hay A, Landers MB,3rd, et al. Fibrinolytic-assisted removal of experimental subretinal hemorrhage within seven days reduces outer retinal degeneration. Ophthalmology 1994;101:672-81.

2. Toth CA, Morse LS, Hjelmeland LM, et al. Fibrin directs early retinal damage after experimental subretinal hemorrhage. Arch Ophthalmol 1991;109:723-9.

3. el Baba F, Jarrett WH,2nd, Harbin TS,Jr, et al. Massive hemorrhage complicating age-related macular degeneration. clinicopathologic correlation and role of anticoagulants. Ophthalmology 1986;93:1581-92.

4. Kiernan DF, Hariprasad SM, Rusu IM, et al. Epidemiology of the association between anticoagulants and intraocular hemorrhage in patients with neovascular age-related macular degeneration. Retina 2010;30:1573-8.

5. Bressler NM, Bressler SB, Childs AL, et al. Surgery for hemorrhagic choroidal neovascular lesions of age-related macular degeneration: Ophthalmic findings: SST report no. 13. Ophthalmology 2004;111:1993-2006.

6. Glatt H, Machemer R. Experimental subretinal hemorrhage in rabbits. Am J Ophthalmol 1982;94:762-73.

7. Gillies A, Lahav M. Absorption of retinal and subretinal hemorrhages. Ann Ophthalmol 1983;15:1068-74.

8. Hochman MA, Seery CM, Zarbin MA. Pathophysiology and management of subretinal hemorrhage. Surv Ophthalmol 1997;42:195-213.

9. Bhisitkul RB, Winn BJ, Lee OT, et al. Neuroprotective effect of intravitreal

triamcinolone acetonide against photoreceptor apoptosis in a rabbit model of subretinal hemorrhage. Invest Ophthalmol Vis Sci 2008;49:4071-7.

10. Scupola A, Coscas G, Soubrane G, et al. Natural history of macular subretinal hemorrhage in age-related macular degeneration. Ophthalmologica 1999;213:97-102.

11. van Zeeburg EJ, van Meurs JC. Literature review of recombinant tissue plasminogen activator used for recent-onset submacular hemorrhage displacement in age-related macular degeneration. Ophthalmologica 2013;229:1-14.

12. Heriot WJ. Intravitreal gas and TPA; an outpatient procedure for submacular hemorrhage. Paper presented at: American Academy of Ophthalmology Annual Vitreoretinal Update; Chicago, IL, 1996.

13. Haupert CL, McCuen BW, Jaffe GJ, et al. Pars plana vitrectomy, subretinal injection of tissue plasminogen activator, and fluid-gas exchange for displacement of thick submacular hemorrhage in age-related macular degeneration. Am J Ophthalmol 2001;131:208-15.

14. Chen CY, Hooper C, Chiu D, et al. Management of submacular hemorrhage with intravitreal injection of tissue plasminogen activator and expansile gas. Retina 2007;27:321-8.

15. Hassan AS, Johnson MW, Schneiderman TE, et al. Management of submacular hemorrhage with intravitreous tissue plasminogen activator injection and pneumatic displacement. Ophthalmology 1999;106:1900-6; discussion 1906-7.

16. Hillenkamp J, Surguch V, Framme C, et al. Management of submacular hemorrhage with intravitreal versus subretinal injection of recombinant tissue plasminogen activator. Graefes Arch Clin Exp Ophthalmol 2010;248:5-11.

17. Wu TT, Kung YH, Hong MC. Vitreous hemorrhage complicating intravitreal tissue plasminogen activator and pneumatic displacement of submacular hemorrhage. Retina 2011;31:2071-7.

18. Singh RP, Patel C, Sears JE. Management of subretinal macular haemorrhage by direct administration of tissue plasminogen activator. Br J Ophthalmol 2006;90:429-31.

19. Kamei M, Estafanous M, Lewis H. Tissue plasminogen activator in the treatment of vitreoretinal diseases. Semin Ophthalmol 2000;15:44-50.

20. Lincoff H, Kreissig I, Stopa M, et al. A 40 degrees gaze down position for pneumatic displacement of submacular hemorrhage: Clinical application and results. Retina 2008;28:56-9.

21. Stopa M, Lincoff A, Lincoff H. Analysis of forces acting upon submacular hemorrhage in pneumatic displacement. Retina 2007;27:370-4.

22. Meyer CH, Scholl HP, Eter N, et al. Combined treatment of acute subretinal haemorrhages with intravitreal recombined tissue plasminogen activator, expansile gas and bevacizumab: A retrospective pilot study. Acta Ophthalmol 2008;86:490-4.

23. Sacu S, Stifter E, Vecsei-Marlovits PV, et al. Management of extensive subfoveal haemorrhage secondary to neovascular age-related macular degeneration. Eye (Lond) 2009;23:1404-10.

24. Matt G, Sacu S, Stifter E, et al. Combination of intravitreal rTPA, gas and ranibizumab for extensive subfoveal haemorrhages secondary to neovascular age-related macular degeneration. Klin Monbl Augenheilkd 2010;227:221-5.

25. Arias L, Mones J. Transconjunctival sutureless vitrectomy with tissue plasminogen activator, gas and intravitreal bevacizumab in the management of predominantly hemorrhagic age-related macular degeneration. Clin Ophthalmol 2010;4:67-72.

26. Guthoff R, Guthoff T, Meigen T, et al. Intravitreous injection of bevacizumab,

tissue plasminogen activator, and gas in the treatment of submacular hemorrhage in age-related macular degeneration. Retina 2011;31:36-40.

27. Treumer F, Roider J, Hillenkamp J. Long-term outcome of subretinal coapplication of rtPA and bevacizumab followed by repeated intravitreal anti-VEGF injections for neovascular AMD with submacular haemorrhage. Br J Ophthalmol 2012;96:708-13.

28. Mayer WJ, Hakim I, Haritoglou C, et al. Efficacy and safety of recombinant tissue plasminogen activator and gas versus bevacizumab and gas for subretinal haemorrhage. Acta Ophthalmol 2013;91:274-8.

29. Kamei M, Misono K, Lewis H. A study of the ability of tissue plasminogen activator to diffuse into the subretinal space after intravitreal injection in rabbits. Am J Ophthalmol 1999;128:739-46.

30. Sobolewska B, Utebey E, Bartz-Schmidt KU, et al. Long-term visual outcome and its predictive factors following treatment of acute submacular hemorrhage with intravitreous injection of tissue plasminogen factor and gas. J Ocul Pharmacol Ther 2014;30:567-72.

31. van Zeeburg EJ, Cereda MG, van Meurs JC. Recombinant tissue plasminogen activator, vitrectomy, and gas for recent submacular hemorrhage displacement due to retinal macroaneurysm. Graefes Arch Clin Exp Ophthalmol 2013;251:733-40.

32. Tadayoni R, Svorenova I, Erginay A, er al. Decreased retinal sensitivity after internal limiting membrane peeling for macular hole surgery. Br J Ophthalmol 2012;96:1513-6.

33. Yushkevich PA, Piven J, Hazlett HC, et al. User-guided 3D active contour segmentation of anatomical structures: Significantly improved efficiency and reliability. Neuroimage 2006;31:1116-28.

34. Moisseiev E, Ben Ami T, Barak A. Vitrectomy and subretinal injection of tissue plasminogen activator for large submacular hemorrhage secondary to AMD. Eur J Ophthalmol 2014;24:925-31.

35. Dewilde E, Delaere L, Vaninbroukx I, et al. Subretinal tissue plasminogen activator injection to treat submacular haemorrhage during age-related macular degeneration. Acta Ophthalmol 2014;92:e497-8.

36. Chang W, Garg SJ, Maturi R, et al. Management of thick submacular hemorrhage with subretinal tissue plasminogen activator and pneumatic displacement for age-related macular degeneration. Am J Ophthalmol 2014;157:1250-7.

37. Kapran Z, Ozkaya A, Uyar OM. Hemorrhagic age-related macular degeneration managed with vitrectomy, subretinal injection of tissue plasminogen activator, gas tamponade, and upright positioning. Ophthalmic Surg Lasers Imaging Retina 2013;44:471-6.

38. Ritzau-Tondrow U, Baraki H, Hoerauf H. Minimally invasive therapy of submacular hemorrhage in exsudative age-related macular degeneration. Ophthalmologe 2012;109:670-5.

39. Lumi X, Sulak M. Treatment of submacular haemorrhage in patients with neovascular age related macular degeneration. Coll Antropol 2013;37 Suppl 1:223-6.

40. Fujikawa M, Sawada O, Miyake T, et al. Comparison of pneumatic displacement for submacular hemorrhages with gas alone and gas plus tissue plasminogen activator. Retina 2013;33:1908-14.

41. Papavasileiou E, Steel DH, Liazos E, et al. Intravitreal tissue plasminogen activator, perfluoropropane (C3F8), and ranibizumab or photodynamic therapy for submacular hemorrhage secondary to wet age-related macular degeneration. Retina 2013;33:846-53.

SUPPLEMENTAL MATERIAL 6.1

Supplemental table 6.1. Absolute volume change (mm³) of
subretinal blood, sub-RPE volume and subretinal fluid; average of two graders

	Week 4	Week 6	Week 12
Intravitreal rtPA, gas and bevacizumab			
Number	10	11	11
Subretinal blood			
Median (95%CI), in mm³	-0.63 (-1.62 – -0.26)	-0.62 (-1.64 – -0.36)	-0.87 (-1.66 – -0.40)
Sub-RPE volume			
Median (95%CI), in mm³	-0.11 (-0.33 – +0.04)	-0.02 (-0.12 – +0.04)	0.0 (-0.21 – +0.03)
Subretinal fluid			
Median (95%CI), in mm³	-0.01 (-0.05 – +0.00)	-0.02 (-0.04 – +0.00)	-0.02 (-0.07 – -0.01)
Subretinal rtPA, vitrectomy, gas and bevacizumab			
Number	10	11	10
Subretinal blood			
Median (95%CI), in mm³	-0.99 (-1.59 – -0.40)	-0.70 (-1.39 – -0.39)	-0.58 (-1.87 – -0.31)
Sub-RPE volume			
Median (95%CI), in mm³	0.00 (-0.09 – +0.08)	-0.03 (-0.08 – 0.00)	-0.03 (-0.59 – +0.09)
Subretinal fluid			
Median (95%CI), in mm³	-0.01 (-0.08 – 0.00)	-0.02 (-0.03 – -0.01)	-0.01 (-0.02 – 0.00)
Difference between treatment groups			
Subretinal blood			
P-value	0.39	0.95	0.81
Median* (95%CI), in mm³	-0.17 (-1.08 – +0.50)	+0.01 (-0.90 – +0.62)	+0.07 (-0.91 – +0.86)
Sub-RPE volume			
P-value	0.25	1.00	0.81
Median* (95%CI), in mm³	+0.11 (-0.06 – +0.40)	0.00 (-0.12 – +0.15)	-0.02 (-0.24 – +0.39)
Subretinal fluid			
P-value	0.80	0.85	0.51
Median* (95%CI), in mm³	0.00 (-0.04 – +0.04)	-0.01 (-0.03 – +0.03)	+0.01 (-0.03 – +0.06)

rtPA = recombinant tissue plasminogen activator; CI=confidence interval.
*A positive difference means that the volume reduction in the intravitreal rtPA group was larger than in the subretinal rtPA group, a negative difference means the opposite

Chapter

7

Phase-Resolved Doppler Optical Coherence Tomographic Features in Retinal Angiomatous Proliferation

Sankha Amarakoon*
Jan Hendrik de Jong*
Boy Braaf
Suzanne Yzer
Tom Missotten
Mirjam E.J. van Velthoven
Johannes F. de Boer

*Joint principal authorship

ABSTRACT

Purpose
To study patients diagnosed with retinal angiomatous proliferation (RAP) based on conventional imaging techniques with phase-resolved Doppler optical coherence tomography (OCT). To detect and localize blood flow in RAP lesions and to compare these findings to conventional imaging, which are mostly invasive and give limited information concerning intra- and transretinal blood flow.

Design
Single-center, consecutive observational case series.

Methods
Single center cohort study. Twelve treatment-naïve patients diagnosed with RAP based on fundus examination, fluorescein angiography, and indocyanine-green angiography, were included. Median age was 79 years (range 65-90). Patients were imaged with an experimental 1,040 nm swept-source phase-resolved Doppler OCT instrument. Abnormal flow was defined as intraretinal neovascularisation or retinal-choroidal anastomosis.

Results
In 11 patients adequate phase-resolved Doppler OCT images were obtained showing abnormal blood flow in the RAP lesion. In 4 patients a retinal-choroidal anastomosis was found, 3 patients showed intraretinal neovascularisation connected with a pigment epithelial detachment, 2 patients showed only intraretinal neovascularisation, and in 2 patients flow was limited to the subretinal or sub-retinal pigment epithelial space.

Conclusions
Phase-resolved Doppler OCT can detect and localize abnormal blood flow within RAP lesions. Blood flow was mostly confined to the intraretinal structures with or without a connecting pigment epithelial detachment; in one-third of patients, a retinal-choroidal anastomosis was detected. The potential of angiography with phase-resolved Doppler OCT to accurately distinguish between normal and pathologic blood flow in addition to structural OCT data without invasive procedures will help to further elucidate both retinal and choroidal vascular pathologies like RAP.

INTRODUCTION

Retinal angiomatous proliferation (RAP) is a distinct form of exudative age-related macular degeneration (AMD).[1,2] In their original reports, Slakter[3] and associates and Yannuzzi and associates[4] hypothesized that RAP was an intraretinal neovascular process that in a later stage extended to the subretinal space eventually progressing into a retinal-choroidal anastomosis. Later, Yannuzzi and associates[5,6] proposed that there might be at least 3 different vasogenic processes involved in the development of RAP lesions, stating that RAP can originate intraretinally, from the choroid or from both simultaneously.

It is estimated that RAP constitutes approximately 10%–15% of newly diagnosed neovascular AMD in Caucasians, whereas in Asian populations the incidence rate is significantly lower.[7,8] In unilateral RAP it has been reported that there is an accumulative annual risk to develop RAP in the other eye that is considerably higher than for any other type of neovascular AMD.[9] RAP lesions are reported in up to 60% of fellow eyes in 3 years.[10] Diagnosing RAP type AMD is clinically important, because, although there is no definite consensus on the best treatment modality for RAP, standard anti-vascular endothelial growth factor (VEGF) monotherapy tends to show persistent activity of the RAP lesion.[11-13] Combination treatment of photodynamic therapy with either triamcinolone or anti-VEGF seems to offer better results, but to date, only relatively small comparative trials have been performed.[14]

The diagnosis of RAP is currently based on a triad of evidence: fundus examination, fluorescein angiography, and indocyanine-green angiography. A telltale sign for RAP on fundus examination is the presence of a single or multiple small intraretinal hemorrhages overlying a retinal vessel.[3] RAP lesions are difficult to distinguish from classic or occult choroidal neovascularization (CNV) on fluorescein angiography. Early stages of RAP can be misinterpreted as classic CNV and later stages of RAP exhibit almost identical signs of occult CNV.[4] Indocyanine-green angiography is considered the standard diagnostic tool for an accurate diagnosis. The hallmark sign of RAP on indocyanine-green angiography is a mid to late phase hot spot, which corresponds to an intraretinal neovascularization or a retinal-choroidal anastomosis.[15,16] Therefore the presence of intraretinal hemorrhage(s), a suspicion of classic or occult CNV on fluorescein angiography and a hot spot on indocyanine-green angiography are evidence to claim the diagnosis of RAP. However, many general ophthalmologists do not have regular access to indocyanine-green angiography, and may therefore misclassify an RAP lesion as another, more common type of CNV.

In the last decade, spectral domain optical coherence tomography (OCT) has become irreplaceable in the management of AMD, though it takes a fairly experienced OCT interpreter to distinguish RAP from other CNV types.[17-19]

Furthermore, it is difficult to visualize the intraretinal process using conventional OCT and impossible to evaluate the transretinal blood flow which seems vital for the diagnosis of RAP. In short, RAP lesions cannot reliably be diagnosed without invasive angiography, and indocyanine-green angiography is of the essence for an accurate diagnosis.

OCT angiography is a new field of imaging of the retinal vasculature and is aimed at discriminating blood vessels from static tissue in a noninvasive and depth-resolved manner. Different approaches for OCT angiography of the retinal vasculature have been proposed by analyzing phase changes or intensity changes in the OCT signal that are caused by moving light-scattering particles.[20-22] Both approaches are capable of providing detailed maps of retinal and choroidal vascular beds. However, in contrast to intensity-based OCT angiography, phase-based OCT angiography is also suited for measuring flow velocities and directions. The use of OCT angiography has recently been demonstrated in polypoidal choroidal vasculopathy[23,24] and exudative macular diseases.[24,25] By providing noninvasive and depth-resolved information about retinal perfusion, OCT angiography is a promising tool in complementing routine conventional imaging.

Our group has developed a phase-stabilized 1,040 nm swept-source OCT system with phase-resolved Doppler OCT modality. With this device, we have demonstrated the detection of tissue reperfusion in a free retinal pigment epithelial-choroid graft after transplantation.[22,26] The phase-resolved Doppler OCT technique used in the current study is based on inter-B-scan comparison of phase changes which considerably improves flow contrasting down to the capillary level.[21] Patients diagnosed with RAP based on conventional techniques were evaluated with this phase-resolved OCT system to detect and localize abnormal blood flow in the region of the RAP lesion.

METHODS AND MATERIALS

Between March 1, 2013 and September 30, 2013, consecutive treatment-naïve patients diagnosed with an RAP lesion in 1 eye were included in this single-center case series. The study was approved by the local internal review board of the Rotterdam Eye Hospital and the Medical Ethical Committee of the Erasmus University Hospital (Rotterdam, The Netherlands). All patients provided written informed consent for the use of the noncommercially available phase-resolved Doppler OCT device.

All patients underwent a complete ophthalmologic examination including slit lamp biomicroscopy, Snellen visual acuity (converted to logMAR for statistical analysis), conventional spectral domain OCT, fundus photography, fluorescein angiography, and indocyanine-green angiography. Patients were included in this

study if they were aged 65 years or older, and had no other active ocular diseases affecting the macula. The diagnosis of RAP was based on a combination of the presence of small intraretinal hemorrhages on fundus examination, the appearance of choroidal neovascularization seen on fluorescein angiography and/or a hyperfluorescent mid to end phase hot spot on indocyanine-green angiography. Fluorescein and indocyanine-green angiographic images were reviewed for confirmation of the RAP diagnosis by 2 independent ophthalmologists (T.M. and J.M.). In case of disagreement, consensus was obtained through side-by-side discussion.

Patients were imaged using a previously developed optical frequency domain imaging system with a phase-resolved Doppler OCT modality. The instrument is based on a swept-source laser (Axsun Technologies Inc, Billerica, Massachusetts, USA) with a central wavelength of 1,040 nm operating at a 100 kHz A-scan rate. The axial resolution was measured to be 6.5 µm in air (4.8 µm in tissue) and the lateral resolution was 25.2 µm. Elaborate technical details of this optical frequency domain imaging instrument were described previously by Braaf et al.[21,22]

In phase-resolved Doppler OCT blood flow is detected noninvasively from phase-changes in the OCT signal caused by moving particles in the retina, especially the erythrocytes and leukocytes in blood vessels. In conventional phase-resolved OCT phase-changes are detected comparing successive A-scans. In high-speed OCT this results in a short time interval between repeated A-scans, which is insufficient to detect low flow velocities in small vessels. Inter-B-scan Doppler OCT was therefore used comparing B-scans instead of successive A-scans to increase the time interval between repeated A-scans and improve flow sensitivity. A backstitched-B-scan protocol was used in which 4 small repeated B-scans were stitched together to form a complete backstitched B-scan. The inter-B-scan time-interval was set to 2.5 ms (250 A-scans), which was found to be effective to detect flow velocities of less than 1 mm/s which is proven to be sufficient to image the retinal capillaries.[21] The phase-resolved Doppler OCT protocol used in this study measured a 3-dimensional data volume consisting of 300 single backstitched B-scans with 2000 A-scans/B-scan over a retinal square area of 3.0 x 3.0 mm and has an acquisition time of 6 seconds per volume. The sample arm power was 1.7 mW on the cornea and measured before every patient examination. The used power is safe according to the American National Standards Institute laser safety standards.

The phase-resolved Doppler OCT scan grid is indicated with a white dashed square on each fundus photograph (**Figures 1-4**, column 1). Fluorescein and indocyanine-green angiographic images were resized to the area of the phase-resolved Doppler OCT scan (**Figures 1-4**, columns 2 and 3, respectively). Phase-resolved Doppler-OCT measurements were processed to Doppler *en face* images (**Figures 1-4**, column 4) and cross-sectional Doppler tomograms (**Figures 1-4**, column 5). B-scans with significant eye motion artifacts were manually removed in

the Doppler en face images to facilitate interpretation and comparison with conventional imaging. Discontinuities in the flow displayed on the Doppler *en face* images were attributed to these eye motion artifacts. The location of the Doppler tomogram is indicated with a red dashed line in the Doppler *en face* image. The Doppler inter-B-scan phase differences (red) were projected over structural B-scans (grayscale) in the Doppler tomograms.

RESULTS

Twelve patients were included in this study based on fundus examination, fluorescein angiography, and indocyanine-green angiography. The median age of the patients was 79 years (range 65-90 years), and the median visual acuity at time of diagnosis was 0.57 logMAR (range 0.14-1.3 logMAR). Phase-resolved Doppler OCT imaging was of very poor quality in 1 patient, owing to the inability to fixate for a prolonged time, making Doppler analysis unreliable. Eleven patients were evaluated in the final analysis, baseline characteristics and examination outcomes are reported in **Table 1**.

In 10 out of 11 patients focal intraretinal hemorrhages were seen on fundus examination suggestive of an RAP lesion. All patients showed characteristics of RAP, with either classic or occult type lesions on fluorescein angiography, and in 10 out of 11 patients a mid to end phase hyperfluorescent hot spot was seen on indocyanine-green angiography.

In 9 out of 11 patients we found abnormal intraretinal blood flow on phase-resolved Doppler OCT. In 3 patients this was found to be connected to sub-retinal pigment epithelial blood flow in a pigment epithelial detachment and in 4 patients it was connected to the choroid, considered to be a retinal-choroidal anastomosis. In 2 out of 11 patients flow was limited to the subretinal or sub-retinal pigment epithelial space. Below, the imaging in all 11 patients is described in more detail.

In 2 patients (Patients 5 and 12) abnormal intraretinal blood flow was detected by phase-resolved Doppler OCT in the absence of a clear retinal-choroidal anastomosis (**Figure 1**). In both patients a small intraretinal hemorrhage was seen on fundus examination (**Figure 1**, column 1) and a hyperfluorescent hot spot on late phase indocyanine-green angiography at the same location (**Figure 1**, column 2). Poorly defined hyperfluorescent areas were found on early phase fluorescein angiography near the foveal avascular zone in both patients (**Figure 1**, column 3).

The Doppler *en face* image of Patient 5 showed enhanced blood flow at the ending of a capillary at the margin of the foveal avascular zone (**Figure 1**, row 1, column 4, red circle).
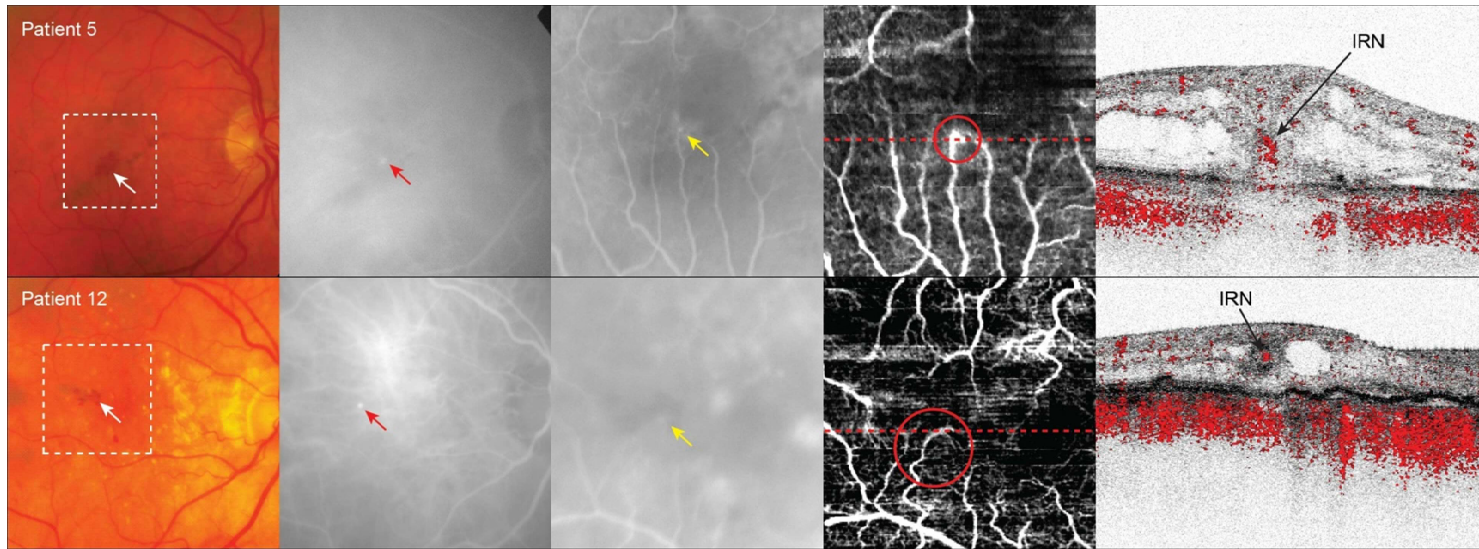
Figure 1. Retinal angiomatous proliferation showing abnormal intraretinal blood flow only. Intraretinal neovascularization (IRN) illustrated by images from Patients 5 and 12. The white dotted square in the fundus photograph (Column 1) indicates the area scanned with phase-resolved Doppler optical coherence tomography (OCT) and the red dotted line (Column 4) corresponds to the location of the tomographic image. The fundus photographs show a small intraretinal hemorrhage (Column 1, white arrows). On late-phase indocyanine green angiography a hyperfluorescent hot spot is seen at the same location (Column 2, red arrows). Poorly defined hyperfluorescent areas are seen on early-phase fluorescein angiography (Column 3, yellow arrows). In Patient 5 (Column 4, top row, red circle), enhanced blood flow at the ending of a capillary at the margin of the foveal avascular zone is detected in the Doppler en face image. The Doppler tomogram reveals the depth-resolved location (Column 5, top row, indicated by "IRN"). In Patient 12 (Column 4, bottom row, red circle), the Doppler en face image depicts a tortuous capillary near the foveal avascular zone. The Doppler tomogram through the ending of this capillary confirms abnormal blood flow confined to the intraretinal structures (Column 5, bottom row, indicated by "IRN").
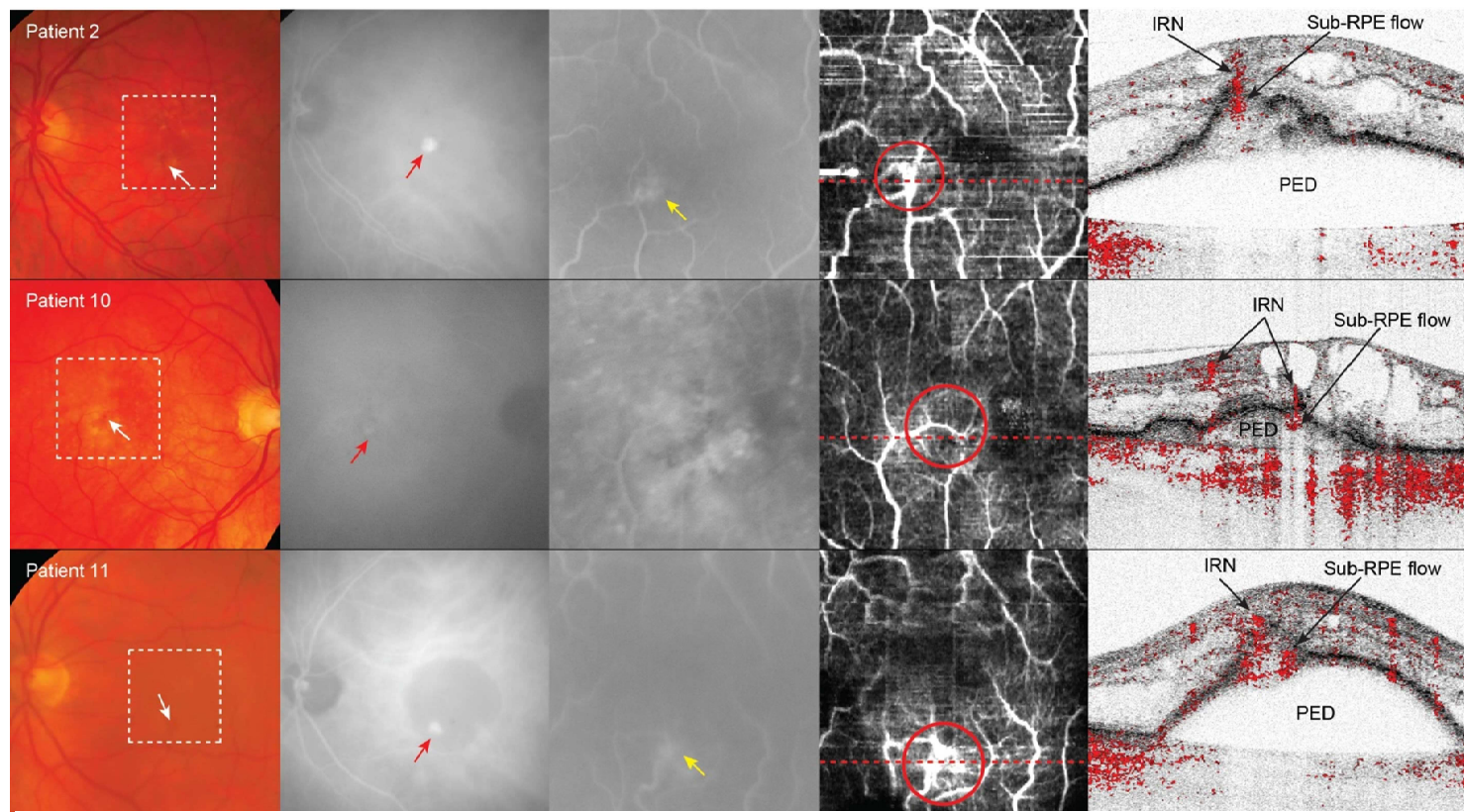
Figure 2. Caption follows on next page.

Figure 2. Retinal angiomatous proliferation showing abnormal intraretinal blood flow related to subretinal flow in a pigment epithelial detachment (PED). Intraretinal neovascularization (IRN) connected to sub–retinal pigment epithelial flow in a pigment epithelial detachment shown in images from Patients 2, 10, and 11. The white dotted square in the fundus photograph (Column 1) indicates the area scanned with phase-resolved Doppler optical coherence tomography (OCT) and the red dotted line (Column 4) corresponds to the location of the tomographic image. Intraretinal hemorrhages are seen on fundus photography in all patients (Col-umn 1, white arrows) and were consistent with the location of the hyperfluorescent hot spot depicted on late-phase indocyanine green angiography (Column 2, red arrows). Early fluorescein angiography shows hyperfluorescent vascular networks in Patients 2 and 11 (Column 3, yellow arrows). (Column 4, top row) The Doppler en face image of Patient 2 shows 2 connecting vessels in an area of enhanced blood flow at the border of the foveal avascular zone (red circle). (Column 5, top row) The Doppler tomogram clearly reveals the depth-resolved information locating abnormal blood flow in the retina (indicated by "IRN") and in the sub–retinal pigment epithe-lial space (indicated by "sub-RPE flow"). (Column 4, middle row) The Doppler en face image of Patient 10 depicts an abnormally curved vessel near the fovea (red circle), of which the Doppler tomogram demonstrates the dissection of this vessel at different depth locations (Column 5, middle row, indicated by "IRN") and that it can be traced to the area under the detached retinal pigment epithe-lium (indicated by "sub-RPE flow"). (Column 4, bottom row) The Doppler en face image of Patient 11 shows an abnormal vascular network (red circle). (Column 5, bottom row) The Doppler tomogram shows an area of abnormal blood flow in the retina continuous to the sub–retinal pigment epithelial region just at the top of the pigment epithelial detachment (indicated by "IRN" and "sub-RPE flow," respectively).
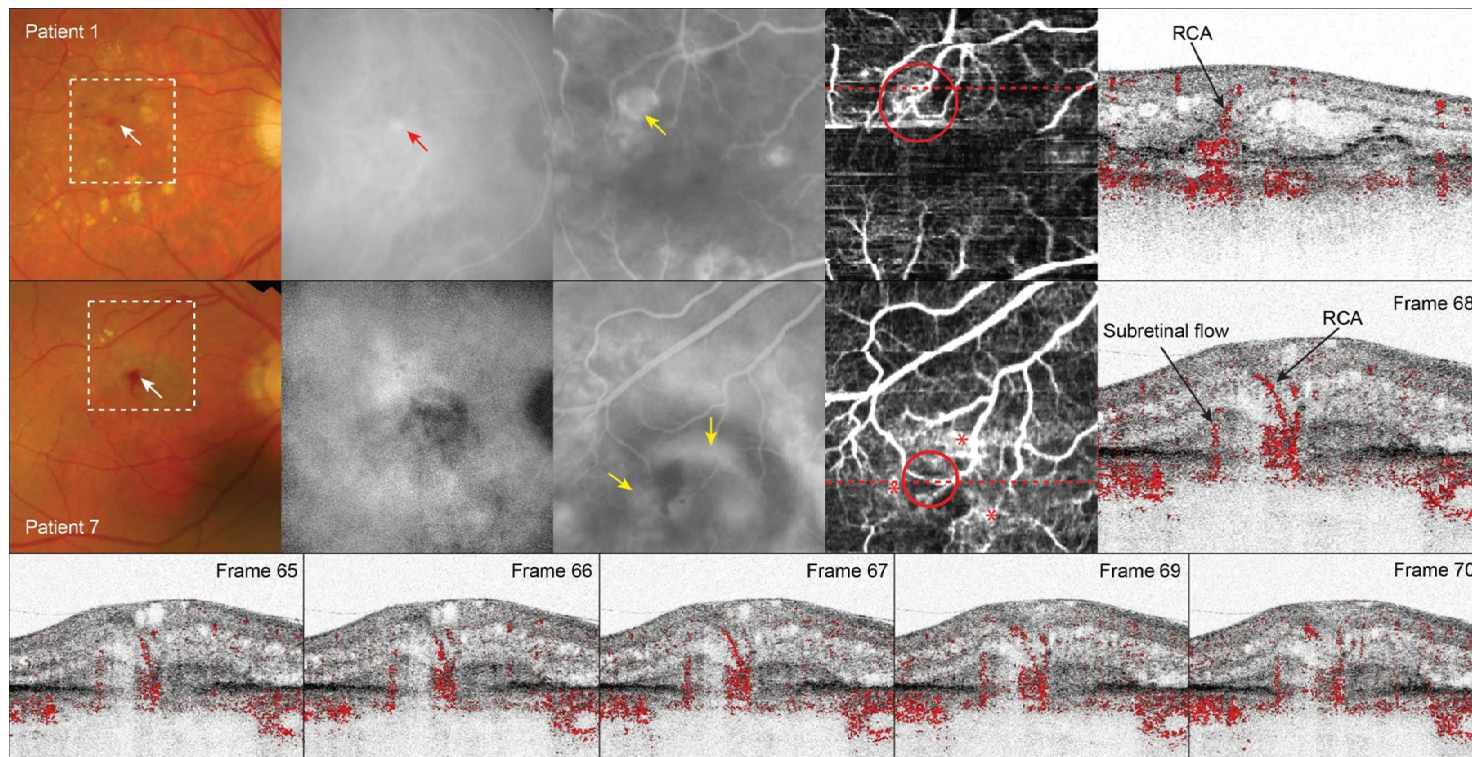
Figure 3. Figure is extended on next page.
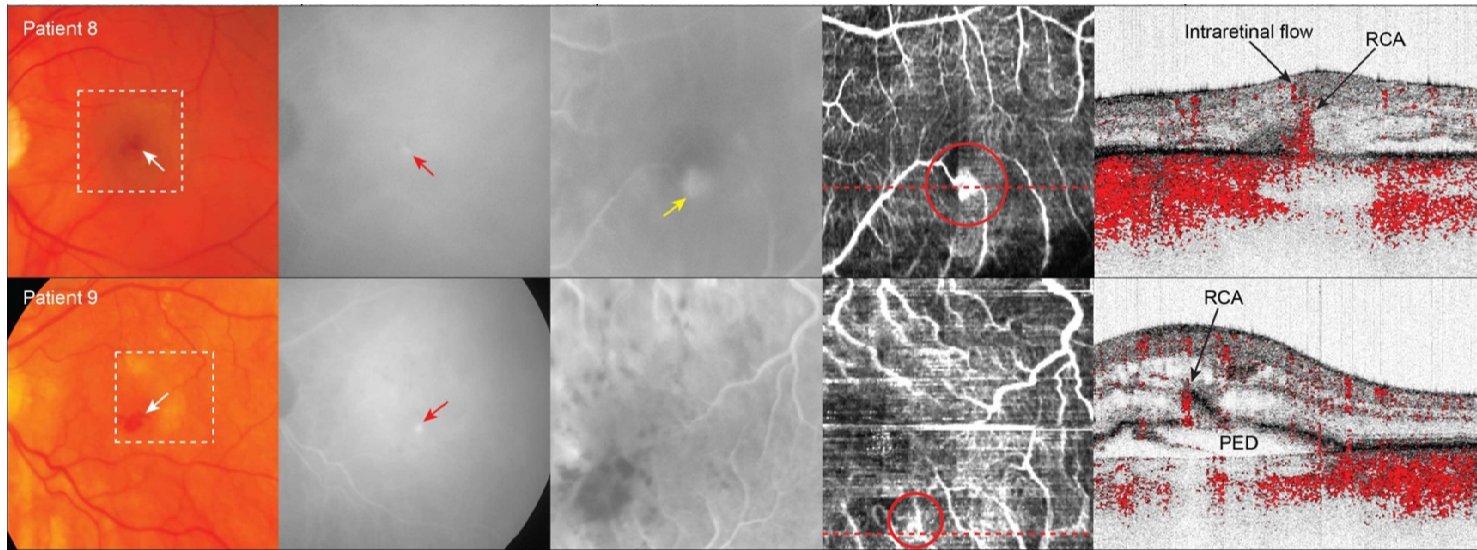
Figure 3. Retinal angiomatous proliferation showing abnormal blood flow through a retinal choroidal anastomosis. Retinal choroidal anastomosis illustrated by images from Patients 1, 7, 8, and 9. The white dotted square in the fundus photograph (Column 1) indicates the area scanned with phase-resolved Doppler optical coherence tomography (OCT) and the red dotted line (Column 4) corresponds to the location of the tomographic image. In all 4 patients intraretinal hemorrhages are seen in the fundus photograph (Column 1, white arrows). (Column 2, red arrows) A hyperfluorescent hot spot on late-phase indocyanine green angiography is seen in Patients 1 (top row), 8 (fourth row), and 9 (bottom row). (Column 3, yellow arrows) Early fluorescein angiography shows abnormal hyperfluor-escent vascular networks in Patient 1 (top row), 7 (second row), and 8 (fourth row). (Column 4) The Doppler en face image of Patients 1 (top row), 8 (fourth row), and 9 (bottom row) show a mesh-like vascular network extending to the margin of the foveal avascular zone (red circles). (Column 5) The Doppler tomogram of Patients 1 (top row), 8 (fourth row), and 9 (bottom row) shows an intraretinal vessel connecting to blood flow detected in the sub–retinal pigment epithelial space (indicated as "RCA"); associated with a pigment epithelial detachment in Patient 9 (bottom row; indicated as "PED"). The Doppler en face image of Patient 7 depicts 2 vessels (Column 4, second row, red circle), surrounded by several abnormal vascular networks (red asterisks). The third row represents a series of Doppler tomograms to illustrate that blood flow is traced in consecutive frames from its intraretinal location to the choroid.
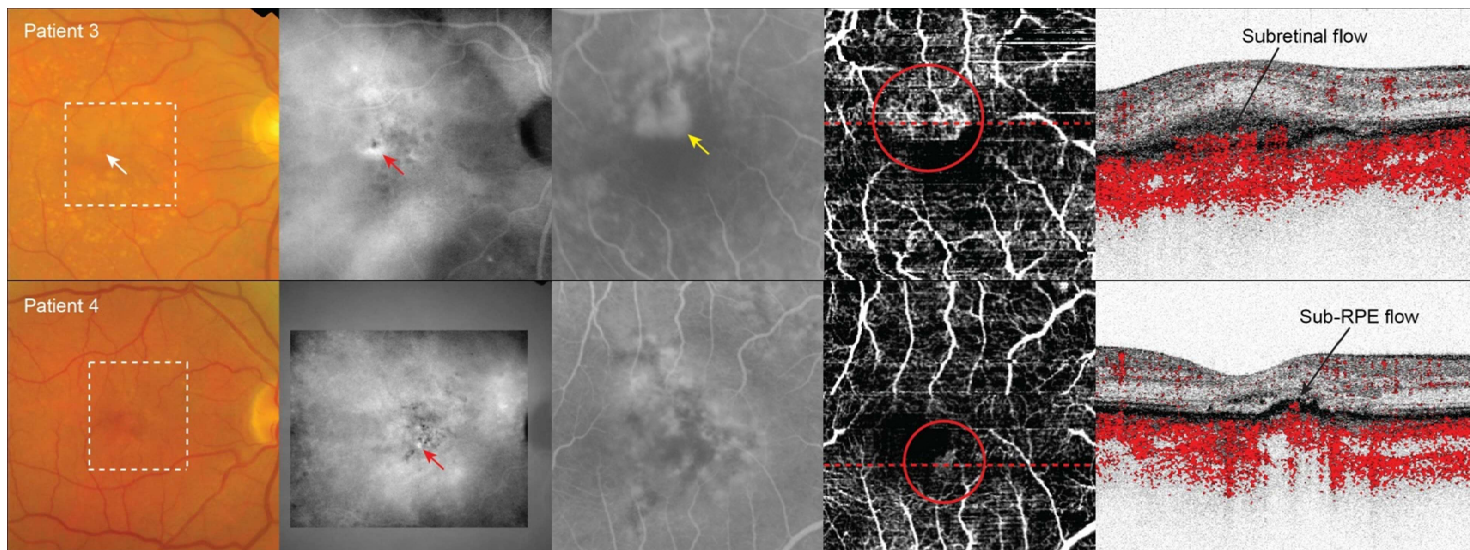
Figure 4. Examples of pure subretinal and sub–retinal pigment epithelial abnormal blood flow. Images from Patients 3 and 4, showing abnormal blood flow on phase-resolved Doppler optical coherence tomography (OCT) confined to the subretinal and subretinal pigment epithelial space, respectively. The white dotted square in the fundus photograph (Column 1) indicates the area scanned with phase-resolved Doppler OCT and the red dotted line (Column 4) corresponds to the location of the tomographic image. Top row: Fundus photograph (Column 1, white arrow) shows an intraretinal hemorrhage; a late-phase hyperfluorescent hot spot is seen on indocyanine green angiography (Column 2, red arrow), and mixed/classic choroidal neovascularization (CNV) on fluorescein angiography (Column 3, yellow arrow). The Doppler en face image shows an abnormal vascular network at the border of the foveal avascular zone (Column 4, red circle). The Doppler tomogram shows abnormal blood flow confined to the subretinal space (Column 5). Row 2: Fundus photograph (Column 1) showing hyperpigmentation; a late-phase hyperfluorescent hot spot on indocyanine green angiography (Column 2, red arrow); and occult CNV (Column 3); Doppler en face image shows an abnormal vascular network at the border of the foveal avascular zone (Column 4, red circle), while it is limited to the sub–retinal pigment epithelial space alone (Column 5, indicated as "sub-RPE flow").

Table 1: Patient characteristics and examination outcomes

Study no.	Sex (M/F)	Age (years)	RAP eye	VA (LogMAR)	SD-OCT		
					IRF	SRF	PED
1	F	82	OD	0.7	+	+	-
2	F	75	OS	0.72	+	+	+
3	M	73	OD	0.24	-	+	-
4	M	67	OD	0.14	-	+	-
5	M	82	OD	0.8	+	+	-
6	*M*	*79*	*OD*	*0.14*	+	+	-
7	M	90	OD	1.28	+	-	-
8	M	65	OS	0.32	+	+	-
9	F	79	OS	0.7	+	-	+
10	M	78	OD	0.44	+	-	+
11	M	90	OS	1.3	+	+	+
12	F	89	OD	0.44	+	-	-

Table 1: Extended

Study no.	FE IRH	FA CNV	ICG Hotspot	PRD-OCT Abnormal flow	Fellow eye
1	+	+	+	RCA	Dry AMD
2	+	+	+	IRNP	Dry AMD
3	+	+	+	AVN, subretinal	Neovascular AMD
4	-	+	+	AVN, sub-RPE	Dry AMD
5	+	+	+	IRN	Neovascular AMD
6	*+*	*+*	*+*	*n/a*	*Neovacular AMD*
7	+	+	-	RCA	Neovascular Glaucoma
8	+	+	+	RCA	Dry AMD
9	+	+	+	RCA	Dry AMD
10	+	+	+	IRNP	Dry AMD
11	+	+	+	IRNP	Dry AMD
12	+	+	+	IRN	Dry AMD

AMD = age-related macular degeneration; AVN = abnormal vascular network; CNV = choroidal neovascularization; F = female; FA = fluorescein angiography; FE = fundus examination; ICG = indocyanine-green angiography; IRF= intraretinal fluid; IRH= intraretinal hemorrhage; IRN = intraretinal neovascularization; IRNP= intraretinal neovascularization with pigment epithelial detachment; LogMAR = logarithm of minimal angle of resolution; M = male; n/a = not applicable; OD = right eye; OS = left eye; PED =pigment epithelial detachment; PRD-OCT = phase-resolved Doppler optical coherence tomography; RAP = retinal angiomatous proliferation; RCA = retinal choroidal anastomosis; RPE = retinal pigment epithelium; SD-OCT = spectral domain optical coherence tomography; SRF = subretinal fluid; VA = visual acuity.

The Doppler tomogram clearly reveals the depth resolved location of an intraretinal neovascularization, by showing abnormal intraretinal blood flow (**Figure 1**, row 1, column 5). A connection of this intraretinal blood flow to the choroid was not detected (**Supplemental video 7.1**).

The Doppler *en face* image of Patient 12 depicted a tortuous capillary near the foveal avascular zone (**Figure 1**, row 2, column 4, red circle). The Doppler tomogram (**Figure 1**, row 2, column 5) through the ending of this capillary confirmed abnormal blood flow confined to the intraretinal structures, considered to be an intraretinal neovascularization.

The location of abnormal intraretinal blood flow seen on phase-resolved Doppler OCT corresponded to the location of the small intraretinal hemorrhage(s) seen on fundus examination, as well as to the hyperfluorescent hot spot on late phase indocyanine-green angiography and the hyperfluorescent areas indicated on early fluorescein angiography.

In 3 patients (Patients 2, 10 and 11) the phase-resolved Doppler OCT images detected abnormal intraretinal blood flow connected to sub-retinal pigment epithelial blood flow in a pigment epithelial detachment (**Figure 2**). Intraretinal hemorrhages were seen on fundus examination in all patients (**Figure 2**, column 1) and were consistent with the location of the hyperfluorescent hotpot depicted on late phase indocyanine-green angiography (**Figure 2**, column 2). In Patient 11 the hyperfluorescent hot spot on indocyanine-green angiography was found at the border of a pigment epithelial detachment (**Figure 2**, row 3, column 2). Early fluorescein angiography showed hyperfluorescent vascular networks in Patient 2 and 11 (**Figure 2**, column 3) and increasing leakage in the late phase fluorescein angiography in all three patients (data not shown).

The Doppler *en face* image of Patient 2 showed two connecting vessels in an area of enhanced blood flow at the border of the foveal avascular zone (**Figure 2**, row 1, column 4, red circle). The Doppler tomogram clearly revealed the depth-resolved information locating abnormal blood flow in the retina (intraretinal neovascularization) and in the sub-retinal pigment epithelial space (**Figure 2**, row 1, column 5).

The Doppler *en face* image of Patient 10 depicted an abnormally curved vessel near the fovea (**Figure 2**, row 2, column 4, red circle). The Doppler tomogram (**Figure 2**, row 2, column 5) demonstrates dissecting this vessel twice at different depth locations (indicated by 'IRN' in the figure) and it showed it could be traced from the inner retinal layers to the area under the detached retinal pigment epithelium.

On the Doppler *en face* image of Patient 11 an abnormal vascular network was seen (**Figure 2**, row 3, column 4, red circle). The Doppler tomogram showed an area of abnormal blood flow in the retina continuous to the sub-retinal pigment epithelial region just at the top of the pigment epithelial detachment (**Figure 2**,

row 3, column 5) without any vessels in the pigment epithelial detachment or along the retinal pigment epithelium connecting to the choroid (**Supplemental video 7.2**).

In all 3 patients, the consecutive cross-sectional phase-resolved Doppler OCT tomograms showed signs of transretinal flow. However, that flow could not be followed to the choroid on consecutive cross-sectional phase-resolved Doppler OCT tomograms. Therefore blood flow is considered confined to the retina alone. There was a direct correlation with the location of the intraretinal neovascularization on phase-resolved Doppler OCT tomogram and the location of the small intraretinal hemorrhages seen on fundus examination and with the hyperfluorescent hot spots on late phase indocyanine-green angiography in all patients.

In 4 patients (Patients 1, 7, 8 and 9) transretinal blood flow was detected with phase-resolved Doppler OCT, traceable from an intraretinal location to the choroid in consecutive frames, considered to be an retinal-choroidal anastomosis (**Figure 3**). In all 4 patients intraretinal hemorrhages were seen on fundus examination (**Figure 3**, column 1), which corresponded to the location of the hyperfluorescent hot spots found on late phase indocyanine-green angiography (**Figure 3**, column 2) in Patients 1, 8 and 9. Indocyanine-green angiography did not reveal a hot spot in Patient 7, although the hemorrhage seen on fundus examination was suggestive for RAP. Early fluorescein angiography showed abnormal hyperfluorescent vascular networks in Patients 1, 7 and 8 (**Figure 3**, column 3) with increasing leakage in the late phase (not shown).

On the Doppler *en face* image of Patient 1 a mesh-like vascular network is shown extending to the margin of the foveal avascular zone (**Figure 3,** row 1, column 4, red circle). On the Doppler tomogram an intraretinal vessel connects to blood flow detected in the sub-retinal pigment epithelial space (indicated as 'RCA' in **figure 3**, row 1, column 5).

The Doppler *en face* image of Patient 7 depicted two vessels (**Figure 3,** row 2, column 4, red circle) extending to region of the hemorrhage seen on fundus examination (**Figure 3**, row 2, column 1). These vessels were surrounded by several abnormal vascular networks (**Figure 3**, row 2, column 4, red asterisks). The Doppler tomogram (**Figure 3**, row 2, column 5) demonstrated the cross-sectional representation of transretinal blood flow (retinal-choroidal anastomosis) and flow extending from or to the choroid. **Figure 3**, row 3, shows a sequence of consecutive frames through the retinal-choroidal anastomosis) illustrating the progression of the blood flow detectable from its intraretinal location to the sub-retinal pigment epithelial space (**Supplemental video 7.3 and 7.4**).

The Doppler *en face* image of Patient 8 showed 2 vessels connecting to an area of blood flow located in the foveal avascular zone (**Figure 3**, row 4, column 4, red circle). The Doppler tomogram showed subretinal blood flow connecting to an

intraretinal vessel, considered a retinal-choroidal anastomosis (**Figure 3**, row 4, column 5).

The Doppler *en face* image of Patient 9 depicted a vascular network (**Figure 3**, row 5, column 4, red circle) near the foveal avascular zone. On the Doppler tomogram a vessel is displayed in the area of a local break in the retinal pigment epithelium, on top of the pigment epithelial detachment (indicated by 'RCA' in **Figure 3**, row 5, column 5). In the surrounding frames it becomes visible that this vessel forms an anastomosis with vessels located within the pigment epithelial detachment and with intraretinal vessels (see also **Supplemental video 7.5**).

The location of the retinal-choroidal anastomosis seen on phase-resolved Doppler OCT was consistent with the location of the intraretinal hemorrhages seen on fundus examination in all patients, and also with the late phase hot spots on indocyanine-green angiography in Patients 1, 8 and 9 and the early hyperfluorescent vascular networks seen on fluorescein angiography in Patients 1, 7 and 8.

In 2 patients (Patients 3 and 4) there was no discernible abnormal blood flow either intraretinally or transretinally (**Figure 4**). Patient 3 showed an intraretinal hemorrhage on fundus examination, whilst in Patient 4 only hyperpigmentation was seen (**Figure 4**, column 1). Both patients revealed a late phase hyperfluorescent hot spot on indocyanine-green angiography (**Figure 4**, column 2). Fluorescein angiography showed a mixed/classic CNV in patient 3 and an occult CNV in patient 4 (**Figure 4**, column 3). On the Doppler *en face* image an abnormal vascular network was seen at the border of the foveal avascular zone in both patients (**Figure 4**, column 4, red circles). The Doppler tomogram of Patient 3 showed abnormal blood flow confined to the subretinal space (**Figure 4**, row 1, column 5) and sub-retinal pigment epithelial space (shown in **Supplemental video 7.6**), while in patient 4 (**Figure 4**, row 2, column 5) it was limited to the sub-retinal pigment epithelial space alone. These findings corresponded to the mixed/classic-type and occult CNV that was seen on fluorescein angiography, respectively.

Figure 5 shows the most representative images from the head-to-head comparison of the spectral domain OCT scan with phase-resolved Doppler OCT tomograms for each of the 4 subcategories described above. For each of the 11 patients a spectral domain OCT scan was chosen that resembled the location of the phase-resolved Doppler OCT as closely as possible. In all images the main overall structures were comparable. Smaller details, for example small intraretinal cysts, seemed slightly better defined on the phase-resolved intensity OCT images. The region of abnormal blood flow localized on the phase-resolved Doppler OCT tomograms corresponded to a high reflective area within or under the retinal tissue on the spectral domain OCT. Patients 8 and 11 are the best examples of this finding.
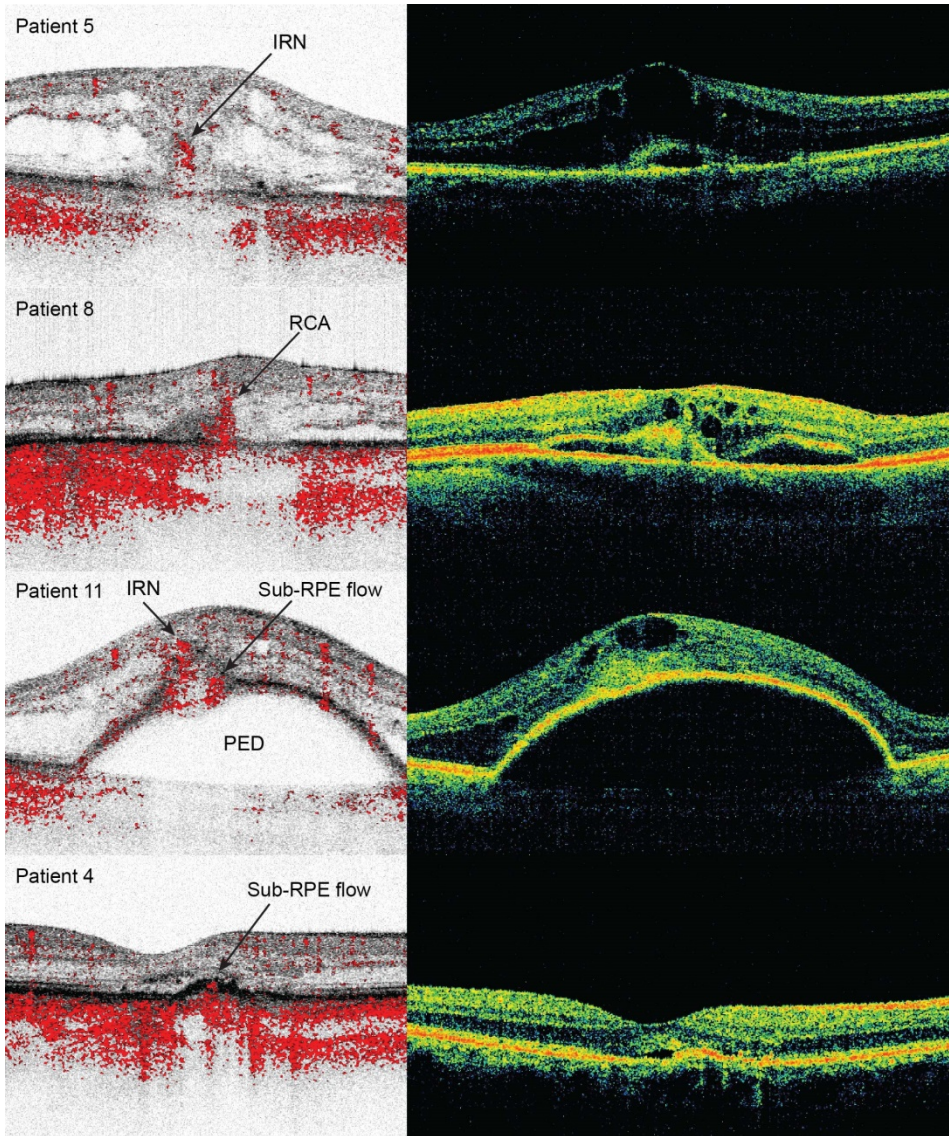
Figure 5. Head-to-head comparison of spectral-domain and phase-resolved Doppler optical coherence tomography (OCT) images. The most representative cases for each of the subtypes of abnormal blood flow detected based on phase-resolved Doppler OCT are shown: Patients 5 (Row 1), 8 (Row 2), 11 (Row 3), and 4 (Row 4), respectively. The left images are the phase-resolved Doppler OCT tomograms and the right images are corresponding spectral-domain OCT images. IRN [intraretinal neovascularization; PED [pigment epithelial detachment; RCA [retinal choroidal anastomosis; RPE [retinal pigment epithelium.

DISCUSSION

In this case series of treatment-naïve RAP patients, phase-resolved Doppler OCT was able to detect and localize the presence of abnormal intra- and transretinal blood flow. Abnormal intra- or transretinal blood flow was detected in 9 out of 11 patients. This abnormal blood flow can be divided into 3 major variations: first, as merely intraretinal (2 patients), second as an intraretinal neovascularisation connected to a pigment epithelial detachment (3 patients), and third as transretinal flow illustrative of a retinal-choroidal anastomosis (4 patients). In 2 patients, blood flow was confined to the sub-retinal pigment epithelial or subretinal space (1 patient each), which seemed more illustrative of typical occult and classic CNV, respectively. The region of the abnormal blood flow on phase-resolved Doppler B-scan tomograms could be correlated to hyperreflective structural changes in the corresponding spectral domain OCT scans.

RAP is considered predominantly an intraretinal neovascularization that responds better to combination treatment including photodynamic therapy than to anti-VEGF monotherapy. Conventional imaging for AMD does not discriminate accurately between intraretinal and subretinal blood flow. While fluorescein angiography is adequate to use in the diagnosis of classic or occult CNV, additional indocyanine-green angiography imaging is preferred to make a diagnosis of RAP. Given the limited access to indocyanine-green angiography in general, the diagnosis of RAP may be underreported. Doppler signals combined with structural data provided by cross-sectional tomograms visualize the depth-localization of retinal blood flow. This enables accurate differentiation between normal and abnormally located blood flow, and between intra- and subretinal or sub-retinal pigment epithelial neovascularization.

Our head-to-head comparison of indocyanine-green angiography with phase-resolved Doppler OCT showed very accurate correspondence in localizing the RAP lesion. In 10 out of 11 patients indocyanine-green angiography showed a hot spot in mid to end phase, that in all cases corresponded to abnormal blood flow seen in the same area on the Doppler *en face* image. However, phase-resolved Doppler OCT showed abnormal transretinal blood flow corresponding to an retinal-choroidal anastomosis in one patient (patient 7, **Figure 3**) who did not show a clear hot spot on indocyanine-green angiography. The hot spot is possibly indiscernible from the underlying occult CNV on indocyanine-green angiography. In Patients 3 and 4 the hot spot on indocyanine-green angiography did not correlate to abnormal intraretinal blood flow seen on phase-resolved Doppler OCT, but to blood flow confined to the subretinal and sub-retinal pigment epithelial space, respectively, which is more illustrative of classic or occult CNV.[27] It has also been suggested before that a small subretinal neovascularization cannot be ruled out when a late phase hot spot is seen on indocyanine-green angiography.[3,6]

Besides accurately determining the depth of abnormal blood flow, and providing highly detailed visualization of the retinal vasculature in the Doppler *en face* images, phase-resolved Doppler OCT has distinct advantages over fluorescein and indocyanine-green angiography as it is noninvasive, easy to perform and has a short measurement time (6 seconds in this study). These advantages allow for repetitive measurements in a safe and more comfortable manner, which is preferable when intensive treatment follow-up is necessary. With the addition of phase-resolved Doppler OCT to the current spectral domain OCT diagnostic evaluation, AMD patients could also benefit from an early and accurate diagnosis of the different subtypes of exudative AMD without resorting to invasive techniques, and which would entail better optimization of treatment management decisions early in the disease.

It is hypothesized that late stage RAP shows a distinct retinal-choroidal anastomosis, while early stages of RAP could be either intraretinal or choroidal in origin.[6] In our study, we probably included patients with late-stage RAP. Four patients presented with a developed retinal-choroidal anastomosis (**Figure 3**) of which it cannot be determined in hindsight whether the origin was retinal or choroidal. In the 3 patients with intraretinal blood flow connecting to sub-retinal pigment epithelial flow in a pigment epithelial detachment, it is likely to hypothesize that these originated intraretinally. With progression of the intraretinal neovascularization it penetrated through the retinal pigment epithelium and formed a pigment epithelial detachment without any connection to the choroid. On the other hand, it can also be argued that the process started in the choroid. After the formation of a retinal-choroidal anastomosis flow and leakage increase locally, causing a pigment epithelial detachment to emerge (comparable to the features seen in Patient 9, **Figure 3**, row 5, column 5). Growth of the pigment epithelial detachment could, in turn, cause a disruption or break of the retinal-choroidal anastomosis, resulting in even more leakage into the pigment epithelial detachment (as displayed in **Figure 2**, column 5) but also a disconnection with the choroidal vasculature. In 2 patients in whom we detected an intraretinal neovascularisation confined to the intraretinal layers, Patient 12 in our opinion strongly supports the hypothesis that a purely intraretinal lesion can occur (**Figure 1**, row 2, column 5). A larger cohort of patients with different stages of RAP is needed to establish the Doppler OCT features further and to clarify the pathophysiology of RAP.

With the current setup of the phase-resolved Doppler OCT system, adequate images were obtained in 11 out of 12 patients. One patient was unable to fixate properly and had an increased instance of movement artifacts. However, even in the presence of poor fixation in most AMD patients, the system was able to obtain good quality images for analysis. The addition of retinal tracking will improve image acquisition, quality, and interpretation.[28,29]

In depicting and interpreting phase-resolved Doppler OCT images it is important to realize that transretinal blood flow is not a pure vertical or horizontal flow. The cross-sectional tomograms in this paper illustrate the most representative images for the series of retinal-choroidal anastomosis or intraretinal neovascularization. Consecutive tomograms from the same area, as shown in **Figure 3**, row 3, show the course and extent of a small vascular meshwork better than one single tomogram. Combining multiple tomogram images into a 3-dimensional layout of the vascular network will provide easier interpretation of similar data sets, showing both the normal and abnormal regions.

Fluorescein angiography is currently the standard in the evaluation of neovasculair AMD. The most important observed features are a hyperfluorescent area in the early phase, leakage in the late phase and pooling of dye in a pigment epithelial detachment. Although our phase-resolved Doppler OCT system is able to detect the low flow velocities of <1 mm/s in retinal capillaries,[21] it is not able to detect leakage from neovascularization in the Doppler *en face* images. In fact, any setup for OCT angiography will not be able to detect leakage, pooling or staining as seen on fluorescein and indocyanine-green angiography, and this should be taken into account when translating OCT angiography from a research setting to clinical practice.

Another limitation of our phase-resolved Doppler OCT system is the current field of view of 10° compared to the 30-50° field of view used in fluorescein and indocyanine-green angiography. The field of view could be enlarged by implementing a retinal tracker allowing for a compilation of several smaller B-scan grids. Another possibility to improve the field of view is to increase the current A-scan rate of 100 kHz. Faster swept-source lasers have been demonstrated with imaging speeds up to 3 MHz. Blatter and associates[30] used a 1.68 MHz swept-source laser to demonstrate OCT angiography with a field of view of 50° based on an intensity variance algorithm.

Jia *et al.*[25] demonstrated blood flow quantification in neovascular AMD patients based on speckle decorrelation angiography. Future developments may also include detecting absolute blood flow velocities and blood flow directions which is only possible using phase-based Doppler OCT. Flow velocities could be of importance in patients with for instance retinal vein obstructions where absolute flow velocities could be compared to the arm-to-retina circulation time measured by fluorescein angiography. Flow directions may also provide more information about the hemodynamic situation in retinal vascular disorders, such as RAP.

In conclusion, we have demonstrated with this small case series that phase-resolved Doppler OCT can pinpoint abnormal intra- and transretinal blood flow in the majority of patients diagnosed with RAP lesions via conventional imaging techniques. The potential of angiography of phase-resolved Doppler OCT is to accurately distinguish between normal and pathologic blood flow and vascular

structures comparable to conventional imaging techniques, but it also provides structural OCT data offering specific depth-location of the abnormal blood flow structures without invasive procedures. This will help to further elucidate both retinal and choroidal vascular pathologies such as RAP.

REFERENCES

1. Hartnett ME, Weiter JJ, Staurenghi G, Elsner AE. Deep retinal vascular anomalous complexes in advanced age-related macular degeneration. *Ophthalmology*. 1996;103(12):2042-2053.

2. Hartnett ME, Weiter JJ, Garsd A, Jalkh AE. Classification of retinal pigment epithelial detachments associated with drusen. *Graefes Arch Clin Exp Ophthalmol*. 1992;230(1):11-19.

3. Slakter JS, Yannuzzi LA, Schneider U, et al. Retinal choroidal anastomoses and occult choroidal neovascularization in age-related macular degeneration. *Ophthalmology*. 2000;107(4):742-53; discussion 753-4.

4. Yannuzzi LA, Negrao S, Iida T, et al. Retinal angiomatous proliferation in age-related macular degeneration. *Retina*. 2001;21(5):416-434.

5. Freund KB, Ho IV, Barbazetto IA, et al. Type 3 neovascularization: The expanded spectrum of retinal angiomatous proliferation. *Retina*. 2008;28(2):201-211.

6. Yannuzzi LA, Freund KB, Takahashi BS. Review of retinal angiomatous proliferation or type 3 neovascularization. *Retina*. 2008;28(3):375-384.

7. Viola F, Massacesi A, Orzalesi N, Ratiglia R, Staurenghi G. Retinal angiomatous proliferation: Natural history and progression of visual loss. *Retina*. 2009;29(6):732-739.

8. Maruko I, Iida T, Saito M, Nagayama D, Saito K. Clinical characteristics of exudative age-related macular degeneration in japanese patients. *Am J Ophthalmol*. 2007;144(1):15-22.

9. Gross NE, Aizman A, Brucker A, Klancnik JM,Jr, Yannuzzi LA. Nature and risk of neovascularization in the fellow eye of patients with unilateral retinal angiomatous proliferation. *Retina*. 2005;25(6):713-718.

10. Campa C, Harding SP, Pearce IA, Beare NA, Briggs MC, Heimann H. Incidence of neovascularization in the fellow eye of patients with unilateral retinal angiomatous proliferation. *Eye (Lond)*. 2010;24(10):1585-1589.

11. Gharbiya M, Parisi F, Cruciani F, Bozzoni-Pantaleoni F, Pranno F, Abdolrahimzadeh S. Intravitreal anti-vascular endothelial growth factor for retinal angiomatous proliferation in treatment-naive eyes: Long-term functional and anatomical results using a modified PrONTO-style regimen. *Retina*. 2014;34(2):298-305.

12. Inoue M, Arakawa A, Yamane S, Kadonosono K. Long-term results of intravitreal ranibizumab for the treatment of

retinal angiomatous proliferation and utility of an advanced RPE analysis performed using spectral-domain optical coherence tomography. *Br J Ophthalmol.* 2014 (epub).

13. Hemeida TS, Keane PA, Dustin L, Sadda SR, Fawzi AA. Long-term visual and anatomical outcomes following anti-VEGF monotherapy for retinal angiomatous proliferation. *Br J Ophthalmol.* 2010;94(6):701-705.

14. Gupta B, Jyothi S, Sivaprasad S. Current treatment options for retinal angiomatous proliferans (RAP). *Br J Ophthalmol.* 2010;94(6):672-677.

15. Yannuzzi LA. Indocyanine green angiography: A perspective on use in the clinical setting. *Am J Ophthalmol.* 2011;151(5):745-751.e1.

16. Fernandes LH, Freund KB, Yannuzzi LA, et al. The nature of focal areas of hyperfluorescence or hot spots imaged with indocyanine green angiography. *Retina.* 2002;22(5):557-568.

17. Truong SN, Alam S, Zawadzki RJ, et al. High resolution fourier-domain optical coherence tomography of retinal angiomatous proliferation. *Retina.* 2007;27(7):915-925.

18. Rouvas AA, Papakostas TD, Ntouraki A, Douvali M, Vergados I, Ladas ID. Angiographic and OCT features of retinal angiomatous proliferation. *Eye (Lond).* 2010;24(11):1633-42; quiz 1643.

19. Matsumoto H, Sato T, Kishi S. Tomographic features of intraretinal neovascularization in retinal angiomatous proliferation. *Retina.* 2010;30(3):425-430.

20. Leitgeb RA, Werkmeister RM, Blatter C, Schmetterer L. Doppler optical coherence tomography. *Prog Retin Eye Res.* 2014;41:26-43.

21. Braaf B, Vermeer KA, Vienola KV, de Boer JF. Angiography of the retina and the choroid with phase-resolved OCT using interval-optimized backstitched B-scans. *Opt Express.* 2012;20(18):20516-20534.

22. Braaf B, Vermeer KA, Sicam VA, van Zeeburg E, van Meurs JC, de Boer JF. Phase-stabilized optical frequency domain imaging at 1-microm for the measurement of blood flow in the human choroid. *Opt Express.* 2011;19(21):20886-20903.

23. Miura M, Makita S, Iwasaki T, Yasuno Y. Three-dimensional visualization of ocular vascular pathology by optical coherence angiography in vivo. *Invest Ophthalmol Vis Sci.* 2011;52(5):2689-2695.

24. Hong YJ, Miura M, Makita S, et al. Noninvasive investigation of deep vascular pathologies of exudative macular diseases by high-penetration optical coherence angiography. *Invest Ophthalmol Vis Sci.* 2013;54(5):3621-3631.

25. Jia Y, Bailey ST, Wilson DJ, et al. Quantitative optical coherence tomography angiography of choroidal neovascularization in age-related macular degeneration. *Ophthalmology.* 2014.

26. van Zeeburg EJ, Braaf B, Cereda MG, van Meurs JC, de Boer JF. Direct blood flow measurements in a free RPE-choroid graft with phase-resolved Doppler OCT. Transl Vis Sci Technol 2015;4(1):2.

27. Moult E, Choi W, Waheed NK, et al. Ultrahigh-speed sweptsource OCT angiography in exudative AMD. Ophthalmic Surg Lasers Imaging Retina 2014;45(6):496–505.

28. Vienola KV, Braaf B, Sheehy CK, et al. Real-time eye motion compensation for OCT imaging with tracking SLO. *Biomed Opt Express.* 2012;3(11):2950-2963.

29. Braaf B, Vienola KV, Sheehy CK, et al. Real-time eye motion correction in phase-resolved OCT angiography with tracking SLO. Biomed Opt Express 2013;4(1):51–65.

30. Blatter C, Klein T, Grajciar B, et al. Ultrahigh-speed non-invasive widefield angiography. *J Biomed Opt.* 2012;17(7):070505.

Chapter

8

Treatment effects in retinal angiomatous proliferation imaged with OCT angiography

Jan Hendrik de Jong
Boy Braaf
Sankha Amarakoon
Maximilian Gräfe
Suzanne Yzer
Koenraad A. Vermeer
Tom Missotten
Johannes F. de Boer
Mirjam E.J. van Velthoven

ABSTRACT

Purpose
This prospective case series is aimed at exploring OCT-angiography (OCT-A) as a treatment monitoring tool in patients treated for retinal angiomatous proliferation (RAP).

Methods
Twelve treatment-naïve RAP patients were included, median age of 79 years (range 65-90). Patients were imaged with an experimental 1,040 nm swept-source phase resolved OCT-A instrument before and after treatment. Treatment consisted of either intravitreal bevacizumab or triamcinolone injections with or without photodynamic therapy (PDT). Abnormal blood flow after treatment was graded as increased, unchanged, decreased or resolved.

Results
OCT-A images before and after treatment could be obtained in 9 patients. Median follow-up period was 10 weeks (range 5-19 weeks). After various treatment, the RAP lesion resolved in 7 patients, in 1 patient the OCT-A depicted decreased flow in the lesion and 1 patient showed unchanged abnormal blood flow. Monotherapy with intravitreal bevacizumab injections resolved RAP in 1 out of 2 patients. Combined therapy of bevacizumab with PDT resolved RAP in 6 out of 7 patients.

Conclusions
OCT-A visualized resolution of abnormal blood flow in 7 out of 9 RAP patients after various short-term treatment sequences. OCT-A may become an important noninvasive monitoring tool for optimizing treatment strategies in RAP patients.

INTRODUCTION

Retinal angiomatous proliferation (RAP), also referred to as type 3 neovascularization, is a distinct variant of exudative age-related macular degeneration (AMD) characterized by intraretinal neovascularization (IRN) with connections to either the retinal vasculature, the choroidal vasculature or both.[1] In more advanced stages, RAP is associated with the formation of a pigment epithelial detachment (PED) and retinal choroidal anastomosis (RCA). RAP represents approximately 15-30% of newly diagnosed patients with exudative AMD.[2-4] The prognosis of RAP is poor with typical rapid progression and, without therapy, ending in a disciform scar and atrophy.[5]

Numerous treatment strategies for RAP have been proposed, but there is no consensus on which treatment is optimal for RAP lesions.[6] Monotherapy with intravitreal anti-vascular endothelial growth factor (VEGF) injections shows favorable short-term results in several studies,[7-12] but requires repeated administration and conflicting long-term outcomes have been reported.[8, 13-16] A combination treatment of intravitreal anti-VEGF or triamcinolone with photodynamic therapy (PDT) seems to lead to a rapid resolution of the consequences of RAP.[17-22] However, there is little data available on how the treatment modalities act on the neovascularization itself and whether all stages of RAP should be treated the same.

Along with funduscopy, spectral domain-optical coherence tomography (SD-OCT)[23] is currently the standard tool for monitoring the effect of treatment of exudative AMD, including RAP. SD-OCT scans provide highly detailed anatomical information on retinal changes in RAP lesions,[24] but without an extension for angiography, it lacks the ability to detect flow, delineate (small) vessels or to image a feeder vessel connecting the intraretinal neovascular complex to the retinal or choroidal vasculature. Active neovascularizations can be revealed by fluorescein angiography (FA) with or without indocyanine green angiography (ICG), but these imaging modalities are invasive and give limited information about the depth location of the intra- and transretinal blood flow. Therefore, they are unsuited for regular follow-up measurements in clinical practice.

OCT angiography (OCT-A) is a new extension to standard OCT and can pinpoint abnormal intra- and transretinal blood flow noninvasively and to monitor treatment effects on neovascularizations, including RAP.[25-28] Our group has developed a phase-resolved 1,040 nm swept-source OCT-system with an OCT-A modality.[29-32] We have demonstrated that OCT-A can identify abnormal intra- and transretinal blood flow in a small case series of 12 RAP patients.[32] We found that abnormal blood flow in RAP was mostly confined to the intraretinal structures and that in one-third of patients an RCA had developed. We hypothesize that OCT-A is also a useful tool for monitoring treatment effects and for improving 'treat and

observe'-style management decisions. This study is aimed at exploring OCT-A as a treatment monitoring tool in patients treated for RAP. The secondary objective was to explore the differences between conventional angiographic imaging and OCT-A.

PATIENTS & METHODS

Twelve treatment-naïve patients diagnosed with an RAP lesion were included in this prospective case series, between March 2013 and September 2013. The study was approved by the local internal review board of The Rotterdam Eye Hospital and the Medical Ethical Committee of the Erasmus University Hospital (Rotterdam, The Netherlands). All patients provided written informed consent.

The patients were examined at baseline by slit lamp biomicroscopy, Snellen visual acuity, conventional SD-OCT, fundus photography, FA and ICG. Inclusion criteria were: age ≥ 65 years, no other active ocular diseases affecting the macula and treatment naïve RAP. RAP was diagnosed by the presence of a small intraretinal hemorrhage on fundus examination, a choroidal neovascularization (CNV) seen on FA and/or a hyperfluorescent mid to end phase hot spot on ICG. Multimodal imaging baseline characteristics of all patients have been previously published by Amarakoon et al.[32] We characterized the visualization of the retinal feeder vessel(s) at baseline by FA and OCT-A as good, fair or poor. The visualization was graded as 'good' if a feeder vessel was visualized connecting to the RAP lesion, as 'fair' if only a faint or interrupted feeder vessel could be recognized, and as 'poor' if none of the surrounding retinal vessels seemed to connect to the lesion.

An experimental optical frequency domain imaging system with a phase-resolved OCT-A modality was used to visualize blood flow at baseline and after treatment. The instrument uses a swept-source laser (Axsun Technologies Inc., Billerica, MA, USA) with a central wavelength of 1,040 nm operating at a 100 kHz A-scan rate. We obtained three-dimensional volume scans consisting of 300 single backstitched B-scans with 2,000 A-scans/B-scan over a retinal square area of 3 x 3 mm and with an acquisition time of 6 seconds per volume. The OCT-A system can detect flow velocities of 0.7 mm/s and higher, which is proven to be sufficient to image the retinal capillaries.[30] Elaborate technical details of this OCT-A instrument have been described previously.[29, 30, 32]

OCT-A measurements were processed to produce OCT-A *en face* images (Column 1 in each presented figure) and cross-sectional OCT-A tomograms (Column 2 and 3 in each presented figure). The OCT-A *en face* images display the phase differences (in white) detected between the vitreoretinal interface and retinal pigment epithelium (RPE). The location of the OCT-A is indicated with a dashed

square on FA images. B-scans with significant eye motion artifacts were manually removed in the OCT-A *en face* images to facilitate interpretation and comparison with follow-up measurements, but some discontinuities in the visualized flow due to eye motion artifacts remained. In the OCT-A tomograms, the inter-B-scan phase differences were overlaid in red on the grayscale structural B-scans. The location of the superimposed OCT-A tomograms is indicated with red dashed lines in the OCT-A *en face* images. Displayed phase-differences are predominantly caused by blood flow, but can also be due to noise, flow shadow artifacts or eye motion artifacts. Flow shadow artifacts (also referred to as projection artifacts)[33] are caused by blood flow signal in large vessels in the inner retina, which produces phase differences in the signal in deeper layers.

The initial treatment schedule of RAP was determined at the ophthalmologist's discretion and consisted of a combination of PDT and 2 or 3 intravitreal injections with bevacizumab or a combination of PDT and an intravitreal injection with triamcinolone. The laser light activation protocol used a wavelength of 689 nm, spot size range of 1.2-2.7 mm, with an intensity of 600 mW/cm^2 and was applied for 83 seconds. The order of treatment steps and the planning of OCT-A measurements were mainly determined by the hospital's and the patient's logistic opportunities. The follow-up period with OCT-A lasted until the first check-up by the ophthalmologist. The presence of abnormal blood flow on OCT-A after treatment was qualitatively categorized as increased, unchanged, decreased or resolved by visual inspection of the whole volume scan.

RESULTS

Twelve RAP patients were included in this study with a median age of 79 years (range 65-90). Baseline characteristics, as well as a comparison of baseline OCT-A with conventional images, have been reported previously.[32] All 12 patients were imaged with OCT-A at baseline. Patients 1 and 6 were excluded from follow-up measurements, because of severe eye movements on the baseline OCT-A scans. Patient 2 did not participate in follow-up treatment and OCT-A measurements because of hospitalization due to other health problems. In the other 9 patients, OCT-A images of sufficient quality were obtained both at baseline and after the initial treatment steps. The median follow-up during this study was 10 weeks (range: 5–19 weeks). A detailed timeline of OCT-A and treatment is indicated in the top right corner of each figure. Patients 7 and 10 were not treated with PDT because of general health issues not allowing them to come in for treatment. Visual acuity at baseline and after the initial treatment scheme is presented in **Table 1**. Median visual acuity changed from 20/50 (range 20/650–20/22) Snellen at baseline to 20/67 (range 20/650–20/20) after treatment.

Table 1: Follow-up period, treatment, OCT-angiography features and visual acuity

Patient*	Follow-up period OCT-A (weeks)	Number of bevacizumab injections	PDT	PDT spot size (mm)	Triam-cinolone	Visualization of feeding vessel(s) at baseline	
						FA	OCT-A
3	15	2	+	2.7	-	Good	Good
4	5	1	+	1.3	-	Poor	Fair
5	10	3	+	1.9	-	Good	Good
7	9	2	-	-	-	Poor	Good
8	13	1	+	1.2	+	Fair	Good
9	12	2	+	1.2	-	Poor	Good
10	9	3	-	-	-	Poor	Good
11	10	2	+	1.2	-	Good	Fair
12	19	2	+	2.7	-	Poor	Good

Table 1: Extended

Patient*	Structural OCT† Baseline			Structural OCT† After treatment			OCT-A Abnormal blood flow after treatment	VA Baseline (Snellen)	VA At first follow-up visit (Snellen)
	IRF	SRF	PED	IRF	SRF	PED			
3	-	+	-	-	-	-	Resolved	20/33	20/22
4	-	+	-	-	+	-	Unchanged	20/22	20/20
5	+	+	-	-	-	-	Resolved	20/100	20/100
7	+	-	-	-	-	-	Decreased	20/650	20/650
8	+	+	-	-	-	-	Resolved	20/40	20/66
9	+	-	+	-	-	-	Resolved	20/100	20/66
10	+	-	+	-	-	+	Resolved	20/50	20/22
11	+	+	+	-	-	+	Resolved	20/200	20/100
12	+	-	-	-	-	-	Resolved	20/40	20/50

IRF= intraretinal fluid; SRF= subretinal fluid; PED= pigment epithelial detachment; PDT= photodynamic therapy; VA= visual acuity. Bevacizumab and triamcinolone were injected intravitreally.

*Patients 1, 2 and 6 were not followed-up with OCT-A after treatment and therefore are not presented in this report.

†The structural OCT of the OCT-A measurements was used to determine the presence of fluids.

OCT angiography

Patients 3 and 4 (see **Figure 1** and **Supplemental figure 8.1**) were diagnosed with RAP based on conventional imaging, but classified as CNV on OCT-A.[32] The abnormal subretinal flow seen in patient 3 responded well to the combination of bevacizumab and PDT (see **Supplemental figure 8.1**). In patient 4 (**Figure 1**) the abnormal sub-RPE flow did not respond to either intravitreal bevacizumab or PDT, while an increase of subretinal fluid was noted at week 1 which was most likely a side-effect of the PDT (**Figure 1**, row 3).

Patient 5 (see **Supplemental figure 8.2**) was firstly treated with bevacizumab after which a OCT-A was performed capturing the effect of only bevacizumab. The RAP lesion initially responded poorly to the bevacizumab injection, but a supplementary PDT resolved the lesion (see **Supplemental figure 8.2**, row 3).

Patient 7 (**Figure 2**) was only treated with bevacizumab during the study period. The baseline OCT-A revealed a clearly delineated RCA, which remained present even after two injections of bevacizumab (**Figure 2**, row 3, column 2). However, the subretinal neovascular component had disappeared after treatment (**Figure 2**, row 3, column 3) as well as most of the intra- and subretinal fluid.

In patient 8 (**Figure 3**), resolution of the abnormal blood flow at the site of the former RAP lesion was observed after PDT alone (**Figure 3**, row 3). After intravitreal injection with triamcinolone and additionally bevacizumab, the subretinal fluid disappeared as well.

In patient 9, the abnormal blood flow as detected with OCT-A resolved after a combination treatment of bevacizumab and PDT (see **Supplemental figure 8.3**). In patient 10, the sub-RPE component of the RAP disappeared after one injection of bevacizumab (see **Supplemental figure 8.4**).

Patient 11 (**Figure 4**) was first treated with bevacizumab and one week after the injection OCT-A indicated that the RAP lesion was still present, but a reduction in PED height was seen (**Figure 4**, row 3). The combination of bevacizumab with PDT resolved the RAP lesion and the sub-RPE fluid disappeared. (**Figure 4**, row 4).

Patient 12 (**Figure 5**) was imaged with OCT-A after a combination of intravitreal bevacizumab and PDT. The diameter of the applied PDT-laser was 2.7 mm and was centered at the hot spot seen on ICG at baseline (**Figure 5**, row 1, column 3, white arrow). The abnormal blood flow on OCT-A had resolved after this combination treatment (**Figure 5**, row 3). However, local areas of non-perfusion in the choroid were detected at week 6 (**Figure 5**, row 3) in the region were the PDT was applied. Because the OCT-A volume scan covers an area of 3x3mm, the major part of the retina and choroid in the scanned area was affected by PDT laser. The reflectivity of the choriocapillaris and choroid was normal in the whole volume scan, indicating that the acquisition of this volume scan was of sufficient quality. A normal density of flow in the choriocapillaris was detected at

the edges of the volume scan (see **Supplemental video 8.1**). Our findings were confirmed by a consecutive OCT-A scan acquired in the same visit at week 6 (see **Supplemental video 8.2**). A partial recovery of choroidal perfusion was seen at week 19 (**Figure 5**, row 4).

Comparison between OCT-A and structural OCT

In 7 out of 7 patients with intraretinal fluid (IRF) before treatment, the IRF had disappeared at the superimposed cross-sectional structural OCT of the last OCT-A (see table 1). In 4 out of 5 patients with subretinal fluid (SRF), the SRF was resolved at the structural OCT. In 1 out of 3 patients with a PED, the PED had disappeared (see **Supplemental figure 8.3**), although the size of the other 2 PED's did decline after treatment (see **Figure 4** and **Supplemental figure 8.4**). Although the decrease of abnormal blood flow in general corresponded well to the decrease of IRF and SRF, the timing was not always similar. The OCT-A of patient 7 (**Figure 2**) showed the presence of abnormal blood flow after treatment, while the intra- and subretinal fluid had already disappeared. On the other hand, the OCT-A images of patient 8 (**Figure 3**, row 4) and 11 (**Figure 4**, row 3) did not show any suspected blood flow after treatment, but the subretinal or sub-RPE fluid persisted.

Comparison of baseline OCT-A and fluorescence angiography

The retinal vasculature detected by OCT-A *en face* images showed a good correspondence to the vasculature revealed by FA (see all figures).[32] However, the retinal capillaries are detected in more detail with OCT-A than with early FA in most patients and seem to suffer less from media opacities like cataract (see figures 8.3-8.5 and **Supplemental figure 8.4**). A good or fair visualization of the retinal feeder vessel was seen in 4 out of 9 patients on FA images and in 9 out of 9 patients on OCT-A *en face* (see **Table 1**). In patient 7 and 9 (**Figure 2** and **Supplemental figure 8.3**), an intraretinal hemorrhage obscured the visualization of the RCA on FA, while the OCT-A signal was not affected by the presence of the hemorrhage. The OCT-A cross-sections were able to display the depth location of the RAP lesions, which is not possible with FA or ICG. The hypercyanescent hot spots seen on ICG showed an accurate correspondence to location of abnormal blood flow on OCT-A in 8 out of 9 patients. A hot spot on ICG was not seen in patient 7 (**Figure 2**), where the OCT-A showed transretinal blood flow representing a retinal choroidal anastomosis

Figure 1: FA and ICG images of patient 4 at baseline and OCT-A images at baseline, week 1 and 5. The measurement and treatment schedule is displayed as a timeline: A=OCT-A; P=photodynamic therapy (PDT);

At baseline, FA demonstrated an occult CNV (Row 1, column 1 and 2) and ICG revealed a late-phase hypercyanescent hot spot on indocyanine green angiography (Row 1, column 3, red arrow). On the OCT-A *en face* at baseline, a neovascularization was seen at the border of the foveal avascular zone (Row 2, column 1, red circle). At the OCT-A tomogram abnormally located blood flow was depicted confined to the sub-retinal pigment epithelial (RPE) space (Row 2, column 2).

At week 1, after PDT, the abnormal vascular network was persisting on the OCT-A *en face* (Row 3, column 1). On the OCT-A tomogram, the abnormal sub-RPE flow was unchanged (Row 3, column 2), whilst an increase of subretinal fluid was noted. An additional injection with intravitreal bevacizumab did not affect the sub-RPE neovascularization, as demonstrated with the OCT-A at week 5 (Row 4). However, a reduction of subretinal fluid was seen (Row 4, column 2).
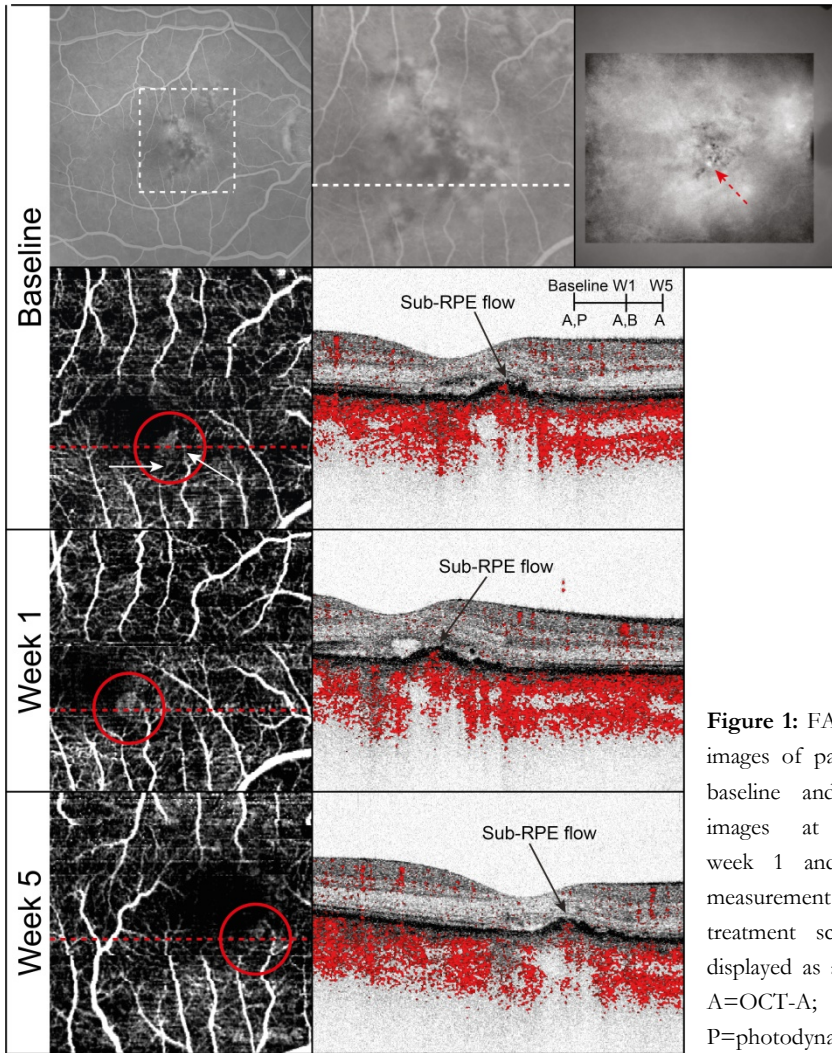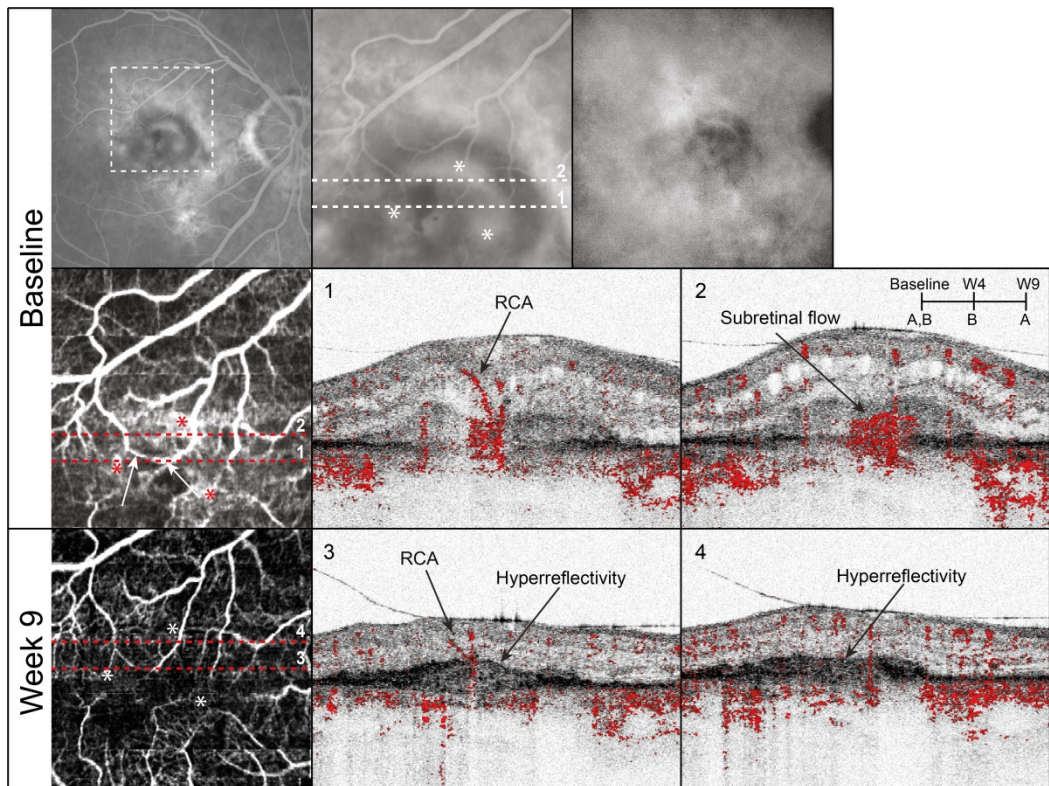
Figure 2: FA and ICG images of patient 7 at baseline and OCT-A images at baseline and week 9. The measurement and treatment schedule is displayed as a timeline: A=OCT-A; B=bevacizumab.

At baseline, early FA showed an abnormal hyperfluorescent vascular network (Row 1, column 1 and 2, white asterisks). ICG did not reveal a late phase hot spot typical for RAP Several areas of abnormal blood flow were observed on the OCT-A en face (Row 2, column 1, red asterisks). A retinal choroidal anastomosis connecting the choroid with inner retinal vessels was found on the baseline OCT-A tomogram 1 (Row 2, column 2, RCA). At the baseline OCT-A tomogram 2, abnormal blood flow in the subretinal space was seen (Row 2, column 3).

The patient was treated with an intravitreal injection of bevacizumab right after baseline OCT-A and at week 4. At week 9 after two bevacizumab injections, the three areas with abnormal blood flow on the OCT-A *en face* had disappeared (Row 3, column 1, white asterisks). The RCA was still seen after treatment at OCT-A tomogram 3 (Row 3, column 2, RCA), while the subretinal neovascularization was resolved, as shown on OCT-A tomogram 4 (Row 3, column 3). A significant reduction of intra- and subretinal fluid from baseline to week 9 was seen, as well as an accumulation of fibrovascular tissue, which is depicted as hyperreflective areas on the structural OCT tomograms.

Figure 3: FA and ICG images of patient 8 at baseline and OCT-A images at baseline, week 1 and 13. The measurement and treatment schedule is displayed as a timeline: A=OCT-A; P=photodynamic therapy (PDT); T=Triamcinolone; B=bevacizumab; Y=YAG laser.

At baseline, a small hyperfluorescent area was seen on FA (Row 1, column 1 and 2, white arrow) and ICG depicted a hypercyanescent hotpsot (Row 1, column 3, red arrow). The OCT-A *en face* at baseline showed two vessels forming an anastomosis in an in an area of increased blood flow at the edge of the foveal avascular zone (Row 2, column 1, red circle). A retinal choroidal anastomosis was seen at the OCT-A tomogram depicting subretinal blood flow connecting to an intraretinal vessel (Row 2, column 2, RCA).

At week 1, after PDT, the OCT-A *en face* as well as the OCT-A tomograms could not detect any abnormal blood flow (Row 3). The OCT-A tomogram showed some hyperreflectivity at the location where the RCA had been seen at baseline (Row 3, column 2). Subretinal fluid was slightly reduced at week 1.

At week 13, another OCT-A was performed which did not display any abnormal blood flow on the OCT-A *en face* (Row 4, column 1, red circle). The structural OCT tomogram showed some hyperreflectivity at the location where the RCA had been seen at baseline (Row 3, column 2). However, no evident abnormal blood flow could be detected in the cross-sections at week 13 (Row 4, column 2).
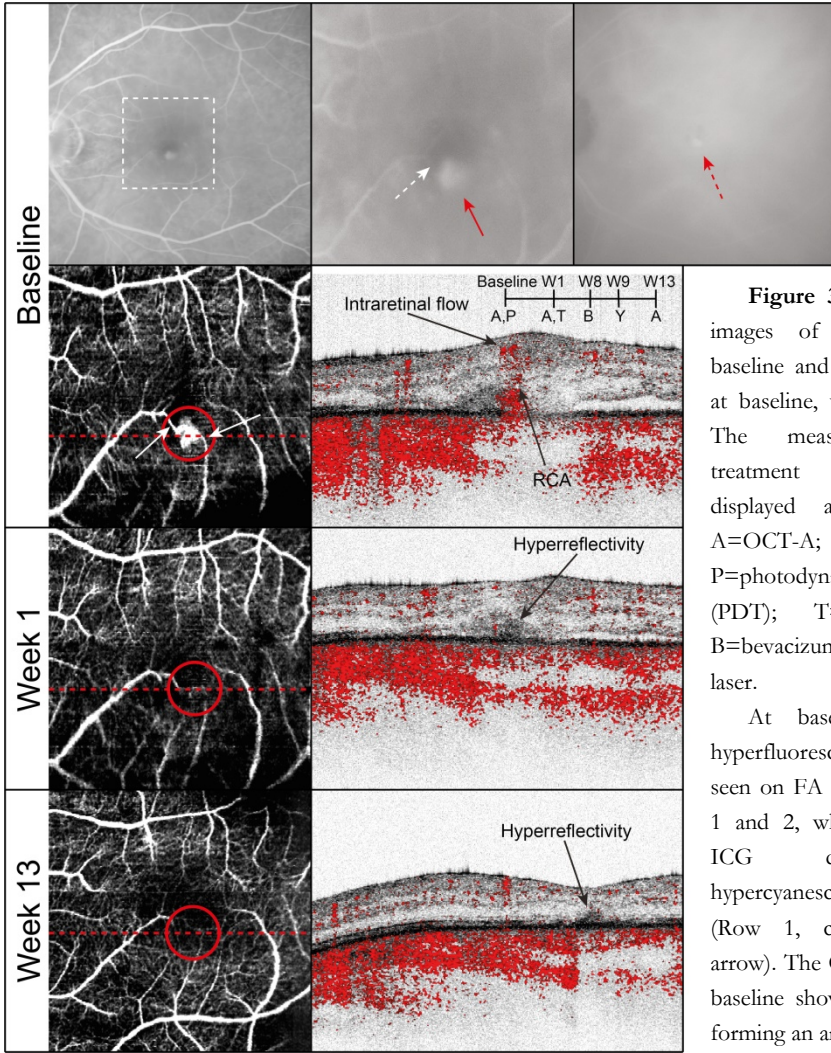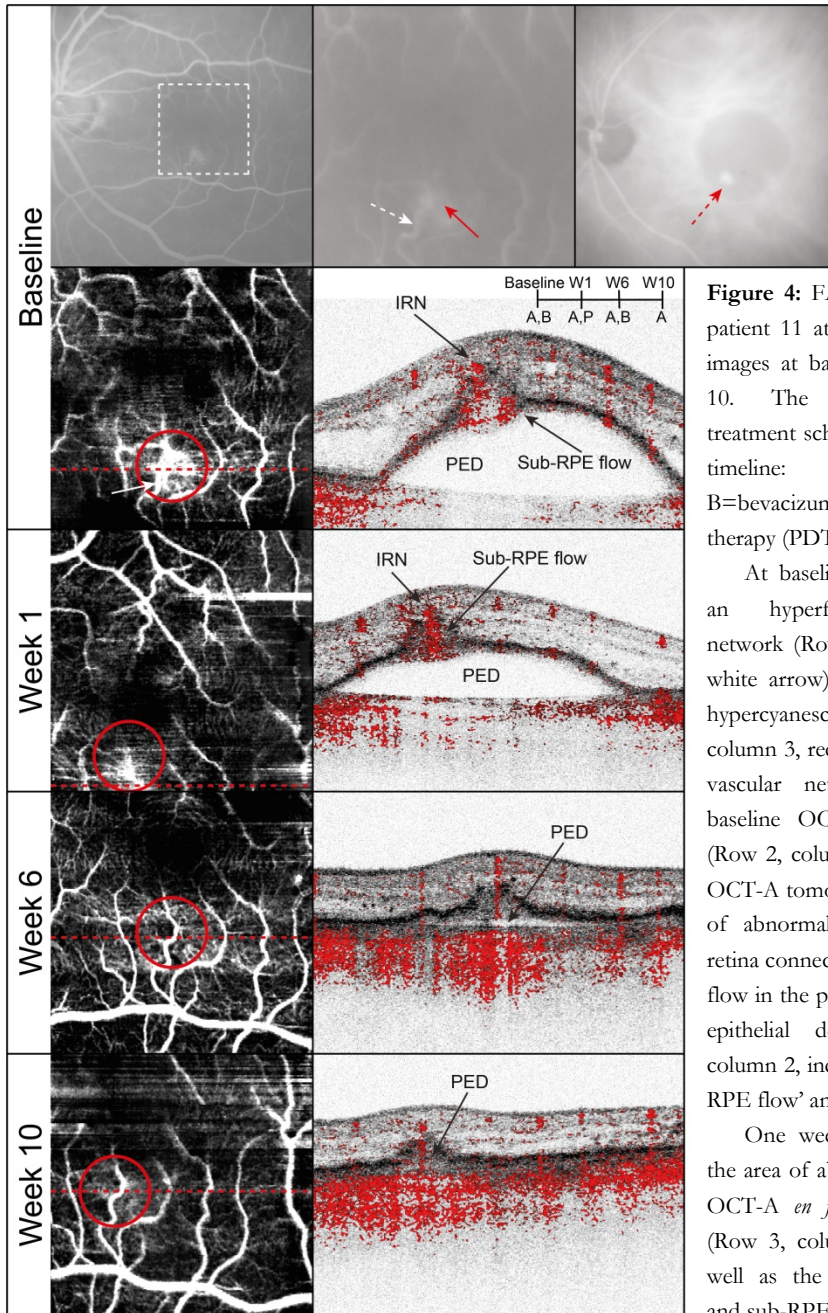
Figure 4: FA and ICG images of patient 11 at baseline and OCT-A images at baseline, week 1, 6 and 10. The measurement and treatment schedule is displayed as a timeline: A=OCT-A; B=bevacizumab ; P=photodynamic therapy (PDT).

At baseline, early FA revealed an hyperfluorescent vascular network (Row 1, column 1 and 2, white arrow) and ICG depicted a hypercyanescent hotpsot (Row 1, column 3, red arrow). An abnormal vascular network was seen at baseline OCT-A *en face* imaging (Row 2, column 1, red circle). The OCT-A tomogram depicted an area of abnormal blood flow in the retina connected to abnormal blood flow in the protrusion of a pigment epithelial detachment (Row 2, column 2, indicated as 'IRN' , 'sub-RPE flow' and 'PED', respectively).

One week after bevacizumab, the area of abnormal blood flow at OCT-A *en face* was still detected (Row 3, column 1, red circle), as well as the abnormal intraretinal and sub-RPE blood flow depicted on the OCT-A tomogram (Row 3, column 2, indicated as 'IRN' and 'sub-RPE flow', respectively). A significant reduction of intra- and subretinal fluid was noted, as well as a decline in PED height.

On the OCT-A images made after PDT at week 6, no abnormal intraretinal or sub-RPE flow could be detected on the *en face* (Row 4, column 1). The phase-differences displayed in the PED are probably flow-shadows of blood flow detected in the inner retina (Row 4, column 2). The remaining sub-RPE fluid detected at week 6 (Row 4, column 2) disappeared after another bevacizumab injection as demonstrated with the structural OCT image at week 10 (see Row 5, column 2), while a small fibrovascular PED remained.
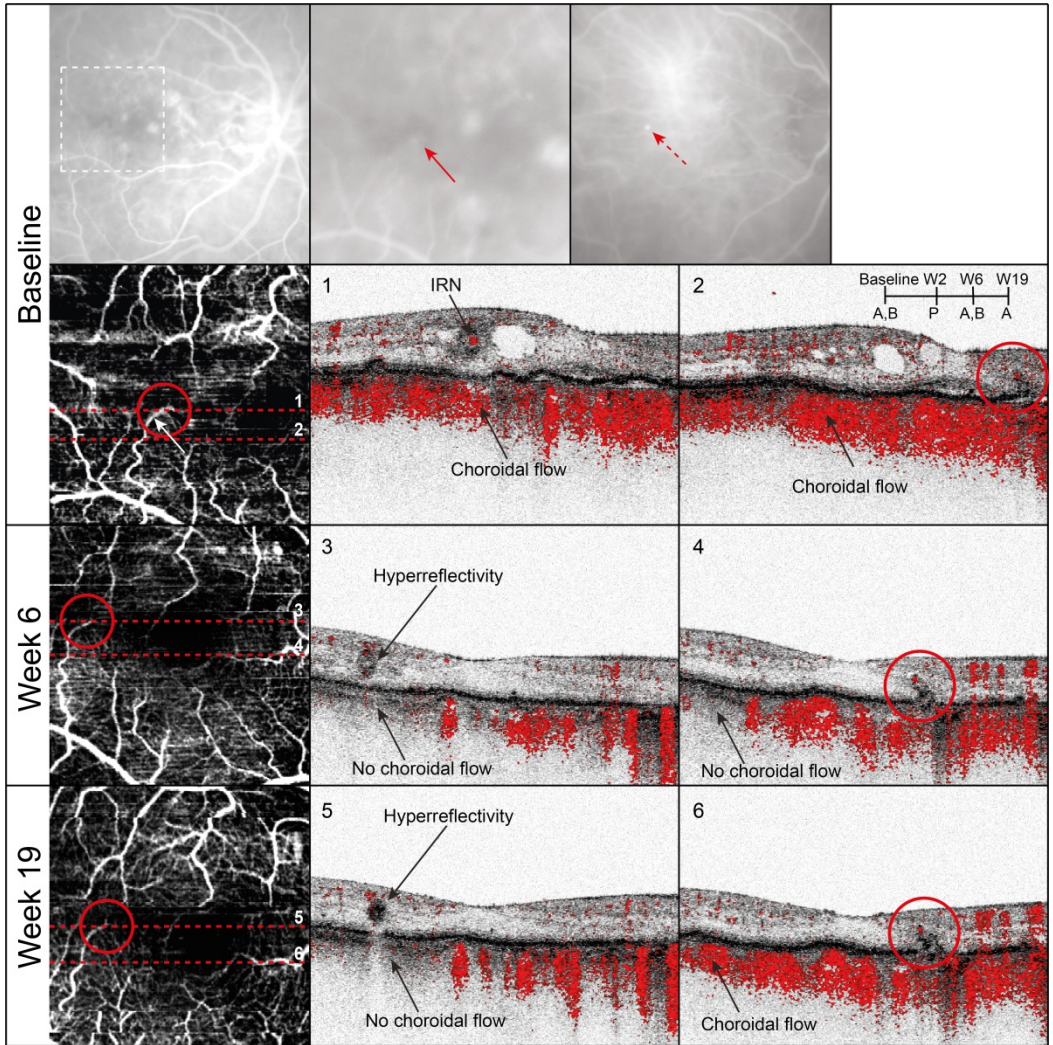
Figure 5: FA and ICG images of patient 12 at baseline and OCT-A images at baseline, week 6 and 19. The measurement and treatment schedule is displayed as a timeline: A=OCT-A; P=photodynamic therapy (PDT); B=bevacizumab.

At baseline, a poorly defined hyperfluorescent area was seen on early FA (Row 1, column 1 and 2, white arrow) and ICG depicted a hypercyanescent hotpsot (Row 1, column 3, red arrow). The OCT-A *en face* image depicted a tortuous capillary with irregular ending near the foveal avascular zone (Row 1, column 1, red circle). OCT-A tomogram 1 made through the ending of this capillary showed abnormal blood flow confined to the inner retina and surrounded by hyperreflectivity (Row 1, column 2, IRN). OCT-A tomogram 2 reveals a cross section through a similar vessel near the foveal avascular zone (Row 1, column 3).

The OCT-A *en face* at week 6 performed after a bevacizumab injection and PDT showed that the ending of the tortuous vessel had become thinner (Row 2, column 1, red circle). On OCT-A tomogram 3, a hyperreflective fibrotic area remained (Row 2, column 2) at the former site of the IRN seen at baseline, without obvious abnormal intraretinal blood. Intraretinal fluid was significantly decreased at week 6. Local areas of non-perfusion were detected in the region of PDT treatment, as shown on OCT-A tomograms 3 and 4 (Row 2, column 2 and 3), whilst choroidal blood flow had been seen at these sites at baseline.

DISCUSSION

In this explorative case series OCT-A images before and after treatment were obtained in 9 RAP patients. At the end of the follow-up period and after various treatment sequences, the RAP lesion was resolved in 7 patients (see Figures 1, 3 and 4 and **Supplemental figures 8.1-8.4**). In 1 patient the OCT-A depicted only decreased flow in the lesion (see **Figure 2**) and 1 patient showed unchanged abnormal blood flow (see **Figure 1**). Monotherapy with intravitreal bevacizumab injections resolved the lesion in 1 out of 2 patients. Combined therapy of bevacizumab with PDT showed resolution in 6 out of 7 patients (see **Figures 1 and 3-5 and Supplemental figures 8.1-8.3**).

This study demonstrates the potential of OCT-A to visualize treatment effects on the angiographic features of RAP. The repeated use of FA to determine the activity of the neovascular lesion is restricted by its invasiveness as well as acquisition time. Therefore, in clinical practice OCT has replaced FA as a standard monitoring tool for exudative AMD treatment, withholding the ophthalmologist information on the blood flow in the neovascular network. We showed that retinal capillaries and feeder vessels are detected in more detail with OCT-A than with early FA in most of the patients of this small case series (see Table 1) and that OCT-A reveals the depth localization of RAP lesions in the cross-sectional images. We demonstrate that OCT-A can monitor the effect of treatment on abnormal blood flow in RAP, without the use of an invasive dye, on *en face* and cross-sectional representations and with a short acquisition time. This broadens the possibilities for the ophthalmologist to evaluate the effect of treatment on retinal and choroidal neovascularizations.

OCT-A might also support the search for an optimal treatment strategy for RAP. Anti-VEGF monotherapy yields promising results for early-stage RAP,[7-12] but long term outcome shows the necessity for repeated injections.[8,13-16] Combination therapy seems to result in better visual outcome[17-22] and a lower retreatment rate.[34,35] Tsai *et al.* reported that the results of anti-VEGF monotherapy for RAP are encouraging, but that concerns remain regarding the development of geographic atrophy and long-term visual outcome.[6] The presented OCT-A data in this study seems to support the hypothesis that a combination of anti-VEGF treatment with PDT leads to rapid resolution of RAP. On the other hand, OCT-A revealed that patient 4 had a small type 1 CNV which did not respond to the combination therapy. If OCT-A had been used in the diagnostic workup of this patient, PDT probably would have been omitted.

Although PDT appears to be efficacious, it has been reported that this treatment may cause thrombus formation in the choroid, leading to a reduction in choroidal perfusion.[36] Patient 12 (**Figure 5**) demonstrates that OCT-A can visualize choroidal nonperfusion (**Figure 5**, row 3, and **Supplemental videos 8.1 and 8.2**), which was most likely caused by PDT treatment. The large spot size of

2.7mm used in this patient might have increased the risk of this collateral damage. Reperfusion was detected after 19 weeks (**Figure 5**, row 4). The range of blood flow velocity in the choriocapillaris was previously reported to be 0.3–3.6 mm/s, while the lower limit of detectable flow velocity in our phase resolved OCT-A system is 0.7 mm/s (see Braaf et al., figure 4)[30]. However, the structural OCT shows normal intensity (**Figure 5**, Row 3, Column 2 and 3) and we could confirm our findings in two different volume scans (**Supplemental videos 8.1 and 8.2**). Therefore, we believe that the risk of not having detected persistent flow in this region of the choriocapillaris is very small. In future studies, OCT-A might be used to further elucidate the occurrence rate of this severe adverse event. The OCT-A system used in this study detected choroidal flow which might be explained by sufficient signal penetration depth of the 1,040nm swept source laser in our study.[37]

The presence of slow abnormal blood flow in small capillaries can be visualized before and after treatment using OCT-A, but fluid leakage is associated with far lower velocities and cannot be detected with OCT-A in the currently available systems. It would be interesting to know whether the absence of abnormal blood flow corresponds to the inactivity of the RAP lesion. In this small case series we found that the absorption of intra- and subretinal fluid on structural OCT mostly corresponds to the disappearance of abnormal blood flow (see Table 1). In some cases however, the disappearance of abnormal blood flow on OCT-A preceded (**Figure 2**) or followed (**Figure 3 and 4**) the absorption of intra- and subretinal fluid on structural OCT. This demonstrates that OCT-A provides additional information compared to standard OCT, which could lead to improved monitoring of treatment outcome and thereby optimizing (re-)treatment decisions. It would be interesting to follow-up patients with OCT-A after discontinuation of treatment to evaluate the role of OCT-A in detecting early reactivations. Although the amount of detail captured by FA seems to be lower than that by OCT-A, FA and ICG could play an important role in validating OCT-A changes after treatment by revealing fluid leakage. However, in daily clinical practice, the amount of residual leakage is monitored by structural OCT alone. Therefore, the additional value of OCT-A in retreatment decisions must be compared primarily to structural OCT.

Strengths of this study include the combination of *en face* images and high resolution cross-sectional images which enabled us to pinpoint the depth of the lesions, and the penetration depth of the 1,040 nm swept source laser which enabled visualization of blood flow in the choroid. Limitations of this explorative study are the small sample size, the short follow-up period, the multiple treatment strategies, the small field of view and the number of eye motions. A longer follow-up period would be needed to evaluate long-term effects of anti-VEGF monotherapy and to establish the recurrence rate of neovascularization after

successful closure of RAP. A larger field of view would be beneficial to monitor several neovascularizations simultaneously or to screen for new neovascularizations when treatment appears to be ineffective. Real-time eye motion correction can result in higher quality flow-information[38] and combined with structural information this allows to search for more subtle treatment effects.

In conclusion, OCT-A detected a decrease in abnormal blood flow after the initial treatment sequence of RAP in 8 out of 9 patients. We have shown that RAP short-term anti-VEGF treatment combined with PDT rapidly results in closure of RAP in this small study. Because of its noninvasiveness, short acquisition time and simultaneous imaging of structural changes, OCT-A appears to be a promising treatment monitoring tool for macular vascular pathologies, such as RAP. A larger trial is warranted using OCT-A to examine treatment effects of combination therapy and monotherapy separately. Interestingly, such a trial would be more feasible at the present time, as the capabilities of our experimental prototype OCT-A are now operative in several commercially available OCT-As.

REFERENCES

1. Yannuzzi LA, Freund KB, Takahashi BS. Review of retinal angiomatous proliferation or type 3 neovascularization. Retina 2008;28(3):375-384.

2. Parravano M, Pilotto E, Musicco I, Varano M, Introini U, Staurenghi G, Menchini U, Virgili G. Reproducibility of fluorescein and indocyanine green angiographic assessment for RAP diagnosis: a multicenter study. Eur J Ophthalmol 2012;22(4):598-606.

3. Massacesi AL, Sacchi L, Bergamini F, Bottoni F. The prevalence of retinal angiomatous proliferation in age-related macular degeneration with occult choroidal neovascularization. Graefes Arch Clin Exp Ophthalmol 2008;246(1):89-92.

4. Slakter JS, Yannuzzi LA, Schneider U, Sorenson JA, Ciardella A, Guyer DR, Spaide RF, Freund KB, Orlock DA. Retinal choroidal anastomoses and occult choroidal neovascularization in age-related macular degeneration. Ophthalmology 2000;107(4):742-53; discussion 753-4.

5. Viola F, Massacesi A, Orzalesi N, Ratiglia R, Staurenghi G. Retinal angiomatous proliferation: natural history and progression of visual loss. Retina 2009;29(6):732-739.

6. Tsai ASH, Cheung N, Gan ATL, Jaffe GJ, Sivaprasad S, Wong TY, Cheung CMG. Retinal angiomatous proliferation. Surv Ophthalmol 2017;62(4):462-492.

7. Reche-Frutos J, Calvo-Gonzalez C, Perez-Trigo S, Fernandez-Perez C, Donate-Lopez J, Garcia-Feijoo J. Ranibizumab in retinal angiomatous proliferation (RAP): influence of RAP stage on visual outcome. Eur J Ophthalmol 2011;21(6):783-788.

8. Gharbiya M, Parisi F, Cruciani F, Bozzoni-Pantaleoni F, Pranno F, Abdolrahimzadeh S. Intravitreal anti-vascular endothelial growth factor for retinal angiomatous proliferation in treatment-naive eyes: long-term functional and anatomical results using a modified PrONTO-style regimen. Retina 2014;34(2):298-305.

9. Shin JY, Yu HG. Optical coherence tomography-based ranibizumab monotherapy for retinal angiomatous proliferation in Korean patients. Retina 2014;34(12):2359-2366.

10. Park YG, Roh YJ. One year results of intravitreal ranibizumab monotherapy for retinal angiomatous proliferation: a comparative analysis based on disease stages. BMC Ophthalmol 2015;15:182-015-0172-2.

11. Chou HD, Wu WC, Wang NK, Chuang LH, Chen KJ, Lai CC. Short-term efficacy of intravitreal Aflibercept injections for retinal angiomatous proliferation. BMC Ophthalmol 2017;17(1):104-017-0497-0.

12. Parodi MB, Donati S, Semeraro F, Danzi P, Introini U, Viola F, Bottoni F, Pucci V, Musig A, Pece A, Azzolini C. Intravitreal Anti-Vascular Endothelial Growth Factor Drugs for Retinal Angiomatous Proliferation in Real-Life Practice. J Ocul Pharmacol Ther 2017;33(2):123-127.

13. Engelbert M, Zweifel SA, Freund KB. "Treat and extend" dosing of intravitreal antivascular endothelial growth factor therapy for type 3 neovascularization/retinal angiomatous proliferation. Retina 2009;29(10):1424-1431.

14. Hemeida TS, Keane PA, Dustin L, Sadda SR, Fawzi AA. Long-term visual and anatomical outcomes following anti-VEGF monotherapy for retinal angiomatous proliferation. Br J Ophthalmol 2010;94(6):701-705.

15. Inoue M, Arakawa A, Yamane S, Kadonosono K. Long-term results of intravitreal ranibizumab for the treatment of retinal angiomatous proliferation and utility of an advanced RPE analysis performed using spectral-domain optical coherence

tomography. Br J Ophthalmol 2014;98(7):956-960.

16. Cho HJ, Lee TG, Han SY, Kim HS, Kim JH, Han JI, Lew YJ, Kim JW. Long-term visual outcome and prognostic factors of Intravitreal anti-vascular endothelial growth factor treatment for retinal angiomatous proliferation. Graefes Arch Clin Exp Ophthalmol 2016;254(1):23-30.

17. Rouvas AA, Chatziralli IP, Theodossiadis PG, Moschos MM, Kotsolis AI, Ladas ID. Long-term results of intravitreal ranibizumab, intravitreal ranibizumab with photodynamic therapy, and intravitreal triamcinolone with photodynamic therapy for the treatment of retinal angiomatous proliferation. Retina 2012;32(6):1181-1189.

18. Freund KB, Klais CM, Eandi CM, Ober MD, Goldberg DE, Sorenson JA, Yannuzzi LA. Sequenced combined intravitreal triamcinolone and indocyanine green angiography-guided photodynamic therapy for retinal angiomatous proliferation. Arch Ophthalmol 2006;124(4):487-492.

19. van de Moere A, Kak R, Sandhu SS, Talks SJ. Anatomical and visual outcome of retinal angiomatous proliferation treated with photodynamic therapy and intravitreal triamcinolone. Am J Ophthalmol 2007;143(4):701-704.

20. Saito M, Iida T, Kano M. Two-year results of combined intravitreal anti-VEGF agents and photodynamic therapy for retinal angiomatous proliferation. Jpn J Ophthalmol 2013;57(2):211-220.

21. Lee MY, Kim KS, Lee WK. Combined intravitreal ranibizumab and photodynamic therapy for retinal angiomatous proliferation. Am J Ophthalmol 2012;153(5):1004-5; author reply 1005.

22. Saito M, Iida T, Kano M, Itagaki K. Two-year results of combined intravitreal ranibizumab and photodynamic therapy for retinal angiomatous proliferation. Jpn J Ophthalmol 2015.

23. Chen TC, Cense B, Pierce MC, Nassif N, Park BH, Yun SH, White BR, Bouma BE, Tearney GJ, de Boer JF. Spectral domain optical coherence tomography: ultra-high speed, ultra-high resolution ophthalmic imaging. Arch Ophthalmol 2005;123(12):1715-1720.

24. Su D, Lin S, Phasukkijwatana N, Chen X, Tan A, Freund KB, Sarraf D. An Updated Staging System of Type 3 Neovascularization using Spectral Domain Optical Coherence Tomography. Retina 2016.

25. Tan AC, Dansingani KK, Yannuzzi LA, Sarraf D, Freund KB. Type 3 Neovascularization Imaged with Cross-Sectional and En Face Optical Coherence Tomography Angiography. Retina 2016.

26. Bhavsar KV, Jia Y, Wang J, Patel RC, Lauer AK, Huang D, Bailey ST. Projection-resolved optical coherence tomography angiography exhibiting early flow prior to clinically observed retinal angiomatous proliferation. Am J Ophthalmol Case Rep 2017;8:53-57.

27. Bansal R, Hemanth V, Mulkutkar S, Singh R, Gupta V, Dogra MR, Gupta A. OCT angiography demonstrates retinal angiomatous proliferation and chorioretinal anastomosis of type 3 neovascularization. Int Ophthalmol 2017.

28. Miere A, Querques G, Semoun O, Amoroso F, Zambrowski O, Chapron T, Capuano V, Souied EH. Optical Coherence Tomography Angiography Changes in Early Type 3 Neovascularization After Anti-Vascular Endothelial Growth Factor Treatment. Retina 2017;37(10):1873-1879.

29. Braaf B, Vermeer KA, Sicam VA, van Zeeburg E, van Meurs JC, de Boer JF. Phase-stabilized optical frequency domain imaging at 1-micron for the measurement of blood flow in the human choroid. Opt Express 2011;19(21):20886-20903.

30. Braaf B, Vermeer KA, Vienola KV, de Boer JF. Angiography of the retina and the

choroid with phase-resolved OCT using interval-optimized backstitched B-scans. Opt Express 2012;20(18):20516-20534.

31. van Zeeburg EJ, Braaf B, Cereda MG, van Meurs JC, de Boer JF. Direct Blood Flow Measurements in a Free RPE-Choroid Graft with Phase-Resolved Doppler OCT. Transl Vis Sci Technol 2015;4(1):2.

32. Amarakoon S, de Jong JH, Braaf B, Yzer S, Missotten T, van Velthoven ME, de Boer JF. Phase-Resolved Doppler Optical Coherence Tomographic Features in Retinal Angiomatous Proliferation. Am J Ophthalmol 2015;160(5):1044-1054.e1.

33. Zhang M, Hwang TS, Campbell JP, Bailey ST, Wilson DJ, Huang D, Jia Y. Projection-resolved optical coherence tomographic angiography. Biomed Opt Express 2016;7(3):816-828.

34. Kaiser PK. Combination therapy with verteporfin and anti-VEGF agents in neovascular age-related macular degeneration: where do we stand?. Br J Ophthalmol 2010;94(2):143-145.

35. Smith BT, Dhalla MS, Shah GK, Blinder KJ, Ryan EH,Jr, Mittra RA. Intravitreal injection of bevacizumab combined with verteporfin photodynamic therapy for choroidal neovascularization in age-related macular degeneration. Retina 2008;28(5):675-681.

36. Schmidt-Erfurth U, Michels S, Barbazetto I, Laqua H. Photodynamic effects on choroidal neovascularization and physiological choroid. Invest Ophthalmol Vis Sci 2002;43(3):830-841.

37. Chen Y, Burnes DL, de Bruin M, Mujat M, de Boer JF. Three-dimensional pointwise comparison of human retinal optical property at 845 and 1060 nm using optical frequency domain imaging. J Biomed Opt 2009;14(2):024016.

38. Braaf B, Vienola KV, Sheehy CK, Yang Q, Vermeer KA, Tiruveedhula P, Arathorn DW, Roorda A, de Boer JF. Real-time eye motion correction in phase-resolved OCT angiography with tracking SLO. Biomed Opt Express 2013;4(1):51-65.

SUPPLEMENTAL MATERIAL CHAPTER 8
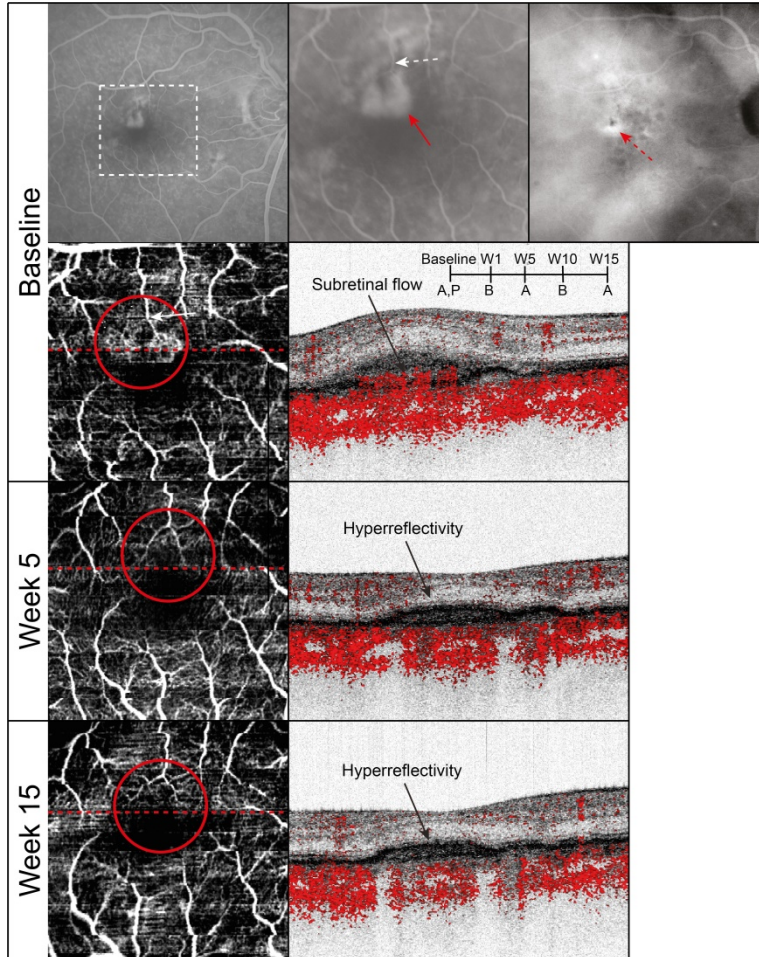
Supplemental figure 8.1: FA and ICG images of patient 3 at baseline and OCT-A images at baseline, week 5 and 15. The measurement and treatment schedule is displayed as a timeline: A=OCT-A; P=photodynamic therapy (PDT); B=bevacizumab.

At baseline, a mixed/classic CNV on FA (Row 1, column 1 and 2, red arrow) and a late phase hypercyanescent hotspot is seen on ICG (column 2, red dashed arrow). At the OCT-A *en face*, an abnormal vascular complex was seen at the border of the foveal avascular zone (Row 2, column 1, red circle). The OCT-A tomogram showed abnormal blood flow protruding from the choroid in the subretinal space (Row 2, column 2). Visualization of the feeding vessels was characterized as good on FA (Row 1, column 2, white dashed arrow) and as good on OCT-A enface (Row 2, column 1, white arrow).

At week 5, after PDT and an intravitreal injection of bevacizumab, the OCT-A *en face* revealed that the abnormal vascular network had disappeared (Row 3, column 1, red circle). On the OCT-A tomogram no abnormal blood was seen, whilst a hyperreflective fibrovascular band remained (Row 3, column 2).

After a second intravitreal bevacizumab injection at week 10, the OCT-A performed at week 15 showed a similar situation as week 5 without evident abnormal blood flow (Row 4).
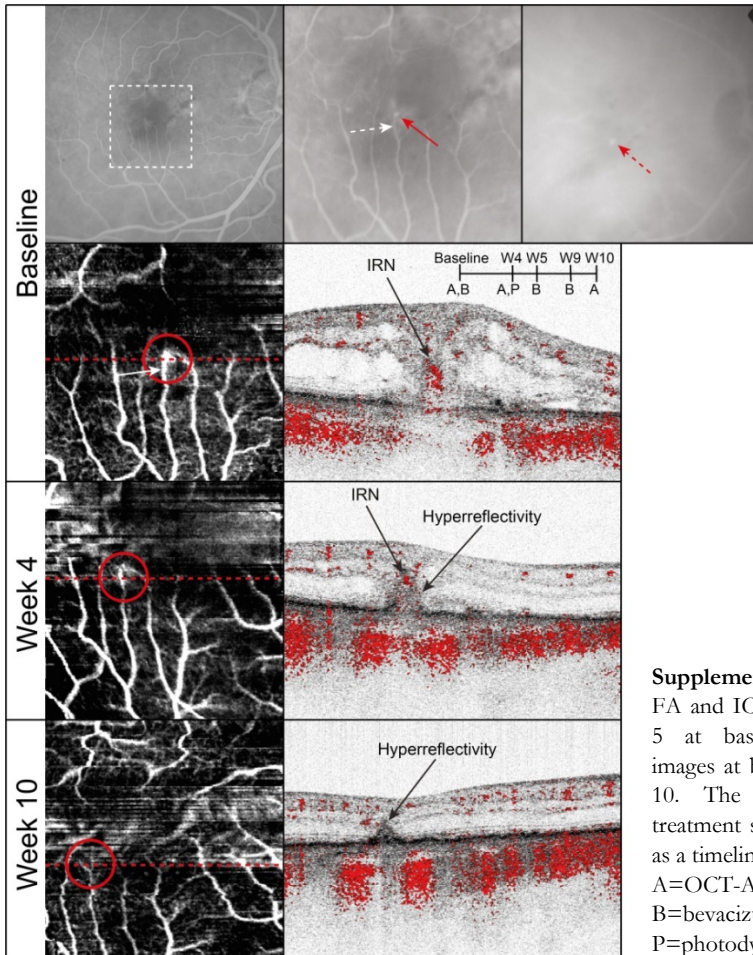
Supplemental figure 8.2:
FA and ICG images of patient 5 at baseline and OCT-A images at baseline, week 4 and 10. The measurement and treatment schedule is displayed as a timeline:
A=OCT-A;
B=bevacizumab;
P=photodynamic therapy.

At baseline, a poorly defined hyperfluorescent area was seen on FA (Row 1, column 1 and 2, red arrow) and a hypercyanescent hotspot on ICG (Row 1, column 3, red dashed arrow). Enhanced blood flow was observed at the end of a capillary at the border of the foveal avascular zone, as displayed at the baseline OCT-A *en face* image (Row 2, column 1, red circle). The OCT-A tomogram shows that the intraretinal neovascularization was located in the outer retina (Row 2, column 2, indicated with 'IRN'). Visualization of the feeding vessels was characterized as good on FA (Row 1, column 2, white dashed arrow) and as good on OCT-A enface (Row 2, column 1, white arrow).

At week 4 after a first bevacizumab injection, the OCT-A *en face* showed the same area of enhanced blood flow (Row 3, column 1, red circle), although smaller in size. This was confirmed on the OCT-A tomogram, which depicts persistent blood flow in the area of hyperreflectivity (Row 3, column 2, 'IRN'). The white area's in the upper third part of the *en face* image are artifacts caused by a failing segmentation algorithm due to a low-intensity signal in that region.

At 10 weeks after baseline, after PDT and two additional intravitreal bevacizumab injections, the OCT-A *en face* did not show the enhanced blood flow at the end of the capillary (Row 4, column 1, red circle), although the quality of the measurement was lower due to increased noise in the central part of the image. On the OCT-A tomogram no suspected blood flow was seen near the hyperreflective area (Row 4, column 2). There is a significant reduction of intra- and subretinal fluid from baseline to week 10.

Supplemental figure 8.3: FA and ICG images of patient 9 at baseline and OCT-A images at baseline and week 12. The measurement and treatment schedule is displayed as a timeline: A=OCT-A; P=photodynamic therapy (PDT); B=bevacizumab.

At baseline, the visualization of an occult neovascularization was obscured by an intraretinal hemorrhage (Row 1, column 1 and 2, red arrow) and a hypercyanescent hotspot was seen on ICG (Row 1, column3, red dashed arrow). At the OCT-A en face image at baseline several abnormally curved vessels were seen (Row 2, column 1, red circle) near the foveal avascular zone. On OCT-A tomogram 1 a vessel can be seen running through a local break in the retinal pigment epithelium (RPE), on top of a pigment epithelial detachment (PED) (Row 2, column 3, indicated as 'RCA')and on OCT-A tomogram 2 a vessel is displayed in the PED (Row 2, column 2, PED). In the adjacent frames it was found that these vessels form an anastomosis with intraretinal vessels. Visualization of the feeding vessels was characterized as poor on FA (Row 1, column 2) and as good on OCT-A enface (Row 2, column 1, white arrow).

At week 12, after two intravitreal injections of bevacizumab and PDT, a normalization of the vascular pattern was seen, as shown at the OCT-A *en face* (Row 3, column 1, red circle). The PED almost completely declined and the intraretinal fluid resolved after treatment, with the RPE break clearly visible on structural OCT tomograms 3 and 4 at the location of the former RCA (Row 3, column 2 and 3).
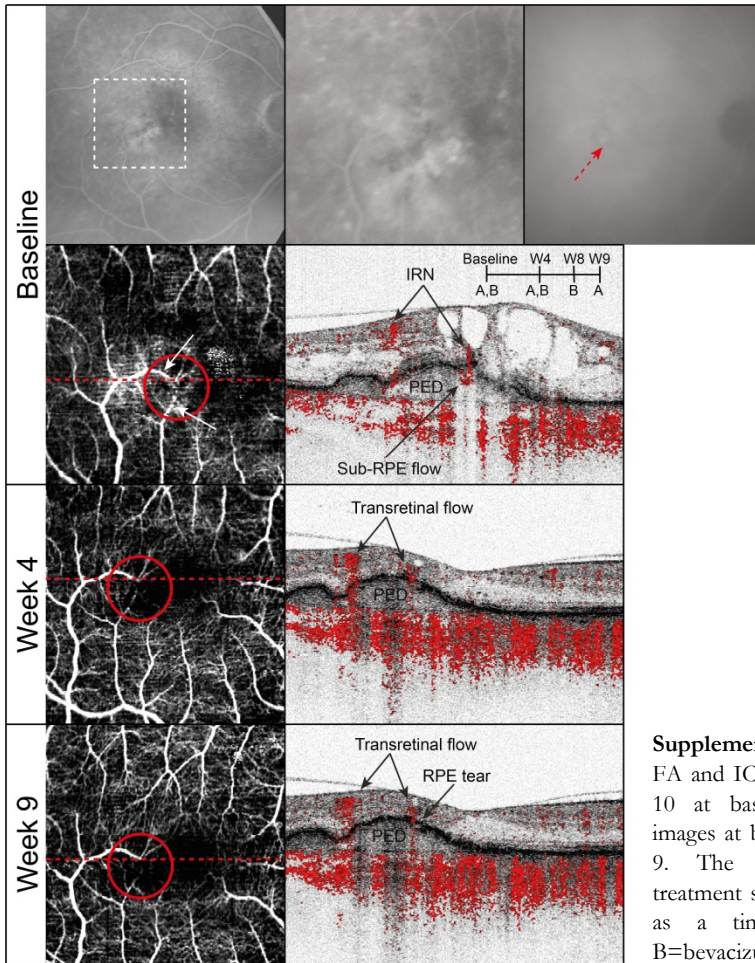
Supplemental figure 8.4: FA and ICG images of patient 10 at baseline and OCT-A images at baseline, week 4 and 9. The measurement and treatment schedule is displayed as a timeline: A=OCT-A; B=bevacizumab.
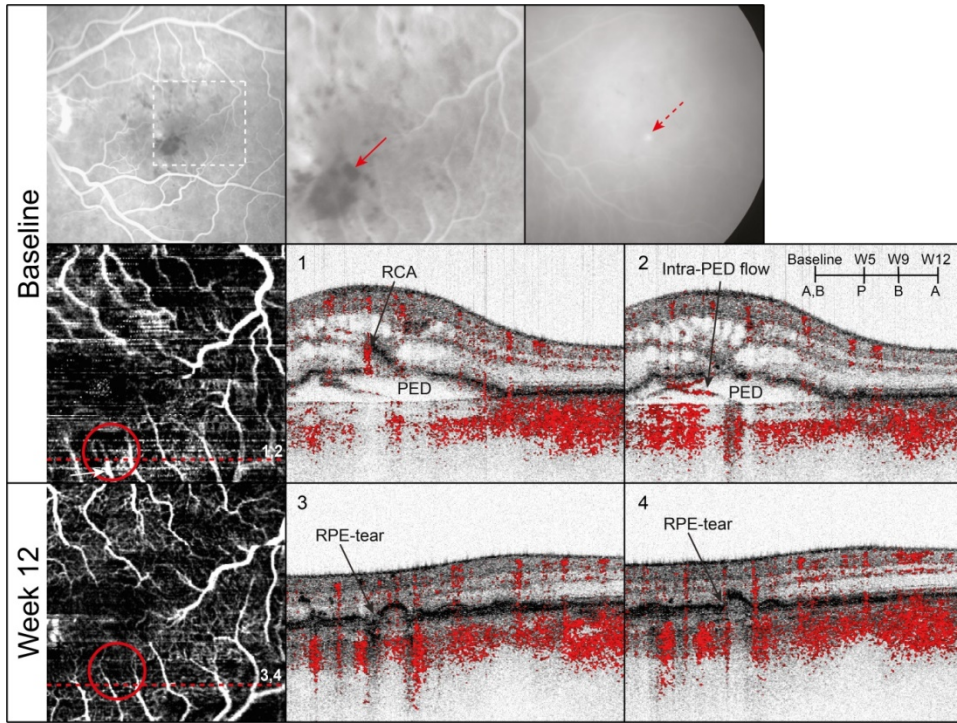
At baseline, an occult neovascularization was seen on FA and a hypercyanescent hotspot on ICG (Row 1, column 3, red dashed arrow). The OCT-A *en face* at baseline depicts a vessel which is strongly curved towards an area of increased blood flow near the fovea (Row 2, column 1, red circle). The OCT-A tomogram depicts the dissection of this vessel at different depth locations (Row 3, column 5, indicated as 'IRN'). The vessel appeared to run from the inner retina through the retinal pigment epithelium (RPE) into the sub-RPE space (indicated as 'sub-RPE flow' in the 'PED'). Visualization of the feeding vessels was characterized as poor on FA (Row 1, column 2) and as good on OCT-A enface (Row 2, column 1, white arrow).

At week 4, after an intravitreal injection of bevacizumab, the abnormal blood flow seen on OCT-A *en face* had disappeared (Row 3, column 1, red circle) and no sub-RPE flow was found in the RPE detachment (Row 3, column 2), while the curved vessel running towards the PED was still present. The amount of intra- and subretinal fluid was significantly reduced.

The patient was treated with two additional injections of bevacizumab at week 4 and 8. At week 9 (Row 4), no obvious differences where noted compared to the OCT-A images at week 4. However, the RPE-break through which the IRN formed a connection with the sub-RPE flow at baseline was still visible on the OCT-A tomogram (Row 4, column 2).

Chapter

9

General discussion

GENERAL DISCUSSION

In this thesis, two ocular diseases were studied: retinal detachment (RD) and age-related macular degeneration (AMD). For both diseases, OCT played a central role in answering the clinical questions. First, the studies on RD are discussed and second, the studies on AMD. Finally, future perspectives are described on the use of OCT in future studies on RD and AMD.

Retinal detachment

RD is a progressive sight-threatening disease that most strongly affects central visual acuity when the macula becomes detached. Treatment of macula-on retinal detachment requires urgent reattachment surgery to prevent macular involvement.[1-4] Since not all patients can benefit from same day surgery due to an already fully booked surgery schedule, preoperative posturing is prescribed to patients who are scheduled for the next day or even the day after. The efficacy and mode of action of this posturing advice are only partly understood and poorly supported by scientific evidence, and therefore, were studied in this thesis.

One of the reasons for the lack of evidence is the requirement of a sufficiently accurate measuring method. Recently, optical coherence tomography (OCT) was used in a Danish clinical trial to study the progression of RD.[5] This study highlighted the use of OCT as a precise instrument to measure RD development in an ethically acceptable manner. Interestingly, in the methods section of the same study, it was documented that patients with bedrest were allowed to sit up for dinner and leave their bed for sanitary interruptions. Therefore, we used OCT in the studies presented in this thesis to measure RD progression, to evaluate the effect of interruptions of preoperative posturing on RD progression and to relate the measured RD progression to potential risk factors for progression.

Efficacy of preoperative posturing

In **chapter 2**, we studied the difference between posturing intervals and interruptions in 198 patients.[6] We demonstrated that OCT was indeed a precise instrument to measure RD development with an intra-rater variability of ±58 µm (95% limits of agreement). We demonstrated that the median RD border displacement during posturing was 1 µm/hour and -149 µm/hour during interruptions, which differed significantly ($p < 0.001$). Therefore, we concluded that preoperative posturing significantly reduces progression of RD. We estimated that patients would progress on average 2.6 mm in a 16-hour period if they would not adhere to the preoperative posturing advice and their activity level would be similar to the light daily activities during the posturing interruptions in this study. This extrapolation underlines the clinical relevance of preoperative posturing and

suggests that patients who the clinician believes may not comply with preoperative posturing may benefit from earlier surgical intervention.

Despite posturing, some patients progressed from baseline. About 22% of patients progressed more than 250 μm from baseline and about 6% of patient progressed more than 20% of their baseline RD–fovea distance. However, the rate of progression is a questionable outcome measure, since progression appeared not be a continues, monotonous process. During interruptions, most patients showed progression, but some regressed extensively during periods of posturing, especially during night time posturing. Patients were admitted at different time points of the day and were scanned at variable time intervals. Therefore, some patients progressed during the first hours of hospitalization due interruptions of posturing, but showed regression overnight and also regression from baseline at the last OCT measurement. Others only showed regression which might be due to admission in the late evening or only showed (some) progression because surgery was performed on the same day of admission to the hospital. The real rate of progression during 48 hours of preoperative posturing can only be revealed if the preoperative period is extended to 48 hours for all patients, which is not ethically acceptable.

Nonetheless, none of the included patients progressed to macula-off status during the follow-up period of the study, while other studies showed a progression rate to macula-off of 0.5-3% in the 2-3 days before surgery.[5,7-9] This seems to indicate that the current policy of the Rotterdam Eye Hospital of preoperative posturing, hospitalization, and surgery within 48 hours is sufficient to prevent macula-off RD. However, some progressive patients were rescheduled to an earlier time point to prevent further progression according to the study protocol. These patients might have progressed to macula-off RD if they were not included in the study.

Risk factors for retinal detachment progression
The efficacy of the preoperative posturing policy does not necessarily justify the costs and burden of hospitalization and continued posturing for all macula-on RD patients. In **chapter 3**, we showed that the correlation between the RD–fovea distance at baseline and the RD–fovea distance at last OCT measurement was 0.98. This indicates that patients with a peripheral RD may show some progression from baseline, but the risk of progression to macula-off remains small. We also showed that the risk of progression is smaller if the amount of subretinal fluid at baseline is smaller. This is in accordance with the theory that the inertia of subretinal fluid during head and eye movements exerts a detaching force on the retina.[5,10-12] The more fluid accumulates under the retina, the more likely the adhesion of the retina to the RPE will be overwhelmed and the RD will further progress. For patients with a large baseline distance between RD and fovea (>4 mm) and a small area of

subretinal fluid (<38 mm^2), a less strict posturing advice or an outpatient preoperative policy might be more convenient to the patients, result in a smaller population of patient who requires hospitalization and still be sufficient to prevent macula-off RD. Patients with a small baseline RD–fovea distance and a large volume of subretinal fluid or bullous appearance should be selected for urgent surgery.

Although the density differences between the retina and the vitreous fluid are rather small,[13] multiple hours or days of sitting and standing upright during daytime might have a cumulative effect and result in accumulation of subretinal fluid in a retinal detachment of the superior quadrants. Due to the increased volume of subretinal fluid, the detaching forces caused by head and eye movements also increase and the RD is more likely to further develop and progress. We showed that a superior RD location is a weak risk factor for progression from baseline. Therefore, we believe that its predictive value is too small to be used as a clinical predictor of RD progression. However, it is still an interesting outcome since the majority of RD patients also has a superior RD at presentation.[6,14] An explanation for the higher progression rate in superior patients might be that these patients are positioned supine preoperatively, which is likely suboptimal for superior RD in terms of counteracting the weak gravity vector. This suggestion is corroborated by the observation that pure temporal retinal detachments, with positioning on their side, show less progression, because the weak gravity vector is now in the correct direction for reattachment. An alternative explanation might be that gravity causes the retina to settle through the vitreous fluid after days of normal activity, resulting in accumulation of subretinal fluid in a retinal detachment of the superior quadrants.

Prolongation of posturing interruptions

An outpatient preoperative policy might be an alternative to hospitalization for patients with a low risk of progression. Because these patients would have to travel home by car or taxi and sit upright, we estimated the effect of prolonged duration of posturing interruptions, as described in **chapter 3**. We measured the progression from baseline in 3 cohorts of 50 patients with an average interruption duration of 22, 41 and 59 minutes respectively. We did not find a statistically significant difference between the three cohorts concerning RD progression from baseline or the progression during the interruptions. The most plausible explanation for this is that movements of the head and eyes are likely to be the driving forces behind RD progression, while patients were mostly sitting upright quietly during the prolongation of interruptions. The force of gravity alone is not enough to detach the retina and the duration of the sitting upright period is too short for gravity to cause an accumulation of subretinal fluid.

Traveling home includes more than prolonged sitting upright alone, like walking to the car, getting in and out of the car, climbing the stairs in an apartment building, and domestic duties. A comparative trial should be performed to study the effect of outpatient care in patients with a low-risk for RD progression. Preventing unnecessary traveling might be achieved by letting the referring ophthalmologist play a key role by liaising with the tertiary clinic to be able to send in patients on the day that there is operation time available. The precise characteristics of the RD as measured with OCT and ultrasound will be helpful in the communication between secondary and tertiary clinics.

Head orientation and head movements

In **chapter 4**, we provide evidence that head motility affects RD progression more than head orientation; i.e. that movements rather than gravity are causing RD progression. We could demonstrate this by measuring the head orientation and motility using a head mounted sensor which contained an accelerometer, gyroscope, and magnetometer. We showed that the strength of the correlation between RD progression and head orientation deviation from advised positioning was moderate, but that the correlation of RD progression with rotational and linear acceleration was much stronger. Therefore, we concluded that preoperative posturing is effective by reducing head movements rather than enforcing head positioning. The clinical significance of the strong correlation between RD progression and head motility is that RD progression will be prevented if patients move their head as little as possible during the preoperative period. This can be accomplished by bed rest and by avoiding unnecessary activities involving head motion. Any required transportation may be done by bed or wheelchair to minimize the number of head and eye movements.

Head movements and saccades

We measured head movements using the head mounted sensor, while saccades are traditionally expected to be able to overcome the forces of retinal adhesion.[12,15] The rotational velocity and acceleration of saccades are typically faster than those of active head rotations.[16-20] However, the radius of the head is greater than the radius of the eye, whereas the magnitude of saccades is smaller than that of head movements.[21] Therefore, the tangential linear acceleration of the components of RD may be in the same range. During a head rotation, the movement of the eye approximates a translational movement. The direction of acceleration and deceleration forces of the fluids at opposite sides of the eye will be almost parallel during rotational head movements and precisely parallel during linear head movements. As a result, the effect on fluid currents within the eye may be limited. During a saccadic eye rotation, however, the direction of acceleration and deceleration forces will be opposite on the opposite sides of the eye, which is likely

to create strong fluid currents of both liquefied vitreous and subretinal fluid. **Supplemental video 9.1** shows a dynamic ultrasound of one of the paticipants of the study presented in **chapter 4** with a bullous retinal detachment. This video demonstrates the effect of a saccade on subretinal fluid displacement, which likely causes retinal traction on the hinge point of the detachment.

Performing clinical studies to measure the effect of head ánd eye movements on the progression of RD might impose an unacceptable burden and progression risk to the patients. Therefore, we used a numerical model **in chapter 5** to determine the effect of a head movement and a saccade on the traction of the vitreous on the retina.[22] The most accurate and most recent material data was used in this model.[23-26] Surprisingly, this model showed that the effect of a head movement on RD progression is much stronger than the effect of a saccade. We show that the peak of the traction loads on the retina caused by head movements and saccades are within the range 30-35 Pa. This is a factor of ten lower than what is measured to be the adhesion force of the retina by Liu *et al.*[27] Since the defined saccadic eye movement was larger than 95% of all saccadic eye movements,[21] it is unlikely that traction caused by most saccadic eye movement will be large enough to overcome the retinal adhesion. However, the defined head movement was small compared to those created by other everyday activities.[20] Therefore it is likely that only head movements can create traction loads in the same order of magnitude as the retinal adhesion. Although this model is a preliminary version and fluid currents are not included, this outcome shows that head movements may play a larger role in RD progression than traditionally thought. However, some factors, like vitreous contraction, might be too complicated to implement in future versions of the model.

Age-related macular degeneration and acute submacular hemorrhage
Age-related macular degeneration (AMD) is a progressive disease of the macula and the leading cause of irreversible legal blindness in elderly people in industrialized countries.[28,29] Submacular hemorrhage (SMH) is a severe complication of exudative AMD, which causes immediate and extensive loss of visual acuity and irreversible damage to the retina and retinal pigment epithelial (RPE) cells.[30-32] Damage to the sensory retinal tissue is due to a limited passage of nutrients to the retina, shrinkage of the outer retinal layers by clot formation with fibrin contraction[31,33] and toxicity of iron and hemosiderin,[34] which can already occur within 24 hours.[33] No controlled trial has yet provided evidence of the superiority of subretinal hemorrhage displacement over no displacement. However, most clinicians act on the observation that without treatment, the visual outcome is poor, whereas pneumatic displacement surgery results in improved visual acuity.[35-38] Displacement of the SMH is achieved by subretinal or intravitreal application of recombinant tissue plasminogen activator (rtPA) to liquefy the fresh

hemorrhage and the application of intravitreal gas to displace the hemorrhage from the macular region. The advantage of intravitreal rtPA and gas over the subretinal rtPA approach is that it is a procedure that can be performed in the office instead of the operation room and therefore potentially at a shorter notice. The intravitreal rtPA and gas procedure is also hypothesized to be less-invasive than subretinal rtPA with vitrectomy and gas and might therefore cause fewer complications, although this is not clearly stated in literature.[35]

OCT volume measurements and complications

In **chapter 6**, two pneumatic displacement approaches were compared on effectiveness and safety in a small randomized controlled trial.[39] In the subretinal rtPA group, patients received pars plana vitrectomy, subretinal administration of rtPA, a tamponade with intravitreal C_3F_8 gas and intravitreal bevacizumab. In the intravitreal rtPA group, rtPA, C_3F_8 gas and bevacizumab were administrated intravitreally. Volumetric OCT measurements were performed of the macula including the SMH. The volume of subretinal blood, subretinal fluid and sub-RPE space was measured in a 2.5 mm cylinder around the fovea by manual annotation. The median relative volume reduction of subretinal blood at 6 weeks postoperatively was 97% in the intravitreal rtPA group and 100% in the subretinal rtPA group and did not differ significantly between the groups (P = 0.56). Therefore, we concluded that both treatment modalities effectively displaced the SMH. The final visual acuity at 12 weeks was >20/200 in 92% in the intravitreal rtPA group and in 82% in the subretinal rtPA group, which was a higher percentage than most retrospective studies have reported after treatment of SMH secondary to AMD.[35] These favorable anatomical and functional outcomes in both groups were obtained despite the occurrence of serious complications in both groups: retinal detachments and recurrent hemorrhages, as well as an elevated IOP after intravitreal rtPA and gas injection causing ischemic disk damage in one patient. We concluded that to avoid undue pressure peaks after intravitreal gas injection, the amount of injected gas should be divided over 2 days.

The advantage of OCT volumetric measurements over standard fundus examinations is that it enables differentiation between subretinal blood, subretinal fluid and the sub-RPE volume. In contrast with fundus examinations, important subretinal hemorrhage thickness changes are not masked on volumetric OCT measurements by a thin remaining subretinal or sub-RPE hemorrhage residue. For that reason, subretinal volume reduction of a hemorrhage is more likely to correlate with survival of the overlying retina than the extent of a hemorrhage. Therefore, we think that OCT volume measurements are a clinically more meaningful and sensitive tool than fundus examinations.

Retinal angiomatous proliferation and OCT angiography

Retinal angiomatous proliferation (RAP) is a distinct variant of exudative age-related macular degeneration (AMD) characterized by intraretinal neovascularization (IRN) with connections to either the retinal vasculature, the choroidal vasculature or both.[40] In more advanced stages, RAP is associated with the formation of a pigment epithelial detachment (PED) and retinal choroidal anastomosis (RCA). The prognosis of RAP is poor with typical rapid progression and, without therapy, ending in a disciform scar and atrophy.[41] Diagnosing RAP-type AMD is clinically important, because standard anti–vascular endothelial growth factor (VEGF) monotherapy tends to show persistent activity of the RAP lesion.[42-44] Numerous treatment strategies for RAP have been proposed, but there is no consensus on which treatment is optimal for RAP lesions.[45,46] A combination treatment of intravitreal anti-VEGF or triamcinolone with photodynamic therapy (PDT) seems to lead to a rapid resolution of the consequences of RAP.[47-52]

The diagnosis of RAP cannot reliably be made based on structural spectral domain OCT (SD-OCT) imaging, since it lacks the ability to detect flow, delineate (small) vessels or to image a feeder vessel connecting the intraretinal neovascular complex to the retinal or choroidal vasculature. Indocyanine green angiography (ICG), which uses invasive fluorescence dye injection, is of the essence for an accurate diagnosis of RAP. However, many general ophthalmologists do not have regular access to ICG, and may therefore misclassify an RAP lesion as another, more common type of CNV. In **chapter 7**, OCT angiography (OCT-A) was used to visualize the RAP lesion at baseline in 11 patients in a noninvasive manner with a custom build, phase-resolved Doppler OCT.[53] We demonstrated that OCT-A can detect and localize abnormal blood flow within RAP lesions. Blood flow appeared to be mostly confined to the intraretinal structures with or without a connecting pigment epithelial detachment. In one-third of patients, a retinal choroidal anastomosis was detected. We concluded that OCT-A enables accurate differentiation between normal and abnormally located blood flow, and between intra- and subretinal or sub–retinal pigment epithelial neovascularization.

Treatment monitoring using OCT angiography

Funduscopy and SD-OCT are currently the standard tools for monitoring the effect of treatment of exudative AMD, including RAP. SD-OCT scans provide highly detailed anatomical information on retinal changes in RAP lesions,[54] but lack the ability to detect flow. Active neovascularizations can be revealed by fluorescein angiography (FA) and ICG, but these imaging modalities are invasive, time-consuming, and give limited information about the depth location of the intra- and transretinal blood flow. Therefore, they are unsuited for regular follow-up measurements in clinical practice and OCT has replaced FA as a standard

monitoring tool for exudative AMD treatment, withholding the ophthalmologist information on the blood flow in the neovascularization.

In **chapter 8**, we studied the OCT-A imaging of 9 RAP patients before and after various treatment sequences.[55] We hypothesized that OCT-A is a useful tool for monitoring treatment effects and to improve 'treat and observe'-style management decisions. We demonstrated that the abnormal blood flow representing the RAP lesions resolved in 7 out of 9 patients. Combined therapy of bevacizumab with PDT showed resolution in 6 out of 7 patients. Monotherapy with intravitreal bevacizumab injections resolved the lesion in 1 out of 2 patients. We showed that retinal capillaries and feeder vessels are detected in more detail with OCT-A than with early FA in most of the patients of this small case series. Nonetheless, FA and ICG could play an important role in validating OCT-A changes after treatment by revealing fluid leakage.

PDT appeared to be efficacious, but it has been reported that this treatment may cause thrombus formation in the choroid, which leads to a reduction in choroidal perfusion.[56] Patient 12 (Chapter 8, Figure 5) demonstrated that OCT-A is able to visualize choroidal non-perfusion, which was most likely a severe side effect of the PDT treatment. Because of its short acquisition time, noninvasiveness and simultaneous imaging of structural changes, we concluded that OCT-A is a promising treatment monitoring tool for macular vascular pathologies, such as RAP.

Future perspectives on the use of OCT in RD and AMD

OCT appeared to be a versatile instrument in studying both RD and AMD. Its histology-like resolution, noninvasiveness and short acquisition time opened the way for various novel applications. In RD, the precise measurements of RD border displacement enabled to study the effect of preoperative posturing and to study risk factors for RD progression. We suggested that OCT should be used in standard clinical care to determine the proximity of the RD border to fovea at presentation. Thereby, OCT can serve as a triage tool to select for urgent or semi-urgent surgery or to select for inpatient or outpatient preoperative care. A large comparative non-inferiority trial or clinical evaluation study would be required to more definitely study the safety of outpatient care by sending selected patients home and evaluate RD progression at their return. This could be combined with measurements of head orientation and head motility, to evaluate the effect of this alternative policy on compliance and RD progression. We envision that in the future, patients are sent home wearing a head-mounted safety sensor warning the patient (and potentially the ophthalmologist) when the amount of head movements exceeds a certain limit. This alternative policy might be cost-saving for both clinics that aim to provide 7 days per week surgery service and clinics that hospitalize patients preoperatively.

In AMD, volumetric measurement of acute SMH were performed to study the efficacy of pneumatic displacement surgery. The evaluation of volumetric changes of acute submacular hemorrhage is currently restricted by manual segmentation. Standard automatic segmentation of the current OCT systems likely fails to recognize the subretinal space in a distorted retina, especially in case of extensive hemorrhage due to the shadowing effect of the subretinal blood. However, since improved automatic segmentation algorithms are currently under development,[57] accurate automatic measurements of SMH may become available in the future. These volumetric measurements could be used in a larger noninferiority trial to compare various treatment strategies for SMH.

Interestingly, OCT-A is currently implemented in several commercially available OCT-A's which opens a new era to study large populations of patients with vessel abnormalities, including RAP. OCT-A will be helpful in distinguishing RAP from the other subtypes of AMD and may serve as a screening tool to detect neovascularizations in the collateral eye or to detect the reactivation rate of neovascularizations after initial treatment. Quantitative measurement of abnormal blood flow would allow to study more subtle treatment effects in all subtypes of exudative AMD. Improved eye or retinal tracking and faster A-scan rates may provide in other, novel applications of OCT which may further improve clinical care of ophthalmic patients.

References

1. Salicone A, Smiddy WE, Venkatraman A, Feuer W. Visual recovery after scleral buckling procedure for retinal detachment. *Ophthalmology*. 2006;113(10):1734-1742.

2. Zhou C, Lin Q, Chen F. Prevalence and predictors of metamorphopsia after successful rhegmatogenous retinal detachment surgery: A cross-sectional, comparative study. *Br J Ophthalmol*. 2016.

3. Rezar S, Sacu S, Blum R, Eibenberger K, Schmidt-Erfurth U, Georgopoulos M. Macula-on versus macula-off pseudophakic rhegmatogenous retinal detachment following primary 23-gauge vitrectomy plus endotamponade. *Curr Eye Res*. 2016;41(4):543-550.

4. Kaufman PL. Prognosis of primary rhegmatogenous retinal detachments. 2. accounting for and predicting final visual acuity in surgically reattached cases. *Acta Ophthalmol (Copenh)*. 1976;54(1):61-74.

5. Hajari JN, Kyhnel A, Bech-Azeddine J, la Cour M, Kiilgaard JF. Progression of foveola-on rhegmatogenous retinal detachment. *Br J Ophthalmol*. 2014;98(11):1534-1538.

6. de Jong JH, Vigueras-Guillén JP, Simon TC, et al. Preoperative posturing of patients with macula-on retinal detachment reduces progression toward the fovea. *Ophthalmology*. 2017.

7. Ehrlich R, Niederer RL, Ahmad N, Polkinghorne P. Timing of acute macula-on rhegmatogenous retinal detachment repair. *Retina*. 2013;33(1):105-110.

8. Ho SF, Fitt A, Frimpong-Ansah K, Benson MT. The management of primary rhegmatogenous retinal detachment not involving the fovea. *Eye (Lond).* 2006;20(9):1049-1053.

9. Wykoff CC, Smiddy WE, Mathen T, Schwartz SG, Flynn HW,Jr, Shi W. Fovea-sparing retinal detachments: Time to surgery and visual outcomes. *Am J Ophthalmol.* 2010;150(2):205-210.e2.

10. Kuhn F, Aylward B. Rhegmatogenous retinal detachment: A reappraisal of its pathophysiology and treatment. *Ophthalmic Res.* 2014;51(1):15-31.

11. Marmor M. Mechanisms of normal retinal adhesion. *In Retina Stephen J. Ryan, Chapter 19.* 2013;1:447-464.

12. Machemer R. The importance of fluid absorption, traction, intraocular currents, and chorioretinal scars in the therapy of rhegmatogenous retinal detachments. XLI edward jackson memorial lecture. *Am J Ophthalmol.* 1984;98(6):681-693.

13. Su X, Vesco C, Fleming J, Choh V. Density of ocular components of the bovine eye. *Optom Vis Sci.* 2009;86(10):1187-1195.

14. Shunmugam M, Shah AN, Hysi PG, Williamson TH. The pattern and distribution of retinal breaks in eyes with rhegmatogenous retinal detachment. *Am J Ophthalmol.* 2014;157(1):221-226.e1.

15. Repetto R, Tatone A, Testa A, Colangeli E. Traction on the retina induced by saccadic eye movements in the presence of posterior vitreous detachment. *Biomech Model Mechanobiol.* 2011;10(2):191-202.

16. Demer JL, Viirre ES. Visual-vestibular interaction during standing, walking, and running. *J Vestib Res.* 1996;6(4):295-313.

17. Wilson SJ, Glue P, Ball D, Nutt DJ. Saccadic eye movement parameters in normal subjects. *Electroencephalogr Clin Neurophysiol.* 1993;86(1):69-74.

18. Abrams RA, Meyer DE, Kornblum S. Speed and accuracy of saccadic eye movements: Characteristics of impulse variability in the oculomotor system. *J Exp Psychol Hum Percept Perform.* 1989;15(3):529-543.

19. Bussone W. Linear and angular head accelerations in daily life. *Master of Science Thesis, Faculty of Mechanical Engineering of the Virginia Polytechnic Institute and State University.* 2005.

20. Arndt S, Cargill R, Selim Hammoud P. **Head accelerations experienced during everyday activities and while riding roller coaster**. *Proceedings of the Human Factors and Ergonomics Society Annual Meeting.* 2004;48(16):1973-1977.

21. Bahill AT, Adler D, Stark L. Most naturally occurring human saccades have magnitudes of 15 degrees or less. *Invest Ophthalmol.* 1975;14(6):468-469.

22. Vroon J, de Jong JH, Aboulatta A, et al. Numerical study of the effect of head and eye movement on progression of retinal detachment. *Biomech Model Mechanobiol.* 2018.

23. Pokki J, Ergeneman O, Sevim S, Enzmann V, Torun H, Nelson BJ. Measuring localized viscoelasticity of the vitreous body using intraocular microprobes. *Biomed Microdevices.* 2015;17(5):85-015-9988-z.

24. Swindle KE, Hamilton PD, Ravi N. In situ formation of hydrogels as vitreous substitutes: Viscoelastic comparison to porcine vitreous. *J Biomed Mater Res A.* 2008;87(3):656-665.

25. Zimmerman RL. In vivo measurements of the viscoelasticity of the human vitreous humor. *Biophys J.* 1980;29(3):539-544.

26. Chen K, Rowley AP, Weiland JD, Humayun MS. Elastic properties of human posterior eye. *J Biomed Mater Res A.* 2014;102(6):2001-2007.

27. Liu X, Wang L, Wang C, Sun G, Liu S, Fan Y. Mechanism of traumatic retinal detachment in blunt impact: A finite element study. *J Biomech.* 2013;46(7):1321-1327.

28. Gunnlaugsdottir E, Arnarsson A, Jonasson F. Prevalence and causes of visual impairment and blindness in icelanders aged 50 years and older: The reykjavik eye study. *Acta Ophthalmol*. 2008;86(7):778-785.

29. Congdon N, O'Colmain B, Klaver CC, et al. Causes and prevalence of visual impairment among adults in the united states. *Arch Ophthalmol*. 2004;122(4):477-485.

30. Benner JD, Hay A, Landers MB,3rd, Hjelmeland LM, Morse LS. Fibrinolytic-assisted removal of experimental subretinal hemorrhage within seven days reduces outer retinal degeneration. *Ophthalmology*. 1994;101(4):672-681.

31. Toth CA, Morse LS, Hjelmeland LM, Landers MB,3rd. Fibrin directs early retinal damage after experimental subretinal hemorrhage. *Arch Ophthalmol*. 1991;109(5):723-729.

32. Bressler NM, Bressler SB, Childs AL, et al. Surgery for hemorrhagic choroidal neovascular lesions of age-related macular degeneration: Ophthalmic findings: SST report no. 13. *Ophthalmology*. 2004;111(11):1993-2006.

33. Glatt H, Machemer R. Experimental subretinal hemorrhage in rabbits. *Am J Ophthalmol*. 1982;94(6):762-773.

34. Hochman MA, Seery CM, Zarbin MA. Pathophysiology and management of subretinal hemorrhage. *Surv Ophthalmol*. 1997;42(3):195-213.

35. van Zeeburg EJ, van Meurs JC. Literature review of recombinant tissue plasminogen activator used for recent-onset submacular hemorrhage displacement in age-related macular degeneration. *Ophthalmologica*. 2013;229(1):1-14.

36. Heriot WJ. Intravitreal gas and tPA: An outpatient procedure for subretinal haemorrhage. proceedings of vail vitrectomy meeting. *Vail: American Society of Retina Specialists*. 1996.

37. Buhl M, Scheider A, Schonfeld CL, Kampik A. Intra-vitreal rt-PA and gas introduction in submacular hemorrhage. *Ophthalmologe*. 1999;96(12):792-796.

38. Hillenkamp J, Surguch V, Framme C, Gabel VP, Sachs HG. Management of submacular hemorrhage with intravitreal versus subretinal injection of recombinant tissue plasminogen activator. *Graefes Arch Clin Exp Ophthalmol*. 2010;248(1):5-11.

39. de Jong JH, van Zeeburg EJ, Cereda MG, et al. INTRAVITREAL VERSUS SUBRETINAL ADMINISTRATION OF RECOMBINANT TISSUE PLASMINOGEN ACTIVATOR COMBINED WITH GAS FOR ACUTE SUBMACULAR HEMORRHAGES DUE TO AGE-RELATED MACULAR DEGENERATION: An exploratory prospective study. *Retina*. 2016;36(5):914-925.

40. Yannuzzi LA, Freund KB, Takahashi BS. Review of retinal angiomatous proliferation or type 3 neovascularization. *Retina*. 2008;28(3):375-384.

41. Viola F, Massacesi A, Orzalesi N, Ratiglia R, Staurenghi G. Retinal angiomatous proliferation: Natural history and progression of visual loss. *Retina*. 2009;29(6):732-739.

42. Gharbiya M, Parisi F, Cruciani F, Bozzoni-Pantaleoni F, Pranno F, Abdolrahimzadeh S. Intravitreal anti-vascular endothelial growth factor for retinal angiomatous proliferation in treatment-naive eyes: Long-term functional and anatomical results using a modified PrONTO-style regimen. *Retina*. 2014;34(2):298-305.

43. Inoue M, Arakawa A, Yamane S, Kadonosono K. Long-term results of intravitreal ranibizumab for the treatment of retinal angiomatous proliferation and utility of an advanced RPE analysis performed using spectral-domain optical coherence tomography. *Br J Ophthalmol*. 2014;98(7):956-960.

44. Hemeida TS, Keane PA, Dustin L, Sadda SR, Fawzi AA. Long-term visual and anatomical outcomes following anti-VEGF monotherapy for retinal angiomatous proliferation. *Br J Ophthalmol.* 2010;94(6):701-705.

45. Gupta B, Jyothi S, Sivaprasad S. Current treatment options for retinal angiomatous proliferans (RAP). *Br J Ophthalmol.* 2010;94(6):672-677.

46. Tsai ASH, Cheung N, Gan ATL, et al. Retinal angiomatous proliferation. *Surv Ophthalmol.* 2017;62(4):462-492.

47. Rouvas AA, Chatziralli IP, Theodossiadis PG, Moschos MM, Kotsolis AI, Ladas ID. Long-term results of intravitreal ranibizumab, intravitreal ranibizumab with photodynamic therapy, and intravitreal triamcinolone with photodynamic therapy for the treatment of retinal angiomatous proliferation. *Retina.* 2012;32(6):1181-1189.

48. Freund KB, Klais CM, Eandi CM, et al. Sequenced combined intravitreal triamcinolone and indocyanine green angiography-guided photodynamic therapy for retinal angiomatous proliferation. *Arch Ophthalmol.* 2006;124(4):487-492.

49. van de Moere A, Kak R, Sandhu SS, Talks SJ. Anatomical and visual outcome of retinal angiomatous proliferation treated with photodynamic therapy and intravitreal triamcinolone. *Am J Ophthalmol.* 2007;143(4):701-704.

50. Saito M, Iida T, Kano M. Two-year results of combined intravitreal anti-VEGF agents and photodynamic therapy for retinal angiomatous proliferation. *Jpn J Ophthalmol.* 2013;57(2):211-220.

51. Lee MY, Kim KS, Lee WK. Combined intravitreal ranibizumab and photodynamic therapy for retinal angiomatous proliferation. *Am J Ophthalmol.* 2012;153(5):1004-5; author reply 1005.

52. Saito M, Iida T, Kano M, Itagaki K. Two-year results of combined intravitreal ranibizumab and photodynamic therapy for retinal angiomatous proliferation. *Jpn J Ophthalmol.* 2015.

53. Amarakoon S, de Jong JH, Braaf B, et al. Phase-resolved doppler optical coherence tomographic features in retinal angiomatous proliferation. *Am J Ophthalmol.* 2015;160(5):1044-1054.e1.

54. Tan AC, Dansingani KK, Yannuzzi LA, Sarraf D, Freund KB. Type 3 neovascularization imaged with cross-sectional and en face optical coherence tomography angiography. *Retina.* 2016.

55. de Jong JH, Braaf B, Amarakoon S, et al. Treatment effects in retinal angiomatous proliferation imaged with OCT angiography. *Ophthalmologica.* 2018:1-11.

56. Schmidt-Erfurth U, Michels S, Barbazetto I, Laqua H. Photodynamic effects on choroidal neovascularization and physiological choroid. *Invest Ophthalmol Vis Sci.* 2002;43(3):830-841.

57. Novosel J, Vermeer KA, de Jong JH, Ziyuan W, van Vliet LJ. Joint segmentation of retinal layers and focal lesions in 3-D OCT data of topologically disrupted retinas. *IEEE Trans Med Imaging.* 2017;36(6):1276-1286.

Chapter

10

Summary

SUMMARY

Two ocular diseases were studied in this thesis: retinal detachment (RD) and age related macular degeneration (AMD). Optical coherence tomography (OCT) played a crucial role in answering the scientific questions as formulated in this thesis. The aim of this thesis was to answer the following questions: 1) if preoperative posturing of macula-on RD influences RD progression; 2) what risk factors for RD progression could be identified; 3) which role head orientation, movement and eye movement play in RD progression; 4) whether intravitreal or subretinal administration of recombinant tissue plasminogen activator (rtPA) in combination with intravitreal gas better stimulates displacement of acute submacular hemorrhages in AMD; 5) what advantage OCT-angiography (OCT-A) has over conventional imaging in diagnosing and treatment monitoring of retinal angiomatous proliferation (RAP), a subtype of AMD.

   Chapter 1 is a general introduction, in which the anatomy of the eye and retina is described, and background information is given on the two diseases under study in this thesis, retinal detachment and age related macular degeneration. The mechanisms responsible for retinal adhesion are discussed as well as the forces causing retinal detachment, especially intraocular currents of vitreous gel and intravitreal fluid caused by head and eye movements. It is explained that preoperative posturing is prescribed for macula-on retinal detachments to prevent RD progression to macula-off for patients waiting for surgery. Furthermore, the pathophysiology, classification and treatment of exudative AMD are described with special attention to RAP, a subtype of exudative AMD characterized by intraretinal neovascularization. Then, an introduction is given on the imaging of the posterior eye using OCT. The principles and limitations of OCT imaging are explained as well as recent developments, like swept source OCT, OCT-A, and wide field OCT.

   In **chapter 2**, the results of the first cohort including 98 patients of a clinical trial studying the effect of preoperative posturing on progression of macula-on RD are presented. Patients were admitted to the ward for bed rest in anticipation of their surgery and were positioned on the side where the RD was mainly located. At baseline and before and after interruptions for meals or toilet visits, a OCT volume scan was performed using a wide-angle Spectralis OCT (Heidelberg Engineering, Heidelberg, Germany). The distance between the nearest point of the RD border and fovea was measured using a custom-built measuring tool. The RD border displacement and the average RD border displacement velocity moving toward (negative) or away (positive) from the fovea were determined for intervals of posturing and interruptions. The median RD border displacement velocity was 1 µm/hour (IQR, -21 to 49 µm/hour) during posturing and -149 µm/hour (IQR,-

406 to 1 μm/hour) during interruptions, a statistically significant difference (P < 0.001). It was concluded that preoperative posturing is effective in reducing progression toward the fovea. Additionally, risk factors for RD progression were studied within this first group of patients, of which a larger baseline RD-fovea distance, a smaller extent of RD, a smaller duration of visual field loss and a superior RD location showed weak but statistically significant correlations with RD progression from baseline.

In **chapter 3**, the effect of prolonging the duration of posturing interruptions by sitting upright is evaluated. The rationale behind this study was that one of the main differences between inpatient and outpatient preoperative posturing is that, in an outpatient care setting, patients would have to travel home in a car or taxi and sit upright. Three cohorts of 50 patients with superior temporal macula-on RD were compared with an average interruption duration of 22, 41 and 58 minutes respectively. The median RD border displacement during interruptions was not statistically significantly different among the cohorts (P = 0.28). Besides re-evaluating the risk factors as studied in the first cohort, ultrasound imaging was used in cohort 3 to evaluate the amount of subretinal fluid (SRF) at baseline as a risk factor for RD progression. The correlation coefficient between SRF area at baseline and relative worst RD progression from baseline was 0.37 (95%CI: 0.04 to 0.66, P = 0.009). It was concluded that we could not find a significant increase of RD progression after prolongation of interruptions by sitting upright and that patients with a larger area of SRF on ultrasound showed an increased risk for RD progression.

Chapter 4 focusses on the relationship between compliance with the preoperative posturing advice and progression of macula-on RD. Furthermore, it was evaluated whether head positioning or head motility contributes most to RD progression. Sixteen patients with macula-on RD were enrolled and admitted to the ward and instructed to posture preoperatively. The head orientation and head linear and rotational acceleration were measured with a head mounted inertial measurement unit (IMU, Shimmer 3, Shimmer Sensing, Ireland). OCT imaging was performed at baseline and before and after natural interruptions of posturing for meals and toilet visits to measure RD progression toward the fovea, similar to the first cohort of the clinical study presented in chapter 2. The correlation coefficient with RD progression was 0.37 (P = 0.001) for compliance, 0.52 (p<0.001) for rotational head acceleration, and 0.49 (p<0.001) for linear head acceleration. The correlation coefficient between RD progression and rotational acceleration was statistically significantly higher than the correlation coefficient between RD progression and compliance (P = 0.034). Therefore, we concluded that preoperative posturing is effective by reducing head movements rather than enforcing head positioning.

In **chapter 5**, a finite element model was developed and used to explore whether eye movements or head movements play the largest role in RD progression. This was done because a clinical trial using RD progression OCT measurement and eye movement measurement would be invasive and therefore far more challenging to perform. The model is based on geometric and material properties reported in literature. The model showed that a mild head movement and a severe eye movement produce similar traction loads on the retina. This implies that strong head movements and not saccadic eye movements are able to cause loads that can trigger and progress an RD. These preliminary results suggest that head movements have a larger effect on RD progression than saccadic eye movements.

Chapter 6 discusses the results of an exploratory randomized clinical trial comparing effectiveness and safety of two treatment modalities to displace an acute submacular hemorrhage (SMH) from the macula. Current management of SMH favors vitrectomy and gas with subretinal administration of rtPA, while intravitreal administration of rtPA and gas might be less invasive but as effective. Twenty-four patients with SMH secondary to AMD were included. The SMH had to exist ≤14 days at time of surgery and SMH thickness had to be between 250 μm and 1,250 μm. Patients were randomized to either intravitreal injections of rtPA, perfluoropropane (C_3F_8) gas, and bevacizumab (n = 12) or vitrectomy with subretinal rtPA administration, intravitreal C_3F_8 gas, and bevacizumab (n = 12). The SMH volume change was measured on spectral domain OCT preoperatively and 6 weeks postoperatively within a 2.5-mm cylinder centered at the fovea. Median relative volume reduction of subretinal blood at 6 weeks postoperatively was 97% (95% confidence interval: 91–99%) in the intravitreal rtPA group and 100% (95–100%) in the subretinal rtPA group and did not differ significantly between groups (P = 0.56). It was concluded that both treatment modalities effectively displaced SMH in this exploratory clinical trial.

In **chapter 7**, we present the results of a study which aimed to describe the features of RAP on OCT-angiography (OCT-A) and to compare these features with conventional imaging. Twelve treatment-naïve patients diagnosed with RAP based on fundus examination, fluorescein angiography, and indocyanine green angiography were included. Patients were imaged with an experimental 1,040 nm swept-source phase-resolved Doppler OCT instrument. Abnormal flow was defined as intraretinal neovascularization or retinal choroidal anastomosis. In 4 patients a retinal choroidal anastomosis was found, 3 patients showed intraretinal neovascularization connected with a pigment epithelial detachment, 2 patients showed only intraretinal neovascularization, in 2 patients flow was limited to the subretinal or sub–retinal pigment epithelial space, and in 1 patient imaging with OCT-A was unsuccessful due to severe eye motions. It was concluded that phase-resolved Doppler OCT is able to detect and localize abnormal blood flow within

RAP lesions. We further concluded that blood flow was mostly confined to the intraretinal structures with or without a connecting pigment epithelial detachment; in one-third of patients a retinal choroidal anastomosis was detected. This study demonstrates the potential of angiography with phase-resolved Doppler OCT to accurately distinguish between normal and pathologic blood.

Chapter 8 evaluates OCT-A as a treatment monitoring tool in patients with RAP in the same patients as described in chapter 7. Treatment consisted of either intravitreal bevacizumab or triamcinolone injections with or without photodynamic therapy (PDT). Abnormal blood flow after treatment was graded as increased, unchanged, decreased or resolved. OCT-A images before and after treatment could be obtained in 9 patients. Median follow-up period was 10 weeks (range 5-19 weeks). After various treatment, the RAP lesion resolved in 7 patients, in 1 patient the OCT-A depicted decreased flow in the lesion and 1 patient showed unchanged abnormal blood flow. Monotherapy with intravitreal bevacizumab injections resolved RAP in 1 out of 2 patients. Combined therapy of bevacizumab with PDT resolved RAP in 6 out of 7 patients. It was concluded that OCT-A visualized resolution of abnormal blood flow in 7 out of 9 RAP patients after various short-term treatment sequences.

Finally, in **chapter 9,** the clinical implications of the aforementioned studies are discussed and novel applications of OCT for future studies are proposed.

Samenvatting

SAMENVATTING

Twee oogheelkundige aandoeningen werden bestudeerd in dit proefschrift: netlviesloslating en leeftijdsgebonden maculadegeneratie (LMD). Optische coherentie tomografie (OCT) speelde een cruciale rol bij het beantwoorden van de wetenschappelijke vragen zoals geformuleerd in dit proefschrift. Het doel van dit proefschrift was om de volgende vragen te beantwoorden: 1) of het pre-operatief houdingsadvies van macula-aan netvliesloslatingen progressie beïnvloedt; 2) welke risicofactoren voor de progressie van netvliesloslatingen konden worden vastgesteld; 3) welke rol de hoofdstand, hoofdbewegingen en oogbewegingen spelen in progressie van netvliesloslatingen; 4) of intravitreale of subretinale toediening van recombinant tissue plasminogen activator (rtPA) in combinatie met intravitreaal gas beter de verplaatsing van acute submaculaire bloedingen bij LMD stimuleert; 5) welk voordeel OCT-angiography (OCT-A) heeft ten opzichte van conventionele beeldvorming bij het diagnosticeren en behandelen van retinale angiomateuze proliferatie (RAP), een subtype van LMD.

Hoofdstuk 1 is een algemene inleiding, waarin de anatomie van het oog en het netvlies wordt beschreven en achtergrondinformatie wordt gegeven over de twee aandoeningen die in dit proefschrift worden bestudeerd, netvliesloslating en leeftijdsgebonden maculaire degeneratie. De mechanismen die verantwoordelijk zijn voor retinale adhesie worden besproken evenals de krachten die een netvliesloslating veroorzaken, in het bijzonder intraoculaire stromingen van het glasachtig lichaam en intravitreaal vocht die op gang komen door hoofd- en oogbewegingen. Er wordt uitgelegd dat preoperatieve houding wordt voorgeschreven voor macula-aan netvliesloslatingen om progressie tot macula-af te voorkomen gedurende de tijd dat patiënten moeten wachten op een operatie. Verder worden de pathofysiologie, classificatie en behandeling van exudatieve LMD beschreven met speciale aandacht voor RAP, een subtype van exudatieve LMD dat gekenmerkt wordt door intraretinale neovascularisatie. Vervolgens wordt een inleiding gegeven over de beeldvorming van het achtersegment van het oog met behulp van OCT. De principes en beperkingen van OCT-beeldvorming worden uitgelegd, evenals recente ontwikkelingen, zoals swept source-OCT, OCT-A en wide field OCT.

In **hoofdstuk 2** worden de resultaten van het eerste cohort gepresenteerd van een klinische studie waarin het effect van preoperatieve houding op de progressie van macula-aan netvliesloslatingen werd onderzocht. 98 patiënten werden opgenomen op de verpleegafdeling van Het Oogziekenhuis Rotterdam voor bedrust in afwachting van hun operatie en werden gepositioneerd op de zijde waar de netvliesloslating zich voornamelijk bevond. Op baseline en voor en na onderbrekingen voor maaltijden of toiletbezoeken werd een OCT-volumescan

gemaakt met behulp van een widefield Spectralis OCT (Heidelberg Engineering, Heidelberg, Duitsland). De afstand tussen het dichtstbijzijnde punt op de netvliesloslatingsrand en de fovea werd gemeten met behulp van een speciaal ontwikkelde meetmethode. De verplaatsing van de netvliesloslatinsrand en de gemiddelde verplaatsingssnelheid van de netvliesloslatingrand die zich in de richting van de fovea (negatief) of bij de fovea vandaan (positief) beweegt werden bepaald voor de intervallen van houding en houdingsonderbrekingen. De mediane verplaatsingssnelheid van de netvliesloslatingrand was 1 µm/uur (IQR, -21 tot 49 µm/uur) tijdens de houdingsintervallen en -149 µm/uur (IQR, -406 tot 1 µm/uur) tijdens houdingsonderbrekingen, wat statistisch significant verschillend was (P <0,001). Er werd geconcludeerd dat het volgen van het preoperatieve houdingsadvies effectief is in het verminderen van de progressie richting de fovea. Bovendien werden risicofactoren voor progressie van netvliesloslatingen bestudeerd binnen deze eerste groep patiënten, waarvan een grotere netvliesloslating-fovea afstand op baseline, een kleinere uitbreiding van de netvliesloslating, een kortere duur van gezichtsveldverlies en een superior locatie van de netvliesloslating een zwakke maar statistisch significante correlatie vertoonden met progressie van netvliesloslatingen vanaf baseline.

In **hoofdstuk 3** wordt het effect geëvalueerd van het verlengen van de duur van houdingsonderbrekingen door middel van rechtop te zitten. De reden voor deze studie was dat een van de belangrijkste verschillen tussen het uitvoeren van een preoperatieve houdingsadvies in een klinisch omgeving of thuis is dat patiënten in een auto of taxi naar huis moeten gaan en dan voor langere tijd rechtop moeten zitten. Drie cohorten van 50 patiënten met een superior temporale macula-aan netvliesloslating met een gemiddelde onderbrekingsduur van respectievelijk 22, 41 en 58 minuten werden vergeleken. De mediane verplaatsing van de netvliesloslatingsrand tijdens onderbrekingen was niet statistisch significant verschillend tussen de cohorten (P = 0,28). Naast het opnieuw evalueren van de risicofactoren zoals beschreven in het eerste cohort, werd in cohort 3 echografie gebruikt om de hoeveelheid subretinaal vocht op baseline te onderzoeken als een risicofactor voor progressie van de netvliesloslating. De correlatiecoëfficiënt tussen het subretinale vocht oppervlak op baseline en de ergste progressie van de netvliesloslating vanaf baseline was 0,37 (95% BI: 0,04 tot 0,66, P = 0,009). Er werd geconcludeerd dat er geen significante toename van progressie van de netvliesloslating was na verlenging van houdingsonderbrekingen door rechtop te zitten en dat patiënten met een groter subretinaal vocht oppervlak op echografie een verhoogd risico op progressie van de netvliesloslating vertoonden.

Hoofdstuk 4 richt zich op de relatie tussen therapietrouwheid van patienten in het naleven van het preoperatieve houdingsadvies en de progressie van macula-aan netvliesloslating. Tevens werd geëvalueerd of de hoofdstand of de hoofdbewegingen het meest bijdragen aan progressie van de netvliesloslatingen.

Zestien patiënten met macula-aan netvliesloslating werden geincludeerd en opgenomen op de verpleegafdeling en geïnstrueerd om de preoperatieve houding aan te nemen. De richting van het hoofd en de lineaire en rotationele versnelling van het hoofd werden gemeten met een aan het hoofd vastgemaakte sensor (intertial measurement unit, IMU, Shimmer 3, Shimmer Sensing, Ierland). OCT-beeldvorming werd uitgevoerd op baseline en voor en na natuurlijke onderbrekingen van de houdingsperiode voor maaltijden en toiletbezoek om progressie van de netvliesloslating richting de fovea te meten, zoals in het eerste cohort van de klinische studie gepresenteerd in hoofdstuk 2. De correlatie tussen progressie van de netvlieslolating en therapietrouwheid was 0,37 (P = 0,001), 0,52 voor rotationele versnelling van het hoofd (P < 0,001) en 0,49 (P < 0,001) voor lineaire versnelling van het hoofd. De correlatie tussen progressie van de netvliesloslating progressie en rotationele versnelling was statistisch significant hoger dan de correlatie tussen progressie van de netvliesloslating en therapietrouwheid (P = 0,034). Daarom concludeerden we dat de preoperatieve houding effectief is door het verminderen van hoofdbewegingen meer dan het vooschrijven van een hoofdstand.

In **hoofdstuk 5** werd een eindig elementenmodel ontwikkeld en gebruikt om te onderzoeken of oogbewegingen of hoofdbewegingen de grootste rol spelen in de progressie van netvliesloslatingen. Dit werd gedaan omdat een klinisch onderzoek naar de progressie van netvliesloslatingen met behulp van OCT-metingen en metingen van de oogbewegingen invasief zou zijn en daarom veel moeilijker om uit te voeren. Het model is gebaseerd op geometrische en materiaaleigenschappen die in de literatuur worden vermeld. Het model toonde aan dat een lichte beweging van het hoofd en een ernstige saccadische oogbeweging vergelijkbare tractiebelastingen produceren op het netvlies. Dit houdt in dat sterke hoofdbewegingen en niet saccadische oogbewegingen belastingen kunnen veroorzaken die een netvliesloslating kunnen doen ontstaan en verergeren. Deze voorlopige resultaten suggereren dat hoofdbewegingen een groter effect hebben op de progressie van netvliesloslatingen dan saccadische oogbewegingen.

Hoofdstuk 6 bespreekt de resultaten van een verkennend, gerandomiseerd klinisch onderzoek waarin de effectiviteit en veiligheid van twee behandelmethoden worden vergeleken om een acute submaculaire bloeding uit de macula te verplaatsen. Het huidige behandeling van submaculaire bloeding is meestal middels vitrectomie en gas met subretinale toediening van recombinant tissue plasminogen activator (rtPA), terwijl intravitreale toediening van rtPA en gas mogelijk minder invasief maar even effectief is. Vierentwintig patiënten met een submaculaire bloeding secundair aan AMD werden geincludeerd. De submaculaire bloeding moest ≤14 dagen bestaan op het moment van de operatie en de submaculaire bloedingsdikte moest liggen tussen 250 μm en 1.250 μm. Patiënten werden gerandomiseerd voor ofwel intravitreale injecties van rtPA,

perfluorpropaan (C_3F_8) gas en bevacizumab (n = 12) of vitrectomie met subretinale rtPA-toediening, intravitreaal C_3F_8-gas en bevacizumab (n = 12). Het volume van de submaculaire bloeding werd door middel van spectraal domein OCT preoperatief gemeten en 6 weken postoperatief binnen een 2,5 mm cilinder rond de fovea. De mediane relatieve volumevermindering van subretinaal bloed 6 weken postoperatief was 97% (95% betrouwbaarheidsinterval: 91-99%) in de intravitreale rtPA-groep en 100% (95-100%) in de subretinale rtPA-groep en verschilde niet significant tussen de groepen (P = 0,56). Er werd geconcludeerd dat beide behandelingsmodaliteiten in dit verkennende klinische onderzoek effectief de submaculaire bloeding verplaatsten.

In **hoofdstuk 7** presenteren we de resultaten van een onderzoek dat gericht was op het beschrijven van de kenmerken van retinale angiomatische proliferatie (RAP) op OCT-angiografie (OCT-A) en om deze kenmerken te vergelijken met conventionele beeldvorming. Twaalf behandelingsnaïeve patiënten met RAP op basis van funduscopy, fluoresceïne-angiografie en indocyanine green angiografie werden geïncludeerd. Patiënten werden in beeld gebracht met een experimentele 1,040 nm swept source phase-resolved Doppler OCT-instrument. Abnormale flow werd gedefinieerd als intraretinale neovascularisatie of retinale choroïdale anastomose. Bij 4 patiënten werd een retinale choroïdale anastomose gevonden, 3 patiënten vertoonden intraretinale neovascularisatie verbonden met een pigmentepitheel loslating, 2 patiënten vertoonden alleen intraretinale neovascularisatie, bij 2 patiënten was de flow beperkt tot de subretinale of sub-retinale pigmentepitheelruimte en bij 1 patiënt was beeldvorming met OCT-A niet succesvol vanwege ernstige oogbewegingen. Er werd geconcludeerd dat phase-resolved Doppler OCT in staat is om abnormale bloedstromen in RAP-laesies te detecteren en te lokaliseren. We concludeerden verder dat de bloedstroom meestal beperkt was tot de intraretinale structuren met of zonder een verbindende pigmentepitheel loslating; bij een derde van de patiënten werd een retinale choroïdale anastomose gedetecteerd. Deze studie toont het potentieel van angiografie met phase-resolved Doppler OCT aan om nauwkeurig onderscheid te maken tussen normale en pathologische bloedstromen.

Hoofdstuk 8 evalueert OCT-A als behandelingsmonitoringstool bij patiënten met RAP bij dezelfde patiënten als beschreven in hoofdstuk 7. De behandeling bestond uit intravitreale bevacizumab- of triamcinolon-injecties met of zonder fotodynamische therapie (PDT). Abnormale doorbloeding na behandeling werd beoordeeld als verhoogd, onveranderd, verlaagd of opgelost. OCT-A-beelden voor en na de behandeling konden bij 9 patiënten worden verkregen. De mediane follow-up periode was 10 weken (bereik 5-19 weken). Na verschillende behandelingen loste de RAP-laesie op bij 7 patiënten, bij 1 patiënt vertoonde de OCT-A een verminderde flow in de laesie en 1 patiënt vertoonde een ongewijzigde abnormale bloedstroom. Monotherapie met intravitreale bevacizumab-injecties

loste RAP op bij 1 van de 2 patiënten. Gecombineerde behandeling van bevacizumab met PDT loste RAP op bij 6 van de 7 patiënten. Geconcludeerd werd dat OCT-A de abnormale bloedstroom visualiseerde bij 7 van de 9 RAP-patiënten na verschillende korte behandelingssequenties.

Ten slotte worden in hoofdstuk 9 de klinische implicaties van de bovengenoemde studies besproken en worden nieuwe toepassingen van OCT voor toekomstige studies voorgesteld.

List of supplemental videos

Supplemental video 5.1 – Numerical model and dynamic ultrasound

Supplemental video 7.1 – RAP Patient 5

Supplemental video 7.2 – RAP Patient 11

Supplemental video 7.3 – RAP Patient 7 – part A

Supplemental video 7.4 – RAP Patient 7 – part B

Supplemental video 7.5 – RAP Patient 9

Supplemental video 7.6 – RAP Patient 3

Supplemental video 8.1 – RAP Patient 12

Supplemental video 8.2 – RAP Patient 12

Supplemental video 9.1 – Dynamic ultrasound of a bullous retinal detachment

These videos can be downloaded from:

https://drive.google.com/open?id=1Qv7ckXyETlIys_Ya42xMxnJOXwrbV2WS

List of Abbreviations

LIST OF ABBREVIATIONS

AMD	Age-related macular degeneration
AVN	Abnormal vascular network
C3F8	Perfluoropropane
CI	Confidence interval
CNV	Choroidal neovascularization
DOR	Diagnostic odds ratio
ETDRS	Early Treatment Diabetic Retinopathy Study
FA	Fluorescein angiography
FD-OCT	Fourier domain optical coherence tomography
FE	Fundus examination
GMP	Good manufacturing practice
ICC	Intraclass correlation coefficient
ICG	Indocyanine-green angiography
ILM	Inner limiting membrane
IMU	Inertial measurement unit
INR	International normalized ratio
IOP	Intraocular pressure
IQR	Interquartile range
IRF	Intraretinal fluid
IRH	Intraretinal hemorrhage
IRN	Intraretinal neovascularization
IRNP	Intraretinal neovascularization with pigment epithelial detachment
logMAR	logarithm of the minimal angle of resolution
MARG	Magnetic angular rate and gravity
OCT	Optical coherence tomography
OCT-A	Optical coherence tomography angiography
OD	Oculus dexter

OFDI	Optical frequency domain imaging
OS	Oculus sinister
PDT	Photodynamic therapy
PED	Pigment epithelial detachment
POI	Point of interest
PRD-OCT	Phase-resolved Doppler optical coherence tomography
RAP	Retinal angiomatous proliferation
RCA	Retinal choroidal neovascularization
RD	Retinal detachment
ROC	Receiver operating characteristic
RPE	Retinal pigment epithelium
rtPA	Recombinant tissue plasminogen activator
SD	Standard deviation
SD-OCT	Spectral domain optical coherence tomography
SLO	Scanning laser ophthalmoscopy
SMH	Submacular hemorrhage
SOP	Standard operation procedure
SRF	Subretinal fluid
SS-OCT	Swept source optical coherence tomography
TD-OCT	Time domain optical coherence tomography
tPA	Tissue plasminogen activator
VA	Visual acuity
VEGF	Vascular endothelial growth factor

PhD Portfolio

PHD PORTFOLIO

Courses	Year	Workload (ECTS)
BROK (Basiscursus Regelgeving Klinisch Onderzoek)	2013	1
Biomedical English writing and communication	2017	2
Scientific integrity	2016	0.3
Laser safety course	2015	0.3
Journal club statistics – Rotterdam Ophthalmic Institute	2015	1.5
Contract research Harrier study training Madrid	2015	0.5
Retinal detachment – Euretina	2017	0.3
Yearly Basic Life Support training	2013-2017	0.5

Seminars and workshops		
SWOO Patient day (oral presentation)	2015	0.5
SWOO Patient day 2017 (oral presentation)	2018	0.5
Retinal detachment patient day 2017 (oral presentation)	2018	1
Scientific seminars The Eye Hospital Rotterdam	2013-2018	2
Scientific seminars Rotterdam Ophthalmic Institute	2013-2018	3
Ophthalmology seminars The Eye Hospital Rotterdam	2013-2018	4
Scientific day Rotterdam Ophthalmic Institute	2014	0.3
Scientific day Rotterdam Eye Hospital	2015	0.3

Oral presentations / poster contributions		
BIOS, San Francisco, USA (oral presentation)	2014	3
ARVO, Orlando, USA (poster contribution)	2014	3
ARVO, Denver, USA (oral presentation)	2015	3

ARVO, Seattle, USA (two poster contributions)	2016	4
EURETINA, Barcelona, Spain (oral presentation)	2017	2
NOG, Maastricht, The Netherlands (oral presentation)	2016	1
NOG, Maastricht, The Netherlands (oral presentation)	2017	1
NOG, Groningen, The Netherlands (oral presentation)	2018	1
DOPS, Nijmegen, The Netherlands (oral presentation)	2016	0.5
WAEH, Rotterdam, NL (oral and poster contribution)	2016	1

Teaching

Master student Erasmus University Rotterdam - Tiarah Simon	2015	1
Internship student Haagse Hogeschool - Koen de Koning	2016	1
Internship student Haagse Hogeschool - Tom den Ouden	2017	2
Master student TU Delft - Jos Vroon	2017	1

Other PhD activities

NOG, Maastricht, The Netherlands	2014	0.3
NOG, Groningen, The Netherlands	2015	0.3
Contract research studies Jetrea, Octave, Harrier, Sequioa	2014-2017	8
Weekly intraocular injections and patient consultation shifts	2013-2017	28

Total		**79.1**

Dankwoord

DANKWOORD

Professor Van Meurs, beste Jan, ik ben er dankbaar voor u als supervisor te hebben gehad. Ik denk dat we elkaar goed aanvulden: u bent van nature meer van de grote lijnen en ik van de details. Dank voor al uw geduld, maar vooral ook voor alle aansporingen om niet in details te blijven hangen. Dank voor al uw vlotte en ter zake doende reacties op vragen, abstracts en manuscripten. Bedankt voor uw mentorschap op momenten dat het minder liep. En dank voor al uw oprechte en positieve opmerkingen als het werk goed was, dat was zeer motiverend!

Koen Vermeer, jouw logisch redeneervermogen was soms onnavolgbaar en confronterend. Als jij zei: 'dat begrijp ik niet', dan wist elke promovendus dat er wat aan de hand was. Dank voor je onvermoeibaarheid in het benoemen van verbeterpunten, deze zijn van onschatbare waarde geweest voor dit proefschrift. Dank dat je altijd bereid was mee te denken, zowel op technisch, klinisch als persoonlijk vlak.

Mirjam van Velthoven, we hebben te kort samengewerkt. Ik heb je zachtaardigheid, goedlachsheid en scherpte gemist de laatste jaren van mijn promotie. Bedankt voor je hulp en je vertrouwen in mij bij de start van mijn promotietraject.

Johannes de Boer, ook met jou is de samenwerking uiteindelijk maar kort geweest. Dank voor je enthousiasme over de OCT projecten en over mijn rol daarin. Dank voor je positiviteit en de kansen die je me geboden hebt.

Netty Dorrestijn, bedankt voor je vertrouwen in mij, bedankt voor je onvermoeibaarheid en je passie voor alle projecten en in het nadenken over de vele praktische en inhoudelijke kanten van mijn promotietraject.

René Wubbels, jouw rol leek vaak wat meer op de achtergrond, maar je inbreng in het ontwerp en de voortgang van de projecten was vaak cruciaal.

Dank aan alle andere oogartsen die op enige wijze een inbreng hebben gehad op de projecten waar ik aan deelgenomen heb. Ik denk aan de medische retina groep: Jose Martinez, Tom Missotten, Suzanne IJzer, Ingeborg van der Born; en aan de vitreoretinale chirurgie groep: Koen van Overdam, Koorosh Faridpooya, Eric Lindstedt, Ellen La Heij, Peter van Etten.

Alle collega's van het ROI en daarbuiten: dank voor jullie gezelligheid en vriendelijkheid, zonder jullie zou het maar een saaie boel zijn geweest! Dank ook voor alle behulpzaamheid en samenwerking. Met het risico iemand te vergeten denk ik terug aan: Aletta, Aline, Angela, Annemiek, Arni, Babak, Boy, Caroline, Elrozy, Elsbeth, Esma, Eva, Gijs, Grzegorz, Jelena, Jetty, Joziena, Juan, Juleke, Heijan, Kari, Kedir, Laurence, Leah, Lisette, Marja, Mark, Mathi, Matteo, Olympia, Robin, Sankha, Saskia, Sonia, Stijn, Susan, Tessa, Verena en Wout. Kedir, thanks for being my paranimf!

Dank aan alle collega's met wie ik heb samen mogen werken op de verpleegafdeling. Jullie hebben me vaak gebeld voor nieuwe patiënten. Zonder jullie gezelligheid en praktische inbreng waren mijn projecten nooit zo vlot verlopen.

Ik dank de studenten met wie ik heb mogen samenwerken die zoveel metingen, berekeningen en programmeerwerk hebben gedaan. Tiarah, Koen, Tom en Jos, jullie inzet en bijdrage overtrof mijn verwachtingen. Dank daarvoor!

Pa en ma, bedankt voor jullie steun en wijze lessen. Dit is eigenlijk niet in woorden uit te drukken. Bedankt dat jullie er altijd voor mij zijn geweest. Afke, Jos, Marijke, Sietske, zwagers, schoonzus, neefjes en nichtjes en overige familie: bedankt voor jullie trouw en gezelligheid. Jos, bedankt dat je mijn paranimf wilt zijn!

Eline en Naomi, jullie aanwezigheid vervult mij met een groots gevoel van vreugde. Niets is motiverender voor mij geweest dan jullie liefde.

Christine, achter elke succesvolle man staat een sterke vrouw. Jij herinnert mij er vaak aan wat er werkelijk toe doet in het leven. Ik bewonder je idealisme, je doorzettingsvermogen, je onvermoeibaarheid en passie die ik zie in de zorg voor onze kinderen en hoe je in het leven staat. Dank voor je begrip, steun, opoffering, wijsheid, humor en liefdevolle aanmoediging.

About the author

ABOUT THE AUTHOR

Jan Hendrik (Henk) de Jong was born on April 19, 1985 in Rotterdam, The Netherlands. He is married to Anuradi Christine de Jong – Bruijn and the father of Eline and Naomi.

He graduated from the Gereformeerde Scholengemeenschap Randstand, Rotterdam, The Netherlands, in 2003. During his medical study he worked for a year as a research student at the hematology department of the Erasmus Medical Center, Rotterdam, The Netherlands, on the efficacy of magnetically enhanced gene delivery to bone marrow stem cells for the use in gene therapy. After graduating from medical school in 2013, he started a PhD project in the Rotterdam Eye Hospital under supervision of Prof. dr. Johannes F. de Boer and Dr. Mirjam E.J. van Velthoven on optical coherence tomography angiography in retinal angiomatous proliferation. After these projects ended, he continued his PhD under supervision of Prof. dr. Jan. C. van Meurs and Dr. Ir. Koenraad A. Vermeer. The topic of this research was the use of optical coherence tomography in treatment monitoring of submacular hemorrhages secondary to age related macular degeneration and the use of optical coherence tomography in studying the effect of preoperative posturing on the progression of macula-on retinal detachment. In 2018 he worked as a phycisian at the neurology department of the Maasstad Ziekenhuis, Rotterdam. In April 2019 he returned to the Rotterdam Eye Hospital as an ophthalmology resident.

LIST OF PUBLICATIONS

De Jong JH, Vigueras Guillén JP, Wubbels RJ, Timman R, Vermeer KA, van Meurs JC. *The influence of prolongation of interruptions of preoperative posturing and other clinical factors on the progress of macula-on retinal detachment.* Article in Press in Ophthalmology Retina, 2019

Smid LM, van Overdam KA, Davidoiu V, **de Jong JH**, de Boer JF, Vermeer KA, van Velthoven MEJ. *Classification and treatment follow-up of a juxtapapillary retinal hemangioblastoma with optical coherence tomography angiography.* Am J Ophthalmol Case Rep. 2019 May 20;15:100472

De Jong JH, de Koning K, den Ouden T, van Meurs JC, Vermeer KA. *The effect of compliance with preoperative posturing advice and head movements on the progression of macula-on retinal detachment.* Translational Vision Science & Technology. 2019;8(2):4.

De Jong JH, Braaf B, Amarakoon S, Gräfe M, Yzer S, Vermeer KA, Missotten T, de Boer JF, Van Velthoven MEJ. *Treatment effects in retinal angiomatous proliferation imaged with OCT angiography.* Ophthalmologica. 2018; 241(3):143–153

Vroon J, **de Jong JH**, Aboulatta A, Eliasy A, van der Helm FCT, van Meurs JC, Wong D, Elsheikh A. *Numerical study of the effect of head and eye movement on progression of retinal detachment.* Biomechanics and Modeling in Mechanobiology. 2018;17(4):975–983

De Jong JH, Vigueras Guillén JP, Simon T, Timman R, Vermeer KA, van Meurs JC. *Preoperative posturing of patients with macula-on retinal detachment retards progression towards the fovea.* Ophthalmology, 2017; 124(10):1510-1522

Novosel J, Vermeer KA, **de Jong JH**, Wang Z, van Vliet L. *Joint segmentation of retinal layers and focal lesions in 3D OCT data of topologically disrupted retinas.* IEEE Transactions on Medical Imaging. 2017;36(6):1276-1286.

Novosel J, Wang ZY, **de Jong JH**, van Velthoven MEJ, Vermeer KA, van Vliet LJ. *Locally-adaptive loosely-coupled level sets for retinal layer and fluid segmentation in subjects with central serous retinopathy.* IEEE 13th International Symposium on Biomedical Imaging (ISBI) 2016, pages 702-705

De Jong JH, van Zeeburg EJT, Cereda MG, van Velthoven MEJ, Faridpooya K, Vermeer KA, van Meurs JC. *Intravitreal versus Subretinal Administration of Recombinant Tissue Plasminogen Activator combined with Gas for Acute Submacular Hemorrhages due to Age Related Macular Degeneration: an Exploratory Prospective Study.* Retina. 2016;36(5):914-925

Amarakoon S, **de Jong JH**, Braaf B, Yzer S, Missotten T, van Velthoven ME, de Boer JF. *Phase-Resolved Doppler Optical Coherence Tomographic Features in Retinal Angiomatous Proliferation.* American Journal of Ophthalmology. 2015;160(5):1044-1054.

Sanchez-Antequera Y, Mykhaylyk O, Van Til NP, Cengizeroglu A, **de Jong JH**, Huston MW, Anton M, Johnston IC, Pojda Z, Wagemaker G, Plank C. *Magselectofection: an integrated method of nanomagnetic separation and genetic modification of target cells.* Blood, 2011; 117(16):e171-81.